# UNIVERSITÀ DI SIENA 1240

Dipartimento di Scienze fisiche, della Terra e dell'ambiente

## Doctoral thesis in physics

XXXV Ciclo

Coordinatore: Prof. Riccardo Paoletti

# Geometric study of classical phase transitions and quantum entanglement

Settore scientifico disciplinare: FIS/02

**Candidate**
Ghofrane Bel Hadj Aissa
University of Siena
Via Roma 56

*Signature* Ghofrane Bel Hadj Aissa

**Supervisor**
Roberto Franzosi
University of Siena
Via Roma 56

*Signature*

**Co-supervisor**
Marco Pettini
University of Aix-Marseille
163 Avenue de Luminy

Academic years 2019/2023

# Abstract

The present work is divided into two parts. First, we discuss how the functional form of thermodynamic observables can be deduced from the geometric properties of subsets of phase space. The geometric quantities taken into account are mainly extrinsic curvatures of the energy level sets of the Hamiltonian of a system under investigation. In particular, it turns out that peculiar behaviors of thermodynamic observables at a phase transition point are rooted in more fundamental changes in the geometry of the energy level sets in phase space. More specifically, we discuss how microcanonical and geometrical descriptions of phase transitions are shaped in the peculiar Kosterlitz–Thouless phase transition and in the special case of the $\phi^4$ model. In the second part, we will focus on the quantification of quantum entanglement, a topic of great current interest. We will derive entanglement and quantum correlation measures, from a geometrical procedure, which are valid for multipartite hybrid states. We also provide a physical and operational meaning of the proposed entanglement measures for pure states. Furthermore, we show that the proposed measures can either be analytically or numerically computed. Finally, we test the validity of the proposed measure through a variety of examples.

# Acknowledgements

First of all, I would like to thank Roberto Franzosi and Marco Pettini for having accepted to supervise this work. I am very grateful for their presence and their ability to guide me in the best possible ways according to my personality.

I would like to thank Ricardo Paoletti for his kind presence and availability, as well as for his sincere advices.

I would also like to thank my fellow office mates in Arcetri in particular (in an order that does not matter) Mattia, Valentin, Beatrice, Marco, and Cristina for their discussions and their help. I would like to thank my dear friends Daniela, and her father Bruno, as well as Maximiliano, Giusy, and Gaston for their support. I am also very grateful to all my friends in the theater for their friendship and kind attention, especially Paolo, Leonardo, Chiara, Giuseppe, and many others.

I cannot thank my parents enough for always supporting me and encouraging me to follow my dreams. This accomplishment would not have been possible without them.

I dedicate this work to God, or to Nature. Whatever you prefer to call it.

# List of publications


[1] G Bel-Hadj-Aissa. *High order derivatives of Boltzmann microcanonical entropy with an additional conserved quantity.* Physics Letters A **384** (24) (2020).

[2] G Bel-Hadj-Aissa, M Gori, R Franzosi, M Pettini. *Geometrical and topological study of the Kosterlitz–Thouless phase transition in the XY model in two dimensions.* Journal of Statistical Mechanics, **2021**, (2021).

[3] G Bel-Hadj-Aissa, M Gori, V Penna, G Pettini, R Franzosi. *Geometrical aspects in the analysis of microcanonical phase-transitions.* Entropy, **384** (22) (2020).

[4] D Cocchiarella, S Scali, S Ribisi, B Nardi, G Bel-Hadj-Aissa, R Franzosi. *Entanglement distance for arbitrary M-qudit hybrid systems.* Physical Review A, **101**, (2020).

[5] A Vesperini, G Bel-Hadj-Aissa, R Franzosi. *Entanglement and quantum correlation measures for quantum multipartite mixed states.* Scientific Reports, **13**, (2023).

# Contents

# Introduction

*"Geometry will draw the soul towards truth and create the spirit of philosophy."*

– Plato, *The Republic.*

Geometry is the language by which Nature manifests itself in the world of forms and matter. It is an elegant and universal language, yet thoroughly and meticulously undisclosed. In the twentieth century, physics witnessed a great sophistication regarding the description of Nature when gravitation and electromagnetism were formulated as field theories in four-dimensional space-time. This gave reason to explore the world around us through broader lenses including geometry. Since then, geometric intuition has been taken more seriously. For example, in the 1970s, it has been shown that all the building blocks of quantum field theory can be formulated in terms of geometrical concepts such as vector bundles, connections, curvatures, covariant derivatives, and spinors. The geometric description of physical concepts is not only elegant but also generally useful. For example, Minkowski's geometrization of special relativity inspired Albert Einstein to formulate general relativity.

In the present work, we will attempt to bring out the usefulness of geometry in two different fields that are still not fully understood and well characterized up to now: classical phase transitions, and the quantification of quantum entanglement. This thesis is divided into two parts. **The first part** will be devoted to the study of classical phase transitions. The characterization of phase transitions remained an open subject for a long time because there were no unified theories of phase transitions taking into account the following two concepts: the occurrence of phase transitions in small systems (for example, a phase transition appearing in a snowflake), and the occurrence of phase transitions in systems without symmetry breaking. We will approach phase transitions using a geometrical way, more precisely, through the geometry and topology of energy level sets in phase space. We will then study a very peculiar phase transition, called the Kosterlitz–Thouless phase transition, which occurs without symmetry breaking. We will show that the phase transition stems from a change in the topology and geometry of the phase space. Finally, we will apply the geometrical and topological analysis to another model, namely the two-dimensional $\phi^4$ model. This model is known to undergo a second-order phase

transition. we will thus show that at the transition point, geometric indicators undergo an abrupt change, which suggests a deeper origin to the phase transition. **The second part** will be dedicated to quantum entanglement. The presence of entanglement in quantum states is widely recognized as one of, if not the, defining property of quantum mechanics. The nature of quantum entanglement is well understood for bipartite pure quantum states. However, this is not the case for pure multipartite entanglement, where entanglement becomes much more complex, and its characterization and quantification are still open subjects. What is even more mysterious is that in the case of mixed multipartite quantum states, other quantum features appear in addition to quantum entanglement. In fact, mixed entangled states can display other types of non-classical correlations such as steering and nonlocality. Even stranger: when unentangled states are mixed, they can display non-classical behavior. Non-locality, steering, entanglement, and any other type of non-classical correlations all belong to a set we call quantum correlations. Following a geometrical method, we will propose a quantum entanglement measure in the case of pure multipartite states. And for mixed multipartite states, we will define a measure of entanglement and a measure of quantum correlations for multipartite states.

PART I

# Geometrical characterization of classical phase transitions

# 1

# Introduction of part I

Phase transitions (PTs) encompass a very large number of phenomena that span from the cosmological scale down to the subnuclear scale and thus cover a huge range of energies and spatial dimensions. Despite their relevance and the extremely vast literature on this topic, a general and complete theory is not yet available. The successful and powerful phenomenological theory due to Landau associates PT with the spontaneous symmetry-breaking phenomenon. However, there are many systems undergoing PT in the absence of symmetry-breaking: the liquid-gas PT which is a first-order transition; systems with continuous symmetry which cannot be broken spontaneously at any finite temperature in dimensions two or lower according to the Mermin–Wagner theorem [112]; systems with local symmetries (gauge theories) which, after the Elitzur theorem [58], undergo PTs in the absence of an order parameter; glasses and supercooled liquids; amorphous and disordered systems; homopolymers and proteins undergoing folding transitions

A paradigmatic example of PT in the absence of symmetry-breaking is provided by the Kosterlitz–Thouless (KT) transitions [101] which manifest in several kinds of two-dimensional systems in condensed matter, such as the XY ferromagnet [110] describing spins on a 2D lattice, or a 2D Bose liquid as in the case of a 2D film of superfluid 4He, with O(2) symmetry [20], or two-dimensional superconductors [136], or a 2D liquid crystal [167], 2D melting into a 'liquid crystal' phase with sixfold orientational order [82], or the 'quasi-condensation' of a uniform 2D fluid of identical bosons [81].

Other transitional phenomena which are experimentally well known but are still at odds with the existing theoretical frameworks are PTs occurring in small systems, far from the thermodynamic limit which is commonly considered as a necessary requisite after the Yang–Lee theory [170]. Among many examples, we can mention the formation of nanoscopic snowflakes [131], Bose-Einstein condensation [103], homopolymer [106] and protein [47] folding. Therefore the motivation for a better understanding of the deep origin of PTs is mainly twofold: there are many PT phenomena occurring without a symmetry-breaking that are obviously not encompassed by the Landau–Ginzburg theory, and there are PTs occurring in nanoscopic or mesoscopic systems (far from the thermodynamic limit) that are not encompassed by the Yang–Lee theory or by the Dobrushin–Ruelle theory [65].

During the last two decades, the mentioned deeper level of description of PTs

has been found to be rooted in a novel and successful explanation of the origin of chaos in Hamiltonian dynamics tackled by means of Riemannian differential geometry [123]. Actually, a Hamiltonian flow can be identified with a geodesic flow on a Riemannian manifold equipped with a suitable metric tensor. Then, by combining together this geometrization of Hamiltonian dynamics with the microcanonical study of PT by means of Hamiltonian dynamics, a question arose naturally: are there peculiar changes in the geometry of the mechanical manifolds in correspondence with a phase transition? The answer turned out in the affirmative and, more precisely, it has been found that the topological properties of certain submanifolds of phase space are at the very grounds of the occurrence of PT. For a system described by a Hamiltonian of the form $H(p,q) = \sum_{i=1}^{N} \frac{1}{2}p_i^2 + V(q_1 \cdots q_N)$, the relevant manifolds are equivalently the energy level sets $\Sigma_E = \{H(p_1 \cdots p_N, q_1 \cdots q_N) = E \in \mathbb{R}\}$ and the balls $\{M_E = H^{-1}((-\infty, E])\}_{E\in\mathbb{R}}$ bounded by the $\Sigma_E$ in phase space, or the potential level sets $\Sigma_v = \{V(a_1 \cdots q_N) = v \in \mathbb{R}\}$ and the balls $\{M_v = V^{-1}((-\infty, v])\}_{v\in\mathbb{R}}$ bounded by the $\Sigma_v$ in configuration space.

The main difference between the topological approach and the usual association of PTs with some kind of singularity of the statistical measures is that the topological approach puts in evidence that all the information concerning the appearance of a PT is already 'encoded' in the interactions among the degrees of freedom of a system. A fact that is upstream of any signature, singular or not, of a PT. Otherwise said, the statistical measures are conceptual tools, not directly accessible to experiments, the singularities of which are used to interpret the occurrence of PTs phenomena, to the contrary the interactions among the constituents of a system have their own physical reality (experimentally accessible) and their knowledge is sufficient to predict the occurrence of a PT by suitably analyzing the energy level sets $H(p_1 \cdots p_N, q_1 \cdots q_N) = E$, or the potential energy level sets $V(q_1 \cdots q_N) = v$.

Besides its application to more traditional transitions [62], this topological approach has been already successfully used to tackle the PT of a gauge model in the absence of an order parameter [122]. Moreover, peculiar topological changes entailing a PT can take place at any finite number of degrees of freedom, thus allowing to go beyond the thermodynamic limit dogma.

Remarkably, topological concepts are at the core of the KT theory independently of the above-mentioned approach, in fact for the planar model of classical spins and for a superfluid two-dimensional film there are spatial vortexes and their cores are holes in the surface where the system lives. Hence a vortex is called a topological defect [100]. Adding holes to a surface makes a change of its homotopy type.

The first part of this thesis will be dedicated to characterizing the KT phase transition of the XY-2D model in a topological framework, however, instead of looking at topological changes in real space, we will focus on certain aspects of the geometry—tightly related to the topology—of the high dimensional manifolds $\Sigma_E$ and $M_E$ in phase space. This is an original work that we have published in [10] and [8]. Using the in-depth study of the geometrical and topological properties of the KT phase transition, we will, at the end of this

part, study another example of application, which is the $\phi^4$ model. This model undergoes a second-order phase transition [38], and through our original work published in [9], we show that geometrical quantities defined in $\Sigma_E$ undergo an abrupt change.

First, we will characterize the Kosterlitz-Thouless (KT) phase transition of the XY 2D model in the microcanonical ensemble from the thermodynamic point of view and we will then investigate the geometry and topology of energy level sets in phase space to verify the Topological Hypothesis on the deep origin of phase transitions. The **Chapter 2** of this part is devoted to a general review of the microcanonical thermodynamics. The first part presents an overview of the microcanonical ensemble thermodynamics. The second part consists of a brief review of the historical pathway that led to the elaboration of the Topological Hypothesis on the origin of phase transitions. In **Chapter 3** the KT phase transition in XY 2D model is characterized within the microcanonical thermodynamic framework previously introduced. The signature of phase transitions in the microcanonical ensemble can be found in the behavior of derivatives of the entropy with respect to the energy. The results of numerical simulations are presented in the last section. In **Chapter 4**, we present a very concise review of Riemannian differential geometry and topology of submanifolds defined as regular level sets of functions in the phase space. In **Chapter 5**, we described the microcanonical thermodynamics of XY 2D model in the geometrical framework introduced in the previous chapter deriving the expression of an extrinsic geometrical estimator of the topological invariants of the regular energy level sets. And, we present the results of Hamiltonian dynamic simulations that investigate the topology and geometry of energy level sets in the phase space endowed with a Euclidean metric. Finally, in **Chapter 6**, we will study, as another example of application, the classical $\phi^4$ model.

# 2

# Review of microcanonical thermodynamics

## 2.1 Introduction

In this chapter, we present an overview of the thermodynamics of phase transitions in the microcanonical ensemble and their origin due to the geometry and topology of phase and configuration space. In Section 2.2, a short review of the thermodynamics of the microcanonical ensemble and of the classification schemes is proposed for phase transitions in such a statistical ensemble. In particular two main classification schemes will be discussed: one (extending the Ehrenfest classification to the microcanonical ensemble) is based on the loss of analyticity of the microcanonical entropy $S_N$ in the thermodynamic limit, the other, more recent, is based on the analysis of the inflection points on derivatives of microcanonical entropy at some order and in finite systems. Both methods will be used to classify the KT phase transition in the XY 2D model in the next chapter. Finally, in Section 2.3 a very brief review is presented on the so called Topological Hypothesis: a conceptual framework where the deep origin of phase transitions in the microcanonical ensemble has been found in topological and geometrical properties of the *support* of the microcanonical measure: the level sets of (potential) total energy in (configuration) phase space.

## 2.2 Thermodynamics in the microcanonical ensemble

### Introduction to microcanonical statistical ensemble

The foundations of classical statistical mechanics are deeply rooted in many body dynamical Hamiltonian systems. Let us consider a Hamiltonian system described by $2N$-degrees of freedom $(p, q) = (p^1, ..., p^n, q^1, ..., q^n)$ in phase space $\Lambda$ and

$$H_N = \frac{1}{2}\sum_{i=1}^{N}(p^i)^2 + V_N(q^1, ..., q^N) \tag{2.1}$$

The dynamic of the system is given by Hamilton equations

$$\begin{cases} \dot{p}^i = -\dfrac{\partial H}{\partial q^i} \\ \\ \dot{q}^i = \dfrac{\partial H}{\partial p^i} \qquad . \end{cases} \tag{2.2}$$

Such equations can be rewritten in a more compact form, introducing the Hamiltonian vector field $X_H$

$$X_H = \sum_{i=1}^{N} \left( -\frac{\partial H}{\partial q^i}\frac{\partial}{\partial p^i} + \frac{\partial H}{\partial p^i}\frac{\partial}{\partial q^i} \right) , \tag{2.3}$$

so that they take the form

$$\frac{\mathrm{d}x^j}{\mathrm{d}t} = X_H^j \ , \quad j = 1, ..., 2N \tag{2.4}$$

where $x^{2i-1} = p^i$ and $x^{2i} = q^i$ for $i = 1, ..., N$. In general, Hamiltonian systems with a number $N \geq 3$ of degrees of freedom are *not* integrable, i.e. it is not possible to find $N$ constant of motion in involution. However, the Poincare-Fermi theorem states that in general for the Hamiltonian systems, $N \geq 3$ guarantees the existence of *only one* constant of motion, the total energy of the system.

**Definition 2.1.** *For Hamiltonian systems with a number $N \geq 3$ of degrees of freedom, the dynamics remain confined on a hypersurface of constant energy*

$$\Sigma_E = \{(p^1, ..p^N, q^1, ..., q^N) \in \Lambda \mid \ H(p,q) = E\} \ . \tag{2.5}$$

If the Hamiltonian system is ergodic on the energy level sets $\Sigma_E$, i.e. the only non-zero measure invariant subspace under the Hamiltonian dynamics is $\Sigma_E$, the Birkoff theorem holds

$$\lim_{T\to+\infty} \frac{1}{T}\int_0^T f(p(t), q(t)) \ \mathrm{d}t = \int_{\Sigma_E} f(p,q) \ \mu \ , \tag{2.6}$$

where $f$ is a real function defined over phase space and $\mu$ is the invariant probability measure on $\Sigma_E$ with respect to the Hamiltonian flow. The probability density $\mu$ can be regarded as the restriction to energy level sets of the invariant probability density $\rho$ defined on $\Lambda$

$$\int_{\Sigma_E} f\mu = \frac{\int_\Lambda f \ \delta\left(H(p,q) - E\right)\rho}{\int_\Lambda \ \delta\left(H(p,q) - E\right)\rho} \ . \tag{2.7}$$

**Theorem 2.1** (Liouville's theorem)**.** *The smooth measure defined in the phase space is invariant under the Hamiltonian flow*

$$\mathcal{L}_{X_H}\rho = 0 \ , \tag{2.8}$$

*where*

$$\rho = \frac{\prod_{i=1}^N \mathrm{d}p^i \wedge \mathrm{d}q^i}{\int_\Lambda \prod_{i=1}^N \mathrm{d}p^i \wedge \mathrm{d}q^i} \ . \tag{2.9}$$

*Proof.* In order to prove this we show that $\mathcal{L}_{X_H}\omega = 0$ where $\omega = \mathrm{d}p^1 \wedge \mathrm{d}q^1 \wedge ... \wedge \mathrm{d}q^N \wedge \mathrm{d}p^N$ is the symplectic volume form. Using the homotopy formula $\mathcal{L}_V = \mathrm{d}\imath_V + \imath_V \mathrm{d}$ and remembering that $\mathrm{d}\omega = 0$ we have that

$$\begin{aligned}\mathcal{L}_{X_H}\omega = \mathrm{d}\imath_{X_H}\omega = \mathrm{d}\sum_{i=1}^{N}\Bigg[ &- \frac{\partial H}{\partial q^i}\,\mathrm{d}q^1 \wedge \mathrm{d}p^1 \wedge ... \wedge \hat{\mathrm{d}p^i} \wedge \mathrm{d}q^i ... \wedge \mathrm{d}p^N \wedge \mathrm{d}q^n + \\ &+ \frac{\partial H}{\partial p^i}\,\mathrm{d}q^1 \wedge \mathrm{d}p^1 \wedge ... \wedge \mathrm{d}p^i \wedge \hat{\mathrm{d}q^i} ... \wedge \mathrm{d}p^N \wedge \mathrm{d}q^N\Bigg] = \\ = \sum_{i=1}^{N}\Bigg[ &- \frac{\partial^2 H}{\partial q^i \partial p^i}\,\mathrm{d}q^1 \wedge \mathrm{d}p^1 \wedge ... \wedge \mathrm{d}p^i \wedge \mathrm{d}q^i ... \wedge \mathrm{d}p^N \wedge \mathrm{d}q^n + \\ &+ \frac{\partial^2 H}{\partial q^i \partial p^i}\,\mathrm{d}q^1 \wedge \mathrm{d}p^1 \wedge ... \wedge \mathrm{d}p^i \wedge \mathrm{d}q^i ... \wedge \mathrm{d}p^N \wedge \mathrm{d}q^N\Bigg] = 0\ .\end{aligned} \tag{2.10}$$

■

Therefore, the measure of the volume is preserved by the dynamics. Coming back to Eq.(2.7), we have

$$\begin{aligned}\int_{\Sigma_E} f\ \mu &= \frac{\int_\Lambda f\,\delta\left(H(p,q)-E\right)\prod_{i=1}^{N}\ \mathrm{d}p^i \wedge \mathrm{d}q^i}{\int_\Lambda\ \delta\left(H(p,q)-E\right)\prod_{i=1}^{N}\ \mathrm{d}p^i \wedge \mathrm{d}q^i} \\ &= \frac{\int_\Lambda\ f\delta\left(H(p,q)-E\right)\prod_{i=1}^{N}\ \mathrm{d}p^i \wedge \mathrm{d}q^i}{\Omega_N(E)}\ ,\end{aligned}$$

where

$$\Omega_N(E) = \int_\Lambda \delta\left(H(p,q)-E\right)\ \prod_{i=1}^{N}\mathrm{d}p^i \wedge \mathrm{d}q^i \tag{2.11}$$

is the area of the energy level sets and it is the *microcanonical partition function*: in some sense, it counts the "number" of configurations compatible with a given constraint (here is the constant energy). From this expression, the specific Boltzmann entropy can be defined

$$S_N(\varepsilon) = \frac{k_B}{N}\ln\left(\frac{\Omega_N(N\varepsilon)}{\Omega_{N0}}\right)\ , \tag{2.12}$$

where $\varepsilon = E/N$ , $N$ is the total number of degrees of freedom, $k_B$ is the Boltzmann constant and $\Omega_0$ is a meaningless arbitrary $N$-dimensional phase space volume scale to have a non-dimensional argument in the logarithm. In what follows we will adopt natural units, i.e. $k_B = 1$.
Thermodynamic relevant observables are generally expressed as the derivatives of the thermodynamic potentials with respect to the parameters that define the correspondent statistical ensemble. For the microcanonical ensemble, the thermodynamic potential is the specific microcanonical entropy $S_N(\varepsilon)$ defined in equation (2.12). The basic macroscopic thermodynamic observable is the

temperature $T$ defined as the first-order derivative of the entropy with respect to the specific energy $\varepsilon$ at fixed volume $v$

$$T = \left(\frac{\partial S}{\partial \varepsilon}\right)_v^{-1} . \tag{2.13}$$

The specific heat is defined as follows

$$c_v = \frac{C_v}{N} = \left(\frac{\partial T}{\partial \varepsilon}\right)_v^{-1} = -\frac{\left(\partial S/\partial \varepsilon\right)_v^2}{\left(\partial^2 S/\partial \varepsilon^2\right)_v} . \tag{2.14}$$

As was noted in the introduction, the microcanonical ensemble is the most fundamental of all statistical ensembles. In fact, from the knowledge of the microcanonical partition functions all the other statistical ensembles can be derived. For instance, let us consider the canonical partition function

$$Z_N(\beta) = \int_\Lambda e^{-\beta H(p,q)} \prod_{i=1}^{N} \mathrm{d}p^i \wedge \mathrm{d}q^i , \tag{2.15}$$

where $\beta = \dfrac{1}{T}$. $T$ is the temperature of the canonical statistical ensemble. This expression can be rewritten as the Laplace transform of the microcanonical partition function $\Omega_N(E)$

$$\begin{aligned} Z_N(\beta) &= \int_0^{+\infty} \mathrm{d}E \int_\Lambda e^{-\beta H(p,q)} \delta(H(p,q) - E) \prod_{i=1}^{N} \mathrm{d}p^i \wedge \mathrm{d}q^i \\ &= \int_0^{+\infty} e^{-\beta E}\, \Omega_N(E)\, \mathrm{d}E . \end{aligned} \tag{2.16}$$

The measure properties of the energy level sets $\Sigma_E$ give the fundamental characterization of the statistical mechanics of microcanonical statistical ensemble and consequently of all other statistical ensembles. Moreover, one can make the link between the canonical specific free energy and the microcanonical specific entropy. In fact, the last equation can be written in this form

$$\begin{aligned} Z_N(\beta) &= \int_0^{+\infty} \exp\left\{-\left[\beta N\varepsilon + N\frac{1}{N}\ln\Omega_N(N\varepsilon)\right]\right\} \mathrm{d}E \\ &= \int_0^{+\infty} \exp\left\{-N\left[\beta\varepsilon - S_N(\varepsilon)\right]\right\} \mathrm{d}E . \end{aligned} \tag{2.17}$$

For large N, we use the saddle point approximation for a fixed $\beta$, we derive $\varepsilon = \varepsilon(\beta)$ such that $h(\varepsilon, \beta) = \beta\varepsilon - S_N\varepsilon$ is minimized, i.e.

$$Z_N(\beta) = \exp\left\{-\frac{N}{2}\left[\beta\tilde{\varepsilon}(\beta) - S(\tilde{\varepsilon}(\beta))\right]\right\} \int_0^{+\infty} \exp\left\{N\frac{\partial^2 S}{\partial \varepsilon^2}|_{\varepsilon=\tilde{\varepsilon}}\left(\varepsilon - \tilde{\varepsilon}\right)^2 + \mathcal{O}(\varepsilon^3)\right\} \mathrm{d}E .$$

Let us consider the function $f_N(\beta) = -\dfrac{1}{N}\log Z_N(\beta)$ that its strictly related to the specific free energy $F_N(\beta) = \dfrac{1}{\beta} f_N(\beta)$ and let us suppose that $S_N$ and $f_N$ converge to the thermodynamic limit to two functions $f_\infty(\beta)$ and $S_\infty(\varepsilon)$. $f_\infty(\beta)$ is then the Legendre transform of $S_\infty(\varepsilon)$, i.e.

$$f_\infty(\beta) = \inf_{\varepsilon \in [0,+\infty[} \left[\beta\varepsilon - S_\infty(\varepsilon)\right] . \tag{2.18}$$

| First order phase transitions | Second order phase transitions |
|---|---|
| $\left\| \frac{\partial G_+(k_{c_i})}{\partial k} - \frac{\partial G_-(k_{c_i})}{\partial k} \right\| = \Delta G_{k_i} > 0$ | $\left\| \frac{\partial^2 G_+(k_{c_i})}{\partial k^2} - \frac{\partial^2 G_-(k_{c_i})}{\partial k^2} \right\| = \Delta G_{k_i^2} > 0$ |

Table 2.1: Summary of the classification scheme of phase transitions adopted by Ehrenfest.

### Phase transition in the microcanonical ensemble: the state of art

As we will see later, according to the topological hypothesis, phase transitions are due to major changes in the topology of the energy level sets. We expect that such dramatic changes can be reflected in a loss of the "smoothness" of the thermodynamic potential defined on these foliated spaces. Is it then possible to associate phase transitions in a microcanonical ensemble with some loss of analyticity of the microcanonical entropy $S$?

Historically, Paul Ehrenfest classified phase transitions in the canonical and grand canonical ensembles based on the behavior of the thermodynamic potential as a function of other thermodynamic variables. First-order phase transitions are those for which the first derivative with respect to one of the thermodynamic variables of the thermodynamic potential $G$ is discontinuous (presence of a "jump" in this derivative). Second-order phase transitions are those for which the second derivative with respect to one of the thermodynamic variables of $G$ is not continuous. Analogously, the $k$th order phase transitions have discontinuities in the $k$th derivatives of $G$. This is summarized in Table 2.1 in the case of the first and second order phase transitions where $\partial G_+(k_{c_i})/\partial k_i = \lim_{k_i \to k_{c_i}^+} (G(k_i)/\partial k_i)$ and $\partial G_-(k_{c_i})/\partial k_i = \lim_{k_i \to k_{c_i}^-} (G(k_i)/\partial k_i)$ ($k_{c_i}$ denotes one of the thermodynamic variables at the critical point). Thus, according to Ehrenfest's classification scheme, the order of the transition is determined by the lowest derivative exhibiting a singular behavior at the critical point. However, such behavior can only occur in the thermodynamic limit, as rigorously proved by Yang and Lee in the grand canonical ensemble [170]. One can wonder if is it possible to extend the Ehrenfest classification scheme to the microcanonical ensemble. As we have seen in the last subsection $f_\infty$ is the Legendre transform of $S_\infty$, then a loss of analyticity of $f_\infty$ can be due to two possible mechanisms: a loss of analyticity of $S_\infty$ or a convex hull in $S_\infty$, where the latest mechanism has been studied in the context of large deviation theory [150].

What if the works on microcanonical ensembles explore "small" systems where the thermodynamic limit is not invoked? Following Ehrenfest classification, no loss of analyticity is expected in the microcanonical entropy in this case. However, other signatures of phase transitions in microcanonical entropy have been proposed. Such classification schemes are linked to the inflection points of the microcanonical entropy and its derivatives. Thus, with this new classification scheme, one can examine phase transitions in systems with a finite number of degrees of freedom. Gross [76] was the first who proposed in the 90s a

classification of phase transitions in the microcanonical ensemble based on the change of the curvature of the entropy $d(k) = \mathrm{d}^2 S/\,\mathrm{d}k^2$ as a function of a conserved quantity, or on the change of the determinant of the matrix $d(k^i)$ in the case of more than one conserved quantity. He proposed two classes of phase transitions, first-order phase transitions with phase separation which involve a latent heat, are characterized by a negative determinant $d(k^i)$ of the entropy $S(k^i)$, and continuous phase transition where two neighboring phases become indistinguishable, are characterized by a zero determinant $d(k^i)$. This idea was refined by Qi and Bachmann [133], where they proposed a definition for a $k$th order phase transitions in the microcanonical ensemble through the analysis of the inflection point of the microcanonical entropy and its derivatives. Their argument goes as follows: since in the canonical ensemble, the order parameter is the temperature, the curve $\langle E\rangle(\beta)$ shows that the phase transition is marked by a sudden decrease in the expectation value of the energy of the system $\langle E\rangle$ at the phase transition. Thus, in the microcanonical ensemble, where the order parameter is the energy, the curve $\beta(E)$ responds least sensitively to energy changes, where $\beta(E) = \mathrm{d}S(E)/\,\mathrm{d}E$. In other words, it causes a change in the monotonicity of $\beta(E)$ which is called an *inflection point of least sensitivity*. And, the classification of phase transitions proposed by Qi and Bachmann in [133], was based on where the inflection point is placed (the point of least sensitivity). For instance, the occurrence of the second-order phase transition is characterized by an inflection point in $\beta(E)$. Whereas the first-order phase transition is outlined by an infection point in $S(E)$, and this seems consistent, in the sense that the first-order phase transition is characterized by a latent heat which can be explained by the energy difference caused by the convex region in $S(E)$ in the case of finite systems (caused by a surface effect), and by an inflection point in the thermodynamic limit[1]. More generally a phase transition of even order $2k$ ($k$ is a positive integer) is associated with a least-sensitive inflection point in the $(2k-1)$th derivative of $S(E)$, and the corresponding negative-valued maximum in the $(2k)$th derivative of $S(E)$. Analogously, a phase transition of odd order $(2k-1)$ occurs if there is a least sensitive inflection point in the $(2k-2)$th derivative of $S(E)$, and the corresponding minimum in the $(2k-1)$th derivative of $S(E)$ is positive. This is summarized in Table **??**, where $S^m$ denotes the $(m)$th derivative of $S$.

## 2.3 Historical motivation of the Topological Hypothesis of phase transitions

The topological theory of phase transitions has its origin in the geometrical formulation of Hamiltonian dynamics in the characterization of chaotic systems. In the mid-'90s, Hamiltonian chaos has been deeply re-investigated [31, 123] from the Riemannian geometrical point of view. It is very well known [97, 71, 3, 109] that trajectories of natural motions can be regarded as geodesic in configuration space endowed with the Jacobi metric. In fact, the paths in configuration space of the representative point of a Lagrangian system, i.e. a mechanical system

[1] It is an open question whether the mechanism proposed by [150] for the emergence of the singularity in the free energy from a convex hull in $S$ is already valid when the convex hull reduces to a single inflection point.

| (2k-1)-th order PT | (2k)-th order PT |
|---|---|
| $S^{(2k-1)} > 0$ | $S^{(2k)} < 0$ |
| $S^{(2k)} = 0$ | $S^{(2k+1)} = 0$ |
| $S^{(2k+1)} > 0$ | $S^{(2k+2)} < 0$ |

Table 2.2: Summary of the classification scheme of phase transitions adopted in the present work.

described by the Lagrangian

$$L\left(q,\dot{q}\right) = \frac{1}{2} g_{ij}\dot{q}^i\dot{q}^j - V \tag{2.19}$$

where $g_{ij}(q)$ is a Riemannian metric on the configuration space, are the geodesics of the energy-dependent Jacobi metric

$$\mathrm{d}s_J = \sqrt{2\left(E-V\right) g_{ij}\dot{q}^i\dot{q}^j}\ . \tag{2.20}$$

Such an introduction of a metric structure allowed describing Hamiltonian chaos in terms of geodesic spread.

Furthermore, it has been shown that critical points of a suitable class of functions on a manifold and their index are strictly related to the topology of the same manifold according to *Morse theory*. In fact, given a generic system of $N$ degrees of freedom described by a Hamiltonian $H = \frac{1}{2}\sum_{i=1}^{N} p_i^2 + V(q_1,\ldots,q_N)$ or equivalently by the corresponding Lagrangian function $L = \frac{1}{2}\sum_{i=1}^{N}\dot{q}_i^2 - V(q_1,\ldots,q_N)$ its dynamics can be identified with a geodesic flow of an appropriate Riemannian differentiable manifold. This differential geometric framework is given by configuration space $M_E = \{q \in \mathbb{R}^N | V(q) < E\}$ endowed with the Jacobian metric defined above. Then, Newton equations are retrieved from the geodesic equations

$$\frac{d^2q^i}{ds^2} + \Gamma^i_{jk}\frac{dq^j}{ds}\frac{dq^k}{ds} = 0\ , \tag{2.21}$$

where $\Gamma^i_{jk}$ are the Christoffel connection coefficients of the manifold. Thus, in this context, the natural question is whether the mechanical manifolds $(M_E, g)$ undergo some peculiar geometrical change when $E$ crosses a critical value $E_c$ that corresponds to a phase transition. And it has been discovered that this is actually the case [123]. Moreover, the peculiar geometrical changes associated with phase transitions were discovered to be also the effects of deeper topological changes of the potential level sets $\Sigma_v^{V_N} := \{V_N(q_1,\ldots,q_N) = v \in \mathbb{R}\}$ in configurations space, and, equivalently, of the balls $\{M_v^{V_N} = V_N^{-1}((-\infty, v])\}_{v\in\mathbb{R}}$ bounded by the $\Sigma_v^{V_N}$. In other words, given a Hamiltonian system undergoing a phase transition, let $v_c = v_c(E_c)$ be the average potential energy corresponding to the

phase transition point, a topological change means that the manifolds $\Sigma^{V_N}_{v<v_c}$ and $\Sigma^{V_N}_{v>v_c}$ are not diffeomorphic, that is, they cannot be transformed one into the other with a differentiable application with the differentiable inverse. Topological changes of these manifolds are related to the presence of critical points of the potential function $V(q)$ in configuration space. To get an intuitive idea of the relationship between critical points of a function in a given space and the topology of its level sets, let us consider a low-dimensional and intuitive case. Given a smooth function $f$, bounded below, such that $f : \mathbb{R}^N \to \mathbb{R}$. Its level sets $\Sigma_u = f^{-1}(u)$ are diffeomorphically transformed one into the other by the flow [86]

$$\frac{dx}{du} = \frac{\nabla f}{\|\nabla f\|^2} \ , \tag{2.22}$$

where $x \in \mathbb{R}^N$, i.e., the points of a hypersurface $\Sigma_{u_0}$ with $u_0 \in [a, b] \subset \mathbb{R}$, are mapped by this flow to the points of another $\Sigma_{u_1}$ with $u_1 \in [a, b]$, provided that $\nabla f$ never vanishes in the interval $[a, b]$. In other words, if in the interval $[a, b]$ the function $f$ has no critical points, all the level sets $\Sigma_u = f^{-1}(u)$, with $u \in [a, b]$, have the same topology. Conversely, the appearance of critical points of $f$ at some critical value $u_c$ breaks the diffeomorphicity among the $\Sigma_{u<u_c}$ and $\Sigma_{u>u_c}$. This is illustrated by one of the simplest possible examples in Figure 2.1. A systematic study is developed within *Morse theory* of the relationship between

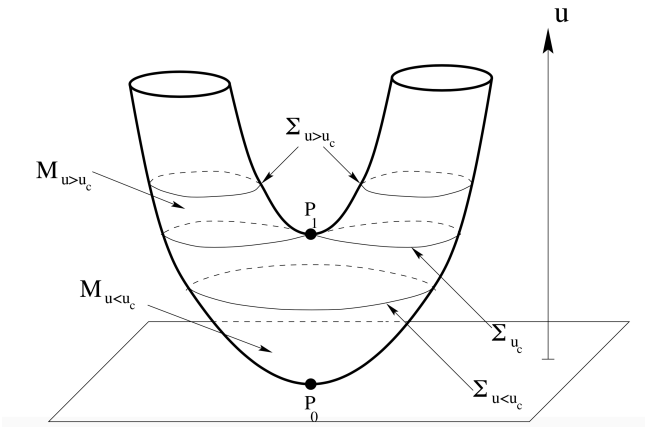


Figure 2.1: The function $f$ is here the height of a point of the bended cylinder with respect to the ground. In $P_1$ it is $df = 0$. The level sets $\Sigma_u = f^{-1}(u)$ below this critical point are circles, whereas above are the union of two circles. The manifolds $M_u = f^{-1}((-\infty, u])$ are disks for $u < u_c$ and cylinders for $u > u_c$

the topological properties of a manifold and the critical points of a suitable class of real-valued functions (Morse functions) defined on it. In particular, if $f \equiv V$, Morse's theory tells us that the existence of critical points of $V$ is associated with topological changes of the hypersurfaces $\{\Sigma_v\}_{v\in\mathbb{R}}$, and also of the $\{M_v\}_{v\in\mathbb{R}}$, provided that $V$ is a good Morse function (that is, bounded below, with no vanishing eigenvalues of its Hessian matrix). In general, finding either analytically or numerically all the critical points of a potential $V(q)$ is a very hard task, often an unfeasible one. Thus in order to get information on the topology of the manifolds of interest one has to resort to the available theorems

in differential topology, like the Pinkall theorem [126]. These theorems relate some total (that is integrated over the whole manifold) geometric property of a manifold with some information on its topology. Note that Morse indexes $\mu_k(M)$ of a manifold $M$ count the number of critical points of degree $k$ (the number of negative eigenvalues of the Hessian of the Morse function). Betti numbers are related with Morse indexes by the inequalities $\mu_k(M) \geq b_k(M)$. The $b_k(M)$ are dimensions of some groups (homology and cohomology of $M$) invariant under diffeomorphisms of $M$.

In this framework, the Topological hypothesis can be formulated as follows: *The basic origin of phase transitions lies in some topological change (or in the way the topology changes) of the support of the measure describing a system at the transition point.* In fact, it can be shown [123] that there is a relationship between geometry and topology of the energy landscape in phase space or in configuration space, and thermodynamic specific entropy

$$S(N\varepsilon) \approx \frac{1}{2N} \log \left[ \mathrm{Vol}\left(\mathcal{S}_1^{2N-1}\right) \sum_{i=0}^{2N-1} b_i\left(\Sigma_{N\varepsilon}\right) + \int_{\Sigma_{N\varepsilon}} \mathrm{d}\sigma \frac{\tilde{\mathcal{R}}(N\varepsilon)}{N!} \right] + r(E), \tag{2.23}$$

where $b_i\left(\Sigma_{N\varepsilon}\right)$ are the Betti numbers of the energy level sets $\Sigma_E$ in phase space. Betti numbers are fundamental topological invariants of a manifold. This approximate formula establishes a relation between thermodynamics and the topology of energy level sets in phase space. It was the starting point for a more rigorous mathematical investigation of the relation between the topology of (potential) energy in (configuration) phase space, and phase transitions. The peculiarity of this approach is that phase transitions are characterized from the point of view of Hamiltonian dynamics. This allows looking for the characterization of phase transitions as more related to the geometrical/dynamical properties of the (potential) energy level sets than to the thermodynamic properties. This has opened up the possibility of predicting whether or not a system will undergo a phase transition from the properties of the potential.

# 3

# Thermodynamics of the Kosterlitz-Thouless phase transition

This Chapter is based on a personal work and has been published in Ref.[8]. Phase transitions at the thermodynamic equilibrium can be heuristically described as an abrupt change of macroscopic properties of the system as the consequence of a small change in *control parameters* that define the statistical ensemble (e.g, the specific energy in the microcanonical ensemble or the temperature in the canonical ensemble). When the "abrupt change of macroscopic properties" of the system coincides with a spontaneous symmetry-breaking phenomenon, it is in general possible to introduce a so-called *order parameter*, that, in some cases, quantitatively measures the emergence of the order in the systems by triggering discontinuities of thermodynamic functions. In these cases, the characterization and classification of phase transitions are quite straightforward: e.g., Landau, for example, provided a classification of phase transitions based on the index of the broken symmetry group. However, it has been observed that phase transitions can also occur in the absence of symmetry breaking. A well-known example is the case of the XY model in two dimensions, where there is a continuous phase transition, yet there is no symmetry breaking, known as the Kosterlitz-Thouless transition. In this case, it is harder to provide a classification of phase transitions in the absence of an order parameter associated with broken symmetry. In this chapter, we will use the most fundamental thermodynamic ensemble, which is the microcanonical ensemble, as seen in the previous Chapter, to study the peculiar Kosterltz-Thouless (KT) phase transition in the 2D XY model. The main features of the KT phase transition are briefly reviewed in Section 3.1. In Section 3.2 we present a method to calculate derivatives up to the 4th order with respect to a specific energy of the specific microcanonical entropy, using a Laplace transform technique. In particular, a computation is performed of the derivatives of the microcanonical entropy, with respect to the energy up to the 4th order, using a Laplace transform technique, and adapted it to the case where the total momentum is conserved. In Section 3.3 we present the algorithm we implemented to sample the energy level sets through the simulation of Hamiltonian dynamics. Finally, in Section 3.4 we present and comment on the results of numerical simulations, looking at the signature of the KT transition in the XY 2D model in the behavior of thermodynamic quantities.

## 3.1 The XY model 2D

### Presentation of the model

The XY model is a 2-vector model on a D-dimensional lattice $\lambda$: a 2-dimensional unit-vector $\mathbf{s}_i = (s_{ix}, s_{iy}) = (\cos\theta_i, \sin\theta_i)$ is associated to each site $i \in \lambda$. The standard Hamiltonian of the XY model in two dimensions is given by

$$H_{\mathrm{stdXY}}(\theta) = -J \sum_{\langle i,j\rangle=1}^{N} \mathbf{s}_i . \mathbf{s}_j = -J \sum_{\langle i,j\rangle \in \lambda\times\lambda} \cos(\theta_i - \theta_j), \tag{3.1}$$

where $\langle i, j\rangle$ indicates all couples of nearest neighbors (resulting in short-range interactions) and $J$ is the coupling constant. Such a model can be regarded as a generalization of the Ising model in the sense that spins can rotate in two dimensions instead of only pointing in two directions.
Moreover, the Hamiltonian is invariant under the continuous $O(2)$ symmetry group because the scalar product of two rotating vectors does not change while the Ising model is invariant under the discrete $Z_2$ symmetry group.
In this work we adopt a modified version of the XY-model on a two dimension lattice ($D = 2$): a kinetic term, quadratic in conjugate momenta $p_i$, has been added at the original Hamiltonian and a fixed constant $2NJ$ has been added to the potential energy in order to recover the potential energy for a set of the coupled harmonic oscillator, i.e.

$$H_{\mathrm{XY}}(\boldsymbol{p}, \boldsymbol{\theta}) = \sum_{i=1}^{n}\sum_{j=1}^{n} \frac{p_{(i,j)}^2}{2} - \mathrm{J}\left[2 - \cos(\theta_{(i,j)} - \theta_{(i,j+1)}) - \cos(\theta_{(i,j)} - \theta_{(i+1,j)})\right] . \tag{3.2}$$

In what follows periodic boundary conditions have been considered, so for a set of $N = n \times n$ spins, we have that $(n + 1, j) = (1, j)$ and $(i, n + 1) = (i, 1)$.
According to Noether's theorem, this system has two first integrals, the total energy $E = H_{\mathrm{XY}}(\boldsymbol{p}, \boldsymbol{\theta})$ and the total momentum $P = \sum_{i\in\Lambda} p_i$ associated to the global $O(2)$ symmetry $\theta_i \to \theta_i + \alpha$.

If one starts bringing the temperature of the spin system down, what happens is that below the Curie temperature (critical temperature $T_c$) they begin to align in a specific direction, which is random[1] and the mean magnetization $\langle M\rangle = 0$. Below $T_c$, the Hamiltonian from above still dictates the behavior of the system, but the newly occupied ground state of the system has lost[2] the original O(2) symmetry of the Hamiltonian.
However according to the Mermin-Wagner theorem [112], there cannot be a spontaneous symmetry breaking in systems with continuous symmetry and short-range interactions in $D \leq 2$ dimensions, which means that the XY model cannot exhibit spontaneous symmetry breaking at finite temperatures, due to its continuous O(2) symmetry.
Why then does one still consider it a phase transition? It's known from numerical simulations that the XY model, has completely different behavior at low and high temperatures. Indeed, by decreasing the temperature up to

[1] In the case of a two-dimensional system, it could be any angle $\theta \in [0, 2\pi)$.
[2] In the case of discrete symmetry, it would be called *a spontaneous symmetry breaking* which would indicate the presence of a phase transition.

$T_c$, the spins start to align in macroscopic regions and this is reminiscent of symmetry breaking, i.e. a shift from an unordered to an ordered phase.
To see this, let's compute the correlation of two spins between the origin and the position $x$ at high temperature. Setting $\kappa = \frac{\mathrm{J}}{T}$, one has

$$\begin{aligned}\langle \mathbf{s}_o . \mathbf{s}_x \rangle &= \langle \cos(\theta_o - \theta_x) \rangle \\ &= \frac{1}{Z_N} \prod_{k=1}^{N} \left( \int_0^{2\pi} \frac{d\theta_k}{2\pi} \right) \cos(\theta_o - \theta_x) e^{\kappa \sum_{\langle i,j \rangle} \cos(\theta_i - \theta_j)} \\ &= \frac{1}{Z_N} \prod_{k=1}^{N} \left( \int_0^{2\pi} \frac{d\theta_k}{2\pi} \right) \cos(\theta_o - \theta_x) \prod_{\langle i,j \rangle} \left[ 1 + \kappa \cos(\theta_i - \theta_j) + O(\kappa^2) \right] \\ &= \frac{1}{Z_N} \prod_{k=1}^{N} \left( \int_0^{2\pi} \frac{d\theta_k}{2\pi} \right) \cos(\theta_o - \theta_x) \left[ 1 + \kappa \cos(\theta_1 - \theta_2) \right] \cdots \end{aligned} \tag{3.3}$$

with

$$\begin{cases} \displaystyle\int_0^{2\pi} \frac{d\theta_1}{2\pi} \cos(\theta_1 - \theta_2) = 0 \\ \\ \displaystyle\int_0^{2\pi} \frac{d\theta_2}{2\pi} \cos(\theta_1 - \theta_2) \cos(\theta_2 - \theta_3) = \frac{1}{2} \cos(\theta_1 - \theta_3) \ . \end{cases} \tag{3.4}$$

The only not null contribution to (3.3) comes from the paths $\gamma$, where each path has length $r = \|x\|$, and a contribution of order $\left(\frac{\kappa}{2}\right)^r \ll 1$. From this follows that the main contribution is given by the shortest path. The correlation length at high temperatures reads then

$$\langle \mathbf{s}_o . \mathbf{s}_x \rangle \approx \left(\frac{\kappa}{2}\right)^r = e^{-r/\xi} \ , \tag{3.5}$$

where $\xi = \ln(2/\kappa)^{-1}$. The equation (3.5) shows that the correlation decays exponentially. At low temperatures, as the fluctuations in the angles are going to be small, at long distances, we take the continuum limit of the lattice model assuming the angle field is slowly varying [3]. Therefore writing

$$\theta_i - \theta_j = a \operatorname{grad} \theta(\mathbf{x}) . \hat{e}_{ij} + \mathrm{O}(a^2),$$

where $a \to 0$ is the lattice spacing and $\hat{e}_{ij}$ is the unit vector along the lattice bond joining sites i and j. Having the Fourier transform of

$$\operatorname{grad} \theta(\mathbf{x}) = \frac{1}{2\pi} \int dq \, (-i\mathbf{q}) e^{-i\mathbf{q}.\mathbf{x}} \tilde{\theta}(\mathbf{q}),$$

and

$$\cos(\theta_i - \theta_j) \approx 1 - \frac{a}{2} \|\operatorname{grad} \theta\|^2,$$

[3] This is called the spin-wave approximation.

the Fourier transform of the Hamiltonian is then

$$\begin{aligned} H &= \frac{\mathrm{J}}{2}\int d^2x \int \frac{d\mathbf{q}\, d\mathbf{q}'}{(2\pi)^2}\mathbf{q}.\mathbf{q}' e^{-i(\mathbf{q}+\mathbf{q}').\mathbf{x}}\,\tilde{\theta}(\mathbf{q})\tilde{\theta}(-\mathbf{q}) \\ &= \int \frac{d\mathbf{q}\, d\mathbf{q}'}{(2\pi)^2}\mathbf{q}.\mathbf{q}'\delta(\mathbf{q}+\mathbf{q}')\tilde{\theta}(\mathbf{q})\tilde{\theta}(-\mathbf{q}). \end{aligned} \tag{3.6}$$

The correlation length reads

$$\begin{aligned} \langle\cos(\theta_0-\theta_r)\rangle = \mathbb{R}e\langle e^{i(\theta_0-\theta_r)}\rangle &= \mathbb{R}e\Big[\sum_{k=0}^{+\infty}\frac{i^k}{k!}\langle\, \underbrace{(\theta_0-\theta_r)^k}_{\mathrm{X}^k}\,\rangle\Big] \\ &= \mathbb{R}e\Big[\sum_{m=0}^{+\infty}\frac{(i)^{2m}}{(2m)!}\langle \mathrm{X}^{2m}\rangle\Big], \end{aligned}$$

where this equality holds because of the Gaussian distribution due to the quadratic and diagonal Hamiltonian (3.6). Knowing that

$$\mathbb{E}\big[X^{2m}\big] = \frac{(2m-1)!\,\langle \mathrm{X}^2\rangle^m}{2^{m-1}\,(m-1)!},$$

one has

$$\langle\cos(\theta_0-\theta_r)\rangle = \sum_{m=0}^{+\infty}\frac{(-1)^m}{2^m m!}\langle \mathrm{X}^2\rangle^m = e^{-\frac{\langle(\theta_0-\theta_r)^2\rangle}{2}}, \tag{3.7}$$

where [4]

$$\langle(\theta_0-\theta_{\mathrm{r}})^2\rangle = \int \frac{d\mathbf{q_1}\, d\mathbf{q_2}}{(2\pi)^2}\big(e^{-i\mathrm{q}_1.\mathrm{r}}-1\big)\big(e^{-i\mathbf{q_2}.\mathbf{r}}-1\big)\langle\tilde{\theta}(\mathbf{q_1})\,\tilde{\theta}(\mathbf{q_2})\rangle\,, \tag{3.8}$$

and

$$\begin{aligned} \langle\tilde{\theta}(\mathbf{q_1})\,\tilde{\theta}(\mathbf{q_2})\rangle &= \frac{\int d[\tilde{\theta}]d[\tilde{\theta}^*]\,\tilde{\theta}(\mathbf{q_1})\,\tilde{\theta}(\mathbf{q_2})\; e^{-\frac{\mathrm{J}}{2\mathrm{T}}\int\frac{d\mathbf{q}\,d\mathbf{q}'}{(2\pi)^2}\mathbf{q}.\mathbf{q}'\delta(\mathbf{q}+\mathbf{q}')\tilde{\theta}(\mathbf{q})\tilde{\theta}(-\mathbf{q})}}{\int d[\tilde{\theta}]d[\tilde{\theta}^*]\; e^{-\frac{\mathrm{J}}{2\mathrm{T}}\int\frac{d\mathbf{q}\,d\mathbf{q}'}{(2\pi)^2}\mathbf{q}.\mathbf{q}'\delta(\mathbf{q}+\mathbf{q}')\tilde{\theta}(\mathbf{q})\tilde{\theta}(-\mathbf{q})}} \\ &= \frac{(2\pi)^2\,\mathrm{T}}{\mathrm{J}\,q_1^2}\delta(\mathbf{q_1}+\mathbf{q_2}). \end{aligned} \tag{3.9}$$

We then have

$$\begin{aligned} \langle(\theta_0-\theta_{\mathrm{r}})^2\rangle &= \frac{\mathrm{T}}{\mathrm{J}}\int d\mathbf{q_1}\, d\mathbf{q_2}\,\frac{\big(e^{-i\mathbf{q_1}.\mathbf{r}}-1\big)\big(e^{-\mathbf{i}\mathbf{q_2}.\mathbf{r}}-1\big)}{q_1^2}\,\delta(\mathbf{q_1}+\mathbf{q_2}) \\ &\approx \frac{\mathrm{T}}{\mathrm{J}}\int_{r^{-1}}^{a^{-1}} dq\;\frac{1}{q} = \frac{\mathrm{T}}{\mathrm{J}}\log\big(\frac{r}{a}\big). \end{aligned} \tag{3.10}$$

Finally, the correlation length at low temperatures reads

$$\langle\mathbf{s}_o.\,\mathbf{s}_x\rangle \propto r^{-\mathrm{T}/\mathrm{J}} \tag{3.11}$$

[4] $\theta_r = \sum_{\mathbf{q}}\tilde{\theta}_{\mathbf{q}}e^{-i\mathbf{q}.\mathbf{r}}$ and $\theta_0 = \sum_{\mathbf{q}}\tilde{\theta}_{\mathbf{q}}$.

At low temperatures the correlation length has an algebraic decay, this confirms the fact that the 2D XY model has completely different behavior in the two regimes. Further, the exponent is not universal but depends on the temperature. This phase is called quasi-ordered.
The minimization of the energy $\delta H/\delta\theta$ leads to $\nabla^2\theta = 0$ which leads to

$$\theta(\alpha) = n\alpha + c, \tag{3.12}$$

where n is called the winding number and describes how many times a spin arrow winds around itself, going around clockwise the vortex center.
The equation (3.12) describes solutions in the form of vortices, which is a special type of topological defect defined by having a non-zero winding number.
One of the discoveries that earned the 2016 Nobel Prize was that topological effects play an important role in certain classical phase transitions. The work of David J. Thouless and J. Michael Kosterlitz explained how two-dimensional materials, like thin films, can have phase transitions despite lacking a truly ordered phase. Their key insight was that vortices are bound tightly together at low temperatures, and yet at high temperature, they become unbound and proliferate. This sharp change in behavior turns out to be universal and explains many unconventional phase transitions such as those found in superfluid helium and superconductors.
The two-dimensional classical XY model studied in this thesis is the simplest physical model with vortices.

### The XY 2D model in the microcanonical ensemble

As we have seen in the last paragraph, we have another integral of motion apart from the total energy, so it is necessary to be precise about the nature of the constraint of the total momentum of the system. It seems natural to consider for the XY model in 2D a particular case of the microcanonical ensemble where also the total momentum is fixed to be $p$, as the dynamic will be confined on hypersurfaces of constant energy over the plane $P = p$.

$$\Sigma_{E,p} = \{x = (p^1, ..p^N, q^1, ..., q^N) \in \Lambda \mid P(x) = p \wedge H(x) = E\} \ . \tag{3.13}$$

It follows that the microcanonical partition function according to Boltzmann's prescription reads

$$\Omega_N(E,p) = \int_\Lambda \delta\left(H(p,q) - E\right)\delta\left(P - p\right) \prod_{i=1}^{N} \mathrm{d}p^i \wedge \mathrm{d}q^i \tag{3.14}$$

so the specific entropy is

$$S_N(\varepsilon, p) = \frac{1}{N}\ln\left(\frac{\Omega(N\varepsilon, p)}{\Omega_0}\right), \tag{3.15}$$

where $\Omega_0$ is an arbitrary constant.

## 3.2 High order derivatives of Boltzmann microcanonical entropy with conserved null total momentum

The starting point to describe microcanonical observables is the definition of the specific entropy

$$S_N(\varepsilon, 0) = \frac{1}{N} \ln \Omega_N(N\varepsilon, 0),$$

in terms of the area of the total energy level sets $\Omega(N\varepsilon, 0)$ as seen in the last section.

To simplify the notation we omit the total momentum fixed to zero in both the argument of microcanonical entropy $S_N(\varepsilon, 0) \to S_N(\varepsilon)$ and of the microcanonical partition function $\Omega_N(E, 0) \to \Omega_N(E)$. All the relevant thermodynamic observables, such as the temperature or the specific heat, can be expressed as a function of the derivatives of the specific entropy $S_N$ with respect to specific energy[5] $\varepsilon$. The derivatives of the specific entropy with respect to the specific energy up to fourth order read

$$\begin{aligned}
\frac{\partial S_N}{\partial \varepsilon} &= \frac{\Omega_N^{'}}{\Omega_N} \,, \\
\frac{\partial^2 S_N}{\partial \varepsilon^2} &= N \left[ \frac{\Omega_N^{''}}{\Omega_N} - \left( \frac{\Omega_N^{'}}{\Omega_N} \right)^2 \right] , \\
\frac{\partial^3 S_N}{\partial \varepsilon^3} &= N^2 \left[ \frac{\Omega_N^{'''}}{\Omega_N} - 3 \frac{\Omega_N^{''}}{\Omega_N} \frac{\Omega_N^{'}}{\Omega_N} + 2 \left( \frac{\Omega_N^{'}}{\Omega_N} \right)^3 \right] \,, \\
\frac{\partial^4 S_N}{\partial \varepsilon^4} &= N^3 \left[ \frac{\Omega_N^{''''}}{\Omega_N} - 4 \frac{\Omega_N^{'''}}{\Omega_N} \frac{\Omega_N^{'}}{\Omega_N} - 3 \left( \frac{\Omega_N^{''}}{\Omega_N} \right)^2 + 12 \frac{\Omega_N^{''}}{\Omega_N} \left( \frac{\Omega_N^{'}}{\Omega_N} \right)^2 - 6 \left( \frac{\Omega_N^{'}}{\Omega_N} \right)^4 \right] \,,
\end{aligned} \tag{3.16}$$

where the prime corresponds to the derivative with respect to the total energy $E = N\varepsilon$. In order to characterize the microcanonical thermodynamics of a given system, a method is needed allowing to calculate of the higher order derivatives of microcanonical entropy (3.16).

In [120] a method is presented by Pearson and Halicioglu, that allows deriving the expression of thermodynamic observables in terms of the average of (specific) kinetic energy and its powers on the $\Sigma_E$ when the *only constraint is the fixed total energy of the system* $H_N = E$ and for systems whose Hamiltonian is of the form

$$\begin{aligned}
H_N(p^1, ..p^N, q^1, ..., q^N) &= K_N(p^1, ..p^N) + V_N(q^1, ..., q^N) \\
&= \sum_{i=1}^{N} \frac{(p^i)^2}{2} + V_N(q^1, ..., q^N) \,,
\end{aligned} \tag{3.17}$$

where $V_N$ is a potential energy invariant for global translation $V_N(q_1 + a, ..., q_N + a) = V_N(q_1, ..., q_N)$, and $K_N$ is the total kinetic energy. Such a method is based

[5] In the microcanonical ensemble, all the thermodynamic observables can be obtained deriving the microcanonical entropy with respect to other state variables, e.g. the pressure $p = T(\partial_v S_N)_\varepsilon$ depends on the derivative of entropy with respect to the volume $v$. In what follows, we do not consider the dependence of the microcanonical entropy on other state variables but the specific energy $\varepsilon = E/N$.

on a Laplace transform technique applied to the microcanonical partition function $\Omega_N(E)$ and it allows performing integration on the $p^i$ variables.
In this thesis, we show how to further develop and adopt such a technique to the case where the total momentum of the system $P_N$ is conserved ad set equal to zero. Let us consider the Laplace transform of the microcanonical partition function $\Omega_N(E)$ (where has been assumed that $P = 0$)

$$\begin{aligned}\mathcal{L}[\Omega_N](t) &= \int_0^{+\infty} e^{-tE}\,\Omega_N(E)\,dE, \\ &= \int \prod_{i=1}^{N} dp^i\,\delta(P) \int \prod_{i=1}^{N} dq^i\, e^{-tH_N(\{p^1,\ldots,p^N,q^1,\ldots,q^N\})} \\ &= \int \prod_{i=1}^{N} dp^i\, e^{-t\sum_{i=1}^{N}\frac{(p^i)^2}{2}}\,\delta(P) \int \prod_{i=1}^{N} dq^i e^{-tV_N(q^1,\ldots,q^N)}\,.\end{aligned} \tag{3.18}$$

In [120] the integration over the $N$ momenta $p^i$ is performed resulting in a Gaussian integral; in the case here considered, however, we have to take into account the constraint on $P_N$. In order to do this we consider the following equality for the Dirac delta function

$$\delta(P) = \frac{1}{2\pi}\int_{-\infty}^{+\infty} ds\, e^{isP}\,, \tag{3.19}$$

so that

$$\begin{aligned}\mathcal{L}[\Omega_N](t) &= \frac{1}{2\pi}\int \prod_{i=1}^{N} dp_i\, e^{-t\sum_{i=1}^{N}\frac{(p^i)^2}{2}} \int_{-\infty}^{+\infty} ds\, e^{isP_N} \int \prod_{i=1}^{N} dq_i e^{-tV_N(q^1\cdots q^N)} \\ &= \frac{1}{2\pi}\int \prod_{i=1}^{N} dp^i \int_{-\infty}^{+\infty} e^{-\frac{t}{2}\sum_k (p^k)^2}\, e^{is\sum_k p_k} \int \prod_{i=1}^{N} dq_i e^{-tV_N(q^1\cdots q^N)} \\ &= \frac{1}{2\pi}\int \prod_{i=1}^{N} dp_i \int_{-\infty}^{+\infty} ds e^{-\frac{t}{2}\sum_k (p_k - is/t)^2} e^{-\frac{Ns^2}{2t}} \int \prod_{i=1}^{N} dq_i e^{-tV_N(q^1\cdots q^N)} \\ &= \frac{1}{(2\pi)^{\left(1-\frac{N}{2}\right)}} \int_{-\infty}^{+\infty} ds\, e^{-\frac{Ns^2}{2t}}\, t^{-N/2} \int \prod_{i=1}^{N} dq_i e^{-tV_N(q^1\cdots q^N)} \\ &= \underbrace{\frac{1}{\sqrt{N}}\,\frac{1}{(2\pi)^{\frac{1}{2}(1-N)}}}_{1/C} \int \prod_{i=1}^{N} dq^i\, t^{-(N-1)/2}\, e^{-tV_N(q^1\cdots q^N)}\,.\end{aligned} \tag{3.20}$$

We now use the Bromwich integral to inverse the Laplace transform

$$\Omega_N(E) = \frac{1}{2\pi i\, C}\int_{\gamma-i\infty}^{\gamma+i\infty} \int \prod_{i=1}^{N} dq^i\, t^{-(N-1)/2}\, e^{t\left[E - V_N\left(q^1\ldots q^N\right)\right]} dt\,,$$

where $\gamma$ is a vertical contour in the complex plane chosen so that all singularities of $t^{-(N-1)/2}$ are on the left of it. After using the residues theorem, one obtains

the final expression for $\Omega_N(E)$ in the form of an integral over the manifold $M_E = \left\{(q^1, ..., q^N) \in \Lambda_q \,|\, V_N(q^1, \ldots, q^N) \leq E\right\}$

$$\Omega_N(E) = \frac{1}{A} \int \prod_{i=1}^{N} dq^i \, \left[E - V_N(q^1 \ldots q^N)\right]^{\frac{N}{2}-\frac{3}{2}} \Theta\left[E - V_N(q^1, \ldots, q^N)\right] \, , \tag{3.21}$$

where

$$A = C\,\Gamma\left(\frac{N}{2} - \frac{1}{2}\right) \, .$$

The first four derivatives of the $\Omega_N(E)$ with respect to the total energy, are then

$$\begin{aligned}
\Omega'_N(E) &= \left(\frac{N}{2} - \frac{3}{2}\right) \frac{1}{A} \int \prod_{i=1}^{N} dq^i \, (E - V_N)^{\frac{N}{2}-\frac{5}{2}} \, \Theta\left(E - V_N\right) \, , \\
\Omega''_N(E) &= \left(\frac{N}{2} - \frac{3}{2}\right)\left(\frac{N}{2} - \frac{5}{2}\right) \frac{1}{A} \int \prod_{i=1}^{N} dq^i \, (E - V_N)^{\frac{N}{2}-\frac{7}{2}} \, \Theta\left(E - V_N\right) \, , \\
\Omega'''_N(E) &= \left(\frac{N}{2} - \frac{3}{2}\right)\left(\frac{N}{2} - \frac{5}{2}\right)\left(\frac{N}{2} - \frac{7}{2}\right) \times \\
&\qquad \times \frac{1}{A} \int \prod_{i=1}^{N} dq_i \big(E - V\big)^{\frac{N}{2}-\frac{9}{2}} \Theta\left(E - V_N\right) \, , \\
\Omega''''_N(E) &= \left(\frac{N}{2} - \frac{3}{2}\right)\left(\frac{N}{2} - \frac{5}{2}\right)\left(\frac{N}{2} - \frac{7}{2}\right)\left(\frac{N}{2} - \frac{9}{2}\right) \times \\
&\qquad \times \frac{1}{A} \int \prod_{i=1}^{N} dq^i \, (E - V_N)^{\frac{N}{2}-\frac{11}{2}} \, \Theta\left(E - V_N\right) \, .
\end{aligned} \tag{3.22}$$

where the dependence of the potential on generalized coordinates $q^i$ has been omitted to simplify the notation. We notice that each derivative of the microcanonical partition function appears divided by $\Omega_N$. Remembering that the microcanonical average $A(q^1 \ldots q^N)$ of any function of generalized coordinates has the form

$$\begin{aligned}
\langle A \rangle_{\mu c} = & \frac{1}{\Omega\, A} \int \prod_{i=1}^{N} dq^i A(q^1 \ldots q^N) \big(E - V_N(q^1 \ldots q^N)\big)^{\frac{N}{2}-\frac{3}{2}} \times \\
& \times \Theta\left(E - V_N(q^1 \ldots q^N)\right) \, ,
\end{aligned} \tag{3.23}$$

and that $\left\langle \big(E - V_N(q^1 \ldots q^N\big)^a \right\rangle_{\mu c} = \langle K_N^\alpha \rangle_{\mu c} = N^\alpha \langle \kappa_N^\alpha \rangle_{\mu c}$ where $\kappa_N$ is the specific kinetic energy, we obtain for the first four order derivatives of the

microcanonical partition function

$$\begin{aligned}
\frac{\Omega'_N}{\Omega_N} &= \left(\frac{N}{2}-\frac{3}{2}\right)\left\langle K_N^{-1}\right\rangle_{\mu c} = \left(\frac{1}{2}-\frac{3}{2N}\right)\left\langle \kappa_N^{-1}\right\rangle_{\mu c} \\
\frac{\Omega''_N}{\Omega_N} &= \left(\frac{N}{2}-\frac{3}{2}\right)\left(\frac{N}{2}-\frac{5}{2}\right)\left\langle K_N^{-2}\right\rangle_{\mu c} = \left(\frac{1}{2}-\frac{3}{2N}\right)\left(\frac{1}{2}-\frac{5}{2N}\right)\left\langle \kappa_N^{-2}\right\rangle_{\mu c} \\
\frac{\Omega'''_N}{\Omega_N} &= \left(\frac{N}{2}-\frac{3}{2}\right)\left(\frac{N}{2}-\frac{5}{2}\right)\left(\frac{N}{2}-\frac{7}{2}\right)\left\langle K_N^{-3}\right\rangle_{\mu c} \\
&= \left(\frac{1}{2}-\frac{3}{2N}\right)\left(\frac{1}{2}-\frac{5}{2N}\right)\left(\frac{1}{2}-\frac{7}{2N}\right)\left\langle \kappa_N^{-3}\right\rangle_{\mu c}, \\
\frac{\Omega''''_N}{\Omega_N} &= (\frac{N}{2}-\frac{3}{2})(\frac{N}{2}-\frac{5}{2})(\frac{N}{2}-\frac{7}{2})(\frac{N}{2}-\frac{9}{2})\left\langle K_N^{-4}\right\rangle_{\mu c} \\
&= (\frac{1}{2}-\frac{3}{2N})(\frac{1}{2}-\frac{5}{2N})(\frac{1}{2}-\frac{7}{2N})(\frac{1}{2}-\frac{9}{2N})\left\langle \kappa_N^{-4}\right\rangle_{\mu c}.
\end{aligned} \tag{3.24}$$

In general, it can be derived that the following expression holds in the case where both *the total energy and the total momentum* are conserved

$$\frac{\Omega_N^{(l)}}{\Omega_N} = \prod_{m=1}^{l}\left(\frac{1}{2}-\frac{2m+1}{2N}\right)\left\langle \kappa^{-l}\right\rangle_{\mu c}, \tag{3.25}$$

where $(l)$ denotes the $l$-th order derivative with respect to $E$, while in [120], where *only the constraint on the total energy is considered*, the previous expression reads

$$\frac{\Omega_N^{(l)}}{\Omega_N} = \prod_{m=1}^{l}\left(\frac{1}{2}-\frac{(2m-1)}{N}\right)\left\langle \kappa^{-l}\right\rangle_{\mu c}. \tag{3.26}$$

As we will observe in what follows, the first expression we derived is more consistent with the geometrical derivation of the expression for the derivatives of $\Omega_N(E)$.

Substituting (3.25) in (3.16), we obtain the derivatives of the microcanonical specific entropy as functions of the microcanonical averages of (powers of) the

specific kinetic energy $\kappa_N$,

$$\begin{aligned}
\frac{\partial S_N}{\partial \varepsilon} =& \left(\frac{1}{2}-\frac{3}{2N}\right)\left\langle \kappa_N^{-1}\right\rangle_{\mu c} \\
\frac{\partial^2 S_N}{\partial \varepsilon^2} =& N\left[\left(\frac{1}{2}-\frac{3}{2N}\right)\left(\frac{1}{2}-\frac{5}{2N}\right)\left\langle \kappa_N^{-2}\right\rangle_{\mu c}-\left(\frac{1}{2}-\frac{3}{2N}\right)^2\left\langle \kappa_N^{-1}\right\rangle_{\mu c}^2\right] \\
\frac{\partial^3 S_N}{\partial \varepsilon^3} =& N^2\Bigg[\left(\frac{1}{2}-\frac{3}{2N}\right)\left(\frac{1}{2}-\frac{5}{2N}\right)\left(\frac{1}{2}-\frac{7}{2N}\right)\left\langle \kappa_N^{-3}\right\rangle_{\mu c}+ \\
& -3\left(\frac{1}{2}-\frac{3}{2N}\right)^2\left(\frac{1}{2}-\frac{5}{2N}\right)\left\langle \kappa_N^{-1}\right\rangle_{\mu c}\left\langle \kappa_N^{-2}\right\rangle_{\mu c}+ \\
& +2\left(\frac{1}{2}-\frac{3}{2N}\right)^3\left\langle \kappa_N^{-1}\right\rangle_{\mu c}^3\Bigg] \\
\frac{\partial^4 S_N}{\partial \varepsilon^4} =& N^3\Bigg[\left(\frac{1}{2}-\frac{3}{2N}\right)\left(\frac{1}{2}-\frac{5}{2N}\right)\left(\frac{1}{2}-\frac{7}{2N}\right)\left(\frac{1}{2}-\frac{9}{2N}\right)\left\langle \kappa_N^{-4}\right\rangle_{\mu c}+ \\
& -4\left(\frac{1}{2}-\frac{3}{2N}\right)^2\left(\frac{1}{2}-\frac{5}{2N}\right)\left(\frac{1}{2}-\frac{7}{2N}\right)\left\langle \kappa_N^{-1}\right\rangle_{\mu c}\left\langle \kappa_N^{-3}\right\rangle_{\mu c}+ \\
& -3\left(\frac{1}{2}-\frac{3}{2N}\right)^2\left(\frac{1}{2}-\frac{5}{2N}\right)^2\left\langle \kappa_N^{-2}\right\rangle_{\mu_c}^2+ \\
& +12\left(\frac{1}{2}-\frac{3}{2N}\right)^3\left(\frac{1}{2}-\frac{5}{2N}\right)\left\langle \kappa_N^{-2}\right\rangle_{\mu c}\left\langle \kappa_N^{-1}\right\rangle_{\mu c}^2+ \\
& -6\left(\frac{1}{2}-\frac{3}{2N}\right)^4\left\langle \kappa_N^{-1}\right\rangle_{\mu c}^4\Bigg].
\end{aligned} \tag{3.27}$$

The microcanonical temperature (2.13) takes the form

$$T=\left[\left(\frac{1}{2}-\frac{3}{2N}\right)\left\langle \kappa^{-1}\right\rangle_{\mu c}\right]^{-1}. \tag{3.28}$$

while the specific heat defined in (2.14) reads

$$c_v=\frac{1}{N}\left[1-\frac{\left(1-\frac{5}{N}\right)\left\langle \kappa_N^{-2}\right\rangle_{\mu c}}{\left(1-\frac{3}{N}\right)\left\langle \kappa_N^{-1}\right\rangle_{\mu c}^2}\right]^{-1}. \tag{3.29}$$

## 3.3 Simulation of the Hamiltonian dynamics

### Presentation of the bilateral symplectic algorithm

Generally, the integration algorithms used for a long time to resolve numerically differential equations create problems on coordinates transformations due to the fact that the Jacobian of these transformations can be different from 1. They are called a non-symplectic coordinate transformation. The time evolution of Hamilton's equations is a symplectomorphism, meaning that it conserves the

symplectic two-form $\mathrm{d}q \wedge \mathrm{d}p$, where $q$ denotes the position coordinates and $p$ the momentum coordinates. Let us consider Hamiltonians of the form

$$H(\mathbf{q},\mathbf{p}) = \sum_{i=1}^{N} \frac{p_i^2}{2} + V(\mathbf{q}) \; . \tag{3.30}$$

In the first order, the evolution equations are

$$\begin{aligned} q(t+\Delta t) &= q(t) + \Delta t p(t) \\ p(t+\Delta t) &= p(t) + \Delta t \, \bar{\nabla} V \left[q(t+\Delta t)\right] \; , \end{aligned} \tag{3.31}$$

where $\bar{\nabla} V = \left( \dfrac{\partial}{\partial q_1} \cdots \dfrac{\partial}{\partial q_N} \right)$ and choosing

$$F(\mathbf{Q},\mathbf{p},\Delta t) = -\mathbf{Q}\cdot\mathbf{P} + \Delta t H(\mathbf{Q},\mathbf{p}) \tag{3.32}$$

as a generating function, one obtains these symplectic (canonical) transformations

$$\begin{aligned} q_i &= -\frac{\partial F}{\partial p_i} = Q_i - \Delta t \frac{\partial H}{\partial p_i} \\ P_i &= -\frac{\partial F}{\partial Q_i} = p_i - \Delta t \frac{\partial H}{\partial Q_i} \; , \end{aligned} \tag{3.33}$$

which coincide with the evolution equations (3.31).
At $\Delta t \to 0$ and $\mathbf{Q} \to \mathbf{q}$, keeping $\mathbf{p}$ fixed, the generating function becomes exactly the generating function of the natural motion of the system. However, at finite $\Delta t$, it would be better to have the symmetric limit e.g. $\Delta t \to 0$ and $\mathbf{P} \to \mathbf{p}$, keeping $\mathbf{q}$ fixed, which can be generated considering this generating function

$$f(\mathbf{Q},\mathbf{p},\Delta t) = \mathbf{q}\cdot\mathbf{P} + \Delta t H(\mathbf{Q},\mathbf{p}) \; . \tag{3.34}$$

In the bilateral symplectic algorithm, developed in [35], these two limits are done together by performing one after the other the two symplectic transformations (3.32) and (3.34). It has then (at the first order) two steps instead of one

$$\begin{aligned} q(t+\Delta t) &= q(t) + \Delta t p(t) \\ p(t+\Delta t) &= p(t) - \Delta t \, \bar{\Delta} V \left[q(t+\Delta t)\right] \\ p(t+2\Delta t) &= p(t+\Delta t) - \Delta t \, \bar{\Delta} V \left[q(t+\Delta t)\right] \\ q(t+2\Delta t) &= q(t+\Delta t) + \Delta t p(t+\Delta t) \; . \end{aligned} \tag{3.35}$$

The first two equations are (3.31) and the others are obtained from

$$\begin{aligned} p_i &= -\frac{\partial f}{\partial q_i} = P_i - \Delta t \frac{\partial H}{\partial q_i} \\ Q_i &= -\frac{\partial f}{\partial P_i} = q_i - \Delta t \frac{\partial H}{\partial P_i} \; , \end{aligned} \tag{3.36}$$

which are generated by (3.34).
In order to work with a more precise integration scheme we used a second-order

bilateral symplectic algorithm, i.e.

$$\begin{aligned} q^{(1)} &= q(t) \\ p^{(1)} &= p(t) - \frac{1}{2}\Delta t\, \bar{\Delta} V\left[q^{(1)}\right] \\ q^{(2)} &= q^{(1)} + \Delta t p^{(1)} \\ p^{(2)} &= p^{(2)} - \frac{1}{2}\Delta t\, \bar{\Delta} V\left[q^{(2)}\right] \\ p^{(3)} &= p^{(2)} \\ q^{(3)} &= q^{(2)} + \frac{1}{2}\Delta t p^{(3)} \\ p^{(4)} &= p^{(3)} - \Delta t\, \bar{\Delta} V\left[q^{(3)}\right] \\ p^{(4)} &= q^{(4)} + \Delta t p^{(3)}\ . \end{aligned} \tag{3.37}$$

### Initialization of the system

The initialization of the system had to be done considering the Hamiltonian dynamics with $H = E$ and the fact that the total momentum has to be equal to zero $P = 0$.

To do so, we considered first the initial value of spin $\theta_{ij}$ as a random variable uniformly distributed in the interval $[0, 2\pi\alpha]$ where $0 < \alpha < 1$. We computed then the potential energy $V(\theta)$ with these initial conditions. If this value was larger than the value of the total energy E, then the variable $\theta_{ij}$ is initialized considering a new variable $\alpha_{\text{new}}$, where $\alpha_{\text{new}} = \alpha/2$. If the new configuration was again not compatible with $E - V = K > 0$, where $K$ is the kinetic energy, we choose the smallest variable $\alpha$ until we found the consistent configuration. Then we initialized the moment. To do so, we divided the set of the spins into two equal subsets $\Lambda_1$ and $\Lambda_2$; then we considered momenta only on one of these two sets, so we had that $\sum_{ij\in\Lambda_1} P_{ij}^2 = K$. To realize this condition we choose a unit vector $v$ on the $\mathcal{S}^{(N/2-1)}$ sphere, and we considered $p_{ij} = \sqrt{2K}\, v_{ij}$ ( where $v_{ij}$ are the components of the unit vector $v$ ). To impose finally the condition on total momentum $P = 0$, we choose $p_{i,j+N/2} = -p_{i,j}$, where $i \in [1, N]$ and $j \in [1, N/2]$. In order to guarantee that the dynamical system uniformly explores the energy level sets at $P = 0$, the averages have been calculated as averages of different trajectories.

## 3.4 Numerical results

We performed Hamiltonian dynamic simulations of the system described by (3.2), with $J = 1$. The numerical integration has been performed setting the total number of time steps $\Delta t = 10^{-3}$ for 250 trajectories and $10^5$ steps to let the system thermalize, and total number of steps for each trajectory is equal to $2 \times 10^6$.
The microcanonical averages are calculated considering the arithmetic average of the time averages along all the trajectories, i.e. if $A_j(i)$ is the value of the

observable $A$ at $i$-th step along the $j$-th trajectory

$$\langle A \rangle_{\mu c} = \frac{1}{N_{trj}} \sum_{j=1}^{N_{trj}} \left( \frac{\sum_{i=1}^{N_{step}} A_j(i)}{N_{steps}} \right) \tag{3.38}$$

In Figure 3.1, the results for the specific heat and the temperature as a function of specific energy have been reported. According to [37] the transition point in the XY 2D model is signaled by a peak in the specific heat. Such a peak becomes narrower and its height converges to a finite value for increasing $N$. The results of our simulations are in agreement with such a qualitative behavior: at $\varepsilon_c$ the specific heat shows a peak that becomes sharper and higher for an increasing number of $N$ and seems to converge to maximal height. In our case, the smallest interval in specific energy we choose for our simulations allowed us to observe a slight drift of the peak for an increasing $N$. This is probably due to the finite size effect already present in the system we considered.
The results of our simulation evidence an inflection point in the temperature curve, in correspondence with the transition-specific energy $\varepsilon_c(N)$. In Figure

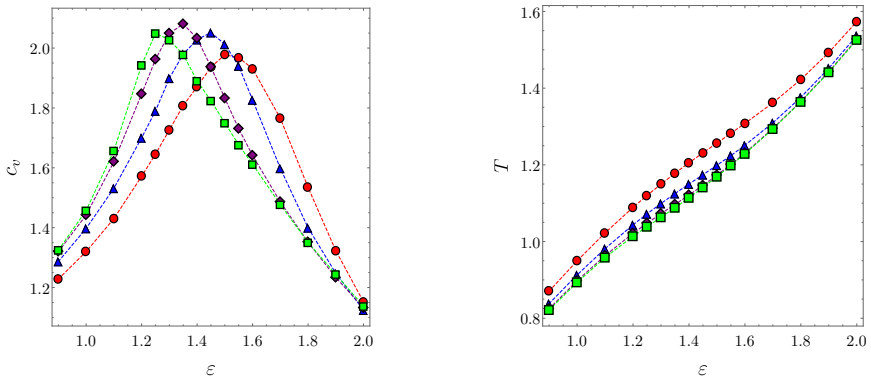


(a) (b)

Figure 3.1: **(a)** Specific heat vs. specific energy and **(b)** Temperature vs. specific energy for $N = 6 \times 6$ (red circles), $N = 10 \times 10$ (blue triangles), $N = 20 \times 20$ (purple diamonds), $N = 40 \times 40$ (green squares).

3.2 both the first and the second-order derivative of the specific entropy have been reported. We observe that also the first-order derivative of the specific entropy shows an inflection point in correspondence of $\varepsilon_c$ for all the studied cases. This is expected as the $\partial_\varepsilon S$ is the inverse of microcanonical temperature. The second derivative of $S_N$ shows a negative maximum at the transition point $\varepsilon_c(N)$, seeming to become an angular point at larger $N$ with

$$\lim_{N\to+\infty} \lim_{\varepsilon\to\varepsilon_c^+} \partial_\varepsilon^3 S_N = 0 \qquad \lim_{N\to+\infty} \lim_{\varepsilon\to\varepsilon_c^-} \partial_\varepsilon^3 S_N > 0 \,.$$

Within the limit of numerical simulation, the observed behavior suggests the emergence of a discontinuity for large $N$ at the transition point in the third-order derivative. The presence of a maximum of the second order derivative for $N \lesssim 20 \times 20$ is consistent with the presence of an inflection point on the first

derivative of $S(E)$. The results on the second order derivative of $S_N$ reinforce the claim that the peak in specific heat can not diverge for large $N$. In fact, the first derivative of entropy (the inverse of the temperature) is expected to converge to a finite strictly positive value for large $N$, so the only possibility for the specific heat to diverge comes from $\partial^2_\varepsilon S_N(\varepsilon_c)$ converging to zero for large $N$ (see equation 2.14). In our case, we observe that $|\partial^2_\varepsilon S_N(\varepsilon_c(N))| > |\partial^2_\varepsilon S_{N'}(\varepsilon_c(N'))|$ when $N > N'$, so the divergence of the specific heat is not expected. Despite the

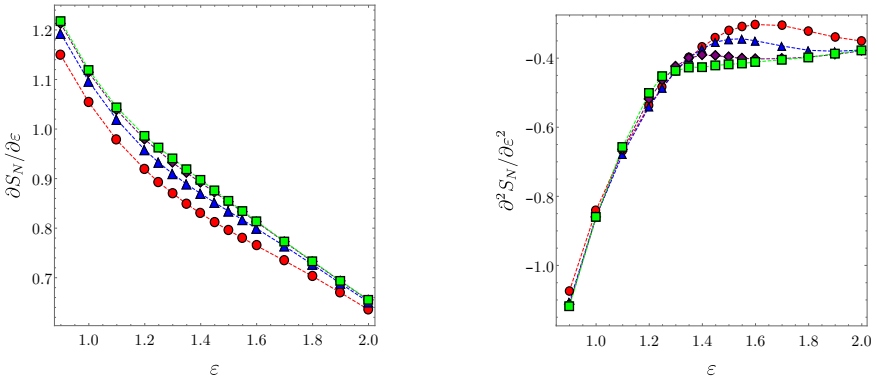


(a) (b)

Figure 3.2: **(a)** First derivative of specific entropy vs. specific energy and **(b)** second derivative of sepcific entropy vs. specific energy for $N = 6 \times 6$ (red circles), $N = 10 \times 10$ (blue triangles), $N = 20 \times 20$ (purple diamonds), $N = 40 \times 40$ (green squares).

relevance of entropy from the thermodynamic point of view, we would be more interested in studying the the behavior of the microcanonical partition function $\Omega_N(N\varepsilon)$ and its derivative with respect to $\varepsilon$, as it has a close relationship with geometry of energy level sets (see Chapter 4). However, the microcanonical partition function $\Omega_N$ is not easy to compare for different values of $N$ due to the fact that it is expected to have an exponential dependence on $N$. The expression of specific entropy (3.15) suggests the introduction of a specific volume $\rho_N(\varepsilon)$ defined as

$$\rho_N(\varepsilon) \equiv \left[\frac{\Omega_N(N\varepsilon)}{\Omega(N\varepsilon_{\min})}\right]^{1/N} , \tag{3.39}$$

where $\Omega(N\varepsilon_{\min})$ is the microcanonical volume at the lowest value of the specific energy $\varepsilon$ so that $\rho(\varepsilon_{\min}) = 1$. Introducing the specific volume $\rho_N$ the microcanonical specific entropy reads

$$S_N(\varepsilon) = \log \rho_N(\varepsilon) , \tag{3.40}$$

from what follows we have

$$\frac{\partial S_N}{\partial \varepsilon} = \frac{\dfrac{\partial \rho_N}{\partial \varepsilon}}{\rho_N} . \tag{3.41}$$

The last expression allows to derive $\rho_N$ by the numerical integration of the function $\partial_\epsilon S_N$, i.e.

$$\rho_N(\epsilon) = \rho_N(\epsilon_{\min}) \exp\left[\int_{\epsilon_{min}}^{\epsilon} \frac{\partial S_N}{\partial \varepsilon}(\epsilon)\right] \, \mathrm{d}\varepsilon \,; . \tag{3.42}$$

The derivatives of $\rho_N$ with respect to specific energy $\varepsilon$ can be obtained deriving equation (3.40), yielding to

$$\begin{aligned}
\frac{\partial \rho_N(\varepsilon)}{\partial \varepsilon} &= \rho_N(\varepsilon)\frac{\partial S_N}{\partial \varepsilon} \\
\frac{\partial^2 \rho_N(\varepsilon)}{\partial \varepsilon^2} &= \rho_N(\varepsilon)\left[\frac{\partial^2 S_N}{\partial \varepsilon^2} + \left(\frac{\partial S_N}{\partial \varepsilon}\right)^2\right] \\
\frac{\partial^3 \rho_N(\varepsilon)}{\partial \varepsilon^3} &= \rho_N(\varepsilon)\left[\frac{\partial^3 S_N}{\partial \varepsilon^3} + 3\frac{\partial S_N}{\partial \varepsilon}\frac{\partial^2 S_N}{\partial \varepsilon^2} + \left(\frac{\partial S_N}{\partial \varepsilon}\right)^3\right] \\
\frac{\partial^4 \rho_N(\varepsilon)}{\partial \varepsilon^4} &= \rho_N(\varepsilon)\left[\frac{\partial^4 S_N}{\partial \varepsilon^4} + 4\frac{\partial^3 S_N}{\partial \varepsilon^3}\frac{\partial S_N}{\partial \varepsilon} + 3\left(\frac{\partial^2 S_N}{\partial \varepsilon^2}\right)^2 + 6\left(\frac{\partial S_N}{\partial \varepsilon}\right)^2\frac{\partial^2 S_N}{\partial \varepsilon^2} + \left(\frac{\partial S_N}{\partial \varepsilon}\right)^4\right] .
\end{aligned} \tag{3.43}$$

In Figure 3.3, the first order derivative of $\partial_\varepsilon \rho(\varepsilon)$ shows a very marked inflection point at the transition energy $\varepsilon_c$. The second order derivative in $\rho_N$ shows a behavior analogous to the specific heat: a peak that becomes sharper at the transition point in the thermodynamic limit. In Figure 3.4 the third-order

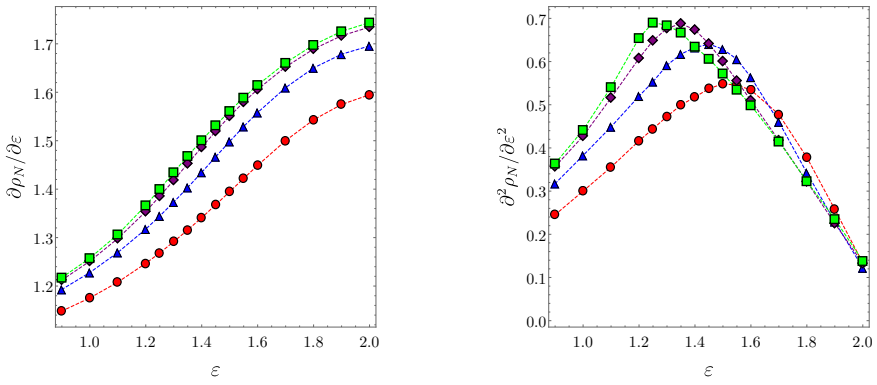


(a) (b)

Figure 3.3: **(a)** : First derivative of the specific volume vs. specific energy for $N = 6 \times 6$ (red circles), $N = 10 \times 10$ (blue triangles), $N = 20 \times 20$ (purple diamonds), $N = 40 \times 40$ (green squares). **(b)**: second derivative of the specific volume vs. specific energy

derivatives of the microcanonical entropy and specific volume have been reported. We notice that the third derivative of the entropy tends to develop a jump for an increasing $N$ in the interval $[1.25, 1.4]$ around the transition point. Within the limit of numerical simulations, this suggests a loss of analyticity in the thermodynamic limit: in fact, this would correspond to a divergence of the 4th order derivative of the entropy at the transition point. One can also note the fact that $\partial_\varepsilon^3 S_N$ is zero at the transition point: this is consistent with the presence of a maximum at the critical point on $\partial_\varepsilon^2 S_N$.
The third order derivative of $\rho_N$ has a stronger signature of the same kind: the slope of the tangent line at the inflection point becomes steeper with an increasing $N$. Also in that case the inflection point has zero value which is

consistent with the presence of a maximum on the second derivative of $\rho_N(\varepsilon)$ and a divergence in $\partial^4_\varepsilon \rho_N$ in the thermodynamic limit. In Figure 3.5, we observe

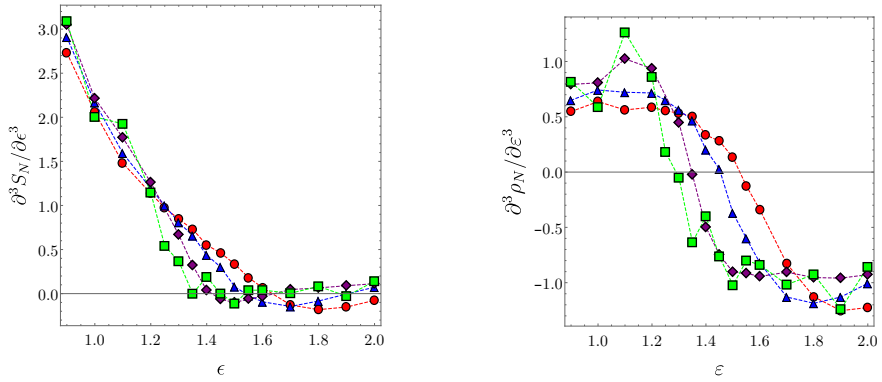


(a) (b)

Figure 3.4: Third order derivative of the specific entropy $S_N$ vs. specific energy **(a)** and third derivative of the specific volume $\rho_N$ vs. specific energy **(b)** for $N = 6 \times 6$ (red circles), $N = 10 \times 10$ (blue triangles), $N = 20 \times 20$ (purple diamonds), $N = 40 \times 40$ (green squares).

that the signal of both the 4th order derivative of $S_N$ and $\rho_N$ is quite noisy, this is probably due to the lack of precision in the numerical estimations of the observables. A longer sampling would probably be required to increase the precision of the simulation. Nevertheless, we observe in both cases a weak signature of a divergence appearing at the transition point for an increasing $N$.

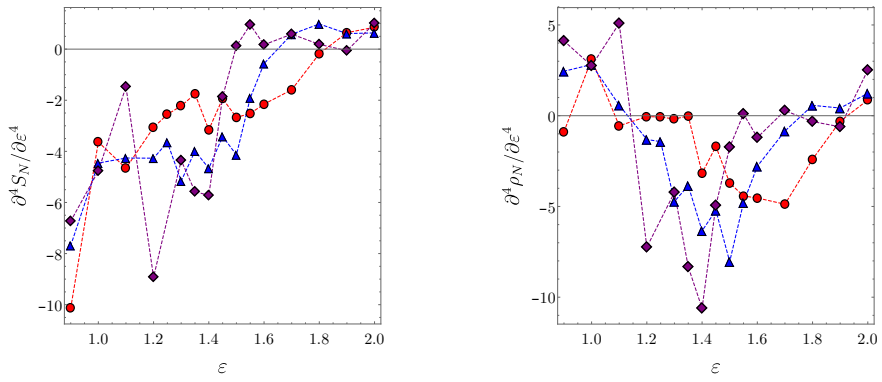


(a) (b)

Figure 3.5: **(a)** : Fourth derivative of the specific entropy vs. specific energy for $N = 6 \times 6$ (red circles), $N = 10 \times 10$ (blue triangles), $N = 20 \times 20$ (purple diamonds). **(b)**: fourth derivative of the specific volume vs. specific energy

## 3.5 Chapter Conclusions

We have seen an inflection point on the first derivative of the entropy at the transition point which corresponds to a negative maximum in the second derivative of the specific entropy for small $N$. According to Bachman classification (Table **??**) the XY 2D model undergoes a second-order phase transition in the microcanonical ensemble. Moreover, within the limit of numerical simulation, we have observed a signal that suggests an asymptotic loss of analyticity of $\partial_\varepsilon^3 S$ at the transition point in the thermodynamic limit. This signature is even more clear in the specific volume $\rho_N$ where both a negative maximum in the second-order derivative and a loss of analyticity of the third-order derivative have been observed at the transition point.

# 4

# Differential geometry and topology of submanifolds

This Chapter is a review of extrinsic differential geometry. A very good introductory course can be found in [96]. We have seen in Chapter 2, the role that the geometry and the topology of phase space have to understand the deep origin of phase transitions. In this Chapter, we present an overview of the geometry and topology of submanifolds $\Sigma_{f_1,...,f_m}$. The differential geometry of such level sets is discussed in Section 4.1, while the topology is discussed through the Pinkall theorem in Section 4.2, which connects the geometry of $\Sigma_{f_1,...,f_m}$ and its topology.

## 4.1 Review of differential extrinsic geometry of codimension $m$ submanifolds

The phase space can be regarded as a $2N$ dimensional manifold where a set of coordinate $\{x^\mu\}_{\mu=1,...,2N}$ can be chosen such that

$$\begin{cases} x^{2\nu-1} = p^{\tilde{\nu}} & \nu = 1, ..., N \\ x^{2\nu} = q^{\hat{\nu}} & \nu = 1, ..., N \end{cases} \tag{4.1}$$

**Definition 4.1.** *Given a set of smooth real functions $\{F^i\}_{i=1,...,m}$ on the phase space $\Lambda$, with $m < 2N$, we define the level sets $\Sigma_{f^1,...,f^m}$ as follows [96]*

$$\Sigma_{f^1,...,f^m} = \left\{ x \in \Lambda \mid F^k = f^k \ , \quad \forall\, k = 1, ..., m \right\} \ . \tag{4.2}$$

If the following condition

$$\mathrm{d}F^1 \wedge ... \wedge \mathrm{d}F^m \neq 0 \tag{4.3}$$

holds for every point on $\Sigma_{f^1,...,f^m}$ then this is a *regular submanifold of codimension $m$.*

In order to give a Riemannian geometrical characterization of such a submanifold, a metric structure (metric tensor) $g$ has to be assigned over the phase space lambda $\Lambda$. In general, this assignment can be quite arbitrary. Nevertheless, for

the sake of consistency with the symplectic structure, we should require that the Riemannian volume form

$$\omega = \sqrt{\det g}\ \ \mathrm{d}x^1 \wedge ... \wedge \mathrm{d}x^{2N} = \sqrt{\det g}\ \ \mathrm{d}p^1 \wedge \mathrm{d}q^1 ... \wedge \mathrm{d}p^N \wedge \mathrm{d}q^N \tag{4.4}$$

is the invariant volume form for the Hamiltonian system, i.e. $\mathcal{L}_{X_H}\omega = 0$. The simplest metric satisfying this condition is the Euclidean one $g = \delta_{\mu\nu}\ \mathrm{d}x^\mu \otimes \mathrm{d}x^\nu$, i.e. the phase space is endowed with the structure of a Euclidean space $\mathbb{E}^{2N}$. Thanks to the metric structure, it is possible to define the *gradient* $\nabla H$ of a function as a vector field such that

$$g(\nabla H, X) = \imath_X \, \mathrm{d}H \tag{4.5}$$

that in components reads

$$\imath_{\nabla H}\, \mathrm{d}x^\mu = (\nabla H)^\mu = g^{\mu\nu}\frac{\partial H}{\partial x^\nu} = \partial^\mu H \ , \tag{4.6}$$

A critical point of the function $H$ is a point where the gradient is null $\nabla H = 0$. Thanks to this definition, the condition (4.3) can be reformulated as the absence of critical points for any function $F^k$ and the linear independence of the $m$ gradient vector fields $\{\nabla F^k\}_{k=1,...,m}$ for any points of $\Sigma_{f^1,...,f^M}$.

**Theorem 4.1.** *The invariant measure of the set $\Sigma_{f^1,...,f^m}$, defined in Eq.4.2, is [123, 96]*

$$\Omega_N(f^1, ..., f^m) = \int_{\Sigma_{f^1,...,f^m}} \sigma_{f^1,...,f^m} \ , \tag{4.7}$$

*where*

$$\sigma_{f^1,...,f^m} = \frac{\sigma_{\Sigma_{f^1,...,f^m}}}{\sqrt{\mathbb{G}(\nabla F^1, .., \nabla F^m)}} \ , \tag{4.8}$$

*with $\mathbb{G}(\nabla F^1, .., \nabla F^m)$ being the Grammian.*

*Proof.* In each point of the regular submanifold of codimension $m$, the tangent bundle of the phase space splits into a tangent bundle to the submanifold $\mathrm{T}\Sigma_{f^1,...,f^m}$ and a normal bundle $\mathrm{N}\Sigma_{f^1,...,f^m}$

$$\mathrm{T}\Lambda|_{\Sigma_{f^1,...,f^m}} = \mathrm{T}\Sigma_{f^1,...,f^m} \oplus \mathrm{N}\Sigma_{f^1,...,f^m} \ , \tag{4.9}$$

where the normal bundle is defined by $\mathrm{N}\Sigma_{f^1,...,f^m} = \mathrm{Span}\{\nabla F^1, ..., \nabla F^m\}$. We define also an *induced* metric (or *first fundamental form*) on such regular submanifold of codimension $m$, which is the assignment to each point of the inner product

$$\langle\ ,\ \rangle : \mathrm{T}\Sigma_{f^1,...,f^m} \times \mathrm{T}\Sigma_{f^1,...,f^m} \longrightarrow \mathbb{R} \ .$$

From the preceding discussion, it follows that it is convenient to introduce an adapted orthonormal frame $\{e_a\}_{a=1,...,2N}$ that allows making explicit the split of the tangent bundle, i.e. $e_{\bar{A}} \in \mathrm{N}\Sigma_{f^1,...,f^m}$ with $\bar{A} = 1, ..., m$ and $e_A \in \mathrm{T}\Sigma_{f^1,...,f^m}$ with $A = m+1, ..., 2N$.

This is equivalent to defining for each point a set of rotation matrix $e_a^\nu$ that allows passing from the coordinate natural frame $\{\partial_1, ..., \partial_{2N}\} = \{\partial_\nu\}_{\nu=1,...,2N}$ to the adapted coordinate orthonormal frame $\{e_1, e_2, ..., e_{2N}\} = \{e_a\}_{a=1,2,...,2N}$, i.e. $e_a = e_a^\nu \partial_\nu$. In analogous way, the inverse matrix $e_\nu^b$ are defined allowing to pass from coordinates covectors $\{\mathrm{d}x^1, ... \mathrm{d}x^{2N}\}$ to adapted covector frame $\{\theta^1, \theta^2, ..., \theta^{2N}\}$ (with $\imath_{e_a}\theta^b = \delta_a^b$), i.e. $\theta^b = e_\mu^b \,\mathrm{d}x^\mu$.
In order to characterize the extrinsic geometry of the regular submanifold $\Sigma_{f^1,...,f^m}$, for any normal vector field $n \in \mathrm{N}\Sigma_{f^1,...,f^m}$, we introduce the *shape* operator $\mathcal{W}_n$ (called also the *Weingarten* operator) giving by the variation of $n$ along the directions tangent to the submanifold at any fixed point, i.e. $\mathcal{W}_n : T\Sigma_{f^1,...,f^m} \longrightarrow T\Sigma_{f^1,...,f^m}$ s.t.

$$\mathcal{W}_n(V) = -D_V n \qquad V \in \mathrm{T}\Lambda|_{\Sigma_{f^1,...,f^m}} \ , \tag{4.10}$$

where $D$ is the *Levi Civita* connection on $(\Lambda, g)$. Let us see first of all that the image of $\mathcal{W}$ is $\subseteq \mathrm{T}\Sigma_{f^1,...,f^m}$, in fact

$$g(\mathcal{W}_n(V), n) = -g(D_V n, n) = -\frac{1}{2} D_V \left[g(n, n)\right] = 0 \ . \tag{4.11}$$

so the Weingarten map can be rewritten in terms of the orthonormal vector basis

$$\mathcal{W}(e_B) = \mathcal{W}_B^A e_A = -D_{e_B} n \quad \Rightarrow \quad \mathcal{W}_B^A = -\theta^A(D_{e_B} n) \ . \tag{4.12}$$

with $A, B = m+1, ..., 2N$. Using the matrices $e_\mu^A$ and $e_B^\nu$ the shape operator can be expressed in terms of natural coordinates $x^\mu$ as

$$\begin{aligned} \left(\mathcal{W}_B^A\right)_n = -\theta^A(D_{e_B} n) &= -e_\mu^A e_B^\nu \ \mathrm{d}x^\mu(D_\nu n) \\ &= -e_\mu^A e_B^\nu \ \mathrm{d}x^\mu \left[\left(\partial_\nu n^\rho + \Gamma_{\nu\lambda}^\rho n^\lambda\right) \partial_\rho\right] \\ &= -e_\mu^A e_B^\nu \ D_\nu n^\mu \ . \end{aligned} \tag{4.13}$$

The eigenvalues $k_1, ..., k_{2N-m}$ of the matrix $\mathcal{W}_n$ are called *principal curvatures*. The average of the principal curvatures at a fixed point is called *mean curvature* $M_n$

$$\begin{aligned} M_n = \frac{1}{2N-m} \sum_{i=1}^{2N-m} k_i &= \frac{1}{2N-m} \mathrm{Tr}\mathcal{W}_n \\ &= -\frac{1}{2N-m} \sum_{A=1}^{2N-m} g(D_{e_A} n, e_A) \ . \end{aligned} \tag{4.14}$$

Let us introduce the Coarea formula (a generalization of the Fubini theorem) which allows expressing the integral of a function over the phase space $\Lambda$ in terms of integrals over the regular submanifolds of $\Lambda$. Let us introduce a coordinate system $\{u^a\}_{a=1,...,2N}$ such that $u^{\bar{A}} = \nabla F^{\bar{A}}$ with $\bar{A} = 1, ..., m$ on a region

$$\mathcal{M}_{[\mathbf{f}_0, \mathbf{f}_1]} = \left\{x \in \Lambda \,|\, f_0^k \leq F^k \leq f_1^k\right\} \ , \tag{4.15}$$

free of critical points of function $f^k$. It follows that the metric $g$ reads

$$g = g_{\mu\nu} \ \mathrm{d}x^\mu \otimes \mathrm{d}x^\nu = g_{ab} \ \mathrm{d}u^a \otimes u^b = g_{\bar{A}\bar{B}} \ \mathrm{d}u^{\bar{A}} \otimes \mathrm{d}u^{\bar{B}} + g_{AB} \ \mathrm{d}u^A \otimes \mathrm{d}u^B \ , \tag{4.16}$$

where, if we consider the inverse matrices of the metric in the two-coordinate system we have

$$g^{\bar{A}\bar{B}} = g^{\mu\nu}\frac{\partial u^{\bar{A}}}{\partial x^{\mu}}\frac{\partial u^{\bar{B}}}{\partial x^{\nu}} = g(\nabla F^{\bar{A}}, \nabla F^{\bar{B}}) \, . \tag{4.17}$$

The Riemannian volume element $\omega$ in the two coordinates systems reads

$$\begin{aligned}\omega &= |\mathrm{det} g_{\mu\nu}|^{1/2} \, \mathrm{d}x^1 \wedge ... \wedge \mathrm{d}x^{2N} = |\mathrm{det} g_{ab}|^{1/2} \, \mathrm{d}u^1 \wedge ... \wedge \mathrm{d}u^{2N} \\ &= |\mathrm{det} g_{\bar{A}\bar{B}}|^{1/2} \mathrm{d}u^1 \wedge ... \wedge \mathrm{d}u^m \underbrace{|\mathrm{det} g_{AB}|^{1/2} \mathrm{d}u^{m+1} \wedge ... \wedge \mathrm{d}u^{2N}}_{\sigma_{\Sigma_{f^1,...,f^m}}} \, ,\end{aligned} \tag{4.18}$$

where $\sigma_{\Sigma_{f^1,...,f^m}}$ is the induced Riemannian area form on the submanifold $\Sigma_{f^1,...,f^m}$. Thus, any integral of a function $\psi(u^{\bar{A}}, u^A)$ on $\mathcal{M}_{[\mathbf{f}_0,\mathbf{f}_1]}$ (defined in Eq.(4.15)) can be expressed as

$$\int_{\mathcal{M}_{[\mathbf{f}_0,\mathbf{f}_1]}} \psi(u^{\bar{A}}, u^A) \, \omega \, , \tag{4.19}$$

which is equal to

$$\int_{\mathbf{f}_0}^{\mathbf{f}_1} \left( \int_{\Sigma_{u^1 ... u^m}} \psi(u^{\bar{A}}, u^A) \sqrt{|\mathrm{det} g_{\bar{A}\bar{B}}|} \sigma_{\Sigma_{u^1 ... u^m}} \right) \mathrm{d}u^1 \wedge \cdots \wedge \mathrm{d}u^m \, . \tag{4.20}$$

Finally, it remains to evaluate $|\mathrm{det} g_{\bar{A}\bar{B}}|^{1/2}$. For any non-zero determinant matrix, we have $\mathrm{det} A^{-1} = (\mathrm{det} A)^{-1}$, so it follows that

$$|\mathrm{det} g_{\bar{A}\bar{B}}|^{1/2} = |\mathrm{det} g^{\bar{A}\bar{B}}|^{-1/2} = \left[ \mathbb{G}(\nabla F^1, .., \nabla F^m) \right]^{-1/2} \tag{4.21}$$

where $\mathbb{G}(X^1, ..., X^m) := \mathrm{det} \left[ g(X^i, X^j)_{i,j=1,...,m} \right]$ is the so-called Grammian (or Gram matrix), so that the expression (4.20) takes the final form

$$\int_{\mathbf{f}_0}^{\mathbf{f}_1} \left( \int_{\Sigma_{u^1,...,u^m}} \psi(u^A, u^{\bar{A}}) \frac{\sigma_{\Sigma_{u^1,...,u^m}}}{\sqrt{\mathbb{G}(\nabla F^1, .., \nabla F^m)}} \right) \mathrm{d}u^1 \wedge ... \wedge \mathrm{d}u^m \, , \tag{4.22}$$

that is usually referred to as *Co-area formula*. When $\psi(u^{\bar{A}}, u^A) = \prod_{\bar{A}=1}^m \delta(u^{\bar{A}} - f^{\bar{A}})$, then the Eq.(4.22) can be interpreted as the microcanonical partition function $\Omega_N(f^1, ..., f^m)$ where $m$ independent first integral of motion $\left\{ F^{\bar{A}} \right\}_{A=1,...,m}$ has been fixed, i.e.

$$\begin{aligned}\Omega_N(f^1, ..., f^m) &= \int_{\Sigma_{f^1,...,f^m}} \frac{\sigma_{\Sigma_{f^1,...,f^m}}}{\sqrt{\mathbb{G}(\nabla F^1, .., \nabla F^m)}} \\ &= \int_{\Sigma_{f^1,...,f^m}} \sigma_{f^1,...,f^m} \, .\end{aligned} \tag{4.23}$$

■

## 4.2 A review of the Pinkall inequality: a bridge between topology and extrinsic geometry

In Section 2.3 we have briefly reviewed the Topological Hypothesis on the origin of phase transitions in the microcanonical ensemble, relying on the topological changes of energy level sets with the appearance of phase transitions. However, it is not possible in general to calculate the topological invariants of a regular $m$-dimensional level set $\Sigma_{f^1,\dots,f^m}$. This problem is, in general, a tough task, as the cohomology groups of a submanifold can be directly computed only in very few cases through algebraic topological techniques. However, it is possible in some cases to calculate or, at least, estimate the topological invariants of submanifolds using the few results existing linking the global geometry with topology. One result of this kind is the well-known Gauss-Bonnet theorem for any two-dimensional surface $\mathcal{M}$ (without boundary)

$$\int_{\mathcal{M}} K_G \ \mathrm{d}s = 2\pi\chi_{\mathrm{eul}}(\mathcal{M}) \ , \tag{4.24}$$

where $\chi_{\mathrm{eul}}$ is the Euler characteristic (which is a topological invariant) of $\mathcal{M}$, and $K_G$ is the so-called Gauss curvature, which is an intrinsic curvature that, in the case of immersion, can be expressed as the product of the principal curvatures, i.e. $K_G = k_1 k_2$. $\mathrm{d}s$ is an element of the area of the surface of $\mathcal{M}$. Although the Gauss-Bonnet theorem admits a generalization to higher even-dimensional manifolds, it is in general not easy to compute the Gauss curvature from the immersion properties: this is why we will look for an extrinsic geometric quantity that can be more easily computed for immersed sub-mediums, such as the regular level sets of first integrals of motions. For this reason, we have considered the so-called *Pinkall's inequality*.

**Definition 4.2.** *For any submanifold $\mathcal{M}^m$ of codimension $m$ immersed in a Euclidean space $\mathbb{E}^n$, the dispersion of the principal curvatures $\{k_i\}_{i=1,\dots n-m}$ is defined as*

$$\sigma^2(k_i) = \frac{1}{(n-m)^2} \sum_{i<j} (k_i - k_j)^2 = \frac{1}{n-m} \sum_{i=1}^{n-m} \left(k_i - \bar{k}\right)^2 \ , \tag{4.25}$$

*where*

$$\bar{k} = \frac{1}{n-m} \sum_{i=1}^{n-m} k_i \ . \tag{4.26}$$

**Definition 4.3.** *Pinkall's inequality [126] reads*

$$\begin{aligned} &\frac{1}{\mathrm{Vol}\left(\mathbf{S}^n\right)} \int_{\mathcal{M}^{(n-m)}} \left[\sigma^2_\xi(k_i)\right]^{(n-m)} \ \mathrm{d}\mu \ \geq \\ &\sum_{i=1}^{(n-m)-1} \left(\frac{i}{n-m-i}\right)^{(n-m)/2-i} b_i\left(\mathcal{M}^{(n-m)}\right) \ , \end{aligned} \tag{4.27}$$

*where* $b_i\left(\mathcal{M}^{(n-m)}\right)$ *are the Betti numbers of the manifold* $\mathcal{M}^{(n-m)}$*, immersed in the Euclidean space* $\mathbb{R}^n$ *(a Betti number is the diffeomorphism-invariant dimension of the* $i$*th cohomology group of the submanifold* $\mathcal{M}^m$ [1]*).* $\mathbf{S}^n$ *is an* $n$*-dimensional sphere of unit radius, and* $\mathrm{d}\mu$ *is the measure on* $\mathcal{M}^{(n-m)}$*.*

We notice that on the right-hand side of Eq.(4.27) there is a weighted sum of Betti numbers: the weights $w_i = [i/(n-i)]^{n/2-i}$ emphasize the contributions coming from the (co)homology groups $H_i(\mathcal{M}^m)$ with $i \simeq n/2$, as can be seen in Figure 4.1 In [122], Pinkall theorem was applied in the case of a system undergoing a

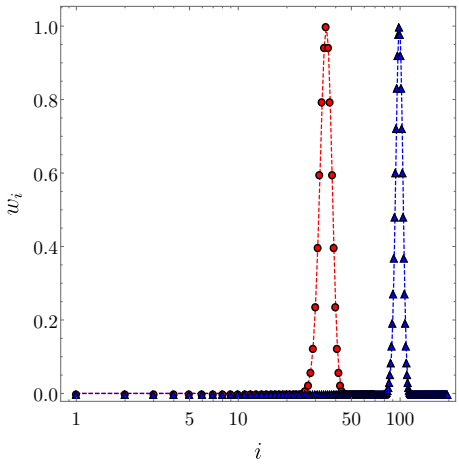


Figure 4.1: Weights $w_i = [i/(n-m-i)]^{(n-m)/2-i}$ appearing in right hand side of Pinkall inequality for $m = 2$ and $n = 2(6 \times 6) = 72$ (red circles) and $n = 2(10 \times 10) = 200$ (blue triangles).

thermodynamic phase transition in the absence of a global symmetry-breaking, where it has been shown that the phase transition is marked by an abrupt change in the geometry and so on the topology of $\Sigma_V$, i.e. the level sets of potential. The geometrical quantity in the left-hand side of Eq.(4.27) is hard to be calculated through numerical simulation of large dynamical systems for two main reasons. The first one concerns the fact that the quantities that can be directly estimated through Hamiltonian dynamic simulations are generally microcanonical averages while in Eq.(4.27) the calculation of the integral on $\mathcal{M}^m$ of the dispersion of principal curvatures is required. The second one is related to the $(n-m)/2$-th power of $\sigma^2_\xi(k_i)$ that for large values of $n$ ($n \gtrsim 100$) become practically untreatable. Such difficulties can be managed thanks to Hölder inequality[135], that allows to consider the $2/(n-m)$ of the integral in Eq.(4.27) for codimension one manifold $\Sigma$

$$\int_\Sigma [\sigma(k_i)]^2 \, \mathrm{d}\mu \;\leq\; \left[\int_\Sigma \left\{[\sigma(k_i)]^2\right\}^{(n-1)/2} \mathrm{d}\mu\right]^{2/(n-1)} \left[\int_\Sigma \mathrm{d}\mu\right]^{1/[1-2/(n-1)]}, \tag{4.28}$$

[1] It is worth to note that Pinkall's inequality becomes an equality if the Betti numbers $\{b_i(\mathcal{M}^m)\}_{i=0,\ldots,n-m}$ are replaced by Morse numbers $\{\mu_i(\mathcal{M}^m)\}_{i=0,\ldots,n-m}$, i.e. the number of critical points of a Morse function on $\mathcal{M}^m$ with index $i$. Therefore, the Pinkall's inequality is a consequence of the so-called *weak Morse inequality*, i.e. $\mu_i(\mathcal{M}^m) \geq b_i(\mathcal{M}^m)$

that for large $n$ becomes

$$\left[\int_{\Sigma} \mathrm{d}\mu\right]^{-1} \int_{\Sigma} \left[\sigma(k_i)\right]^2 \mathrm{d}\mu \leq \left[\int_{\Sigma} \left\{\left[\sigma(k_i)\right]^2\right\}^{n/2} \mathrm{d}\mu\right]^{2/n} \tag{4.29}$$

Moreover, Hölder inequality becomes an equality when $[\sigma(k_i)]^n$ equals its average value almost everywhere on $\Sigma$. So we can introduce a reminder $r(\Sigma)$, the last equation is rewritten as

$$\left[\int_{\Sigma} \mathrm{d}\mu\right]^{-1} \int_{\Sigma} \left[\sigma(k_i)\right]^2 \mathrm{d}\mu = \left[\int_{\Sigma} \left\{\left[\sigma(k_i)\right]^2\right\}^{n/2} \mathrm{d}\mu\right]^{2/n} - r(\Sigma) \tag{4.30}$$

where we recognize on the left-hand side the average with respect to the measure $\mathrm{d}\mu$ of the dispersion of principal curvatures. In the case where the dispersion of the principal curvatures of $\Sigma$ displays a limited variability from point to point, the remainder $r(\Sigma)$ appears to be a small correction and, consequently, the Hölder inequality is tight

$$\begin{aligned} \langle\left[\sigma(k_i)\right]^2\rangle_{\mu} &\sim \left[\int_{\Sigma} \left\{\left[\sigma(k_i)\right]^2\right\}^{n/2} \mathrm{d}\mu\right]^{2/n} - r(\Sigma) \\ &= \left[\mathrm{Vol}\left(\mathbb{S}^n\right) \sum_{i=1}^{n} \left(\frac{i}{n-i}\right)^{n/2-i} b_i\left(\Sigma\right)\right]^{2/n} - r(\Sigma) \end{aligned} \tag{4.31}$$

under the hypothesis that $\mathrm{d}\mu$ is the induced Riemmanian manifold over $\Sigma$.

# 5

# Differential geometry and topology of submanifolds in XY 2D model

This Chapter presents our original work that has been published in Ref.[10]. Here, we will use the mathematical framework explored in the last Chapter for codimension $m$ submanifolds $\Sigma_{f^1,\dots,f^m}$ to adapt it to the case of XY 2D model. We have seen in Chapter 3 that the two conserved quantities in the XY 2D model are the Hamiltonian $H = E$ and the total momentum $P = p$. We will then present in this Chapter the bridge between thermodynamics and geometry of $\Sigma_{p,E} = \{x \in \Lambda \,|\, H(x) = E \ \wedge \ P(x) = p\}$. Then, we will present the calculations of some geometrical observables of $\Sigma_{p,E}$. Finally, we present and discuss the numerical results of Hamiltonian dynamics simulations allowing to estimate the averages and variances of the geometrical quantities investigated on $\Sigma_{0,N\varepsilon}$ have been reported as functions of specific energy $\varepsilon$ for different values of $N$.

## 5.1 Link between thermodynamics and geometry of the submanifolds $\Sigma_{p,E}$

In the present Section, we investigate the relationship between the thermodynamics of a (generalized) microcanonical ensemble where both the total energy

$$H = \frac{1}{2}\sum_{\tilde{\mu}=1}^{N} p^{\tilde{\mu}} p_{\tilde{\mu}} + V_N(q) \tag{5.1}$$

and the total momentum

$$P = \sum_{\tilde{\mu}=1}^{N} p^{\tilde{\mu}} \tag{5.2}$$

are fixed quantities and the geometry of the regular submanifolds $\Sigma_{p,E}$ in phase space.
The first step to study the extrinsic geometry in this particular case consists in defining the normal bundle on $\Sigma_{p,E}$. This requires calculating both the gradient of the total momentum

$$\nabla P = \sum_{\tilde{\mu}} \partial_{\tilde{\mu}} \implies \|\nabla P\| = N^{1/2} \,, \tag{5.3}$$

and the gradient of the Hamiltonian $H$

$$\nabla H = \sum_{\tilde{\mu}} p^{\tilde{\mu}} \partial_{\tilde{\mu}} + \sum_{\hat{\mu}} \partial^{\hat{\mu}} V \partial_{\hat{\mu}} \implies \|\nabla H\| = \left[ \sum_{\tilde{\mu}} p^{\tilde{\mu}} p_{\tilde{\mu}} + \|\hat{\nabla} V\|^2 \right]^{1/2}, \quad (5.4)$$

where $\hat{\nabla} f = \partial^{\hat{\mu}} f \partial_{\hat{\mu}}$ is the gradient referred only to set of generalized coordinates $q^{\hat{\mu}}$.
Two normal vector fields can be associated with the two gradient fields in absence of critical points

$$\begin{aligned} n_P &= \frac{\nabla P}{\|\nabla P\|} = \frac{\sum_{\tilde{\mu}} \partial_{\tilde{\mu}}}{N^{1/2}} \\ n_H &= \frac{\nabla H}{\|\nabla H\|} = \frac{\sum_{\tilde{\mu}} p^{\tilde{\mu}} \partial_{\tilde{\mu}} + \sum_{\hat{\mu}} \partial^{\hat{\mu}} V \partial_{\hat{\mu}}}{\left[ \sum_{\tilde{\mu}} p^{\tilde{\mu}} p_{\tilde{\mu}} + \|\hat{\nabla} V\|^2 \right]^{1/2}} \end{aligned} \quad (5.5)$$

Following the definition given for the microcanonical volume $\Omega_N$ based on the Co-area formula given in Chapter 4, Eq.(4.23) reads in this case

$$\begin{aligned} \Omega_N(E,p) &= \int_\Lambda \delta(H(p,q) - E)\, \delta(P - p)\, \omega = \int_{\Sigma_{p,E}} \left( \frac{\sigma_{\Sigma_{p,E}}}{\sqrt{\mathbb{G}(\nabla H, \nabla P)}} \right) \sigma_{E,p} \\ &= \int_{\Sigma_{p,E}} \chi\, \sigma_{\Sigma_{p,E}} = \int_{\Sigma_{p,E}} \sigma_{p,E}\ , \end{aligned} \quad (5.6)$$

where $\chi = \left( \sqrt{\mathbb{G}(\nabla H, \nabla P)} \right)^{-1}$ and

$$\begin{aligned} \sqrt{\mathbb{G}(\nabla H, \nabla P)} &= \sqrt{\det \begin{bmatrix} g(\nabla H, \nabla H) & g(\nabla H, \nabla P) \\ g(\nabla P, \nabla H) & g(\nabla P, \nabla P) \end{bmatrix}} \\ &= \sqrt{\|\nabla H\|^2 \|\nabla P\|^2 - (g(\nabla H, \nabla P))^2}. \end{aligned} \quad (5.7)$$

Since the microcanonical thermodynamic observables defined in Chapter 3 are expressed as the derivatives of the microcanonical partition function with respect to the specific energy, it is useful to provide a derivation formula for the integral of functions over $\Sigma_{p,E}$ with respect to the energy *at fixed p*.
Let us define the two functions $f \in C^\infty(\Lambda)$ and $F : (E_1, E_2) \to \mathbb{R}$

$$F(E,p) = \int_{\Sigma_{p,E}} f\ \sigma_{p,E} \quad (5.8)$$

We will derive in what follows the explicit form of the operator $\mathcal{A}_E(\cdot)$ acting over functions $f$, s.t.

$$\frac{\partial F}{\partial E}(E,p) = \int_{\Sigma_{p,E}} \mathcal{A}_E(f)\ \sigma_{p,E} \quad (5.9)$$

To derive such an operator with respect to the energy, let us consider the definition of the derivative of a function with respect to $E$. In what follows we

adopt this notation: $F'(E,p) = \partial_E F(E,p)$ and $\Omega'(E) = \partial_E \Omega(E,p)$

$$\begin{aligned} F'(E,p) &= \lim_{\Delta E \to 0} \frac{\int_{\Sigma_{p,E+\Delta E}} f\ \sigma_{p,E} - \int_{\Sigma_{p,E}} f\ \sigma_{p,E}}{\Delta E} \\ &= \lim_{\Delta E \to 0} \frac{\int_{\phi(\Sigma_{p,E},\Delta E)} f\ \sigma_{p,E} - \int_{\Sigma_{p,E}} f\ \sigma_{p,E}}{\Delta E} \\ &= \lim_{\Delta E \to 0} \frac{\int_{\Sigma_{p,E}} \phi^*_{\Delta E}(f\ \sigma_{p,E}) - \int_{\Sigma_{p,E}} f\ \sigma_{p,E}}{\Delta E} \\ &= \int_{\Sigma_{p,E}} \left[ \lim_{\Delta E \to 0} \frac{\phi^*_{\Delta E}(f\ \sigma_{p,E}) - f\ \sigma_{p,E}}{\Delta E} \right] \\ &= \int_{\Sigma_{p,E}} \mathcal{L}_\xi (f\, \sigma_{p,E}) \end{aligned} \tag{5.10}$$

In the second equality, the pullback of the one-parameter diffeomorphism $\phi(\cdot, \Delta E)$ among energy level sets generated by the vector field $\xi$, has been applied on the argument of the integral in order to evaluate it on $\Sigma_{p,E}$. In the last term, we recognize that the argument of the integral is the Lie derivative along the vector field $\xi$ of the $(2N-2)$-form $\alpha = f\sigma_{p,E} = f\chi\sigma_{\Sigma_{p,E}}$, so we obtain

$$\mathcal{L}_\xi (f\sigma_{p,E}) = \xi(f\chi)\sigma_{\Sigma_{p,E}} + f\chi\mathcal{L}_\xi \left(\sigma_{\Sigma_{p,E}}\right). \tag{5.11}$$

As we are interested in a derivation with respect to $E$ at fixed $p$, the vector field $\xi$ has to fulfill the two following conditions:

$$\begin{aligned} \mathrm{d}H\,(\xi) &= 1 \\ \mathrm{d}P\,(\xi) &= 0 \end{aligned} \tag{5.12}$$

and using the gradient definition (4.5), we obtain

$$\begin{aligned} g\,(\nabla H,\, \xi) &= 1 \\ g\,(\nabla P,\, \xi) &= 0. \end{aligned} \tag{5.13}$$

After further calculations, we obtain

$$\xi = c\, \left( \nabla H - g\,(\nabla H,\, \nabla P)\, \frac{\nabla P}{\|\nabla P\|^2} \right), \tag{5.14}$$

with $c = \left( \|\nabla H\|^2 - \dfrac{g\,(\nabla H, \nabla P)^2}{\|\nabla P\|^2} \right)^{-1}$.

We are interested in studying the extrinsic geometry of submanifolds of codimension two $\Sigma_{p,E}$ when $p$ is fixed while $E$ can change. So, we simplify the problem by considering $\Sigma_{p,E}$ as a codimension one submanifold, immersed on $\Sigma_p$, on which the level sets $H = E$ can evolve. We introduce then the projector operator $\mathbb{P}_{\Sigma_{p,E}}$ for vectors on the tangent bundle $\mathrm{T}\Sigma_p$, i.e.

$$\mathbb{P}_{\Sigma_{p,E}}(X) = X - g(X, n_P) n_P. \tag{5.15}$$

Let us redefine the two normal vector fields on $\Sigma_{p,E}$ (see Figure 5.1 for a visualization of the following vectors)

$$\begin{aligned} n_1 &= \frac{\nabla P}{\|\nabla P\|} \\ n_2 &= \frac{\mathbb{P}_{\Sigma_{p,E}}(n_H)}{\|\mathbb{P}_{\Sigma_{p,E}}(n_H)\|} = \frac{\mathbb{P}_{\Sigma_{p,E}}(\nabla H)}{\|\mathbb{P}_{\Sigma_{p,E}}(\nabla H)\|}, \end{aligned} \tag{5.16}$$

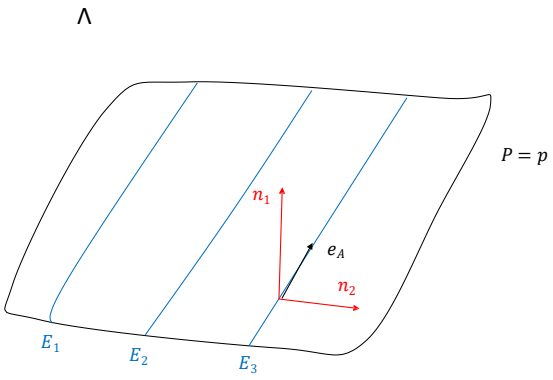


Figure 5.1: Level sets $H = E$ over the submanifolds $P = p$ immersed on $\Lambda$

where $n_2$ is the normal vector field to energy level sets over $\Sigma_p$. We notice that

$$\begin{aligned}\mathbb{P}_{\Sigma_{p,E}}(\nabla H) &= \nabla H - g\left(\nabla H, \frac{\nabla P}{\|\nabla P\|}\right)\frac{\nabla P}{\|\nabla P\|} = \nabla H - \frac{1}{N}g(\nabla H, \nabla P)\,\nabla P \\ &= \nabla H - \frac{1}{N}P\,\nabla P = \nabla H - \frac{1}{N}\nabla\left(\frac{P^2}{2}\right) = \nabla f_{Hp}\,,\end{aligned}$$

where we have introduced the function $f_{Hp}$. With the definition of such new function $f_{Hp}$, the vector field $\xi$ we introduced in equation (5.14) can be more easily expressed as follows

$$\xi = \frac{\nabla f_{Hp}}{\|\nabla f_{Hp}\|^2}\,. \tag{5.17}$$

It is natural to introduce the differential forms $\theta^1 = e^1_\mu\,\mathrm{d}x^\mu$ and $\theta^2 = e^2_\mu\,\mathrm{d}x^\mu$, that in terms of derivatives of $f_{Hp}$ and $P$, i.e.

$$\begin{aligned}\imath_{n_1}\theta^1 = e^1_\mu n^\mu_1 = e^1_\mu\frac{\partial^\mu P}{\|\nabla P\|} = 1 \quad &\Rightarrow \qquad e^1_\mu = \frac{\partial_\mu P}{\|\nabla P\|} \\ \imath_{n_2}\theta^2 = e^2_\mu n^\mu_2 = e^2_\mu\frac{\partial^\mu f_{Hp}}{\|\nabla f_{Hp}\|} = 1 \quad &\Rightarrow \qquad e^2_\mu = \frac{\partial_\mu f_{Hp}}{\|\nabla f_{Hp}\|}\end{aligned} \tag{5.18}$$

yielding to

$$\begin{aligned}\theta^1 &= \frac{\partial_\mu P\,\mathrm{d}x^\mu}{\|\nabla P\|} = \frac{\mathrm{d}P}{\|\nabla P\|} \\ \theta^2 &= \frac{\partial_\mu f_{Hp}\,\mathrm{d}x^\mu}{\|\nabla f_{Hp}\|} = \frac{\mathrm{d}f_{Hp}}{\|\nabla f_{Hp}\|}\,.\end{aligned} \tag{5.19}$$

With this notation, the volume form on phase space can be rewritten as follows

$$\begin{aligned}\omega = \mathrm{d}x^1 \wedge ... \wedge \mathrm{d}x^{2N} &= \det(e_b^\mu)\ \theta^1 \wedge \theta^2 \wedge ... \wedge \theta^{2N} \\ &= \theta^1 \wedge \theta^2 \wedge \underbrace{\theta^{2+1} \wedge ... \wedge \theta^{2N}}_{\sigma_{\Sigma_{p,E}}} \\ &= \theta^1 \wedge \theta^2 \wedge \sigma_{\Sigma_{p,E}}\ .\end{aligned} \tag{5.20}$$

where $\imath_\xi \sigma_{\Sigma_{p,E}} = \|\nabla f_{Hp}\|^{-1} \imath_{n_2} \left(\theta^{2+1} \wedge ... \wedge \theta^{2N}\right) = 0$ and $\mathcal{L}_V \omega = (\mathrm{div}\, V)\, \omega$. We have also used the fact that a Riemannian volume is a maximal form, i.e. $\mathrm{d}\omega = 0$. Finally, we obtain

$$\mathcal{L}_\xi \left(\sigma_{\Sigma_{p,E}}\right) = \|\nabla f_{Hp}\|^{-1}\, \mathrm{div}\,(n_2) \sigma_{\Sigma_{p,E}}\ , \tag{5.21}$$

that substituted in Eq.(5.11), yields

$$\begin{aligned}\mathcal{L}_\xi(f\sigma_{p,E}) &= \left(\frac{\mathcal{L}_\xi\,(f\,\chi)}{\chi} + f\ \|\nabla f_{Hp}\|^{-1}\, \mathrm{div}\,(n_2)\right) \chi\, \sigma_{\Sigma_{p,E}} \\ &= \mathcal{A}_E(f)\, \sigma_{p,E}\ .\end{aligned} \tag{5.22}$$

So we obtain

$$\frac{\partial F(E,p)}{\partial E} = \int_{\Sigma_{p,E}} \mathcal{A}_E(f)\ \ \sigma_{p,E} \tag{5.23}$$

that generalizes to higher derivatives

$$F^{(k)}(E,p) = \int_{\Sigma_{p,E}} \mathcal{A}_E^k(f)\ \ \sigma_{p,E} = \int_{\Sigma_{p,E}} \underbrace{\mathcal{A}_E(\mathcal{A}_E(...(\mathcal{A}_E}_{k-\text{times}}(f)))) \ \ \sigma_{p,E}\,. \tag{5.24}$$

By simply putting $f = 1$, one obtains

$$\Omega'(E) = \int_{\Sigma_{p,E}} \left(\frac{\mathcal{L}_\xi\,(\chi)}{\chi} + \ \frac{\mathrm{div}\,(n_2)}{\|\nabla f_{Hp}\|}\right) \chi\, \sigma_{\Sigma_{p,E}}\ , \tag{5.25}$$

with

$$\begin{aligned}\mathcal{L}_\xi\,(\chi) = \nabla_\xi\,(\chi) &= \frac{1}{\|\nabla f_{Hp}\|^2}\, \nabla_{\nabla_{f_{Hp}}} \left(\frac{1}{\|\nabla f_{Hp}\|\, N^{1/2}}\right) \\ &= \left(-\frac{1}{2\,N^{1/2}}\right) \frac{1}{\|\nabla f_{Hp}\|^2}\, \frac{2\,g\left(\nabla f_{Hp},\, \nabla_{\nabla_{f_{Hp}}} \nabla f_{Hp}\right)}{\|\nabla f_{Hp}\|^3} \\ &= -\frac{\mathrm{Hess} f_{Hp}\left(\nabla_{f_{Hp}}, \nabla_{f_{Hp}}\right)}{\|\nabla f_{Hp}\|^5\, N^{1/2}}\ ,\end{aligned} \tag{5.26}$$

where we have used the definition of the Hessian two-covector

$$\mathrm{Hess} f(X,Y) \equiv g(\nabla_X \nabla f, Y) = X \mathrm{d}f(Y) - \mathrm{d}f(\nabla_X Y)\ . \tag{5.27}$$

Finally, we obtain

$$\Omega'(E) = \int_{\Sigma_{p,E}} \left(-\frac{\mathrm{Hess} f_{Hp}\left(\nabla_{f_{Hp}}, \nabla_{f_{Hp}}\right)}{\|\nabla f_{Hp}\|^4} + \frac{\mathrm{div}\,(n_2)}{\|\nabla f_{Hp}\|}\right) \sigma_{p,E}\ . \tag{5.28}$$

So the inverse of the microcanonical geometrical temperature is given by

$$T_{\rm geo}^{-1}(E,p) = \frac{\int_{\Sigma_{p,E}} \operatorname{div}\xi \quad \sigma_{p,E}}{\int_{\Sigma_{p,E}} \quad \sigma_{p,E}} = \int_{\Sigma_{p,E}} \operatorname{div}\xi \quad \mu = \langle \operatorname{div}\xi \rangle_{\mu c}(p,E) \ , \quad (5.29)$$

where $\langle\cdot\rangle_{\mu c}(p,E)$ indicates the averages over the energy level sets $\sigma_{p,E}$ with the probability measure $\mu$.

## 5.2 Geometrical and topological observables in XY 2D model

As we are interested on the extrinsic geometry of $\Sigma_{p,E}$, we introduce the mean curvature along the vector $n_2$ and according to the equation (4.14), we have

$$\begin{aligned} M_{n_2} &= -\frac{1}{2N-2}\sum_{A=1}^{2N-2} g(\nabla_{e_A} n_2, e_A) \\ &= -\frac{1}{2N-2}\left[\sum_{i=1}^{2} g(\nabla_{n_i} n_2, n_i) + \sum_{A=1}^{2N-2} g(\nabla_{e_A} n_2, e_A) - \sum_{i=1}^{2} g(\nabla_{n_i} n_2, n_i)\right] \\ &= -\frac{1}{2N-2}\left[\sum_{\tilde\mu} g(\nabla_{\partial_{\tilde\mu}} n_2, \partial_{\tilde\mu}) + \sum_{\hat\mu} g(\nabla_{\partial_{\hat\mu}} n_2, \partial_{\hat\mu}) + \right. \\ &\qquad\qquad \left. - g(\nabla_{n_1} n_2, n_1) - g(\nabla_{n_2} n_2, n_2)\right] \\ &= -\frac{1}{2N-2}\left[\operatorname{div}(n_2) - g(\nabla_{n_1} n_2, n_1)\right] \ . \end{aligned} \quad (5.30)$$

The second term of the last equation in (5.30) is null. In fact, from $\nabla_{\nabla P}\nabla f_{Hp} = 0$ (for more details see Appendix A) it follows

$$\begin{aligned} \nabla_{n_1} n_2 &= \frac{1}{\|\nabla P\|}\nabla_{\nabla P}\left(\frac{\nabla f_{Hp}}{\|\nabla f_{Hp}\|}\right) \\ &= \frac{\nabla_{\nabla P}\nabla f_{Hp}}{\|\nabla P\|\|\nabla f_{Hp}\|} - \frac{(\nabla_{\nabla P}\nabla f_{Hp},\, \nabla f_{Hp})\,\nabla f_{Hp}}{\|\nabla P\|\|\nabla f_{Hp}\|^3} = 0 \ . \end{aligned} \quad (5.31)$$

Finally the mean curvature $M_{n_2}$ of $\Sigma_{p,E}$ reads

$$M_{n_2} = \frac{1}{2N-2}\left[\frac{\mathrm{Hess} f_{Hp}(\nabla f_{Hp}, \nabla f_{Hp})}{\|\nabla f_{Hp}\|^3} - \frac{\Delta f_{Hp}}{\|\nabla f_{Hp}\|}\right] \ . \quad (5.32)$$

To explore the topology of $\Sigma_{p,E}$ we consider them as co-dimension one manifold immersed in the Euclidean space $\Sigma_p$ and we compute the dispersion of the principle curvatures $\sigma^2_{n_2}(k_i)$ (that according to Pinkall theorem presented in Chapter 4 is strictly related with topology).

$$\sigma^2_{n_2}(k_i) = \langle k_i^2\rangle - \langle k_i\rangle^2 = \frac{\mathrm{Tr}(\mathcal{W}^2_{n_2})}{2N-2} - \frac{(\mathrm{Tr}\mathcal{W}_{n_2})^2}{(2N-2)^2} \ , \quad (5.33)$$

where

$$\begin{aligned}
\mathrm{Tr}(\mathcal{W}^2_{n_2}) &= \sum_{A=1}^{2N-2} g(-\nabla_{(-\nabla_{e_A} n_2)} n_2, e_A) = -\sum_{A=1}^{2N-2} g(n_2, \nabla_{\nabla_{e_A} n_2} e_A) \\
&= -\left[ \sum_{A=1}^{2N-2} g\left(n_2, \nabla_{e_A}\nabla_{e_A} n_2\right) + g(n_2, [\nabla_{e_A} n_2, e_A]) \right] \\
&= \sum_{A=1}^{2N-2} \left[ g\left(\nabla_{e_A} n_2, \nabla_{e_A} n_2\right) + g(n_2, [e_A, \nabla_{e_A} n_2]) \right] \\
&= \sum_{\mu=1}^{2N} g\left(\nabla_\mu n_2, \nabla_\mu n_2\right) + \sum_{A=1}^{2N-2} g(n_2, [e_A, \nabla_{e_A} n_2]) - g\left(\nabla_{n_2} n_2, \nabla_{n_2} n_2\right) \\
&= \sum_{\mu=1}^{2N} \|\nabla_\mu n_2\|^2 - \|\nabla_{n_2} n_2\|^2 + \sum_{A=1}^{2N-2} g(n_2, [e_A, \nabla_{e_A} n_2])
\end{aligned} \tag{5.34}$$

The first term of equation (5.34) is giving by

$$\begin{aligned}
\sum_{\mu=1}^{2N} \|\nabla_\mu n_2\|^2 = \sum_{\mu=1}^{2N} \Bigg[ & \frac{\partial_\mu \partial^\rho f_{Hp}\, \partial_\rho \partial_\gamma f_{Hp}}{\|\nabla f_{Hp}\|^2} + \frac{\partial^\rho f_{Hp} \partial_\rho f_{Hp}}{\|\nabla f_{Hp}\|^6} \left(\partial_\mu \partial_\nu f_{Hp}\, \partial^\nu f_{Hp}\right)\left(\partial_\gamma \partial_\sigma f_{Hp}\, \partial^\sigma f_{Hp}\right) + \\
& - 2 \frac{\left(\partial_\mu \partial^\rho f_{Hp}\, \partial_\rho f_{Hp}\right)\left(\partial_\gamma \partial_\nu f_{Hp}\, \partial^\nu f_{Hp}\right)}{\|\nabla f_{Hp}\|^4} \Bigg] \delta^\gamma_\mu \\
= \sum_{\mu=1}^{2N} & \left[ \frac{\partial_\mu \partial^\rho f_{Hp}\, \partial_\rho \partial_\gamma f_{Hp}}{\|\nabla f_{Hp}\|^2} - \frac{\left(\partial_\mu \partial^\rho f_{Hp}\, \partial_\rho f_{Hp}\right)\left(\partial_\gamma \partial_\nu f_{Hp}\, \partial^\nu f_{Hp}\right)}{\|\nabla f_{Hp}\|^4} \right] \delta^\gamma_\mu \\
= \mathrm{Tr} & \left[ \frac{\left(\mathrm{Hess} f_{Hp}\right)^2}{\|\nabla f_{Hp}\|^2} \right] - \frac{\left(\mathrm{Hess} f_{Hp}\, \nabla f_{Hp}\right)^2}{\|\nabla f_{Hp}\|^4} \, .
\end{aligned} \tag{5.35}$$

Knowing that

$$\nabla_{n_2} n_2 = \frac{\partial^\mu f_{Hp}}{\|\nabla f_{Hp}\|} \nabla_\mu n_2 \, ,$$

the second term then reads

$$\begin{aligned}
\|\nabla_{n_2} n_2\|^2 &= \frac{1}{\|\nabla f_{Hp}\|^2}\, g\left(\partial^\mu f_{Hp}\, \nabla_\mu n_2, \partial^\sigma f_{Hp}\, \nabla_\sigma n_2\right) \\
&= \frac{1}{\|\nabla f_{Hp}\|^2} \left[ \frac{\left(\|\mathrm{Hess} f_{Hp}\right)\left(\nabla f_{Hp}\right)\|^2}{\|\nabla f_{Hp}\|^2} + \right. \\
&\qquad \left. - \frac{\|\left(\mathrm{Hess} f_{Hp}\right)\left(\nabla f_{Hp}\right)^2\|^2}{\|\nabla f_{Hp}\|^4} \right].
\end{aligned} \tag{5.36}$$

The last term of equation (5.34) is a measure of the integrability of the vector field distribution $\{n_1, e_{\bar{A}}\}_{\bar{A}=2+1,\ldots,2N}$ in the sense of the Froebenius' Theorem .

In particular, if these fields form a closed algebra

$$[n_1, e_{\bar{A}}] \in \text{Span}\{n_1, e_{2+1}, ..., e_{2N}\} \tag{5.37}$$

then $\sum_{\bar{A}=3}^{2N} g(n_2, \left[\nabla_{e_{\bar{A}}} n_2, e_{\bar{A}}\right]) = 0$.
It is convenient to rephrase this condition in the language of differential forms. Let us introduce the annihilator 1-form $\eta$ defined as

$$\begin{aligned}\eta &= \left[\partial_{\tilde{\mu}} H - (\partial_{\tilde{\nu}} H \partial^{\tilde{\nu}} P)\partial_{\tilde{\mu}} P\right] \mathrm{d}q^{\tilde{\mu}} + \left[\partial_{\hat{\mu}} H - (\partial_{\hat{\nu}} H \partial^{\hat{\nu}} P)\partial_{\hat{\mu}} P\right] \mathrm{d}p^{\hat{\mu}} \\ &= [\partial_{\tilde{\mu}} H - (\partial_{\tilde{\nu}} H \partial^{\tilde{\nu}} P)\partial_{\tilde{\mu}} P]\mathrm{d}q^{\tilde{\mu}} + \partial_{\hat{\mu}} H \mathrm{d}p^{\hat{\mu}}\end{aligned} \tag{5.38}$$

such that

$$\eta(n_1) = \eta(e_A) = 0\,. \tag{5.39}$$

So if $\mathrm{d}\eta$ is an annihilator 2-form on the space $\text{Span}\{n_1, e_{2+1}, ..., e_N\}$ then the fields $\{n_1, e_A\}_{A=2+1,...,N}$ are in involution, i.e.

$$\begin{aligned}&0 = \mathrm{d}\eta(X, Y) = X\eta(Y) - Y\eta(X) - \eta([X, Y]) = -\eta([X, Y]) \\ &\forall X, Y \in \text{Span}\{n_1, e_1, ..., e_{2N-2}\}\,.\end{aligned} \tag{5.40}$$

For the 1-form $\eta$ defined in (5.38) we can evaluate explicitly $\mathrm{d}\eta$,

$$\begin{aligned}\mathrm{d}\eta =&[\partial_{\tilde{\rho}}\partial_{\tilde{\mu}} H - (\partial_{\tilde{\rho}}\partial_{\tilde{\nu}} H \partial^{\tilde{\nu}} P + \partial_{\tilde{\nu}} H \partial_{\tilde{\rho}}\partial^{\tilde{\nu}} P)\partial_{\tilde{\mu}} P - (\partial_{\tilde{\nu}} H \partial^{\tilde{\nu}} P)\partial_{\tilde{\rho}}\partial_{\tilde{\mu}} P]\ \mathrm{d}q^{\tilde{\rho}} \wedge \mathrm{d}q^{\tilde{\mu}} + \\ &+ \partial_{\hat{\rho}}\partial_{\hat{\mu}} H\ \mathrm{d}p^{\hat{\rho}} \wedge \mathrm{d}p^{\hat{\mu}}\ .\end{aligned} \tag{5.41}$$

The terms of the form $\partial_{\tilde{\rho}}\partial_{\tilde{\mu}} f$ and $\partial_{\hat{\rho}}\partial_{\hat{\mu}} f$ are symmetric in the permutation of the indexes and so are null. The derivative of order $k \geqslant 2$ of the function $P$ are null as it is a linear function in $p^{\tilde{\mu}}$. So the only non trivial term is $\left(\partial_{\tilde{\rho}}\partial_{\tilde{\nu}} H \partial^{\tilde{\nu}} P\right)\partial_{\tilde{\mu}} P\ \mathrm{d}p^{\tilde{\rho}} \wedge \mathrm{d}p^{\tilde{\mu}}$: as $\left(\partial_{\tilde{\rho}}\partial_{\tilde{\nu}} H \partial^{\tilde{\nu}} P\right)\partial_{\tilde{\mu}} P = N$ it is not antisymmetric with respect to the indexes $\tilde{\rho}$, $\tilde{\mu}$ and the term is zero. So it follows that $\mathrm{d}\eta = 0$. Finally

$$\begin{aligned}\mathrm{Tr}(\mathcal{W}_{n_2}^2) = \mathrm{Tr}\left[\frac{\left(\mathrm{Hess} f_{Hp}\right)^2}{\|\nabla f_{Hp}\|^2}\right] - \frac{\left(\mathrm{Hess} f_{Hp}\,\nabla f_{Hp}\right)^2}{\|\nabla f_{Hp}\|^4} + \\ - \frac{1}{\|\nabla f_{Hp}\|^2}\left[\frac{\left(\|\mathrm{Hess} f_{Hp}\right)\left(\nabla f_{Hp}\right)\|^2}{\|\nabla f_{Hp}\|^2} - \frac{\|\left(\mathrm{Hess} f_{Hp}\right)\left(\nabla f_{Hp}\right)^2\|^2}{\|\nabla f_{Hp}\|^4}\right]\end{aligned} \tag{5.42}$$

## 5.3 Numerical Results

All the details of the calculations of the geometrical observables seen in the last section are in Appendix A. In the case of geometrical observables, we are also interested on the computation of the averages with respect to the Riemannian induced measure $\sigma_{\Sigma_{0,E}}$, i.e.

$$\langle A \rangle_{geo} = \frac{\int_{\Sigma_{0,E}} A\ \sigma_{\Sigma_{0,E}}}{\int_{\Sigma_{0,E}} \sigma_{\Sigma_{0,E}}}. \tag{5.43}$$

As the Hamiltonian dynamics simulations allow to sample the submanifold $\Sigma_{0,E}$ according to the microcanonical measure, we have to express the geometric

averages (5.43) as a function of the microcanonical averages calculated according to Eq.(3.38). As shown in [61], the geometrical averages can be estimated as follows

$$\langle A \rangle_{geo} = \frac{\langle A\chi^{-1} \rangle_{\mu c}}{\langle \chi^{-1} \rangle_{\mu c}} \tag{5.44}$$

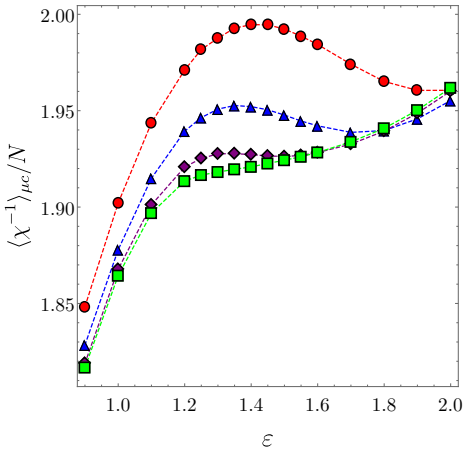


Figure 5.2: Microcanonical average of the inverse of the density of states $\chi^{-1}$ for the XY 2D model as a function of specific energy $\varepsilon$ for $N = 6 \times 6$ (red circles), $N = 10 \times 10$ (blue triangles), $N = 20 \times 20$ (purple diamonds), $N = 40 \times 40$ (green squares).

In principle $\chi^{-1}$ is not an intensive observable: so it is expected to depend on $N$

$$\begin{aligned} \langle \chi^{-1} \rangle_{\mu c} &= N^{1/2} \left\langle \sqrt{2K + \|\nabla V_N\|^2} \right\rangle \approx N^{1/2} \left\langle \sqrt{N\left[2\kappa + (\partial_{\hat{\mu}} V_N)^2\right]} \right\rangle_{\mu c} \\ &\approx N \sqrt{2\langle \kappa \rangle_{\mu c} + \langle (\partial_{\hat{\mu}} V_N)^2 \rangle_{\mu c}}\,, \end{aligned} \tag{5.45}$$

where in the second equality we considered $\|\nabla V_N\|^2 \approx N \left(\partial_{\hat{\mu}} V_N\right)^2$, because the system has nearest neighbors interactions and the transnational invariance holds for any spin (due to the periodic boundary conditions). We can consider both the microcanonical average of the specific kinetic energy $\langle \kappa \rangle_{\mu c}$ and the derivative of the potential $\left(\partial_{\hat{\mu}} V_N\right)^2_{\mu c}$ as intensive quantities so that we can argue that $\chi^{-1} \approx N$.
In Figure 5.2, we observe that at the transition point, the maximum of $\chi^{-1}$ tends to disappear in favor of a point of non-differentiability preceding an inflection point with an increasing $N$. Despite the fact that this observable has no geometrical interpretation, we observe a signature of the transition.

In Figure 5.3, we observe an agreement with a precision $\lesssim 10^{-3}$ between the new thermodynamic method that has been developed in this work and the geometrical method. We notice also an important deviation of the Pearson Halicioglu method [120] (where the constraint on total momenta has not been considered. See Chapter 3) with respect to the other two methods ($\approx 5 \times 10^{-2}$ for $N = 6 \times 6$). This effect is stronger for smaller systems.

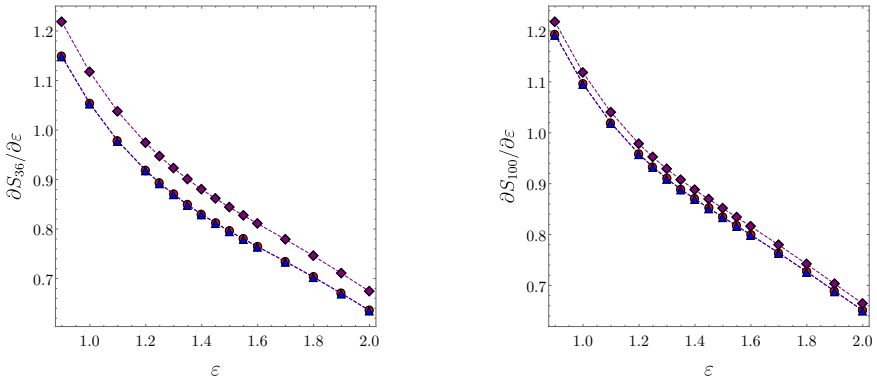


(a) (b)

Figure 5.3: First order derivative with respect to specific energy at fixed total momentum $P = 0$ of microcanonical entropy $S_N$ for $N = 6 \times 6$ **(a)** and for $N = 10 \times 10$ **(b)**. The different markers correspond to different calculation methods: the method we have used in this work (red circles), the geometrical method (blue triangles), and the original Pearson Halicioglu formula where the constraint on total momenta has not been considered (purple diamonds).

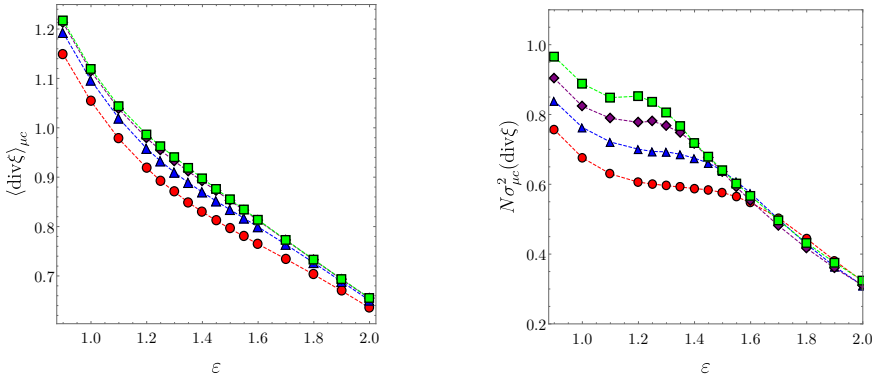


(a) (b)

Figure 5.4: Micorcanonical average of div$\xi$ **(a)** and microcanonical variance of div$\xi$ **(b)** for $N = 6 \times 6$ (red circles), $N = 10 \times 10$ (blue triangles), $N = 20 \times 20$ (purple diamonds), $N = 40 \times 40$ (green squares).

In Figure 5.4, we notice a strong qualitative and quantitative agreement between $\langle \mathrm{div}\xi \rangle_{\mu c} = T^{-1}_{\mathrm{geo}}$ and the first derivative of the specific thermodynamic entropy observed in Chapter 3 (Figure 3.2).
We notice also an asymptotic loss of differentiability of the variance of div$\xi$ as a function of the specific energy $\varepsilon$. In fact $\sigma^2_{\mu c}(\mathrm{div}\xi)$ shows a horizontal inflection point preceding the formation of a "knee" at the transition point, which becomes sharper with an increasing $N$.

In Figure 5.5, we observe a remarkable accordance between the average of the mean curvature calculated using microcanonical and geometrical measures.

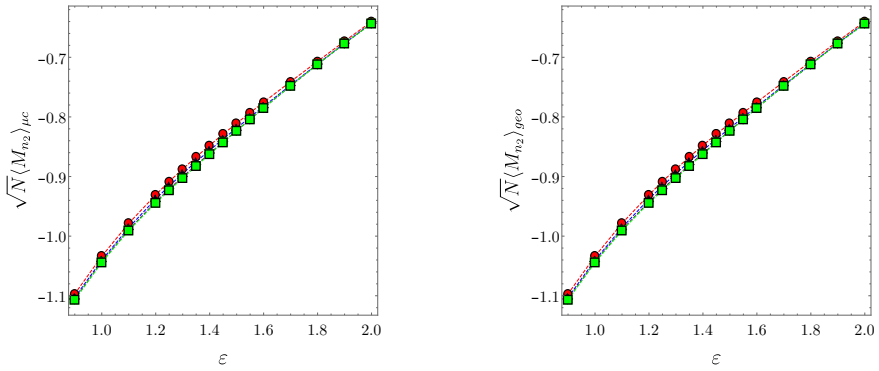


(a) (b)

Figure 5.5: Microcanonical average of mean curvature **(a)** and the geometrical average of mean curvature **(b)** for $N = 40 \times 40$ (green squares) and $N = 6 \times 6$ (red circles).

We observe also a weak change on the slop of $\sqrt{N}\,\langle M_{n_2}\rangle$ at the transition point. Since the average of the mean curvature is not an intensive observable, we add empirically the factor $\sqrt{N}$ that allows to compare the curves at different $N$. However, for the variance of the mean curvature in Figure 5.6, we observe an abrupt change on the concavity of the curve in both cases (Geometrical and microcanonical measures), which is more marked with an increasing $N$. This is interesting because it is directly related to the geometry of $\Sigma_{0,E}$.

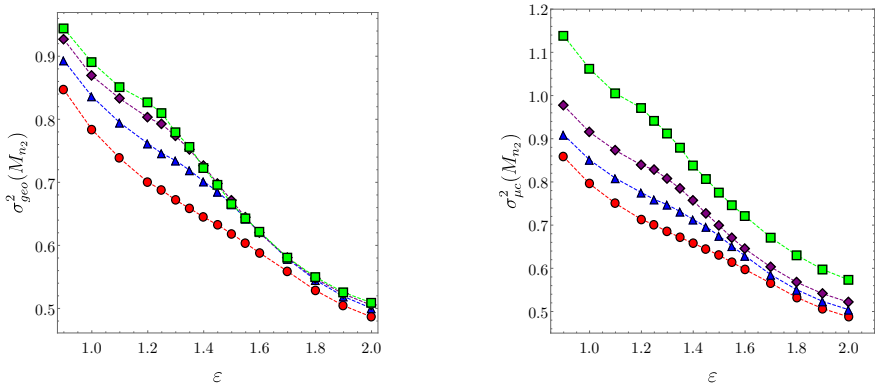


(a) (b)

Figure 5.6: Geometrical variance of the mean curvature **(a)** and microcanonical variance of the mean curvature **(b)** for $N = 6\times6$ (red circles), $N = 10\times10$ (blue triangles), $N = 20 \times 20$ (purple diamonds) and $N = 40 \times 40$ (green squares).

We recognize also in Figure 5.7 that there is an important agreement between the geometrical and microcanonical averages of the dispersion of the principal curvatures. This is the main observable we are interested in because this makes the link between geometry and topology according to Pinkall's theorem as

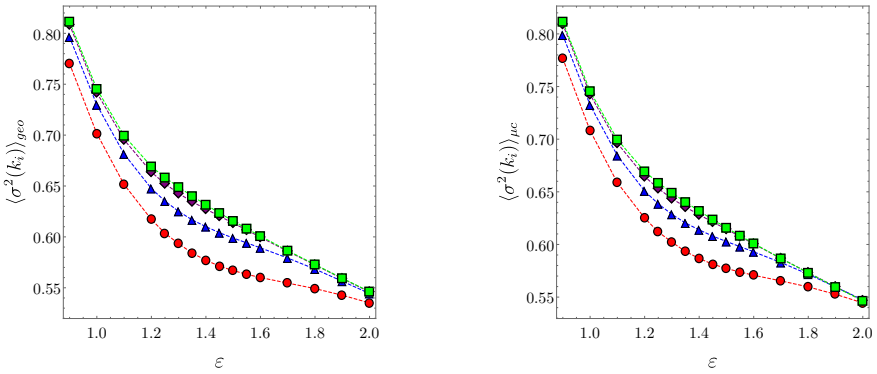


(a) (b)

Figure 5.7: Geometrical average of the dispersion of the principal curvatures **(a)** and the microcanonical average of the dispersion of the principal curvatures **(b)** for $N = 6 \times 6$ (red circles), $N = 10 \times 10$ (blue triangles), $N = 20 \times 20$ (purple diamonds) and $N = 40 \times 40$ (green squares).

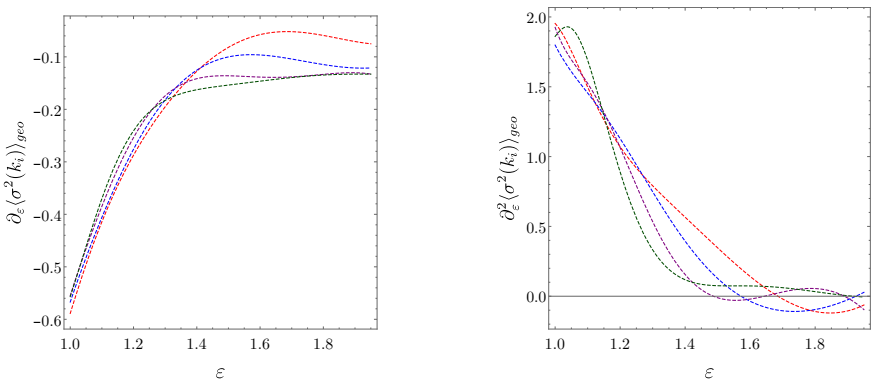


(a) (b)

Figure 5.8: First order derivative with respect to the specific energy of the geometrical average of the dispersion of the principal curvatures **(a)** and second order derivative with respect to the specific energy of the geometrical average of the dispersion of the principal curvatures **(b)** for $N = 6 \times 6$ (red), $N = 10 \times 10$ (blue), $N = 20 \times 20$ (purple) and $N = 40 \times 40$ (green).

explained in Chapter 4. We notice a sudden change in the concavity of $\langle\sigma^2(k_i)\rangle$ at the transition point which becomes sharper with an increasing $N$. We observe that such an estimator of median topology behaves linearly above the transition point and like a branch of parabola below the transition point. In order to put in evidence this point we performed an eighth-order polynomial fitting of $\langle\sigma^2(k_i)\rangle_{geo}$ as a function of the specific energy and we considered then the derivatives with respect to the specific energy of the fitted function up to the second order, presented in Figure 5.8. $\partial_\varepsilon\langle\sigma^2(k_i)\rangle_{geo}$ shows an asymptotic loss of differentiability at the transition point and the corresponding loss of continuity

is marked on $\partial_\varepsilon^2 \langle \sigma^2(k_i) \rangle_{geo}$ which is due to the presence of a steeper jump at the transition point with an increasing $N$.

## 5.4 Chapter conclusions

We have seen that $T_{geo}^{-1}$ and the thermodynamic inverse temperature are in remarkable accordance. We have also seen that for $\partial_\varepsilon S$, we observe a good agreement between the thermodynamic method developed in this work and the geometric method. Moreover, we have observed a change, either on the slope or on the concavity, of the geometrical observable curves, at the transition point. We have also observed an abrupt change in the concavity of $\langle \sigma^2(k_i) \rangle$. This suggests that the KT phase transition is a mild phase transition in the sense that we have to consider derivatives up the second order to observe a clear signal of the transition. Moreover, $\langle \sigma^2(k_i) \rangle$ is a geometrical quantity estimating topological invariants of the level sets as we have seen in Chapter 4. So, this suggests that the 2D KT phase transition has a deep and very origin in the way the topology changes with respect to the energy. In particular, as $\langle \sigma^2(k_i) \rangle$ is a geometrical estimator of the median topology, we argue that we observe a change in the rate of appearance of high dimensional holes on $\Sigma_{0,E}$ with energy. We have also seen the loss of differentiability of $\sigma_{\mu c}^2(\mathrm{div}\xi)$ in the thermodynamic limit, which is probably related to the loss of differentiability of the second order derivative of the microcanonical specific entropy. In fact, we notice that according to [123] the second order derivative of microcanonical entropy can be expressed using our notations, as follows

$$\frac{\partial^2 S_N}{\partial \varepsilon^2} = N \left[ \sigma_{\mu c}^2(\mathrm{div}\xi) + \langle \mathcal{L}_\xi \mathrm{div}\xi \rangle_{\mu c} \right] . \tag{5.46}$$

We can argue that the asymptotic loss of differentiability observed in Figure 3.2(b) has a geometrical origin in the loss of differentiability of $N\sigma_{\mu c}^2(\mathrm{div}\xi)$.

# 6

# Another example of application: the $\phi^4$ model

The work depicted here is one of our original works and can be found in Ref.[9]. Here, we will discuss two $\phi^4$ models, one with nearest neighbors and the other with mean-field interactions. The models can undergo a second-order phase transition. We will see, as done for the KT phase transitions, that the signature of the phase transition can be detected from an abrupt change in geometrical quantities defined on the energy level sets.

## 6.1 The model

In what follows two different versions of a $\phi^4$ model are considered. These are defined through nearest-neighbor interactions and through long-range interactions, respectively. These models are in some sense "paradigmatic" in that they both undergo a second-order phase transition due to the $\mathbb{Z}_2$ symmetry-breaking, the same of the 2D Ising model. The $\phi^4$ models are defined by the Hamiltonian

$$H = \sum_{\mathbf{j}} \frac{1}{2}\pi_{\mathbf{j}}^2 + V(\phi) \tag{6.1}$$

where

$$V(\phi) = \sum_{\mathbf{j}} \left[ \frac{\lambda}{4!}\phi_{\mathbf{j}}^4 - \frac{\mu^2}{2}\phi_{\mathbf{j}}^2 + \frac{J}{D} \sum_{\mathbf{k}\in I(\mathbf{j})} (\phi_{\mathbf{j}} - \phi_{\mathbf{k}})^2 \right] , \tag{6.2}$$

$\pi_{\mathbf{j}}$ is the conjugate momentum of the variable $\phi_{\mathbf{j}}$ that defines the position of the $\mathbf{j}^{th}$ particle. In the case of the two-dimensional model, $\mathbf{j} = (j_1, j_2)$ denotes a site of a two dimensional lattice, the number of nearest neighbors is $D = 4$ and $I(\mathbf{j})$ are the nearest neighbour lattice sites of the $\mathbf{j}^{th}$ site. The coordinates of the sites are integer numbers $j_k = 1, \ldots, N_k$, $k = 1, 2$, so that the total number of sites in the lattice is $N = N_1\, N_2$. Furthermore periodic boundary conditions are assumed. In the case of the mean-field model $\mathbf{j} = 1, \ldots, N$ denotes the indices of the $2N$ canonical coordinates of the system, $D = N - 1$ and $I(\mathbf{j}) = 1, \ldots, N$.

The Hamiltonian equations of motion read

$$\begin{aligned} \dot{\phi}_{\mathbf{j}} &= \pi_{\mathbf{j}} \,, \\ \dot{\pi}_{\mathbf{j}} &= -\frac{\partial V}{\partial \phi_{\mathbf{j}}} \end{aligned} \quad . \tag{6.3}$$

The local potential displays a double-well shape whose minima are located at $\pm\sqrt{3!\mu^2/\lambda}$ and to which it corresponds the ground-state energy per particle $e_0 = -3!\mu^4/(2\lambda)$. At low energies, the system is dominated by an ordered phase where the time averages of the local fields are not vanishing. By increasing the system energy the local $\mathbb{Z}_2$ symmetry is restored and the averages of the local fields are zero.

### 2-d $\phi^4$ model.

In the case of the two-dimensional model, we have[1]

$$\Delta H = N(1 + 4J - \mu^2) + \frac{\lambda}{2!}\|\phi\|^2 \,, \tag{6.4}$$

where $\|\phi\| = \sqrt{\sum_{\mathbf{j}} \phi_{\mathbf{j}}^2}$. In addition, it results

$$\|\nabla H\| = \sqrt{2K + \|\nabla V\|^2} \,, \tag{6.5}$$

where $K$ stands for the total kinetic energy $K = \sum_{\mathbf{j}} \pi_{\mathbf{j}}^2/2$ and

$$\nabla_{\mathbf{k}} V = \frac{\lambda}{3!}\phi_{\mathbf{k}}^3 + (4J - \mu^2)\phi_{\mathbf{k}} - J \sum_{\mathbf{j}\in I(\mathbf{k})} \phi_{\mathbf{j}} \,. \tag{6.6}$$

The Hessian matrix of the Hamiltonian function is

$$\mathcal{H} = \begin{pmatrix} \mathbb{1} & 0 \\ 0 & \mathcal{H}_V \end{pmatrix} , \tag{6.7}$$

where the entries of the Hessian matrix $\mathcal{H}_V$ of the potential function $V$ result

$$(\mathcal{H}_V)_{\mathbf{ij}} = \partial^2_{\mathbf{ij}} V = \left(\frac{\lambda}{2!}\phi_{\mathbf{j}}^2 + 4J - \mu^2\right)\delta_{\mathbf{i},\mathbf{j}} - J\delta_{\mathbf{j},I(\mathbf{i})} \,.$$

Finally, it is

$$\partial^3_{\mathbf{ijk}} V = \lambda \delta_{\mathbf{i},\mathbf{j}} \delta_{\mathbf{j},\mathbf{k}} \phi_{\mathbf{j}} \,.$$

[1] From Eq.(6.1), we have

$$\partial_{\pi_{\mathbf{k}}} H = \sum_{\mathbf{j}} \pi_{\mathbf{j}} \delta_{\mathbf{jk}} = \pi_{\mathbf{k}} \quad \Rightarrow \quad \partial^2_{\pi_{\mathbf{k}}\pi_{\mathbf{k}}} H = 1 \,.$$

Thus, we have

$$\frac{\partial H}{\partial \phi_{\mathbf{k}}} = \frac{\partial V}{\partial \phi_{\mathbf{k}}} \,,$$

and

$$\frac{\partial^2 H}{\partial \phi_{\mathbf{k}}^2} = 4J - \mu^2 + \frac{\lambda}{2!}\phi_{\mathbf{k}}^2 \quad \Rightarrow \quad \Delta H = N(1 + 4J - \mu^2) + \frac{\lambda}{2!}\|\phi\|^2 \,.$$

### Mean-field $\phi^4$ model.

The analogous quantities for the case of the mean-field model are the following. $\Delta H$ has the same form of (6.4), whereas

$$\nabla_{\mathbf{k}} V = \frac{\lambda}{3!}\phi_{\mathbf{k}}^3 + \left[4J\frac{N}{N-1} - \mu^2\right]\phi_{\mathbf{k}} - \frac{4J}{N-1}\mathcal{M}\,, \tag{6.8}$$

where we have introduced the total magnetization

$$\mathcal{M} = |\sum_{\mathbf{j}} \phi_{\mathbf{j}}|\,. \tag{6.9}$$

In this case the Hessian matrix $\mathcal{H}_V$ of the potential function $V$ is

$$(\mathcal{H}_V)_{\mathbf{ij}} = \partial^2_{\mathbf{ij}} V = \left[\frac{\lambda}{2!}\phi_{\mathbf{j}}^2 + 4J\frac{N}{N-1} - \mu^2\right]\delta_{\mathbf{i,j}} - \frac{4J}{N-1}\,,$$

and $\partial^3_{\mathbf{ijk}} V$ has the same form of the 2−d case.

## 6.2 Numerical results

As we did for the KT phase transition, we have derived the caloric curve $T(E)$ and the specific heat $C_v(E)$ of the two models. In addition to the thermodynamic quantities, we have measured geometric quantities as the average of the Ricci curvature $K_R(q, \dot{q})$ (see Appenix B for details). The main outcome of our analysis is the better effectiveness of the geometric indicators as phase-transitions detectors with respect to the traditional thermodynamic indicators, with the exception of the order parameter. In a recent paper [122], by resorting to geometric indicators, it has been possible to unambiguously characterize and explain the phenomenology of a system that undergoes a thermodynamic phase transition in the absence of a global symmetry-breaking and thus in the absence of an order parameter.

### 2-d $\phi^4$ model

In this section, we report the results of the simulations performed for the $2d$ $\phi^4$ model (with nearest-neighbor interactions). The order parameter $M = \langle\mathcal{M}\rangle/N$ - an average of the total magnetization $\mathcal{M}$ defined in (6.9) - is reported as a function of the energy density $\epsilon = E/N$ in Fig.6.1: the bifurcation pattern of $M(E/N)$ is typical of a second-order phase transition.

Figure 6.1 allows one to determine the critical energy density $\epsilon_c$ of the phase-transition, which is found to be $\epsilon_c \approx 11.1$.

As seen for the KT phase transition, a typical signature of a phase transition is provided by the shape of the caloric curve $T(E)$, i.e. the temperature as a function of the energy. The caloric curve of the $2d$ $\phi^4$ model is reported in Fig.6.2. We clearly see that it displays an inflection point just at the critical energy density value identified by the bifurcation point of the order parameter - highlighted with the vertical dashed line in Fig. 6.2 - and this is in perfect agreement with the proposition proposed by Bachmann [133]

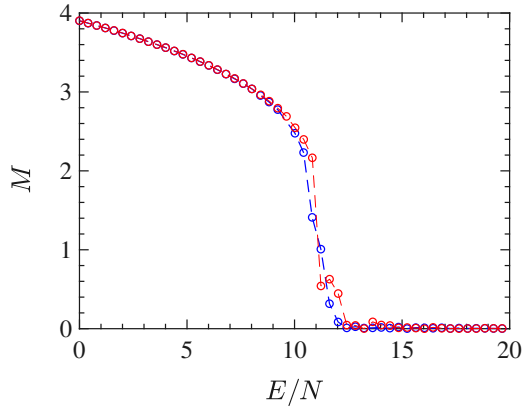


Figure 6.1: The figure shows the plot of the quantity order parameter $M$ vs the energy density $E/N$ for $128 \times 128$ particles (blue circles) and $48 \times 48$ particles (red circles).

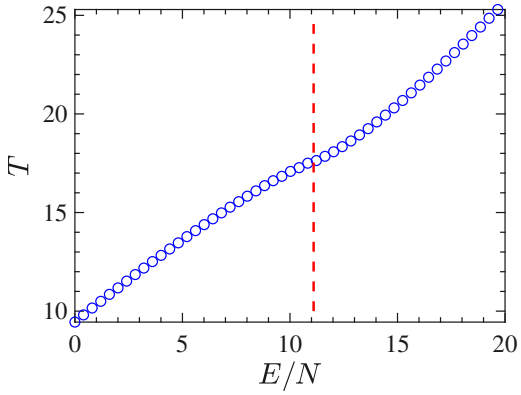


Figure 6.2: The figure reports the temperature, as a function of $E/N$ for the $2-d$ $\phi^4$ model for $128 \times 128$ particles.

In Fig.6.3, the curve of the inverse temperature $\beta$ as a function of $E/N$ shows an inflection point, located by the dashed vertical line.

The expected growth with the system size, of the peak of the specific heat in correspondence with the phase-transition is shown in Fig. 6.4. The curve of the specific heat $C_V$ vs the energy-density $E/N$ has been computed for different lattice sizes, that is, $24 \times 24$ sites (open circles), $48 \times 48$ sites (open squares) and $128 \times 128$ sites (crosses).

Fig. 6.5 reports the second derivative of the entropy with respect to the energy $E$. As mentioned above, the divergence of the specific heat stems from the vanishing of this derivative. This figure displays the outcomes of a numerical derivation of the curve $\beta(E)$ obtained for systems of different sizes: $24 \times 24$ lattice sites (open circles), and $48 \times 48$ lattice sites (crosses). In addition, Fig. 6.5 reports the values of $N\partial^2 S/\partial E^2$ vs $E/N$ in the case of a system with $24 \times 24$

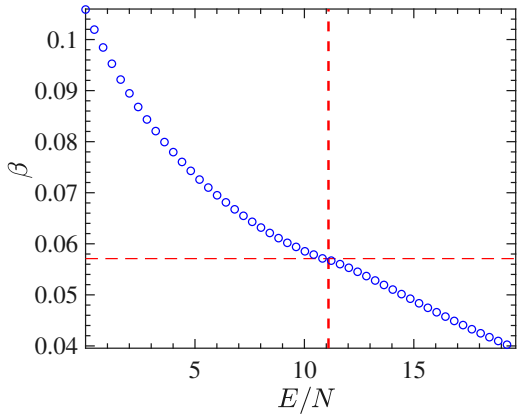


Figure 6.3: $\beta$ vs $E/N$ in the case of the $2d$-$\phi^4$ model with $128 \times 128$ particles.

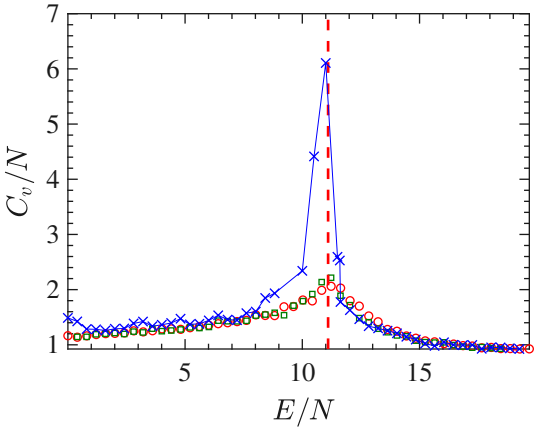


Figure 6.4: $C_v/N$ vs $E/N$. The lattice sizes are: $24 \times 24$ (open circles), $48 \times 48$ (open squares) and $128 \times 128$ (crosses).

(open squares), $48 \times 48$ (full circles) and $128 \times 128$ (stars) lattice sizes. The figure shows distinctly the transition point, corresponding to a discontinuity of the fourth order of the derivative of $S$.

In Figure 6.6 the curve $\langle \triangle H \rangle / N$ vs $E/N$ is reported, that is the time average of the Laplacian of the Hamiltonian function per degree of freedom, and again it clearly shows an inflection point at the transition energy density. The quantity $\langle \triangle H \rangle / N$ has a geometric meaning but of a different kind with respect to those related to the extrinsic curvature of the energy level sets. In fact, as shown in Appendix B, it turns out that the Laplacian of the Hamiltonian [in Eq.(B.15)] coincides, apart from a constant, with the Ricci-curvature of a Riemannian manifold, an enlarged configurational space-time endowed with a metric due to Eisenhart [123, 52]. The geodesics of this manifold are just the natural motions of the Newton equations associated with the Hamiltonian of the system.

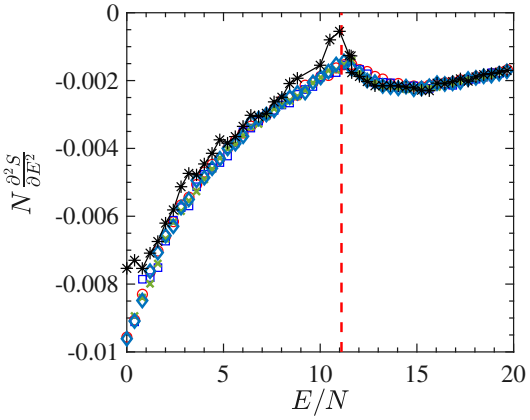


Figure 6.5: $N\partial^2 S/\partial E^2$ vs $E/N$ derived with a numeric derivative of the curve $\beta(E/N)$. Symbols refer to $24 \times 24$ (open squares), $48 \times 48$ (full circles) and $128 \times 128$ (stars) lattice sizes, respectively.

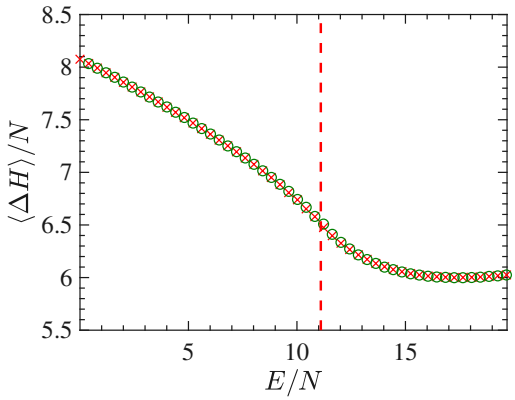


Figure 6.6: Figure reports the time average of $\Delta H/N$ as a function of $E/N$ in the case of a system with $24 \times 24$ lattice sites.

### Mean-field $\phi^4$ model

In the present section, we report the results of the numerical simulations performed for the mean-field $\phi^4$ model. Also, this model undergoes a second-order phase transition which is clearly displayed by the bifurcation of the order parameter $M = \langle \mathcal{M} \rangle / N$, the magnetization, versus the energy density $\epsilon = E/N$, as is shown in Figure 6.7 where the critical energy density of the phase transition point is found to be $\epsilon_c \approx 25$.

With respect to the $2d$ model, the long-range interactions make this system harder to simulate. In fact, considerable difficulties have been encountered in computing stabilized time averages of the same quantities computed for the $\phi^4$ model with short-range interactions. These difficulties depend on the worsening of the properties of self-averaging of this model for energy values close to the transition point, clearly due to the long-range interactions. Besides that, and again except for the order parameter, the mean-field model undergoes a phase

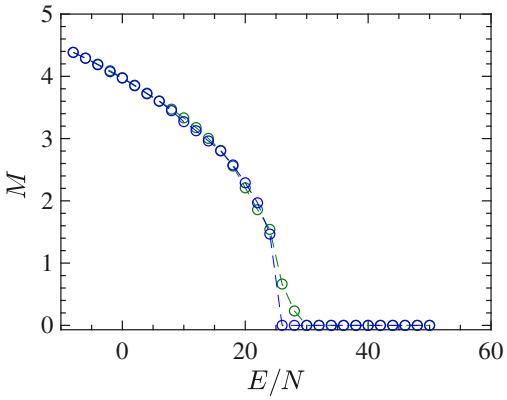


Figure 6.7: The order parameter $M$ for the mean-field $\phi^4$ model is reported vs $E/N$ for 1024 particles (green circles) and 2048 particles (blue circles).

transition that appears much "softer" than the one undergone by the $2d$ model. This fact is put in evidence by the basic thermodynamic functions $T(E/N)$

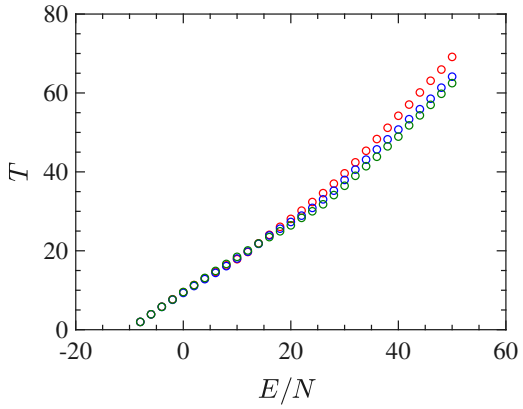


Figure 6.8: $T$ vs $E/N$ for the mean-field $\phi^4$ model. $N = 4096$ red circles, $N = 2048$ blue circles, $N = 1024$ green circles.

and $\beta(E/N)$, reported in Figures 6.8 and 6.9, respectively. In particular the curve $\beta(E/N)$ does not display at all any feature to identify the presence of a transition. All in all, these functions are not very helpful neither to clearly identify the presence of a phase transition nor, possibly, its transition point.

In Figure 6.10 we report the derivative $N\partial^2 S/\partial E^2$ as a function of $E/N$ worked out in the same way as previously done for the short-range model. The energy density pattern of this derivative is found to be very noisy, even after many millions of integration time steps, and this goes together with a very bad outcome for the specific heat, which, on purpose, is not reported here.

To the contrary, and together with the order parameter, Figure 6.11 shows an interesting pattern of the time average of the Ricci curvature of the mechanical

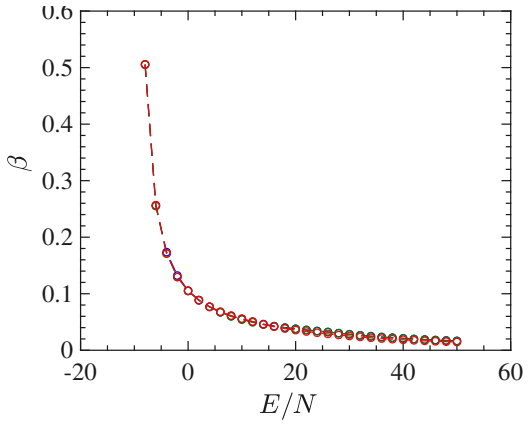


Figure 6.9: The figure shows the curve $\beta$ vs $E/N$ for the mean-field $\phi^4$ model. $N = 4096$ red circles, $N = 2048$ blue circles, $N = 1024$ green circles.

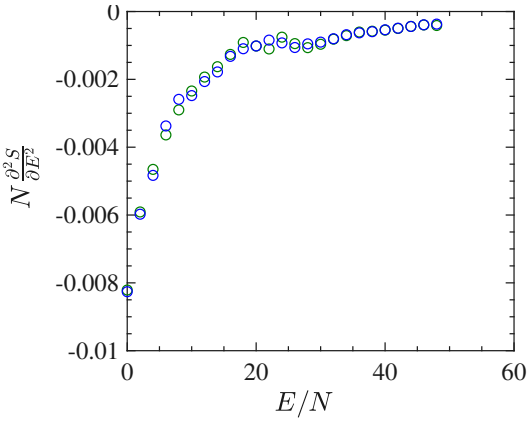


Figure 6.10: The figure shows the plot of the quantity $N\partial^2 S/\partial E^2$ vs $E/N$ derived with a numeric derivative of the curve $\beta(E)$ for 1025 particles.

manifold $(M \times \mathbb{R}^2, g_e)$ (see Appendix B) as a function of the energy density. The pattern of $\langle \Delta H \rangle (E/N)/N$ displays a "cuspy" point in correspondence with the vertical red dashed line locating the phase transition point. Of course, within the obvious limits of numerical outcomes, such a "cuspy" point appears as an abrupt change of the second derivative of the Ricci curvature - with respect to the energy - because above the transition point, its pattern appears convex (of positive second derivative), whereas just below the transition point the values of the Ricci curvature appear to align along a straight segment, thus with a vanishing second derivative. Loosely speaking, this is reminiscent of similar jumps of the second derivative with respect to the energy of an average curvature function which has been found for a gauge model [122].

## 6.3 Chapter conclusions

We have considered the second-order phase transitions stemming from the same kind of $\mathbb{Z}_2$ symmetry-breaking phenomenon occurring in two $\phi^4$ models.

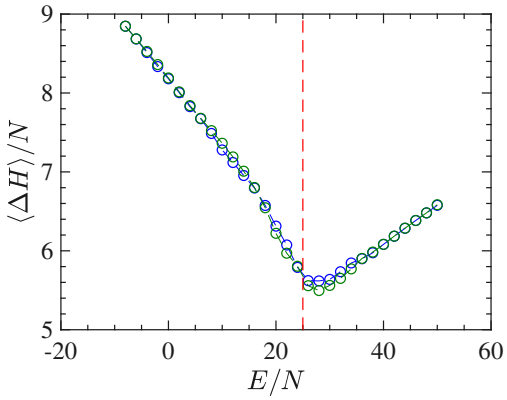


Figure 6.11: The figure shows the plot of the quantity $\langle \Delta H \rangle / N$ vs $E/N$ for 1024 particles (green circles) and 2048 particles (blue circles).

Besides the standard detection of the presence of a phase transition through the bifurcation of an order parameter, we have focused on basic geometric properties of different manifolds, highlighting that the values of thermodynamic observables, like temperature and specific heat, and their functional dependence on the energy are the consequences of more fundamental changes with the energy of curvature properties of the energy level sets in phase space. The conceptual interest of this fact is that a phase transition phenomenon can be seen as just depending on the interaction potential of the forces acting among the degrees of freedom of a system, that is, the possibility for a system of undergoing a phase transition is already "encoded" in its Hamiltonian function and thus can be read in the variation of some extrinsic curvature properties of the hypersurfaces $H(p, q) = E$ foliating the phase space. When the variations with energy in the geometry of these level-set manifolds are too "mild", as is the case of the mean-field $\phi^4$ model, one can again recover a rather sharp geometric signature of the transition by considering the energy variation of the Ricci curvature of a manifold the geodesics of which are the motions of the system. In other words, in both cases, a phase transition phenomenon can be seen as stemming from a deeper level than the usual one which consists of attributing them to a loss of analyticity of the statistical measures in the thermodynamic limit. The statistical measures represent an "epistemic" description of the occurrence of phase transitions, in which statistical measures do not correspond to physically measurable entities, whereas the forces acting among the degrees of freedom of a system belong to an "ontic" level because forces are real physical entities, velocities of the kinetic energy and potentials can be in principle measured so that for energy conserving closed system the quantities entering the relation $H(p, q) = E$ are real physical ones.

Finally, since geometric indicators, like the Ricci curvature, are independent of the order parameter among the other thermodynamic quantities, the proposed geometric analysis can be applied also in the case of systems that undergo phase transitions in absence of a global symmetry breaking and thus in the absence of an order parameter.

# 7

# Conclusion of part I

In this part, different aspects of the 2D KT phase transition are studied. On the one side, the study of the microcanonical thermodynamics of the XY 2D model is granted to detect and classify the KT phase transition at finite $N$, and to generalize it to the thermodynamic limit. On the other side, the topological and geometrical characterization of the submanifolds $\Sigma_{p,E} = \{x \in \Lambda \mid P(x) = 0 \ \wedge \ H(x) = E\}$ allowed to predict the KT phase transition and at any finite N. Moreover, We studied the phase transition occurring in the $\phi^4$ model, using the geometrical and topological scheme.

At the end of this investigation, we have obtained the following results:

- The development of the Laplace transform technique to calculate the derivatives of the microcanonical specific entropy with respect to the specific energy up to the fourth order and in *presence of the constraint* $P = 0$ for the total momentum of the system.
- Through the study of the microcanonical thermodynamics of the KT phase transition in 2D model, we conclude that it is a second order phase transition, both according to a classification recently proposed by Bachmann[133] and extended microcanonical classification *à la* Ehrenfest, discussed in Chapter 3.
- We rephrase the microcanonical thermodynamics for systems with conserved total momentum in terms of the Riemannian geometry of energy-total momentum level sets $\Sigma_{E,p}$ in phase space $\Lambda$ endowed with Euclidian metric.
- We numerically verified that the first order derivative of the microcanonical entropy calculated both with our Laplace transform technique and with the geometrical method are in full agreement.
- We showed how to calculate a geometrical estimator of the median topology of $\Sigma_{E,p}$ thanks to the Pinkall inequality, i.e. the geometrical average of the dispersion of the principal curvatures $\langle \sigma^2(k_i) \rangle$ of $\Sigma_{0,E}$.
- We found the *geometrical origin* of KT phase transition in the change, either on the slope or on the concavity, of the geometrical observable curves (the average and the variance of the extrinsic mean curvature, the

divergence of the vector field $\xi$ generating the diffeomorphism among the level sets $\Sigma_{0,E}$, etc.), at the transition point.

- We found convincing evidence that the 2D KT phase transition has *the deep and very origin in a topological change of the submanifolds* $\Sigma_{0,E}$ signaled by the abrupt change of the concavity of $\langle \sigma^2(k_i) \rangle$. In fact, what we observed might be interpreted as a change in the rate of appearance of high dimensional holes of $\Sigma_{0,E}$ with energy at the transition point.

- The proposed geometrical analysis has been also fruitful in the study of the $\phi^4$ model example since all the studied geometrical quantities were found to have an abrupt change at the phase transition.

# PART II

# Geometrical characterization of quantum entanglement

# 1

# Introduction of part II

In this part of the thesis, we will characterize quantum entanglement through the study of projective Hilbert spaces. Quantum entanglement is one of the most subtle and intriguing phenomena in nature. It is a quantum mechanical phenomenon in which quantum states shared between two or more parties cannot be described as separated states, even if the parties are spatially separated. This leads to correlations between observable physical properties of the systems. The potential usefulness of quantum entanglement has been demonstrated in various applications such as quantum teleportation, quantum cryptography, and quantum dense coding. Despite its key role, entanglement remains elusive and the problem of its characterization and quantification is still open [147, 69].

Quantum mechanics is grounded in a formalism in which the states of a quantum system are vectors in a complex Hilbert space $\mathcal{H}$. Nonetheless, it is well-known that such a formulation is redundant since vectors differing only in normalization and global phase are physically equivalent [11]. The use of this equivalence relation leads to the space where quantum states live in complex projective Hilbert spaces $P(\mathcal{H})$. A famous example of a projective Hilbert space is the Bloch sphere, which is actually a natural way of introducing the notion of a qubit [114], that is at the same time also a standard tool in the study of the polarization of photons [143]. The concept of distance in this space was first introduced via the Fubini Study metric by Provost and Vallee in [132], where they have shown that the distance between nearby states is related to quantum fluctuations.

The goal of this part of the thesis is to show that despite the fact that quantum states live in a strange and abstract projective Hilbert space, it is possible to speak of its geometry and extract valuable information from it through the Fubini Study metric. In fact, we will construct an entanglement measure for pure and mixed states from an adapted application of the Fubini Study metric. This part will depict our original work on quantum entanglement and quantum correlation done in Ref.[41] and Ref.[154]. In **Chapter 2**, we will tackle some important concepts of projective Hilbert spaces. In **Chapter 3** we will review some basic concepts of quantum entanglement. Then, in **Chapter 4**, we will illustrate the procedure that led us to the construction of an entanglement measure for multipartite pure states. We named the proposed entanglement measure *entanglement distance*. Next, in **Chapter 5**, we will

talk about the physical interpretation of the entanglement distance. This will be important for the analysis that will be done in **Chapter 6** of the examples of application of the proposed measure. In **Chapter 7**, we extend the proposed entanglement measure to mixed multipartite states. We will illustrate how we have constructed a quantum correlation measure for multipartite mixed states, which led us to the construction of an entanglement measure for mixed states. And finally, in **Chapter 8**, we will apply these both measures to some examples of mixed states, to show the validity of the proposed measures.

# 2

# Review of projective Hilbert spaces

In this Chapter, we review some notions of projective geometry. We will first start by giving a general definition of projective spaces in section 2.1. Then, in Section 2.2, we will give an example of a projective space, that is the projective Hilbert space. At the end of this chapter, we will briefly discuss the Fubini study metric, which is a metric that can be endowed in the projective Hilbert space

## 2.1 What is a projective space?

In Euclidean Geometry two distinct lines intersect unless they are parallel. In the setup of projective geometry, one enlarges the geometric setup by claiming that two distinct lines will always intersect. Even if they are parallel they have an intersection. One of the easiest examples to illustrate a projective space is the road (see Figure 2.1) that becomes narrower as it moves away from the observer's eye. Euclidean geometry alone will not be able to describe this. In

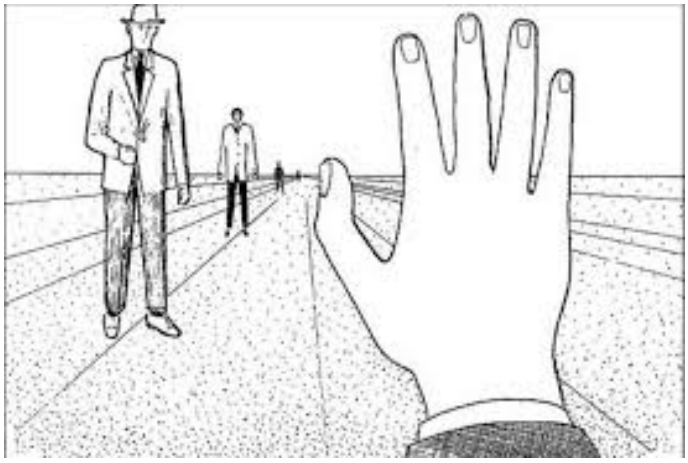

Figure 2.1: Parallel lines seem to intersect at infinity at a vanishing point.

fact, the two parallel lines forming the road intersect at a vanishing point at infinity. Euclidean geometry is thus not sufficient to describe the geometry in projective space. Actually, Euclidean geometry is a subset of projective geometry.

Projective geometry was invented shortly after Renaissance painters invented perspective geometry to project and paint the world as it is in a realistic way. To create a faithful image of the three-dimensional world, perspective geometry provided a theoretical explanation of a basic empirical fact about vision; namely, when we see parallel lines it generally looks as if they meet at some point very far away on the horizon. This led to the establishment of some fundamental rules for perspective drawing by Renaissance artists

(1) The image of a straight line is a straight line.

(2) Each family of parallel lines converges towards a vanishing point.

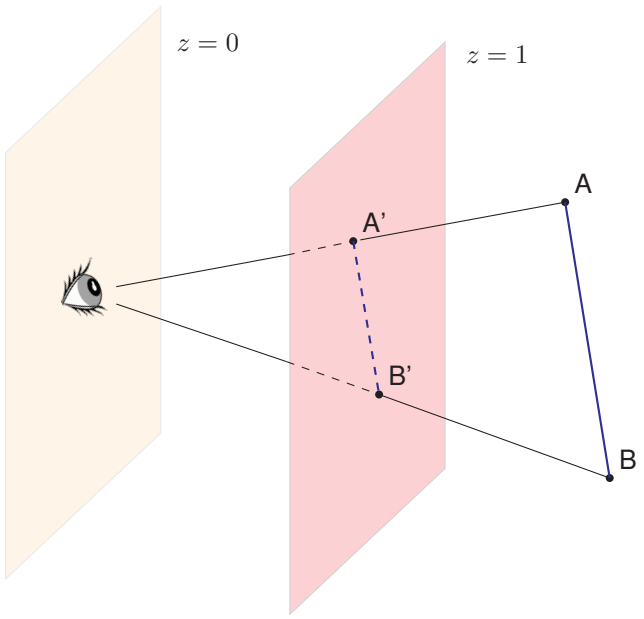


Figure 2.2: One point perspective

An example of the first rule is applied in Figure 2.2. The straight line $(AB)$ is projected into a straight line $(A'B')$ to the $z = 1$ plane which symbolizes the painter's canvas. Another way to consider the first rule is the following: the projected line $(A'B')$ is merely the result of the intersection of the plane $z = 1$ and the plane passing from the observer's eye and containing $(AB)$. Another thing to note is that points lying on the plane $z = 0$ do not have images, since they are invisible to the observer's eye. The line that crosses the points $A$ and $A'$ (or $B$ and $B'$) is actually a light ray that enters the eye's observer.

The second rule can be understood by taking the following example: suppose we want to represent in perspective a square tiling, for instance of a floor (see Figure 2.3). Suppose a painter is standing straight in front of a square tile. The floor is underneath him and he wants to paint what he sees. To include depth in his image, he cannot merely paint the square tiling with parallel lines in figure 2.3. Instead, he must first draw the horizon line as in Figure 2.4, which will depend on the tilt of his head then he has to find the vanishing points to which families of parallel lines converge. For example in Figure 2.4, the parallel lines

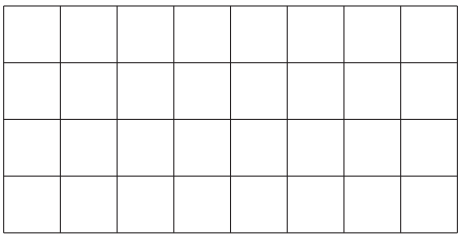

Figure 2.3: Euclidean vision of a square tiling

on the floor that are facing the painter converge into a single vanishing point (in black) at the Horizon. Whereas, the diagonals of the squares (in red) converge towards another vanishing point. The horizon added by the artist is a line that he seems to see very far from him. This means that the squares in front of him are not very distorted, unlike the ones far away from him. Without the horizon, the parallel lines would not be converging. It is as if, the artist added a line at infinity to his canvas to which each family of parallel lines converges. Thus, we say that the painter's canvas is no longer a Euclidean plane. It is a projective space because the line at infinity added completes the Euclidean flat plane on which the painter was painting. The space is now richer than an ordinary Euclidean space, because, every two parallel lines intersect at a point. More precisely, the Canvas is said to be a projective real plane, generally denoted as follows $P\left(\mathbb{R}^2\right) \equiv \mathbb{R}P^2$.

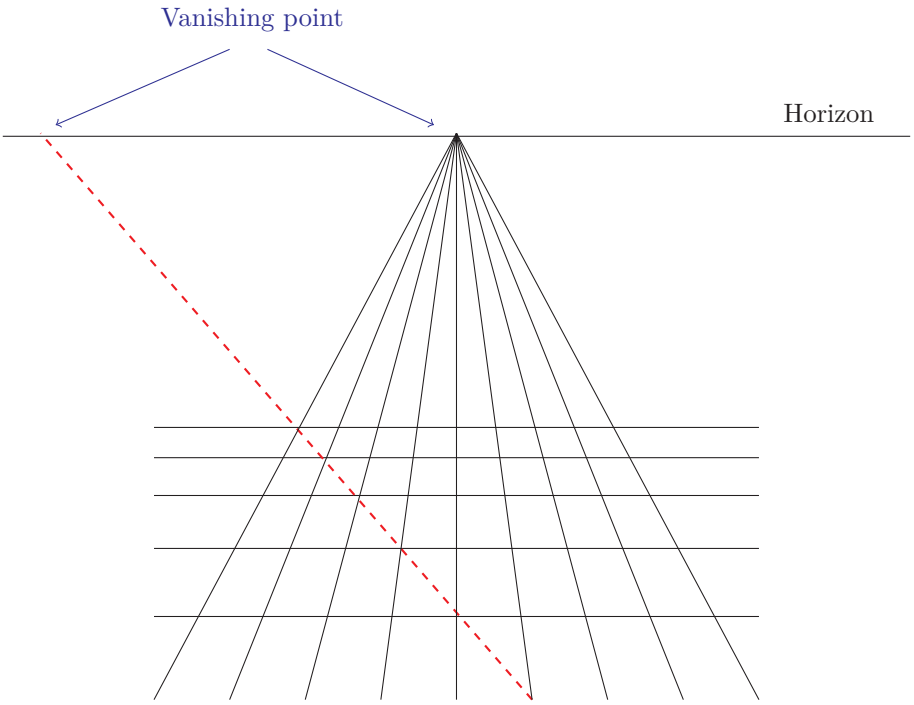


Figure 2.4: Projective vision of a square tiling

We can thus represent a projective real plane as in Figure 2.5, where we have added a line at infinity and where each family of parallel lines converges towards a point belonging to that line. We can think of the line at infinity as the horizon line added to the Canvas by a painter. However, in the early 1800,

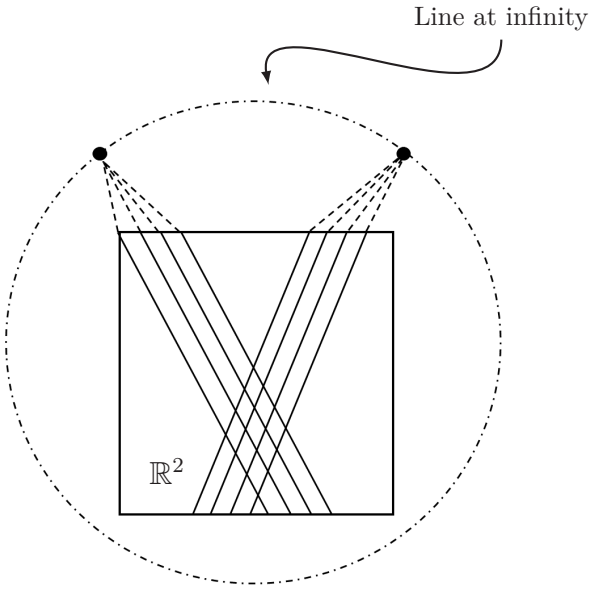


$\mathbb{R}P^2$

Figure 2.5: Real projective plane

a completely new way of thinking about the projective plane was introduced, which completely changed the direction of the subject and introduced new kinds of ideas and techniques. It was the idea of describing the projective spaces with homogeneous coordinates that was introduced by August Ferdinand Möbius in 1827 [115, 145]. In this version of the projective plane, points are lines through the origin in $\mathbb{R}^3 \setminus \{0\}$ for reasons that will become clear in a while. To see that this representation of the projective plane is equivalent to the one given in Figure 2.5, let us use the embedding of $\mathbb{R}^2$ in $\mathbb{R}^3$, see Figure 2.6. One point in $\mathbb{R}^2$ is given by the intersection of a line through the origin in $\mathbb{R}^3$. The ad-hoc points at infinity added to $\mathbb{R}^2$ in Figure 2.5 are now given by the lines in the $xy$ plane, in Figure 2.6, that are parallel to $\mathbb{R}^2$, since a parallel line meets $\mathbb{R}^2$ at infinity. Each line is actually extended to infinity in both directions so, to avoid confusion, we use the word *ray*, rather than line through the origin. The ray is not an object composed of a large number of points, we have to think of it as a single object, representing a single projective point. The projective space in this representation is parameterized by lines through the origin. A line is determined by two points, so a line through the origin is determined by any nonzero vector. For this reason, we say that the projective plane is the set of rays in $\mathbb{R}^3 \setminus \{(0,0,0)\}$, which is written in a shortened form as $\mathbb{R}^3 \setminus \{0\}$. Since all rays that are not parallel to $\mathbb{R}^2$ intersect it, we conclude that there is a one-to-one correspondence between points in $\mathbb{R}^2$ and the rays that are not

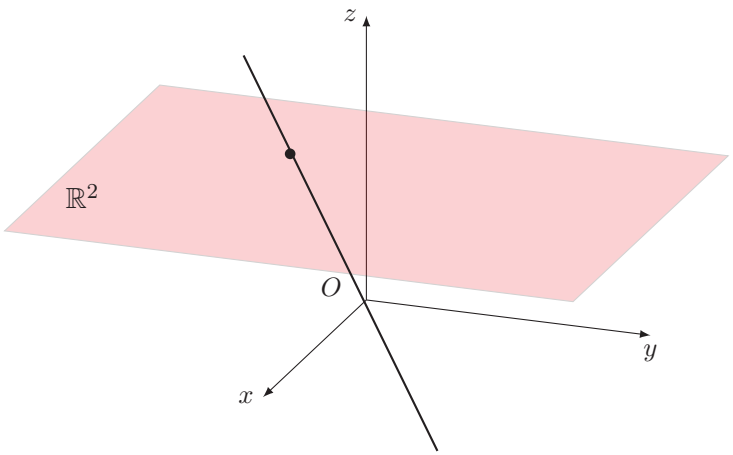


Figure 2.6: Embedding of $\mathbb{R}^2$ in $\mathbb{R}^3$

parallel to $\mathbb{R}^2$. And, rays at the origin are in one-to-one correspondence with the directions of parallel lines in $\mathbb{R}^2$. To see this, we must remember that a ray is the result of the intersection of two planes. Thus, a ray in the $xy$ plane (at the origin) is the intersection of the $xy$ plane and a plane passing through it. As a result, a ray in the $xy$ plane is in a one-to-one correspondence with a line in Euclidean space, see Figure 2.7.

We can organize all these lines defined in all directions by introducing homogeneous coordinates (also called projective coordinates). Suppose a plane,

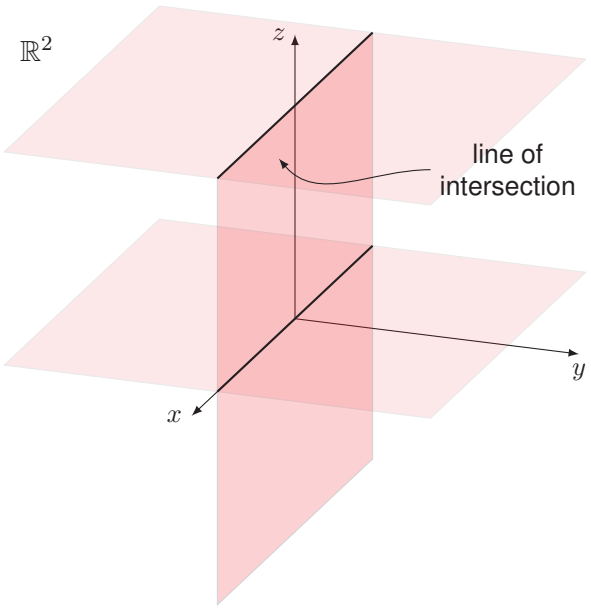


Figure 2.7: Rays in the $xy$ plane are in one-to-one correspondence with directions in the Euclidean space.

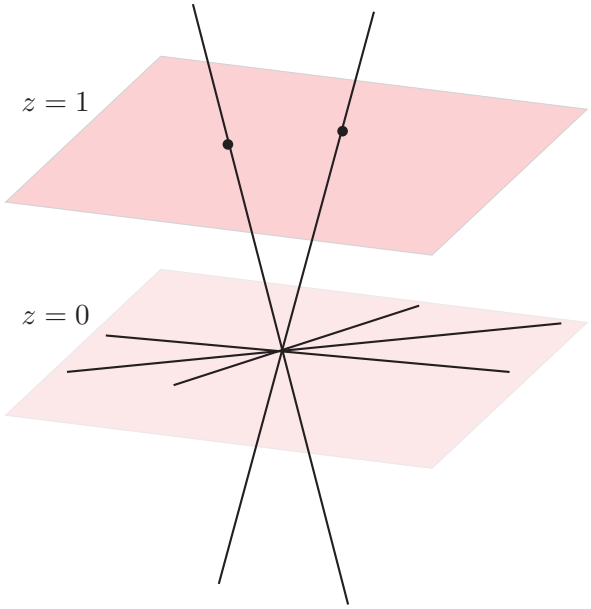


Figure 2.8: Homogeneous coordinates

for example, the $z = 1$ plane (Figure 2.8). Then, most of the rays will meet this plane at a point. The only rays which are not going to intersect with the $z = 1$ plane are the ones that are lying in the $z = 0$ plane. In this representation, we are actually using a vector space construction of the projective plane, since we can represent a ray by a vector through the origin in $\mathbb{R}^3$. Thus, any ray can be described by a vector $\vec{v} = (x, y, z)$, and any multiple of this vector is given by $\lambda\vec{v}$. It is especially interesting to choose $\lambda$ such that the $z$ coordinate of the new vector is equal to 1, that is $\vec{v}' = \lambda\vec{v} = (x', y', 1)$, and this means that $\lambda$ has to be equal to $1/z$. Therefore, the new vector must be $\vec{v}' = (x/z, y/z, 1)$. We can conclude that the line trough $\vec{v} = (x, y, z)$ has Euclidean coordinates $(X = x/z, Y = y/z)$. So, this is a way of transferring from a 3-dimensional scale-invariant, using homogeneous coordinates, to the 2-dimensional description, using the ordinary Cartesian coordinates, i.e.

$$\underbrace{\begin{pmatrix} x \\ y \\ z \end{pmatrix}}_{\text{Homogeneous coordinates}} \longrightarrow \underbrace{\begin{pmatrix} X = x/z \\ \\ Y = y/z \end{pmatrix}}_{\text{Affine coordinates}} . \tag{2.1}$$

Rays from the origin which are not horizontal can intersect a given plane at a point $(x, y, z)$ and intersect another plane at another point that can be obtained by scaling $(x, y, z)$. Meaning that rays are exactly in one-to-one correspondence with points in the Cartesian plane. On the other hand, the horizontal rays at $z = 0$ correspond to points at infinity in the Cartesian plane (since a given horizontal ray intersects a Cartesian plane in an ideal point at infinity). This can be seen as follows: a point in Cartesian coordinates $(1, 2)$, becomes $(1, 2, 1)$ in homogeneous coordinates. If a point $(1, 2)$ moves towards infinity it becomes $(\infty, \infty)$ in Cartesian coordinates and $(1, 2, 0)$ in homogeneous coordinates.

More formally, a projective space in any dimension can be defined as follows [168, 45]

**Definition 2.1.** *Let $\mathbb{F}$ be a field and let $\mathbf{V}$ be a finite-dimensional $\mathbb{F}$-vector space. The projective space of $\mathbf{V}$ denoted $P(\mathbf{V})$ is the set of one-dimensional vector subspaces of $\mathbf{V}$*

$$P(\mathbf{V}) = \{\mathbf{V} \setminus \{0\} / (v \sim \lambda v), \quad \lambda \in \mathbb{F}^*\}, \tag{2.2}$$

*where $v \in \mathbf{V}$.*

If $\dim \mathbf{V} = n+1$, then $\dim P(\mathbf{V}) = n$. If we fix a basis $\{e_0, \cdots, e_n\}$ of $\mathbf{V}$, then $\mathbf{V} \cong \mathbb{F}^{n+1}$, we denote $P\left(\mathbb{F}^{n+1}\right) = P^n\mathbb{F} = \mathbb{F}P^n$. Fixing a basis $\{e_0, \cdots, e_n\}$ yields a unique decomposition

$$v = \sum_{i=0}^{n} x_i e_i \ .$$

Thus

$$v \sim \lambda v \Rightarrow (x_0, \cdots, x_n) = (\lambda x_0, \cdots, \lambda x_n) \ .$$

We get

$$\mathbb{F}P^n = \mathbb{F}^{n+1} \setminus (\{0\} / (v \sim \lambda v), \quad \lambda \in \mathbb{F}^*) \ .$$

In general, we note the equivalence class of $v$

$$[v] = [x_0 : \cdots : x_n] \ .$$

The rules to construct a projective space using a coordinate system are

(1) A point in projective space $\mathbb{F}P^n$ is $p = [v]$ and it has $\left(\dim [P(\mathbf{V})] + 1\right)$ coordinates $(x_0, \cdots, x_n)$.

(2) $x_i \in \mathbb{F}$.

(3) Not all $x_i$ are zero.

(4) $(x_0, \cdots, x_n) = (\lambda x_0, \cdots, \lambda x_n)$ for $\lambda \in \mathbb{F}^*$

## 2.2 Projective Hilbert spaces

In quantum mechanics, an arbitrary quantum state in Hilbert space $\mathcal{H}$ of a quantum system is described as follows

$$|\psi\rangle = \sum_i a_i |e_i\rangle \ , \tag{2.3}$$

where $\{|e_i\rangle\}$ is a set of orthonormal basis vectors for $\mathcal{H}$ . The $a_i$ are complex numbers. This means that the state $|\psi\rangle$ is a vector in $\mathcal{H}$ with coordinates $(a_1, a_2, \cdots, a_i, \cdots)$. We know that, if any state $|\psi\rangle$ is multiplied by a complex factor $c$, the resulting state must be equivalent to the original one, apart from the special case where $c = 0$. Thus, we can define an equivalence relation

$$(a_1, a_2, \cdots, a_{n+1}) \sim (ca_1, ca_2, \cdots, ca_{n+1}) \ , \ \forall\, c \in \mathbb{C} \setminus \{0\} \ . \tag{2.4}$$

We can write this equivalence relation as

$$[a] = [a_1 : \cdots : a_{n+1}] \tag{2.5}$$

If we look back at definition 2.1 of projective spaces, we will realize that we actually defined the homogeneous coordinates of a point in $P\left(\mathbb{C}^{n+1}\right) = \mathbb{C}P^n$. We can thus define projective Hilbert spaces as follows [169]

**Definition 2.2.** *A finite projective Hilbert space $P\left(\mathcal{H}^{n+1}\right) \equiv P\mathcal{H}^n$ is defined as a complex projective space $P\left(\mathbb{C}^{n+1}\right) = \mathbb{C}P^n$. Thus, the projective Hilbert space is the space consisting of all complex lines in $\mathbb{C}^{n+1}$*

$$\mathbb{C}P^n = \left\{ \boldsymbol{z} = [z_0, \cdots, z_n] \in \mathbb{C}^{n+1} \setminus \{0\} \right\} / \left\{ \boldsymbol{z} \sim \lambda \boldsymbol{z}\,,\ \lambda \in \mathbb{C}^* \right\}, \tag{2.6}$$

*where $\boldsymbol{z}$ is a vector in $\mathbb{C}^{n+1}$, expressed in terms of the homogeneous coordinates (or projective coordinates), and the equivalence relation $\boldsymbol{z} \sim \lambda \boldsymbol{z}$ means that any vector $\lambda \boldsymbol{z}\,,\ \lambda \in \mathbb{C}^*$ represents the same ray as $\boldsymbol{z}$, provided that the coefficient $\lambda$ is not zero.*

In the projective Hilbert space $\mathcal{H}P^n$, we can define a metric, called the Fubini–Study metric, which is a Kähler metric (see Appendix D for an introduction to Khäler manifolds). This metric was actually described first in 1904 and 1905 by Guido Fubini and Eduard Study [63, 148]. Given two rays $|\psi\rangle$ and $|\phi\rangle$ on $P\mathcal{H}^n$, we can define a transition probability as follows

$$\cos(\theta)^2 = \frac{|\langle\phi|\psi\rangle|^2}{\langle\phi|\phi\rangle\langle\psi|\psi\rangle}\,, \tag{2.7}$$

where $\theta$ is the angle between the two rays. However, a ray in a projective space is considered as a point in the projective space. Thus, the angle $\theta$ between two rays in $P\mathcal{H}^n$ can be thought of as a distance between two points $|\psi\rangle$ and $|\phi\rangle$. If we Taylor expand Eq.(2.7) up to the second order and if we set $\mathrm{d}\theta$ equal to $\mathrm{d}s$, where $\mathrm{d}s$ denotes an infinitesimal distance, and take $\phi = \psi + \mathrm{d}\psi$, we get

$$\mathrm{d}s^2 = \frac{\langle\psi|\psi\rangle\langle\mathrm{d}\psi|\,\mathrm{d}\psi\rangle - \langle\mathrm{d}\psi|\psi\rangle\langle\psi|\,\mathrm{d}\psi\rangle}{\langle\psi|\psi\rangle^2}\,. \tag{2.8}$$

This is the Fubini Study metric defined in projective Hilbert spaces. In the case where $|\psi\rangle$ is normalized, Eq.(2.8) can also be written in the following way [68]

$$\mathrm{d}s^2 = \langle d\psi|d\psi\rangle - \frac{1}{4}|\langle\psi|d\psi\rangle - \langle d\psi|\psi\rangle|^2\,. \tag{2.9}$$

For a more detailed description of the Fubini Study metric, see Appendices D and C.

# 3

# Entanglement: general discussion

In this Chapter, we briefly discuss basic notions of quantum entanglement. Quantification of entanglement is an important task in quantum information theory. As we will see, the quantification of entanglement in a system can be achieved in two different approaches: an axiomatic approach and an operational approach. We will be interested in the axiomatic approach. Entanglement measures in the axiomatic approach have to fulfill certain axioms. In particular, they have to be non-increasing under Local Operations and Classical Communications (LOCC). For this reason, we will first define entanglement in multipartite states in Section 3.1. Then, we will review the notion of quantum operations in Section 3.2 and LOCC in Section 3.3. Next, in Section 3.4, we will introduce the notion of entanglement measures. And, finally, in Sections 3.5 and 3.6, we will briefly talk about the notion of the classification of entangled states and why it is important.

## 3.1 Quantum entanglement

The total projective Hilbert space $P\mathcal{H}$ of a system composed of two subsystems is the tensor product of the subsystems projective Hilbert spaces $P\mathcal{H}$, i.e. $P\mathcal{H} = P(\mathcal{H}_1 \otimes \mathcal{H}_2)$. A pure quantum state $|\psi^{12}\rangle$ is described by rays in $P\mathcal{H}$, and it is said to be separable if it can be expressed as a tensor product

$$|\psi^{12}\rangle = |\psi^1\rangle \otimes |\psi^2\rangle \ . \tag{3.1}$$

In other words, a pure state is separable if and only if there are no correlations between the subsystems. If $|\psi^{12}\rangle$ is not separable, it is called entangled.

There is a more general way to define entanglement in a bipartite system, and it is via the so called-Schmidt decomposition. Suppose that the above bipartite state is now expressed in a more general form, i.e. as a superposition of states

$$|\psi^{12}\rangle = \sum_{i=0}^{n} \sum_{j=0}^{m} c_{ij} \, |\psi_i^1\rangle \otimes |\psi_j^2\rangle \ , \tag{3.2}$$

where $n$ and $m$ are the dimensions of $\mathcal{H}_1$ and $\mathcal{H}_2$ respectively. We clearly see from equations (3.1) and (3.2), that: the state $|\psi^{12}\rangle$ is separable if and only if the rank of the matrix $C$ with coefficients $c_{ij}$ is equal to 1. To detect

entanglement in a bipartite state, we can express the state in Eq.(3.2) in a particular way, called the *Schmidt decomposition*

$$|\psi^{12}\rangle = \sum_{i=0}^{p} \chi_i \, |\phi_i^1\rangle \otimes |\phi_i^2\rangle \ , \tag{3.3}$$

where $(\{|\phi_i^1\rangle\}, \{|\phi_i^2\rangle\})$ are sets of orthonormal vectors in $P\mathcal{H}_1$, and $P\mathcal{H}_2$, respectively, and $p$ is called the Schmidt rank. The coefficient $\chi_i$ are the unique values of the matrix $C$, satisfying $\sum_i \chi_i = 1$. Thus, in terms of the Schmidt decomposition, we have: a state $|\psi^{12}\rangle \in P\left(\mathcal{H}_1 \otimes \mathcal{H}_2\right)$ is entangled iff its Schmidt rank $c$ is strictly larger than 1.

Unfortunately, there is no such expansion of general vectors when three or more subsystems are combined. In the case of more than two systems, the notion of entanglement becomes more complicated. It is interesting to use the example of pure three-qubit systems first, as it already shows the increasing richness of entanglement features compared to bipartite pure states. We will then generalize the concepts encountered in three-qubit systems to multipartite states.

A pure three-partite state is called *fully separable* if and only if it can be written in the form

$$|\psi_{fs}\rangle = |\psi_1\rangle \otimes |\psi_2\rangle \otimes |\psi_3\rangle \ . \tag{3.4}$$

Another possible situation, which arises when we go beyond the bipartite framework, is that two of the three parties share some entanglement, while they share no entanglement with the other parties.

A pure three-partite state is called *bi-separable* with respect to partition 12|3, if and only if it can be written in the form

$$|\psi_{bs}\rangle = |\psi_{12}\rangle \otimes |\psi_3\rangle \ , \tag{3.5}$$

where $|\psi_{12}\rangle$ is an entangled state defined in $P\left(\mathcal{H}_1 \otimes \mathcal{H}_2\right)$.

The last class of pure tripartite entanglement is what is called *genuine (of fully) tripartite entangled states*. A pure three-partite state is a genuine tripartite entangled if and only if it is neither fully separable nor bi-separable with respect to any bipartition.

In the case of a quantum system consisting of $n$ subsystems, entangled states show further structure. Indeed, in the multipartite case, apart from fully separable and fully entangled states, there also exists the notion of partial separability. The starting point of entanglement theory in a multipartite pure state $|\psi\rangle \in P\left(\mathcal{H}^{\otimes M}\right)$ is to define the set of unentangled states. This corresponds to product states, i.e. to vectors of the type

$$|\psi\rangle = |\psi_1\rangle \otimes \cdots \otimes |\psi_M\rangle \ . \tag{3.6}$$

A state vector is entangled if it is not of this form. Entangled vectors are themselves grouped into different classes of "equivalent" entanglement.

## 3.2 Quantum operations

A quantum operation (also known as a quantum process) is a mathematical formalism used to describe a general class of transformations that a quantum system can undergo. For example, the dynamics of a closed quantum system are characterized by a unitary transformation. However, the formalism of quantum operations describes not only the unitary time evolution or symmetry transformations of isolated systems but also the effects of measurement and interaction with the environment, thus the dynamic of open quantum systems.

A very elegant explanation of quantum operations is provided in Nielson and Chuang book [116], in Chapter 8. A simple way to describe the dynamics of an open quantum system is to consider it as the result of an interaction between the quantum system we are interested in and a given environment. And both, form a closed quantum system. Figure 3.1 shows a schematic representation of

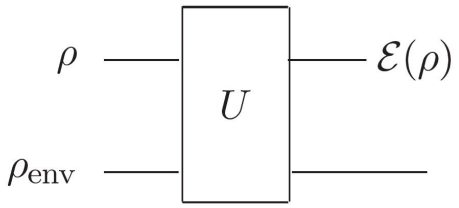


Figure 3.1: Schematic representation of the interaction of a system, represented by $\rho$ and an environment. After interaction with an environment, the final state is denoted by $\mathcal{E}(\rho)$. The figure was taken from [116]

the process. The system, described by the state $\rho$, enters a box, in which it is coupled with the environment through a unitary operation $U$. The final state, after the transformation, is $\mathcal{E}(\rho)$. The mathematical expression of the process is

$$\mathcal{E}(\rho) = \text{Tr}_{\text{env}} \left( U \left( \rho \otimes \rho_{\text{env}} \right) U^{\dagger} \right) , \tag{3.7}$$

where the interaction system-environment is considered to be represented -for the sake of simplicity to understand the concept now- with $\rho \otimes \rho_{\text{env}}$, i.e. with a product state. In the case where the unitary operation does not involve any interaction with an environment, the final state reads $\mathcal{E}(\rho) = \tilde{U} \rho \tilde{U}^{\dagger}$, where $\tilde{U}$ is the part of $U$ that acts only on $\rho$.

A more elegant way to describe quantum operations [116] is the *Operator-sum representation*. In this representation, as we will see, the dynamics of the principle system can be described without having to explicitly consider the properties of the environment. We assume in this representation that the initial state of the environment is of the form $|e_0\rangle \langle e_0|$[1], and its final state is represented by a set of states $\{|e_n\rangle\}$, forming an orthonormal basis. A general mathematical

[1]We assumed that the initial state of the environment is pure. This is not a restriction, since even in the case where the initial state of the environment is mixed, we still can purify the system. See [116] for a more detailed explanation.

description of the process depicted in Figure 3.1 can thus be rewritten as follows

$$\begin{aligned}\mathcal{E}(\rho) &= \sum_n \langle e_n| U \Big[\rho \otimes |_0\rangle \langle e_0|\Big] U^\dagger |e_n\rangle \\ &= \sum_n E_n \rho E_n^\dagger \,, \end{aligned} \tag{3.8}$$

where

$$E_n = \langle e_n|U|e_0\rangle \tag{3.9}$$

are operators on the projective Hilbert space of the principal system. Equation (3.8) is known as the operator-sum representation of $\mathcal{E}$. The operators $\{E_n\}$ are known as the *operation operators* or as *Kraus operators*.

Another way to express quantum operations is as follows: suppose we measure the environment in the basis $|e_n\rangle$. From Eq.(3.8) and (3.9), we see that projecting the state of the environment into $|e_n\rangle \langle e_n|$, yields an intermediate state $\rho_n = E_n \rho E_n^\dagger$, which if we normalize it, we get

$$\rho_n = \frac{E_n \rho E_n^\dagger}{\mathrm{Tr}\left(E_n \rho E_n^\dagger\right)} \,. \tag{3.10}$$

And on the other hand, if we compute the probability of getting the outcome $n$, we will find (the proof is done in [116])

$$p(n) = E_n \rho E_n^\dagger \,. \tag{3.11}$$

Equations 3.10 and 3.11, yield

$$E_n \rho E_n^\dagger = p_n \rho_n \,. \tag{3.12}$$

Thus, a quantum operation can be written in terms of the intermediate states $\rho_n$ as

$$\mathcal{E}(\rho) = \sum_n p(n)\rho_n = \sum_n E_n \rho E_n^\dagger \,. \tag{3.13}$$

Properties of quantum operations

(1) A quantum operator $\mathcal{E}$ is a linear map between spaces of trace class[2] operators defined on Hilbert spaces.

(2) If we demand conservation of the probability, we need to set $\mathrm{Tr}\left(\mathcal{E}(\rho)\right) = 1$, and this yields

$$\begin{aligned} 1 &= \mathrm{Tr}\left(\mathcal{E}(\rho)\right) \\ &= \mathrm{Tr}\left(\sum_n E_n^\dagger E_n \rho\right), \quad \forall\ \rho \\ &\Rightarrow \sum_n E_n^\dagger E_n = 1 \,. \end{aligned} \tag{3.14}$$

[2] A trace-class operator is a linear operator for which a trace can be defined and it is a finite number independent of the choice of the basis used to compute the trace.

In this case, the quantum operations are called *trace preserving*, and in the case where $\sum_n E_n^\dagger E_n \leq 1$, they are called non-trace-preserving.

(3) $\mathcal{E}$ is completely positive.

Examples of quantum operations

(1) *Local Unitary operations*: One of the most important classes of quantum operations that can act on quantum states is that of the unitary operators $U$ [108]. They are bounded linear operators $U : P\mathcal{H} \to P\mathcal{H}$, that satisfy $U^\dagger U = UU^\dagger = \mathbb{1}$.

(2) *Measurement*: Another important type of quantum operation is quantum measurements. There are two types of measures

a) **Projective measurement:** it is also called von Neumann measure and it is described by a Hermitian operator $O$, such that

$$O = \sum_m m\Pi_m \ , \tag{3.15}$$

where $\Pi_m$ is the projector onto the eigenspace of $O$ with eigenvalue $m$ and they satisfy $\sum_m \Pi_m = \mathbb{1}$ and $\Pi_m \Pi_{m'} = \delta_{mm'}$.

b) **Generalised measurement:** also called Positive Operator Valued Measure (POVM). It is described by a collection of measurement operators $M_i$, that satisfy $\sum_i M_i^\dagger M_i = \mathbb{1}$. They can be projectors, but not necessarily.

Example: assume a single qubit in a state $\rho = |0\rangle\langle 0|$ interacts with an environment through

$$U = |0\rangle\langle 0| \otimes \mathbb{1} + |1\rangle\langle 1| \otimes \sigma_x \ , \tag{3.16}$$

where $|0\rangle\langle 0|$ and $|1\rangle\langle 1|$ act on the system and $\mathbb{1}$ and $\sigma_x$ act on the environment. In this case, Kraus operators defined in Eq.(3.9), are $E_0 = |0\rangle\langle 0|$ and $E_1 = |1\rangle\langle 1|$.

## 3.3 Local operations and classical communication (LOCC)

With the recent explosion of interest in quantum computing, new questions have arisen, particularly about measurements performed by multiple parties on spatially separated quantum systems. If the parties lack the ability to communicate quantum information, then they are restricted from performing quantum operations on their individual local subsystems and then communicating classical information about the results of their actions to the other parties.

## Definition

Imagine a bipartite system, shared by Alice and Bob spatially separated from each other, and suppose that Alice performs an operation on her side. Such operations, performed exclusively within Alice's (or Bob's) laboratory are called local operations. Alice then communicates the outcome to Bob. Depending on the result, he performs his operation, obtains the result, communicates it to Alice, and so on. This complicated procedure is called LOCC. They are thus a way to operate locally on part of the system and communicate the result of this operation classically to another part, where usually another local operation is performed conditioned on the information received. LOCC can be used to transform entangled states into other entangled states, but they cannot generate entangled states out of product states. Thus, the possible transformations between states are strictly limited by using LOCC.

Let us give an example: suppose Alice and Bob share an entangled quantum state $|\psi\rangle = (1/\sqrt{2})\,(|00\rangle + |11\rangle)$. Knowing that they only have access to arbitrary operations on their local systems (including measurement) and classical communication, they wonder into what other states $|\varphi\rangle$ the initial state $|\psi\rangle$ can be transformed. Suppose they choose the following protocol:

(1) Alice chooses to perform two outcomes measurements, described by measurement operators

$$M_1 = \begin{pmatrix} \cos\theta & 0 \\ 0 & \sin\theta \end{pmatrix} \qquad M_2 = \begin{pmatrix} \sin\theta & 0 \\ 0 & \cos\theta \end{pmatrix} . \tag{3.17}$$

Thus, after the measurement, the initial state $|\psi\rangle$ is either

$$|\psi_1\rangle = \cos\theta\,|00\rangle + \sin\theta\,|11\rangle \ , \tag{3.18}$$

or

$$|\psi_2\rangle = \cos\theta\,|11\rangle + \sin\theta\,|00\rangle \ . \tag{3.19}$$

(2) If Alice finds the state in Eq.(3.18), she does nothing. If she find the state in Eq.(3.19), she applies a NOT gate (the Pauli matrix $\sigma_x$), and gets

$$|\psi_2\rangle' = \cos\theta\,|01\rangle + \sin\theta\,|10\rangle \ . \tag{3.20}$$

(3) She then communicates classically the results saying to Bob, if she got the state in Eq.(3.18) or the one in Eq.(3.20).

(4) Bob does nothing if the state is the one in Eq.(3.18) and applies a NOT gate if the state is the one in Eq.(3.19).

This means that regardless of the measurement outcomes obtained by Alice, they get the state

$$|\varphi\rangle = \cos\theta\,|00\rangle + \sin\theta\,|11\rangle \ . \tag{3.21}$$

Thus, Alice and Bob have transformed their initial entangled $|\psi\rangle = (1/\sqrt{2})\,(|00\rangle + |11\rangle)$ into the state $|\varphi\rangle = \cos\theta\,|00\rangle + \sin\theta\,|11\rangle$ using only local operations on their individual systems, and classical communication.

**Remark:** Alice and Bob can convert an entangled state to another, but can never increase the amount of entanglement in a state.

LOCC can be generalized to many parties spatially separated from each other. For example, $M$ parties can share a composite system in an entangled state. As we saw in the above example, even if restricted to local operations assisted with communication through a classical channel, the parties can still modify the entanglement properties of the system, and in particular, they can try to convert one entangled state into another, but can never increase the entanglement. This possibility leads to natural ways of defining equivalence relations in the set of entangled states, where equivalent states are then said to contain the same kind of entanglement. This classification of entanglement is interesting in quantum information theory because the parties can use two states -that differ from each other by LOCC- for exactly the same tasks[3]. It has been shown in [14], that if we have many copies of a given bipartite state $|\psi\rangle$, applying LOCC leads to identifying all bipartite pure-state entanglement with that of the Einstein-Podolsky-Rosen state $1/\sqrt{2}\,(|00\rangle + |11\rangle)$ [54].

Thus, LOCCs are important for two reasons

(1) They play a major role in defining good entanglement measures.

(2) They allow for a classification of entangled states.

However, LOCC protocols have proven to be extremely challenging. Indeed, they involve a sequence of measurements for each of which the outcome must be known in order to determine the next step in the protocol, and in addition, the way in which the state of the system is transformed by that outcome plays an important role in determining what will happen at that next step. In fact, a number of studies have considered the significance of the number of rounds of communication used by the parties. In the bipartite case, it has been shown that for the task of transforming a system from one pure state to another, multiple rounds are not necessary [107]. However, for mixed-state purification scenarios (see Chapter 7 for the characterization of entanglement in mixed states), it has been shown [17] that two rounds of communication are needed. The question of whether or not it can be helpful to use an infinite number of rounds has also been studied. And it was shown for example in [39] that infinite rounds are required. Thus, it is still not clear how many series are needed to represent LOCC.

## Mathematical formulation

In the previous section, we gave a mathematical structure of general local operations applied to a given system. However, in addition to local operations, LOCC protocols contain also classical communication. How can we describe this

[3]Another classification of entangled states has been proposed [19, 50] using SLOCC: Stochastic local operations and classical communications In this classification, the equivalence between two states is not necessarily deterministic. We will not develop this concept as it will not be useful in what follows.

mathematically? Even considering only two rounds (i.e. classical communication from Alice to Bob and then from Bob to Alice), this turns out to be a difficult problem to define mathematically. However, fortunately, it has been shown that LOCCs are contained within the set of *separable operations*. We will define them in while, let us first summarize the different existing classes of operations in the literature. They have been summarized by the Horodecki family in Ref.[92]

***C1***- *Class of local operations*: No classical communications between Alice and Bob in this case. The mathematical formulation is quite trivial: $\mathcal{E}_{AB}(\rho) = (\mathcal{E}_A \otimes \mathcal{E}_B)(\rho)$, where $\mathcal{E}_A$ and $\mathcal{E}_B$ are locals quantum operations.

***C2a***- *Class of "one-way" forward LOCC operations*: in this case, the classical communications are only from Alice to Bob. The example of the shared entangled state by Alice and Bob, given above, belongs to this class. The mathematical structure of this operation is: $\mathcal{E}_{\overrightarrow{AB}}(\rho) = \sum_i V_A^i \otimes \mathbb{1}_B \Big( \left[\mathbb{1}_A \otimes \mathcal{E}_B^i\right] \rho \Big) \left(V_A^i\right)^\dagger \otimes \mathbb{1}_B$, where $V_A^i$ and $\mathcal{E}_B^i$ are the local operations applied by Alice, and Bob respectively, with $\mathcal{E}_B^i$ being deterministic.

***C2b***- *Class of "one-way" backward LOCC operations*: it has the same mathematical structure then ***C2a***, but with the roles of Alice and Bob interchanged.

***C3***- *Class of "two-way" classical communication*: Both, Alice and Bob are allowed to communicate with each other. The mathematical structure of this class is complicated. It has been done in Ref.[48]. We will not develop it here. It's the next class that interests us.

***C4***- *Class of separable operations*: These are operations with product Kraus operators:

$$\mathcal{E}_{AB}^{sep}(\rho) = \sum_i A_i \otimes B_i \, \rho \, A_i^\dagger \otimes B_i^\dagger \, , \tag{3.22}$$

where $\sum_i A_i^\dagger A_i \otimes B_i^\dagger B_i = \mathbb{1} \otimes \mathbb{1}$. This class of operations have been considered in [134, 151].

***C5***- *Positive partial transpose (PPT) operations*[4]*:* The simplest example of such operations is $\rho \to \rho \otimes \rho_{\mathrm{PPT}}$. That is a process of adding some PPT state.

There is an order of inclusions [92], between these different classes: $C1 \subset C2a, C2b \subset C3 \subset C4 \subset C5$. Thus, the set of all LOCC is contained in the set $C4$ of all separable operations. It has been shown in [18] that any LOCC is separable, but the opposite is not true. Therefore, for a given $M$-partite state

[4] A general pure or mixed multipartite state (see Chapter 7 for the study of mixed states) $\rho^{A_1,A_2,\cdots,A_N}$ is called fully separable if it can be expressed as a convex combination of product states with respect to the partition $A_1, A_2, \cdots, A_N$. And $\rho^{A_1,A_2,\cdots,A_N}$ is said to have positive partial transpose if the operator obtained by taking a partial transpose with respect to any subset of parties is positive semi-definite.

$\rho$, we can define a completely positive trace-preserving map (CPTP), described by separable Kraus operators of the form

$$A_\alpha = \bigotimes_{k=0}^{M-1} A_k^{\alpha_k} = A_0^{\alpha_0} \otimes A_1^{\alpha_1} \cdots \otimes A_{M-1}^{\alpha_{M-1}} \ , \tag{3.23}$$

that can describe a LOCC protocol on $\rho$, i.e.

$$\mathcal{E}_{\mathrm{LOCC}}(\rho) = \sum_\alpha A_\alpha \rho A_\alpha^\dagger \ . \tag{3.24}$$

## 3.4 Entanglement quantification

There are two approaches to quantifying entanglement: the axiomatic approach and the operational one. In the last one, the entanglement is linked to the operational tasks. For example, the system is more entangled if it allows for better performance of some tasks, such as teleportation. In other words, the operational approach quantifies the usefulness of a state for a certain protocol that requires entanglement. The first approach is also called the abstract approach [87], in which one writes down a list of properties one demands from a measure.

### Operational approach

Entanglement cost and entanglement of distillation

The entanglement cost $E_c(\rho)$ is defined as follows: suppose $n_{\mathrm{in}}$ input singlets[5] and a protocol, i.e. a family of LOCC transforming the $n_{\mathrm{in}}$ input singlets onto $n_{\mathrm{out}}$ output copies of the state $\rho$. The minimal rate of singlets that have to be used to create many copies of $\rho$ via LOCC is defined as the entanglement cost

$$E_C(\rho) = \inf_{\mathrm{LOCC}} \lim_{n_{\mathrm{out}}\to\infty} \frac{n_{\mathrm{in}}}{n_{\mathrm{out}}} \tag{3.25}$$

The entanglement of distillation $E_D(\rho)$ is defined as the dual way of $E_c(\rho)$, that is

$$E_D(\rho) = \sup_{\mathrm{LOCC}} \lim_{n_{\mathrm{in}}\to\infty} \frac{n_{\mathrm{out}}}{n_{\mathrm{in}}} \ , \tag{3.26}$$

which is basically the optimal singlet distillation rate from many copies of $\rho$.

### Axiomatic approach

Since abstract quantification is based on a list of some properties that need to be fulfilled, let us begin by lying them out. We will then give some examples of entanglement measures

Axioms for a bona fide measure of quantum entanglement

[5] In Dirac notation, a singlet state $|\psi\rangle$ is usually represented as follows: $|\psi\rangle = (|01\rangle + |10\rangle)$.

As a tool for entanglement quantification, an entanglement measure (also called entanglement monotone) has to quantify the amount of entanglement in a given state. The conditions that any entanglement measure $E(\rho)$ has to satisfy, were first introduced in Ref.[153]. Here we list these properties without any deep discussion and suggest Refs.[48, 92, 77]

(1) If the state $\rho$ is separable, then $E(\rho) = 0$.

(2) The function $E(\rho)$ should not change under local unitary transformations

$$E(\rho) = E\left[\left(\prod_{\mu=0}^{M-1} U_\mu\right)\rho\left(\prod_{\mu=0}^{M-1} U_\mu\right)^\dagger\right], \tag{3.27}$$

where $U_\mu$ is an abbreviation for $\mathbb{1}_0 \otimes \cdots U_\mu \cdots \otimes \mathbb{1}_{M-1}$.

(3) Since entanglement cannot be produced by LOCC, an entanglement measure cannot increase under LOCC operations

$$E(\mathcal{E}_{\mathrm{LOCC}}(\rho)) \leq E(\rho)\,, \tag{3.28}$$

where $\mathcal{E}_{\mathrm{LOCC}}(\rho)$ is a CPTP map.

(4) Convexity of $E(\rho)$

$$E\left(\sum_i p_i\rho_i\right) \leq \sum_i p_i E(\rho_i)\,. \tag{3.29}$$

(5) Additivity of $E(\rho)$

$$E(\rho_1 \otimes \rho_2) = E(\rho_1) + E(\rho_2)\,. \tag{3.30}$$

**Remarks:** properties (1), (2) and (3) are required for a good entanglement measure. In fact, requirement (1) is quite a trivial one. The second one, says that any good entanglement measure is supposed to give the same result for states that differ only by local unitary operations. Indeed, a unitary transformation does not change the physical content of a state, but only our way of representing it. In the case of an $M$ composite system, we can distinguish between local and global unitary operations. Local unitary operations have a form $U = U_1 \otimes U_2 \otimes \cdots \otimes U_M$, where $U_i$ are arbitrary unitary operations that act independently on each subsystem. These operations cannot change relations between subsystems. Global unitary operations do not have this form and, as a result, they can make the subsystems interact. The third requirement says that any good measure of entanglement is not supposed to increase with LOCC, since the parties can never create entanglement by only using local operations and classical communications. Note that, requirement (3) implies requirement (2). It is usually preferable to show that an entanglement measure fulfills a stronger version of requirement (3), which is the non-increase *on average* under LOCC [156], i.e.

$$\sum_\alpha p_\alpha E(\rho_\alpha) \leq E\left(\rho\right)\,, \tag{3.31}$$

where (see Section 3.2)

$$\rho_\alpha = \frac{A_\alpha \rho A_\alpha^\dagger}{\mathrm{Tr}\left[A_\alpha \rho A_\alpha^\dagger\right]} \,, \tag{3.32}$$

are the Kraus operators describing some LOCC protocol and

$$p_\alpha = \mathrm{Tr}\left[A_\alpha \rho A_\alpha^\dagger\right] \tag{3.33}$$

is the probability of obtaining outcome $\alpha$. However, it is not necessary for an entanglement measure to fulfill properties (4) and (5). The convexity property is often demanded, but not all measures fulfill it. The logarithmic negativity constitutes a good example of being a strong entanglement measure that is not convex [128]. The additivity property is difficult to prove for many measures [129].

Examples of entanglement measures

- **von Neumann entropy:** It is a measure for bipartite pure states. Although the Schmidt rank $p$ defined in Eq.(3.3), detects entanglement in pure bipartite states. It does not quantify entanglement. A quantification of entanglement is possible with the Schmidt coefficients $\chi_i$. In fact, a natural measure called *entropy of entanglement* or *von Neumann entropy*, consists in taking the entropy of the distribution specified by the squares of the coefficients

  $$S_{1(2)} = -\,\mathrm{Tr}\left(\rho_{1(2)} \log \rho_{1(2)}\right) \,. \tag{3.34}$$

  If the entropy is 0 then there is only a single coefficient equal to 1, and the state is not entangled. But as soon as the entropy is positive the state is entangled. To see why entropy is finer than the Schmidt rank, let us take an example. Suppose the following bipartite pure states

  $$|\psi\rangle = \frac{1}{\sqrt{2}}\,|00\rangle + \frac{1}{\sqrt{2}}\,|11\rangle \quad \text{and} \quad |\phi\rangle = \sqrt{1-\epsilon}\,|00\rangle + \sqrt{\epsilon}\,|11\rangle \,.$$

  For $0 < \epsilon < 1/2$, both states have the same Schmidt rank, but the first one has entanglement entropy 1, whereas the second has entanglement entropy going to 0 as $\epsilon \to 0$.

- **Entanglement of formation:** The first measure of entanglement that has been proposed for mixed states (entanglement in mixed states will be studied in Chapter 7) is the entanglement of formation [17]. It is defined

as the convex roof[6]of the von Neumann entropy.

$$E_F(\rho) = \inf_{\rho=\sum_i p_i|\psi_i\rangle\langle\psi_i|} \sum_i p_i S\left(|\psi_i\rangle\langle\psi_i|\right) \ . \tag{3.35}$$

If $\rho$ is pure, $E_f(\rho)$ boils down to von Neumann entropy. The question of whether the entropy of formation is fully additive is not yet solved

- **Concurrence:** A very popular measure for the quantification of bipartite quantum entanglement is the concurrence [166, 138]. For a bipartite pure state $|\psi\rangle$, it is defined as follows

$$C\left(|\psi\rangle\right) = \sqrt{2\left[1 - \mathrm{Tr}(\rho_i^2)\right]}\,, \tag{3.36}$$

where $i = 1, 2$ denotes the $i$th subsystem. The Concurrence has been generalized for multiparticle pure states in arbitrary dimensions [138, 21]

$$C\left(|\psi\rangle_M\right) = \sqrt{2\left[1 - \mathrm{Tr}(\rho_{\mathcal{A}}^2)\right]}\,, \tag{3.37}$$

where $\rho_{\mathcal{A}}$ is the reduced density matrix across the bipartition $\mathcal{A}$ of the pure state $|\psi\rangle_M$. For mixed states, this definition is extended via the convex roof construction.

- **Distance measures:** These measures are based on a natural intuition, that the closer the state is to the separable set $\mathcal{S}$, the less entangled it is.

$$E_D(\rho) = \inf_{\sigma\in\mathcal{S}} D(\rho||\sigma) \tag{3.38}$$

where $D(\rho||\sigma)$ is a measure of distance between $\rho$ and $\sigma$, and where the infimum is taken over all separable states. It has been shown that such a function is monotonic under CPTP. Monotonicity turned out to be a condition for the distance to be a measure of distinguishability of quantum states [152, 64]. One of the first distance measures that have been constructed is the relative entropy of entanglement [151]

$$E_R(\rho) = \inf_{\sigma\in\mathcal{S}} S(\rho||\sigma)\,, \tag{3.39}$$

where the distance $S(\rho||\sigma)$ is the relative entropy $S(\rho||\sigma) = \mathrm{Tr}\left[\rho\left(\log\rho - \log\sigma\right)\right]$. It is actually the quantum mechanical analog of relative entropy.

- **The geometrical measure of entanglement:** An often-used entanglement measure for multiparticle systems is the geometric measure of

[6]The so-called convex roof construction is a strategy for defining entanglement measures for mixed states. We start by defining a measure of entanglement for pure states $E(|\psi\rangle\langle\psi|)$, then we define

$$E(\rho) = \inf_{\rho=\sum_i p_i|\psi_i\rangle\langle\psi_i|} \sum_i p_i\, E(|\psi_i\rangle\langle\psi_i|)\,,$$

as a measure of quantum correlation/entanglement on the set of mixed states. The infimum is taken over all possible decompositions of the state $\rho = \sum_i p_i\,|\psi_i\rangle\langle\psi_i|$ into pure states $|\psi_i\rangle\langle\psi_i|$.

entanglement [162, 161, 5]. It is quite similar to the Distance measure since it also quantifies the distance to the separable states. For a given multiparticle state $|\psi\rangle$, one can define the following quantity

$$\Lambda(\psi) = \sup_{\phi \in \mathcal{S}} |\langle\phi|\psi\rangle| , \tag{3.40}$$

where the supremum is taken over all separable states. Then, one can define the geometrical measures as follows

$$E_G(|\psi\rangle) = 1 - \Lambda(\psi)^2 , \tag{3.41}$$

The geometric measure is a multipartite entanglement measure, and its generalization to mixed states through the convex roof construction has been done and used in [78, 162]

## 3.5 Entanglement as a resource

Local operations and classical communications cannot generate entangled states out of product states, they can be used to transform entangled states into other entangled states, as seen in Section 3.3. This captures the intuitive notion that quantum entanglement is something precious and its value cannot be freely increased. This suggests that entanglement can be elevated from being just an interesting fundamental phenomenon to being useful in performing practical tasks. In fact, since local operations and classical communications are the most physical and concrete operations we can perform in laboratories, it is thus very reasonable to consider what information processing tasks can be performed when restricted to LOCC. The study of entanglement as a valuable and precious feature, when only restricted operations such as LOCC are available, is called resource theory [88]. Here, the main idea is that one defines some subset of all possible quantum operations as the set of free operations. For instance, the free operations can represent all available quantum operations implementable in a specific experimental setup. All states that can be generated using free operations from some fixed initial state are called free states. A state that is not part of the free states is thus called resourceful, i.e. an entangled state is a resource. However, resource theory is more general, for example, an experimentalist may only be able to maintain coherence in a quantum system for a short amount of time because of limited ability to mitigate environmental noise. In this case, coherence is the resource.

The following example depicts very well the meaning behind the resource theory of quantum entanglement. It was first given by Rob Spekkens and then taken up by Chitambar et al. in [40]:

*" The set of all shapes that can be generated by a compass and a ruler could represent "free states" of a resource theory, with the action of the compass and ruler being the free operations. Therefore, in this resource theory, all the shapes that cannot be generated by a compass and ruler are considered as resources."*

Entanglement is the most useful resource for various quantum communication protocols like quantum teleportation [13, 139, 51, 98, 93], dense coding [12, 28, 29] and secret sharing [85, 72] which gives the quantum advantage over the classical communication protocols

## 3.6 Entanglement classification

We can distinguish several types of entanglement, depending on which particle is entangled with the others, and at which amount. Being able to classify and detect the entanglement type of a state is a key competence in many areas of quantum information, such as quantum computing. In fact, some entangled states appear in quantum algorithms to be more efficient than other entangled states. In this context, we may want to partition entangled states into different classes [67].

The finest distinction is the one based on local unitary (LU) operations. Two $M$-partite state vectors $|\psi\rangle$, $|\phi\rangle$ defined in $P\left(\mathcal{H}_{\psi}^{\otimes M}\right)$ and $P\left(\mathcal{H}_{\phi}^{\otimes M}\right)$ of dimension $\prod_{\mu=1}^{M} \mathrm{d}_{\mu}$, are considered equivalently entangled if they differ only by a local unitary basis change [160]:

$$|\psi\rangle \sim_{\mathrm{LU}} |\phi\rangle \iff |\psi\rangle = (U_1 \otimes \cdots \otimes U_M)\,|\phi\rangle \ , \tag{3.42}$$

where $U_{\mu}$, $\mu = 1, \cdots, M$ is an LU operator of dimension $\mathrm{d}_{\mu} \times \mathrm{d}_{\mu}$. In the case of bipartite systems, i.e. $M = 2$, we have

$$(U_1 \otimes U_2)\,|\psi\rangle = \sum_{i=0}^{p} \chi_i \,(U_1\,|\alpha_i\rangle) \otimes (U_2\,|\beta_i\rangle) \ , \tag{3.43}$$

where we have used the Schmidt decomposition, defined in Eq.(3.3). Because any orthonormal basis can be mapped onto any other basis by a unitary operation, we see that two bipartite state vectors are LU equivalent if and only if their Schmidt coefficients coincide.
LU equivalence is physically meaningful and feasible in the case of bipartite systems. In fact, the Schmidt coefficients $\chi_i$ are merely the set of eigenvalues of each of the reduced density matrices. Thus, a LU equivalence of two bipartite states can be seen experimentally by using for example quantum state tomography. Thus, from an operational point of view, LU equivalence is justified because we cannot create entangled states from separable states by local unitary basis changes only.

However, as seen in the previous section 3.5, resource theories provide a natural and more concrete way to rigorously compare the resources held in different quantum states. Two states possess the same resource if it is possible to transform one into the other using the free operations of the resource theory (meaning the only available operations). Thus, from an operational point of view, it is better to classify entangled states through LOCC, which is a coarser notion of "equivalent entanglement" through the addition of classical communications. Two states which are LOCC–equivalent are equally useful for any kind of application.

However, although physically and operationally well-defined, no clear mathematical description of LOCC equivalence has been identified so far. In fact, we have seen in Section 3.3, that already for two rounds, the mathematical structure of LOCC is complex. A more general classification has been proposed, whose physical interpretation is less satisfactory, but whose mathematical description

is easier to implement, is the notion of stochastic LOCC equivalence (SLOCC) [50]. Two pure states are said to be equivalent if they can be transformed into each other by LOCC with some nonzero probability. As in Section 3.3, a SLOCC consists of several rounds in each of which the parties perform operations on their respective systems, depending on previous measurement results. However, in a SLOCC protocol, one does not need all the rounds to be done perfectly. Meaning that a transformation of $|\psi\rangle$ into $|\phi\rangle$ is possible, if there is a LOCC protocol enabling the transformation, but without imposing that it has to be achieved with certainty. One can think of the protocol as splitting into different branches with each measurement, that is done by each party. Each branch can be represented by a local operator $A_i$ that is applied locally on the state being shared among the parties. And two $M$-partite states $|\psi\rangle$ and $|\phi\rangle$ are said to be SLOCC equivalent if

$$(A_1 \otimes A_2 \otimes \cdots \otimes A_M)\,|\psi\rangle = \lambda\,|\phi\rangle \quad \lambda \in \mathbb{C}\,. \tag{3.44}$$

This is possible only if the transformation is realized with matrices that have unit determinant 1, i.e. $\det A_i = 1$. In other words, two states $|\psi\rangle$ and $|\phi\rangle$ are said to be SLOCC equivalent if and only if they can be transformed into each other by means of local invertible operators. It has been shown [50] that there are two inequivalent kinds of genuine tripartite entanglement via SLOCC, namely the

$$|\mathrm{GHZ}\rangle = \frac{1}{\sqrt{2}}\left(|000\rangle + |111\rangle\right) \tag{3.45}$$

and

$$|\mathrm{W}\rangle = \frac{1}{\sqrt{3}}\left(|001\rangle + |010\rangle + |100\rangle\right) \tag{3.46}$$

states.

# 4

# Entanglement measure in pure states

This Chapter depicts an original work that we published in Ref.[41]. As seen in the previous Chapter, entanglement is an essential resource for progressing in the field of quantum-based technologies. It is the most useful resource for various quantum communication protocols. Therefore, it is of practical interest to quantify this resource to estimate the efficiency of such protocols. Although many aspects of quantum entanglement have been studied extensively [92], entanglement remains elusive and the problem of its classification [6, 137, 105, 73, 66] and quantification is still not well understood in higher dimensional systems [146, 70]. So far, several different approaches have been developed to quantify the variety of states available in the quantum regime [92]. Entropy of entanglement is uniquely accepted as a measure of entanglement for pure states of bi-partite systems [130], while for the same class of mixed states, entanglement of formation [166], entanglement distillation [17, 15, 90] and relative entropy of entanglement [153] are largely acknowledged as faithful measures. The development of quantum information theory and the increasing experimental demand for quantum states manipulation led to develop measures enfolding more general states. For multi-partite systems, a broad range of measures has covered pure states [50, 25] and mixed states [43] among which, a Schmidt measure [57] and a generalisation of concurrence [33] have been proposed. In the last years, the variety of paths adopted to tackle the problem led to estimation-oriented approaches based on the quantum Fisher information [125, 95, 141]. Due to the deep connection between the quantum Fisher information and a statistical distance [23], the geometry of entanglement has been studied in the case of two qubits [104]. While the mentioned measures address mainly qubits systems, the necessity for noise tolerance and reliability in quantum tasks opened the way to study higher dimensional states, the qudits [99]. In noise-tolerant schemes, magic-state-distillation protocols outperform their qubits counterparts [32] while a proof of enhanced security for quantum key distribution tasks is derived in [144]. In addition, a recent experimental realization confirmed the superiority of qudits in certifying entanglement in noisy environments [53]. At the same time, a different measure of entanglement for such systems appeared, such as a measure for highly symmetric mixed qudit states [4] and the concurrence in arbitrary Hilbert space dimensions [138]. Finally, a geometric measure for $M$-qudit pure states has been proposed in [83].

In this chapter, we propose a geometrical entanglement measure, called *Entanglement distance*, that can be computed for either pure or mixed states of M-qudit hybrid systems[1]. Our work has been done in Ref.[41]. We will derive our measure from the Fubini Study metric defined in projective Hilbert spaces. We will prove that it fulfills all the requirements for a good measure of quantum entanglement [156, 79, 153].

## 4.1 Entanglement distance

A qudit, is a state in a $(d-1)$-dimensional projective Hilbert space and a hybrid $M$-qudit is a state in $P\mathcal{H}^{\otimes M} := P\left(\mathcal{H}_{d_0} \otimes \mathcal{H}_{d_1} \otimes \cdots \otimes \mathcal{H}_{d_{M-1}}\right)$. The dimension of the projective Hilbert space $P\mathcal{H}^{\otimes M}$ is $\left[\left(\prod_\mu d_\mu\right) - 1\right]$. We saw in Chapter 2, that a projective Hilbert space carries the Fubini-Study metric, that can be expressed in quantum mechanics in the following way [68]

$$\mathrm{d}s^2 = \langle d\psi | d\psi\rangle - \frac{1}{4}|\langle\psi|d\psi\rangle - \langle d\psi|\psi\rangle|^2 \,, \tag{4.1}$$

where $|\psi\rangle$ is a generic normalised state and $|d\psi\rangle$ is an infinitesimal variation of such a state.

We want to use the Fubini Study metric to construct an entanglement measure. For this reason, we will start by imposing the invariance of the Fubini Study metric under local unitary operations [151, 128]. As a matter of fact, the action of $M$ arbitrary $\mathrm{SU}(d_\mu)$ local unitary operators $U_\mu$ $(\mu = 0, \ldots, M-1)$ on a given state $|s\rangle$, generates a class of states

$$|U, s\rangle = \prod_{\mu=0}^{M-1} U_\mu |s\rangle \,, \tag{4.2}$$

that share the same degree of entanglement. In the above equation, $U_\mu$ is an abbreviation for $\mathbb{1}_0 \otimes \cdots U_\mu \cdots \otimes \mathbb{1}_{M-1}$, i.e. for each $\mu$, $U_\mu$ operates on the $\mu$th qudit. Thus we define an infinitesimal variation of the state (4.2) as

$$|dU, s\rangle = \sum_{\mu=0}^{M-1} d\tilde{U}_\mu |U, s\rangle \,, \tag{4.3}$$

where there is no summation on the index $\mu$ and each infinitesimal $\mathrm{SU}(d_\mu)$ transformation $d\tilde{U}_\mu$ operates on the $\mu$-th qudit. Such infinitesimal transformation can be written as

$$d\tilde{U}_\mu = -i(\mathbf{n}\cdot\mathbf{T})_\mu \, d\xi^\mu \tag{4.4}$$

where $(\mathbf{n}\cdot\mathbf{T})_\mu := \mathbf{n}_\mu \cdot \mathbf{T}_\mu$, $\mathbf{n}_\mu$ is a unit vector in $\mathbb{R}^{d_\mu^2-1}$, $\xi^\mu$ are real parameters, and where we denote by $T_{\mu a}$, $a = 1, \ldots, d_\mu^2 - 1$, the generators of $\mathfrak{su}(d_\mu)$ algebra (see Appendix E). From Eq. (4.1), with this choice, we obtain the following

[1] A hybrid system is a system formed by subsystems with different Hilbert space dimensions. For example, a system formed with a qubit and a qutrit is a hybrid system.

expression for the Fubini-Study metric $g(\mathbf{v})$,

$$\begin{aligned} g(\mathbf{v}) &= \sum_{\mu\nu} g_{\mu\nu}(\mathbf{v}) d\xi^\mu d\xi^\nu \\ &= \sum_{\mu\nu} \Big[ \langle s|(\mathbf{v}\cdot\mathbf{T})_\mu (\mathbf{v}\cdot\mathbf{T})_\nu |s\rangle - \langle s|(\mathbf{v}\cdot\mathbf{T})_\mu |s\rangle\langle s|(\mathbf{v}\cdot\mathbf{T})_\nu |s\rangle \Big] d\xi^\mu d\xi^\nu \ . \end{aligned} \tag{4.5}$$

In the latter equation, the real unit vectors $\mathbf{v}_\mu$ are derived by a rotation of the original ones according to

$$\mathbf{v}_\nu \cdot \mathbf{T}_\nu = U_\nu^\dagger \mathbf{n}_\nu \cdot \mathbf{T}_\nu U_\nu \ , \tag{4.6}$$

where there is no summation on the index $\nu$.

**Definition 4.1** (**Entanglement distance**). *The entanglement distance for a general M-qudit state $|s\rangle$ is defined as*

$$\begin{aligned} E(|s\rangle) &= \min_{\{\mathbf{v}_\mu\}_\mu} \mathrm{Tr}\, g(\mathbf{v}) \\ &= \min_{\{\mathbf{v}_\mu\}_\mu} \sum_{\mu=0}^{M-1} \Big[ \langle s|(\mathbf{v}\cdot\mathbf{T})_\mu^2 |s\rangle - \langle s|(\mathbf{v}\cdot\mathbf{T})_\mu |s\rangle^2 \Big] \ . \end{aligned} \tag{4.7}$$

*where the* min *is taken over all the possible orientations of the unit vectors $\mathbf{v}_\mu \in \mathbb{R}^{\mathrm{d}_\mu^2 - 1}$, and where we have adopted the following notation*

$$(\mathbf{T}\cdot\mathbf{v})_\mu := \mathbb{1}_0 \otimes \cdots (\mathbf{T}\cdot\mathbf{v})_\mu \cdots \otimes \mathbb{1}_{(M-1)} \tag{4.8}$$

**Definition 4.2.** *In the case of an M-qubit state $|s\rangle$, the entanglement distance simplifies to*

$$E(|s\rangle) = \min_{\{\mathbf{v}_\mu\}_\mu} \Big[ M - \sum_{\mu=0}^{M-1} \langle s| \left(\boldsymbol{\sigma}\cdot\mathbf{v}\right)_\mu |s\rangle^2 \Big] \ , \tag{4.9}$$

*where $\boldsymbol{\sigma}$ is the Pauli vector and $\mathbf{v}_\mu \in \mathbb{R}^3$, with $||\mathbf{v}_\mu|| = 1$.*

**Lemma 4.1.** *In the case of a multipartite qubits system, the entanglement distance is*

$$E(|s\rangle) = 2 \sum_{\mu=0}^{M-1} S_L^\nu = \sum_\mu \Big( 1 - \mathrm{Tr}\left[ (\rho^\mu)^2 \right] \Big) \ , \tag{4.10}$$

*where $S_L^\nu$ is the Linear entropy [113, 24] of the reduced state $\rho_\mu$, and $\mathrm{Tr}\left[(\rho^\mu)^2\right]$ is the purity computed for subsystem $\mu$.*

*Proof.* Lemma 4.1 will be proven in Chapter 5. ■

**Proposition 4.1.** *The entanglement distance for a general M-qudit state $|s\rangle$ defined in Eq.*(4.7) *can be expressed in two other different forms, in which there is no dependence on the orientations $\mathbf{v}_\mu$ and thus, no minimization procedure. The first is the following*

$$E(|s\rangle) = \sum_{\mu=0}^{M-1} \left[ \mathrm{Tr}(A_\mu) - 2(d_\mu - 1) \right] \ , \tag{4.11}$$

*where*

$$A_\mu = \sum_{ij} \left[ \langle s|T_{\mu i}T_{\mu j}|s\rangle - \langle s|T_{\mu i}|s\rangle\langle s|T_{\mu j}|s\rangle \right] . \tag{4.12}$$

*This is done by expressing the trace of the Fubini Study metric in the following way*

$$g_{\mu\mu}(\mathbf{v}_\mu) = \sum_{ij} v_{\mu i}v_{\mu j}A_{\mu ij} . \tag{4.13}$$

*The second way of expressing the entanglement distance is the following*

$$E(|s\rangle) = \sum_{\mu=0}^{M-1} \left[ \frac{2(d_\mu - 1)}{d_\mu} - \sum_{k=1}^{d_\mu^2-1} \langle s|T_{\mu k}|s\rangle^2 \right] , \tag{4.14}$$

*where we have used the fact that (see Appendix E)*

$$\mathrm{Tr}(A_\mu) = \frac{2(d_\mu^2 - 1)}{d_\mu} - \sum_{k=1}^{d_\mu^2-1} \langle s|T_{\mu k}|s\rangle^2 , \tag{4.15}$$

*with $T_{\mu k}$, $k = 1, \ldots, d_\mu^2 - 1$ are the generators of $\mathfrak{su}(d_\mu)$ algebra.*

**Definition 4.3.** *We name entanglement metric (EM) $\tilde{g}$ the Fubini-Study metric associated to $\{\tilde{\mathbf{v}}_\mu\}_\mu$*

$$\tilde{g} = g(\{\tilde{\mathbf{v}}_\mu\}_\mu) , \tag{4.16}$$

*where $\{\tilde{\mathbf{v}}_\mu\}_\mu$ denotes the set of M-directions that minimize the trace of the Fubini Study metric (i.e. the set of directions minimizing Eq.(4.7)).*

**Proposition 4.2.** *States that differ from one another by local unitary transformations have the same form of $\tilde{g}$. Thus, a classification of multipartite entangled states is possible through the EM.*

## 4.2 Properties of the entanglement distance

In what follows, we will show some important properties that the proposed measure fulfills. We will mostly use Eq.(4.9), to illustrate all the proofs, i.e. the entanglement distance for multipartite qubit states. However, all the following proofs can be trivially generalized to eq.(4.7), i.e. to the entanglement distance for general hybrid multipartite states.

**Proposition 4.3.** *The entanglement distance for a general hybrid M-qudit system is positive semi-definite*

$$E(|s\rangle) \geq 0 . \tag{4.17}$$

*Proof.* We can show that (see App. E)

$$\mathrm{Tr}(A_\mu) \geq \frac{2(d_\mu^2 - 1)}{d_\mu} - \frac{2(d_\mu - 1)}{d_\mu} , \tag{4.18}$$

which induces,

$$\mathrm{Tr}(A_\mu) - 2(d_\mu - 1) \geq 0 . \tag{4.19}$$

Thus,

$$E(|s\rangle) \geq 0 \, . \tag{4.20}$$

■

**Lemma 4.2.** *For a maximally entangled state $|s\rangle$, the expectation value of the generators is equal to zero, i.e.*

$$\langle s|T_{\mu k}|s\rangle = 0 \tag{4.21}$$

*for each $\mu = 0, \ldots, M-1$ and $k = 1, \ldots, d_\mu^2 - 1$.*

As a result of Lemma 4.2, the entanglement measure for a maximally entangled state is thus

$$E(|s\rangle) = \sum_{\mu=0}^{M-1} \frac{2(d_\mu - 1)}{d_\mu} \, , \tag{4.22}$$

We will use Lemma 4.1 to show that the entanglement distance does not increase under LOCC. Since LOCC are a subset of separable operations (see Chapter 3), We will first proceed by showing in Lemmas 4.3 and 4.4 that the local purities $\mathrm{Tr}\left[(\rho^\mu)^2\right]$ cannot decrease, on average, under separable operations. This has been proved in Ref.[7]. We will adopt their proof to our work and notation. The following proofs can be easily generalized to the entanglement distance for multipartite qudits systems, i.e. Eq.(4.7).

**Lemma 4.3.** *Local purities cannot decrease, on average, under local operations.*

*Proof.* Let $\mathcal{H}P^{\otimes M} = P\left(\bigotimes_{\mu=0}^{M-1} \mathcal{H}_\mu\right)$ be the projective space of the joint Hilbert spaces of $M$-partite system. Then, let $\phi_\mu$ be a CPTP map acting only on the $\mu$th subsystem via the set of Kraus operators $\{A_\mu^{\alpha_\mu}\}$, where $\sum_{\alpha_\mu} A_\mu^{\alpha_\mu \dagger} A_\mu^{\alpha_\mu} = \mathbb{1}_\mu$. The action of the Kraus operators on the $\mu$th subsystem is (see Eq.(3.10)) is

$$\rho_{\alpha_\mu} = \frac{1}{p_{\alpha_\mu}} A_\mu^{\alpha_\mu} \rho A_\mu^{\alpha_\mu \dagger} \, , \tag{4.23}$$

where $\rho_{\alpha_\mu}$ is the state of the system after the local operation on subsystem $\mu$ has given $\alpha_\mu$ as a result, and $p_{\alpha_\mu}$ is the probability of getting the state $\rho_{\alpha_\mu}$. Suppose $\rho_\nu = \mathrm{Tr}_{\nu^c}(\rho)$ is the reduced state of the $\nu$th subsystem associated to $\rho$ and $(\rho_\nu)_{\alpha_\mu} = \mathrm{Tr}_{\nu^c}(\rho_{\alpha_\mu})$ is the reduced state of the $\nu$th subsystem associated to $\rho_{\alpha_\mu}$. Two situations arise

1. If $\nu = \mu$, then the reduced state after outcome $\alpha$ is obtained reads

$$(\rho_\nu)_{\alpha_\mu} = \frac{1}{p_{\alpha_\mu}} A_\mu^{\alpha_\mu} \rho_\nu A_\mu^{\alpha_\mu \dagger} \, . \tag{4.24}$$

From the polar decomposition of $A_\mu^{\alpha_\mu}\sqrt{\rho_\nu}$ (see Nielson and Chuang book [116], in Chapter 12), it follows that there exists $V_{\alpha_\mu}$ unitary such that

$$\sqrt{\rho_\nu}A_\mu^{\alpha_\mu\dagger}A_\mu^{\alpha_\mu}\sqrt{\rho_\nu} = V_{\alpha_\mu}A_\mu^{\alpha_\mu}\rho_\nu\, A_\mu^{\alpha_\mu\dagger}V_{\alpha_\mu}^\dagger \ . \tag{4.25}$$

Taking the sum over $\alpha_\mu$ of the above equation, we get

$$\begin{aligned}\rho_\nu &= \sum_{\alpha_\mu} V_{\alpha_\mu}A_\mu^{\alpha_\mu}\rho_\nu\, A_\mu^{\alpha_\mu\dagger}V_{\alpha_\mu}^\dagger \\ &= \sum_{\alpha_\mu} p_{\alpha_\mu}V_{\alpha_\mu}\left(\rho_\nu\right)_{\alpha_\mu}V_{\alpha_\mu}^\dagger \ .\end{aligned} \tag{4.26}$$

This leads to the majorization relation (see Theorem 11 in Ref.[117] or Chapter 12 in [116])

$$\boldsymbol{\lambda}\left(\rho_\nu\right) \prec \sum_{\alpha_\mu} p_{\alpha_\mu}\,\boldsymbol{\lambda}\left[\left(\rho_\nu\right)_{\alpha_\mu}\right] \ , \tag{4.27}$$

where $\boldsymbol{\lambda}\left(\sigma\right)$ is the vector of eigenvalues of $\sigma$ arranged in decreasing order.

2. If $\nu \neq \mu$, then $\left(\rho_\nu\right)_{\alpha_\mu}$ is the state of the $\nu$th subsystem after an operation has been applied on the $\mu$th subsystem, and in this case, we have

$$\rho_\nu = \sum_{\alpha_\mu} p_{\alpha_\mu}\left(\rho_\nu\right)_{\alpha_\mu} \ . \tag{4.28}$$

We get again the majorization relation

$$\boldsymbol{\lambda}\left(\rho_\nu\right) \prec \sum_{\alpha_\mu} p_{\alpha_\mu}\,\boldsymbol{\lambda}\left[\left(\rho_\nu\right)_{\alpha_\mu}\right] \ . \tag{4.29}$$

Purity is a Schur-convex function, i.e.

$$x \prec y \qquad \Longrightarrow \qquad f\left(x\right) \leq f\left(y\right) \ . \tag{4.30}$$

Equations (4.27) and (4.30) yield

$$\mathrm{Tr}\left[\left(\rho_\nu\right)^2\right] \leq \mathrm{Tr}\left[\left(\sum_{\alpha_\mu} p_{\alpha_\mu}\left(\rho_\nu\right)_{\alpha_\mu}\right)^2\right] . \tag{4.31}$$

Knowing that purity is a convex function, we have finally

$$\mathrm{Tr}\left[\left(\rho_\nu\right)^2\right] \leq \sum_{\alpha_\mu} p_{\alpha_\mu}\,\mathrm{Tr}\left[\left(\left(\rho_\nu\right)_{\alpha_\mu}\right)^2\right] . \tag{4.32}$$

Thus we have shown that the action of $\phi_\mu$ on $\rho$ will not decrease, on average, the local purity of any reduced state $\rho_\nu$. ■

Lemma 4.3 can be generalized as follows to separable operations.

**Lemma 4.4.** *local purities cannot decrease, on average, under separable operations.*

*Proof.* Let $\mathcal{H}P^{\otimes M} = P\left(\bigotimes_{\mu=0}^{M-1}\mathcal{H}_\mu\right)$ be the projective space of the joint Hilbert spaces of $M$-partite system, and let $\phi$ be a *separable* CPTP map described by Kraus operators $\mathcal{A}_\alpha$. Because $\phi$ is separable, it can be represented with Kraus operators of the form (see Eq.(3.22))

$$\mathcal{A}_\alpha = \bigotimes_{\mu=0}^{M-1} A_\mu^{\alpha_\mu} = A_0^{\alpha_0}\otimes A_1^{\alpha_1}\otimes\cdots\otimes A_{M-1}^{\alpha_{M-1}}\ , \tag{4.33}$$

where $\alpha = \{\alpha_0,\alpha_1,\cdots,\alpha_{M-1}\}$ and $\{A_\mu^{\alpha_\mu}\}$ operators acting on the $\mu$th subsystem via the CPTC map $\phi_\mu$.

In Lemma 4.3, we have shown that the action of each local operation $\phi_\mu$ does not decrease, on average, the local purities. Now, knowing that the majorization relation forms a partial order (see [117, 7]), we have transitivity. Meaning that if

$$\boldsymbol{\lambda}(\rho_\nu) \prec \sum_{\alpha_\mu} p_{\alpha_\mu}\boldsymbol{\lambda}((\rho_\nu)_{\alpha_\mu})$$

and

$$\boldsymbol{\lambda}((\rho_\nu)_{\alpha_\mu}) \prec \sum_{\alpha'_{\mu'}} p_{\alpha'_{\mu'}}\boldsymbol{\lambda}((\rho_\nu)_{\alpha_\mu\,\alpha'_{\mu'}})\ ,$$

then by transitivity, we have

$$\boldsymbol{\lambda}(\rho_\nu) \prec \sum_{\alpha_\mu\,\alpha'_{\mu'}} p_{\alpha_\mu}p_{\alpha'_{\mu'}}\boldsymbol{\lambda}\left[(\rho_\nu)_{\alpha_\mu\,\alpha'_{\mu'}}\right]\ , \tag{4.34}$$

where $(\rho_\nu)_{\alpha_\mu\,\alpha'_{\mu'}}$ is the density matrix $\rho_\nu$ after local operations are performed on $\mu$th and the $\mu'$th subsystems.

Using the fact that the purity is a Schur-convex function, we have

$$\mathrm{Tr}\left[(\rho_\nu)^2\right] \le \sum_\alpha p_\alpha\,\mathrm{Tr}\left((\rho_\nu)_\alpha\right)\ , \tag{4.35}$$

where $p_\alpha = \prod_{\mu=0}^{M-1} p_{\alpha_\mu}$, such that $\sum_\alpha p_\alpha = 1$ and $(\rho_\nu)_\alpha \equiv (\rho_\nu)_{\alpha_1\,\alpha_2\cdots\alpha_M}$.

Therefore, we have shown that local purities cannot decrease, on average, under separable operations $\phi$. ■

**Theorem 4.1.** *The proposed entanglement measure has the following properties:*

(1) $E(|s\rangle) = 0$ *for a fully separable state.*

(2) *E is invariant under unitary local operations.*

(3) $E(|s\rangle)$ *is non-increasing, on average, under LOCC.*

(4) $E(|s\rangle)$ *is additive.*

**Remark:** The convexity of an entanglement measure requirement is important only in the case where the measure can be extended to mixed states. This is not our purpose in this chapter. We will extend the proposed entanglement measure to mixed stated in Chapter 7.

*Proof.*

(1) From Eqs. (E.5) and (4.15) we get $E(|s\rangle) = 0$ for a separable state $|s\rangle$.

(2) This follows trivially from the construction of the proposed entanglement measure (see Eq.4.2).

(3) From Lemma 4.1, we have that

$$E(|s\rangle) = \sum_{\mu} \left(1 - \mathrm{Tr}\left[(\rho^{\mu})^2\right]\right) . \tag{4.36}$$

And from Lemma 4.4, we have shown

$$\mathrm{Tr}\left[(\rho^{\mu})^2\right] \leq \sum_{\alpha} p_{\alpha}\, \mathrm{Tr}\left((\rho^{\mu})_{\alpha}\right) , \tag{4.37}$$

where $p_{\alpha} = \prod_{\mu=0}^{M-1} p_{\alpha_{\mu}}$, such that $\sum_{\alpha} p_{\alpha} = 1$ and $(\rho^{\mu})_{\alpha} \equiv (\rho^{\mu})_{\alpha_1\, \alpha_2 \cdots \alpha_M}$. We have thus,

$$\begin{aligned} 1 - \mathrm{Tr}\left[(\rho^{\mu})^2\right] &\geq 1 - \sum_{\alpha} p_{\alpha}\, \mathrm{Tr}\left((\rho^{\mu})_{\alpha}\right) \\ &\equiv \sum_{\alpha} p_{\alpha} \left(1 - \mathrm{Tr}\left[\,(\rho^{\mu})_{\alpha}\,\right]\right) . \end{aligned}$$

Summing over all the subsystems, we get

$$\begin{aligned} \sum_{\mu=0}^{M-1} \left[1 - \mathrm{Tr}\left(\,(\rho^{\mu})^2\,\right)\right] &\geq \sum_{\mu=0}^{M-1} \left[\sum_{\alpha} p_{\alpha} \left(1 - \mathrm{Tr}\left[\,(\rho^{\mu})_{\alpha}\,\right]\right)\right] \\ &\equiv \sum_{\alpha} p_{\alpha} \left[\sum_{\mu=0}^{M-1} \left(1 - \mathrm{Tr}\left[\,(\rho^{\mu})_{\alpha}\,\right]\right)\right] \end{aligned}$$

Thus, we have

$$E(\rho) \geq \sum_{\alpha} p_{\alpha} E(\rho_{\alpha}) . \tag{4.38}$$

Meaning that the proposed entanglement measure cannot increase, on average, under separable operation. Thus, we immediately have that the proposed Entanglement is non-increasing, on average, under LOCC, because LOCC operations are a subset of separable operations (see Section 3.3).

(4) Let us suppose a pure state $\rho$, expressed as a tensor product of two subsystems, i.e. $\rho = \rho_0 \otimes \rho_1 = |s_0\rangle\langle s_0| \otimes |s_1\rangle\langle s_1|$. Let us assume, for the sake of simplicity, that the subsystems are qubits. From Eq.(4.9), we get the entanglement measure for the state $\rho$, that is

$$\begin{aligned} E(\rho) &= \min_{\{\mathbf{v}_\mu\}_\mu} \sum_{\mu=0}^{1} \left[ 1 - \left[ \mathrm{Tr}\left( \rho_0 \otimes \rho_1 \ (\boldsymbol{\sigma}\cdot\mathbf{v})_\mu \right) \right]^2 \right] \\ &= 2 - \max_{\{\mathbf{v}_\mu\}_\mu} \underbrace{\sum_{\mu=0}^{1} \left[ \mathrm{Tr}\left( \rho_0 \otimes \rho_1 \ (\boldsymbol{\sigma}\cdot\mathbf{v})_\mu \right) \right]^2}_{\mathcal{A}} , \end{aligned} \tag{4.39}$$

where $\sum_{\mu=0}^{1} (\boldsymbol{\sigma}\cdot\mathbf{v})_\mu$ is shortened notation for $\Big( (\boldsymbol{\sigma}\cdot\mathbf{v})_0 \otimes \mathbb{1} + \mathbb{1} \otimes (\boldsymbol{\sigma}\cdot\mathbf{v})_1 \Big)$. Thus, we have

$$\begin{aligned} \mathcal{A} &= \sum_{\mu=0}^{1} \left[ \mathrm{Tr}\left( \rho_0 \otimes \rho_1 \ (\boldsymbol{\sigma}\cdot\mathbf{v})_\mu \right) \right]^2 \\ &= \underbrace{\left[ \mathrm{Tr}\left( \rho_0 \otimes \rho_1 \ ((\boldsymbol{\sigma}\cdot\mathbf{v})_0 \otimes \mathbb{1}) \right) \right]^2}_{\mathcal{B}_1} + \underbrace{\left[ \mathrm{Tr}\left( \rho_0 \otimes \rho_1 \ (\mathbb{1} \otimes (\boldsymbol{\sigma}\cdot\mathbf{v})_1) \right) \right]^2}_{\mathcal{B}_2} \end{aligned} \tag{4.40}$$

And now, let us compute one of the parts, for example, $\mathcal{B}_1$

$$\begin{aligned} \mathcal{B}_1 &= \left( \sum_{i_0 i_1} \langle i_0| \otimes \langle i_1| \left[ |s_0\rangle\langle s_0| \otimes |s_1\rangle\langle s_1| \left( (\boldsymbol{\sigma}\cdot\mathbf{v})_0 \otimes \mathbb{1} \right) \right] |i_0\rangle \otimes |i_1\rangle \right)^2 \\ &= \left( \sum_{i_0 i_1} \langle i_0|s_0\rangle \langle i_1|s_1\rangle \langle s_0| (\boldsymbol{\sigma}\cdot\mathbf{v})_0 |i_0\rangle \langle s_1|i_1\rangle \right)^2 \\ &= \langle s_0| (\boldsymbol{\sigma}\cdot\mathbf{v})_0 |s_0\rangle^2 \ . \end{aligned}$$

The computation of $\mathcal{B}_2$ is similar, and we get

$$\mathcal{B}_2 = \langle s_1| (\boldsymbol{\sigma}\cdot\mathbf{v})_1 |s_1\rangle^2 \ .$$

Thus, $\mathcal{A}$ reads

$$\mathcal{A} = \langle s_0| (\boldsymbol{\sigma}\cdot\mathbf{v})_0 |s_0\rangle^2 + \langle s_1| (\boldsymbol{\sigma}\cdot\mathbf{v})_1 |s_1\rangle^2 \ . \tag{4.41}$$

Finally, replacing $\mathcal{A}$ in eq.(4.39), we get

$$E(\rho_0 \otimes \rho_1) = 2 - \max_{\mathbf{v}_0} \langle s_0| (\boldsymbol{\sigma}\cdot\mathbf{v})_0 |s_0\rangle^2 - \max_{\mathbf{v}_1} \langle s_1| (\boldsymbol{\sigma}\cdot\mathbf{v})_1 |s_1\rangle^2$$

This is equivalent to

$$\min_{\mathbf{v}_0}\left(1-\langle s_0|\left(\boldsymbol{\sigma}\cdot\mathbf{v}\right)_0|s_0\rangle^2\right)+\min_{\mathbf{v}_1}\left(1-\langle s_1|\left(\boldsymbol{\sigma}\cdot\mathbf{v}\right)_1|s_1\rangle^2\right)$$

Thus,

$$E(\rho_0\otimes\rho_1)=E(\rho_1)+E(\rho_2) \tag{4.42}$$

This can be generalized to any M-qubits system, and also to any M-qudit system, since the entanglement measures for qubits and qudits in Equations (4.14) and (4.9) have the same structure, i.e. based on the trace of the product of the state system $\rho$ and the operators $\left(\boldsymbol{\sigma}\cdot\mathbf{v}\right)_\mu$ for qubits or $\left(\boldsymbol{T}\cdot\mathbf{v}\right)_\mu$ for qudits.

■

## 4.3 Chapter conclusions

So far, many successful measures of entanglement for bipartite systems have been proposed [166, 158, 128, 155]. And various entanglement measures for multipartite systems have been proposed [57, 164, 113, 159, 24, 33] too. However, there is currently no such measure that is both analytically simple to calculate and applicable to hybrid multipartite systems. In this chapter (the work has been done in Ref.[41]), we have proposed an entanglement measure, that we named *entanglement distance*, for hybrid multipartite pure states. It is analytically easy to compute. In fact, this will be the task of the next Chapter, i.e. we will compute the entanglement distance for a variety of examples. We have shown in this Chapter that it fulfills all the requirements for a good measure of entanglement. That is: *i*) the entanglement distance is zero for a fully separable state, *ii*) it is invariant under unitary local operations, *iii*) it is non-increasing on average, under LOCC, and *iv*) it is additive.

# 5

# Physical interpretation of the entanglement distance

This chapter is based on a personal work. In Chapter 4, we have presented the calculations that led to the construction of the entanglement distance. In this Chapter, we want to dive a little bit deeper than presenting only complex calculus, we want to give a simple physical interpretation and the intuition behind such a measure. We will show that the proposed entanglement distance has the physical interpretation of a lack of knowledge of the spin of the subsystems. If the spin of all the subsystems can be known, then the entanglement distance is equal to zero. However, if the spin of one of the subsystems cannot be known, the measure is different from zero. During an experiment, the spin is a random variable. And a way to measure the lack of knowledge of a random variable is the variance. We will show that the entanglement distance is actually the sum of the spin variances computed for each subsystem. We will prove this for qubit systems. However, this can be trivially generalized to qudit systems. First, in Section 5.1, we will briefly review the variance of a random variable in classical physics. Then, in Section 5.2, we will see how we define the spin variance for quantum systems. We will show in Section 5.3 that the variance of the spin of the $\mu$th qubit in a multipartite state is actually the distance squared defined in the Bloch ball. Next, Section 5.4 will be about expressing the $\mu$th spin variance in terms of the $\mu$th spin probability distribution, because, this will be helpful to express in Section 5.5 the spin variance in terms of the Linear entropy.

## 5.1 The variance of a random variable in classical physics

In probability theory, the expectation value of a random variable $X$ with a finite list of possible outcomes $x_1, \ldots, x_n$, is defined as $\mathbb{E}[X] = p_1x_1 + p_2x_2 + \cdots + p_nx_n$, where $p_i$ is the probability of obtaining the value $x_i$. In general, randomness prevents the outcome of a single random experiment from being predicted. However, the strong law of large numbers makes it possible to better predict the result if a large number of experiments of the same type are performed. Let us take a basic example of an expectation value calculation in classical probability theory, which will be useful thereafter for a comparison with the spin expectation value in quantum mechanics. Suppose we roll 4 times an unbiased die and record the number of one. After rolling the die 4 times, we may for

example not get the number 1, thus $X = 0$. Or, we may get 4 times the number 1, so $X = 4$, etc. And each of these different outcomes has a probability of occurrence. This is summarized in the following table. The expectation value

| $X$ | 0 | 1 | 2 | 3 | 4 |
|---|---|---|---|---|---|
| $p(x)$ | 0.48 | 0.39 | 0.11 | 0.015 | 0.0007 |

Table 5.1: $X$ can take five different values with different probabilities $p(x)$.

is thus equal to $E(X) = 0.66$ and it predicts the average value obtained for $X$ if the experiment is repeated a very large number of times. The uncertainty on the random variable is measured with the variance, defined as follows

$$\mathrm{Var}[X] = \mathbb{E}\left[X^2\right] - \mathbb{E}[X]^2 \ ,$$

or with its square root, which is the standard deviation.

## 5.2 The variance of the spin in quantum mechanics

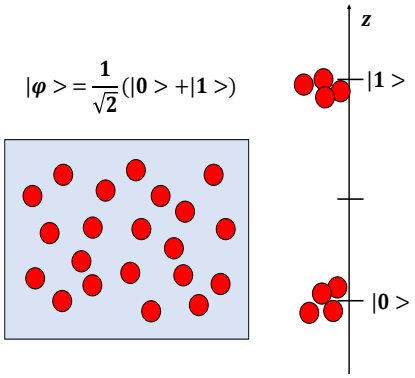


Figure 5.1: Schematic setup of a quantum measurement through a Stern-Gerlach apparatus. The experiment allows computing the expectation value of the spin along the direction $\mathbf{z}$ of a system prepared in the state $|\psi\rangle = (|0\rangle + |1\rangle)/\sqrt{2}$. Experimentally, a large number of systems (red spheres) are prepared in the state $|\psi\rangle$, and each system is projected either on $|0\rangle$ or on $|1\rangle$ with equal probabilities.

In quantum mechanics, an experimental setup is described by the state $\psi$ of the system that is defined as a ray in a projective Hilbert space $\mathcal{PH}$ and the observable $\hat{O}$ to be measured. The expectation value of $\hat{O}$ in a normalized state $\psi$ is denoted as

$$\begin{aligned} \langle \hat{O} \rangle_\psi &= \langle \psi | \hat{O} | \psi \rangle \\ &= \sum_i a_i |\langle a_i | \psi \rangle|^2 \ , \end{aligned} \tag{5.1}$$

where $|a_i\rangle$ are eigenvectors of $\hat{O}$ with eigenvalues $a_i$ and $|\langle a_i|\psi\rangle|^2$ is the probability of obtaining the eigenvalue $a_i$. The spin $\vec{S}$ of a quantum system

is a vector observable, i.e. $\vec{S} = S_x\vec{e}_x + S_y\vec{e}_y + S_z\vec{e}_z$, if expressed in Cartesian coordinates. The hat is omitted here since there is no classical variable we can confuse the spin with. Systems having spin 1/2 can have their spin described by the Pauli matrices $(\sigma_x, \sigma_y, \sigma_z)$, that span the space of observables of the complex 2-dimensional Hilbert space

$$S_x = \frac{h}{2}\begin{pmatrix} 0 & 1 \\ 1 & 0 \end{pmatrix}, \quad S_y = \frac{h}{2}\begin{pmatrix} 0 & -i \\ i & 0 \end{pmatrix}, \quad S_z = \frac{h}{2}\begin{pmatrix} 1 & 0 \\ 0 & -1 \end{pmatrix},$$

where $h$ is the Planck constant. In what follows, the study of the spin 1/2 will be done only through the Pauli matrices, i.e. $h/2$ will be omitted. The difference between the die example is that in quantum mechanics, measuring the spin of a quantum system collapses its wave function. Thus, the expected value in quantum mechanics does not refer to the average value of the results that one would obtain after many trials on the same system as for the die. In fact, if we observe the system's spin many times, we will get the same result, because of the collapse of the wave function that would have occurred during the first trial. Instead, we prepare several quantum systems in the same state and observe the spin of each of them, then average the results obtained for each system (see Figure 5.1).

As for any random variable, the expectation value of the spin along a given direction indicates the lack of knowledge one has on the spin along that direction. Let us give some examples to illustrate this better.

**Example 5.1.** *Suppose the following separable state $|\psi_1\rangle = |0\rangle \otimes |0\rangle$, where both systems are prepared in the spin up along the direction* $\mathbf{z}$*. And, suppose that two local observers 1 and 2 measure through a Stern-Gerlach apparatus the spins of the two subsystems along the direction* $\mathbf{z}$*. The expectation value of the spin along* $\mathbf{z}$ *of each system in this state is equal to one, i.e. $\langle\psi_1| \sigma_z \otimes \mathbb{1} |\psi_1\rangle = \langle\psi_1| \mathbb{1} \otimes \sigma_z |\psi_1\rangle = 1$, where $\sigma_z$ has $\{|0\rangle, |1\rangle\}$ as eigenvectors. This means that each observer knows perfectly the state of the subsystem he is measuring. They do not have any lack of knowledge about the subsystems spin they are measuring.*

**Example 5.2.** *Suppose now that the state of the second system in the previous example is rotated along the* $\mathbf{y}$ *direction, for example, $|\psi_2\rangle = |0\rangle \otimes (|0\rangle + |1\rangle)(1/\sqrt{2})$. In this case, the expectation values of the two spin systems along* $\mathbf{z}$ *are $\langle\psi_2| \sigma_z \otimes \mathbb{1} |\psi_2\rangle = 1$ and $\langle\psi_2| \mathbb{1} \otimes \sigma_z |\psi_2\rangle = 0$. The second system is in an equal superposition of states $|0\rangle$ and $|1\rangle$, which implies that when the second observer measures along* $\mathbf{z}$*, the spin measure will be in one of the two states with equal probabilities. Thus, the second observer completely lacks knowledge about the state of the subsystem along the* $\mathbf{z}$ *direction. However, $|+\rangle = (|0\rangle + |1\rangle)(1/\sqrt{2})$ is an eigenstate of $\sigma_x$, giving $\langle\psi_2| \mathbb{1} \otimes \sigma_x |\psi_2\rangle = 1$. This means that there is no lack of knowledge along the* $\mathbf{x}$ *direction. The state of the second subsystem is completely determined along the* $\mathbf{x}$ *direction.*

Importantly, the lack of knowledge about a subsystem's spin cannot be canceled if the subsystem is entangled. Let us take again some examples.

**Example 5.3.** *Suppose that the spin of the qubits in the GHZ state, i.e.*

$$|GHZ\rangle = \frac{1}{\sqrt{2}}\left(|000\rangle + |111\rangle\right) \ , \tag{5.2}$$

*is measured locally. A local observer will notice that whatever the direction of observation* $\mathbf{v}$*, the expectation values of the spin are invariably zero, i.e.* $\langle GHZ|\, \sigma_v \otimes \mathbb{1} \otimes \mathbb{1}\, |GHZ\rangle = \langle GHZ|\, \mathbb{1} \otimes \sigma_v \otimes \mathbb{1}\, |GHZ\rangle = \langle GHZ|\, \mathbb{1} \otimes \mathbb{1} \otimes \sigma_v\, |GHZ\rangle = 0\,,\ \forall\, \mathbf{v} \in \mathbb{R}^3$*.*

**Example 5.4.** *On the other hand, if a local observer measures locally the spin of the W state, i.e.*

$$|W\rangle = \frac{1}{\sqrt{3}}\left(|001\rangle + |010\rangle + |100\rangle\right) \ , \tag{5.3}$$

*he will find that along* $\mathbf{z}$*, he gets the biggest spin expectation value, i.e. the less lack of knowledge:* $\langle W|\, \sigma_z \otimes \mathbb{1} \otimes \mathbb{1}\, |W\rangle = \langle W|\, \mathbb{1} \otimes \sigma_z \otimes \mathbb{1}\, |W\rangle = \langle W|\, \mathbb{1} \otimes \mathbb{1} \otimes \sigma_z\, |W\rangle = 1/3$*. Thus, along the* $\mathbf{z}$ *direction, a local observer can decrease the lack of knowledge he has about the spin of the measured subsystem. This is impossible for the GHZ state. This is due to the fact that the W state can be partially expressed as a superposition of states, whereas the GHZ state cannot. The expectation values calculated for the W state are different from zero along* $\mathbf{z}$ *simply because the state is expressed in terms of the eigenvectors of* $\sigma_z$*. We would have had obviously the same result if W was expressed in terms of the eigenvectors of* $\sigma_v$ *and observed along* $\mathbf{v}$*.*

The take-home message here is that, in the case of separable qubits, the lack of spin knowledge can always be eliminated by finding the appropriate direction in which the system's state is not in a superposition of states. This is not the case for a maximally entangled qubit. Entangled systems are by definition systems whose states cannot be fully separated into tensor product states. Thus, the superposition of states is not merely a feature of the measurement, as for separable states. The lack of knowledge does not depend only on the observer and the direction from which he observes the system. Thus, the expectation value calculated locally in different states informs one on the lack of knowledge one has on a qubit, and thus on the degree of entanglement of the subsystem to the rest of the system.

For fully separable states, the expectation value yields 1 along the right direction, which means that the state of the qubit can be fully determined in that direction. However, in the case of entangled states, such as the W-state, there exists a direction in which one can decrease the lack of knowledge one has on each qubit, but can never completely eliminate it, i.e. the expectation value of the spin will always be less than 1. For maximally entangled states such as the GHZ-state, such direction does not exist, the lack of knowledge is completely out of the observer's hand. More generally, the expectation value of the $\mu$th spin along a given direction can be positive or negative. To define a clear quantity that is equal to zero for a maximum lack of knowledge and 1 when the $\mu$th spin is fully known, we can take the square of the expectation value. That is, for a

generic $M$-qubits state $|\psi\rangle \in \mathcal{H}P = P\left(\bigotimes_{\mu=0}^{M-1}\mathcal{H}_\mu\right)$, the $\mu$th spin expectation value squared

$$\langle(\boldsymbol{\sigma}\cdot\mathbf{v})^\mu_M\rangle^2_\psi = \left(\langle\psi|\mathbb{1}^0\otimes\ldots(\boldsymbol{\sigma}\cdot\mathbf{v})^\mu\cdots\otimes\mathbb{1}^{M-1}|\psi\rangle\right)^2 \quad \in \quad [0,1]\ ,$$

where $\mathbf{v}^\mu \in \mathbb{R}^3$ with $||\mathbf{v}^\mu|| = 1$ and $\boldsymbol{\sigma}^\mu$ is the Pauli vector applied on the $\mu$th qubit, is a good quantity for quantifying the lack of knowledge an observer has on the $\mu$th qubit. In fact, we have

i) If $\exists\,\mathbf{w}^\mu \in \mathbb{R}^3$ s.t $\langle(\boldsymbol{\sigma}\cdot\mathbf{w})^\mu\rangle^2_\psi = \max_{\mathbf{v}_\mu}\langle(\boldsymbol{\sigma}\cdot\mathbf{v})^\mu_M\rangle^2_\psi = 1$

$\Longrightarrow$ The $\mu$th qubit is fully separable from the rest of the system.

ii) If $\exists\,\mathbf{w}^\mu \in \mathbb{R}^3$ s.t $0 < \langle(\boldsymbol{\sigma}\cdot\mathbf{w})^\mu\rangle^2_\psi = \max_{\mathbf{v}_\mu}\langle(\boldsymbol{\sigma}\cdot\mathbf{v})^\mu_M\rangle^2_\psi < 1$

$\Longrightarrow$ The $\mu$th qubit is entangled to the system.

iii) If $\langle(\boldsymbol{\sigma}\cdot\mathbf{v})^\mu_M\rangle^2_\psi = 0\ ,\ \forall\,\mathbf{v}^\mu$

$\Longrightarrow$ The $\mu$th qubit is maximally entangled to the system.

To define a quantity that vanishes for separable qubits and gives 1 for maximally entangled qubits, we may resort to the spin variance. The $\mu$th spin variance is a good measure of entanglement of the $\mu$th subsystem

$$\min_{\mathbf{v}^\mu}\mathrm{Var}\left[(\boldsymbol{\sigma}\cdot\mathbf{v})^\mu\right] = \min_{\mathbf{v}^\mu}\left[1-\langle(\boldsymbol{\sigma}\cdot\mathbf{v})^\mu_M\rangle^2_\psi\right]\ , \tag{5.4}$$

where $\langle((\boldsymbol{\sigma}\cdot\mathbf{v})^\mu_M)^2\rangle_\psi = 1$. It vanishes for separable qubits and gives 1 for maximally entangled qubits.

The entanglement distance proposed in Eq.(4.9) in Chapter 4 is exactly the sum of $\min_{\mathbf{v}^\mu}\mathrm{Var}\left[(\boldsymbol{\sigma}\cdot\mathbf{v})^\mu\right]$, defined Eq.(5.4)

$$E(|\psi\rangle) = \sum_{\mu=0}^{M-1}\min_{\mathbf{v}^\mu}\mathrm{Var}\left[(\boldsymbol{\sigma}\cdot\mathbf{v})^\mu\right]\ . \tag{5.5}$$

The entanglement distance measures thus the sum of the lack of knowledge computed for each subsystem.

## 5.3 The variance of a spin $1/2$ and the Bloch sphere

The general form of a single pure state along a given direction $\mathbf{n} \in \mathbb{R}^3$ is

$$|\psi_n\rangle = \cos\left(\frac{\theta_1}{2}\right)|0\rangle + e^{i\varphi_1}\sin\left(\frac{\theta_1}{2}\right)|1\rangle\ , \tag{5.6}$$

and its density matrix reads

$$\rho = |\psi_n\rangle \langle_n \psi| = \frac{1}{2} \left(\mathbb{1} + \boldsymbol{\sigma} \cdot \mathbf{n}\right) \ , \tag{5.7}$$

where $\boldsymbol{n}$ is its Bloch vector

$$\mathbf{n} = \begin{pmatrix} r \sin\theta_1 \cos\varphi_1 \\ r \sin\theta_1 \sin\varphi_1 \\ r \cos\theta_1 \end{pmatrix} \ . \tag{5.8}$$

and where the radius $r$ is equal to 1 for pure states. An experimenter can observe this state along a given direction

$$\mathbf{v} = \begin{pmatrix} \sin\theta_2 \cos\varphi_2 \\ \sin\theta_2 \sin\varphi_2 \\ \cos\theta_2 \end{pmatrix} \ , \tag{5.9}$$

where $||\mathbf{v}|| = 1$. And since he has access to the angles $\theta_2$ and $\varphi_2$, he can choose the direction he wants. The spin expectation value of $|\psi_n\rangle$ along a given direction $\mathbf{v}$ reads

$$\mathrm{Tr}\left( |\psi_n\rangle \langle_n \psi| \left(\boldsymbol{\sigma} \cdot \mathbf{v}\right) \right) = \langle\psi_n| \left(\boldsymbol{\sigma} \cdot \mathbf{v}\right) |\psi_n\rangle \ = \mathbf{n} \cdot \mathbf{v} \tag{5.10}$$

**Lemma 5.1.** *Given a pure M-partite state* $\rho = |\psi\rangle \langle\psi| \in \mathcal{H}P^{\otimes M} = P\left(\bigotimes_{\mu=0}^{M-1} \mathcal{H}_\mu\right)$*, we have the following equality*

$$\mathrm{Tr}\left[ \left(\rho \left(\mathbb{1}^0 \otimes \cdots \boldsymbol{\sigma}^\mu \cdots \otimes \mathbb{1}^{M-1}\right)\right] = \mathrm{Tr}\left(\rho^\mu \boldsymbol{\sigma}^\mu\right) = \mathbf{n}^\mu \ , \tag{5.11}$$

*where*

$$\rho^\mu = \frac{1}{2} \left(\mathbb{1} + \left(\mathbf{n} \cdot \boldsymbol{\sigma}\right)^\mu\right) \ , \tag{5.12}$$

*is the density matrix of the* $\mu$*th subsystem, and* $\mathbf{n}^\mu$ *is the Bloch vector of the* $\mu$*th subsystem, with* $||\mathbf{n}^\mu|| \leq 1$*.*

*Proof.* For a generic $M$-qubit state $\rho = |\psi\rangle \langle\psi| \in \mathcal{H}P^{\otimes M} = P\left(\bigotimes_{\mu=0}^{M-1} \mathcal{H}_\mu\right)$, we have

$$|\psi\rangle = \sum_{i_0 \ldots i_{M-1}} C_{i_0 \ldots i_{M-1}} |i_0\rangle \otimes \cdots \otimes |i_{M-1}\rangle \ . \tag{5.13}$$

Thus, the density matrix of the above pure state is

$$\rho = \sum_{\substack{i_0 \ldots i_{M-1} \\ j_0 \ldots j_{M-1}}} C^*_{j_0 \ldots j_{M-1}} C_{i_0 \ldots i_{M-1}} |i_0\rangle \otimes \cdots \otimes |i_{M-1}\rangle \ \langle j_0| \otimes \cdots \otimes \langle j_{M-1}| \ .$$

The density matrix of the first qubit for example reads

$$\rho^0 = \sum_{k_1 \ldots k_{M-1}} \sum_{\substack{i_0 \ldots i_{M-1} \\ j_0 \ldots j_{M-1}}} C^*_{j_0 \ldots j_{M-1}} C_{i_0 \ldots i_{M-1}} \langle k_1| \otimes \cdots \otimes \langle k_M - 1| \times$$

$$\times \left( |i_0\rangle \otimes \cdots \otimes |i_{M-1}\rangle \ \langle j_0| \otimes \cdots \otimes \langle j_{M-1}| \right) |k_1\rangle \otimes \cdots \otimes |k_{M-1}\rangle \ ,$$

which gives

$$\begin{aligned} \rho^0 &= \sum_{\substack{i_0 \dots i_{M-1} \\ j_0 \dots j_{M-1}}} C^*_{j_0 \dots j_{M-1}} C_{i_0 \dots i_{M-1}} |i_0\rangle \ \langle j_0| \, \delta_{i_1 \, j_1} \dots \delta_{i_{M-1} \, j_{M-1}} \\ &= \sum_{\substack{i_0 \dots i_{M-1} \\ j_0}} C^*_{j_0, i_1 \dots i_{M-1}} C_{i_0 \dots i_{M-1}} |i_0\rangle \ \langle j_0| \ . \end{aligned}$$

The expectation value of the spin of the first qubit in the above $M$-qubits state is

$$\begin{aligned} \mathrm{Tr}\left(\rho^0 \boldsymbol{\sigma}^0\right) &= \sum_{k_0} \sum_{\substack{i_0 \dots i_{M-1} \\ j_0}} C^*_{j_0 \dots i_{M-1}} C_{i_0 \dots i_{M-1}} \langle k_0 | i_0 \rangle \ \langle j_0| \, \boldsymbol{\sigma}^0 \, |k_0\rangle \\ &= \sum_{\substack{i_0 \dots i_{M-1} \\ j_0}} C^*_{j_0 \dots i_{M-1}} C_{i_0 \dots i_{M-1}} \langle j_0 | \boldsymbol{\sigma}^0 | i_0 \rangle \ . \end{aligned} \tag{5.14}$$

On the other hand, using Eq.(5.13), we have

$$\begin{aligned} \mathrm{Tr}\left[\rho \, \boldsymbol{\sigma}^{\,0}_M\right] &= \sum_{k_0 \dots k_{M-1}} \langle k_0 \dots k_{M-1}| \left( |\psi\rangle \langle \psi| \ \boldsymbol{\sigma}^{\,0}_M \right) |k_0 \dots k_{M-1}\rangle \\ &= \sum_{k_0 \dots k_{M-1}} \sum_{\substack{i_0 \dots i_{M-1} \\ j_0 \dots j_{M-1}}} C^*_{j_0 \dots j_{M-1}} C_{i_0 \dots i_{M-1}} \langle k_0 \dots k_{M-1}| \times \\ &\qquad \times \left( |i_0 \dots i_{M-1}\rangle \ \langle j_0 \dots j_{M-1}| \, \boldsymbol{\sigma}^{\,0}_M \right) |k_0 \dots k_{M-1}\rangle \\ &= \sum_{k_0 \dots k_{M-1}} \sum_{\substack{i_0 \dots i_{M-1} \\ j_0 \dots j_{M-1}}} C^*_{j_0 \dots j_{M-1}} C_{i_0 \dots i_{M-1}} \left( \delta_{k_0 i_0} \delta_{k_1 i_1} \dots \delta_{k_{M-1} i_{M-1}} \right) \times \\ &\qquad \times \left( \delta_{j_1 k_1} \dots \delta_{j_{M-1} k_{M-1}} \right) \langle j_0 | \boldsymbol{\sigma}^{\,0}_M | k_0 \rangle \\ &= \sum_{\substack{i_0 \dots i_{M-1} \\ j_0 \dots j_{M-1}}} C^*_{j_0 \dots j_{M-1}} C_{i_0 \dots i_{M-1}} \left( \delta_{j_1 i_1} \delta_{j_{M-1} i_{M-1}} \right) \langle j_0 | \boldsymbol{\sigma}^0_M | i_0 \rangle \\ &= \sum_{\substack{i_0 \dots i_{M-1} \\ j_0}} C^*_{j_0 \dots i_{M-1}} C_{i_0 \dots i_{M-1}} \langle j_0 | \boldsymbol{\sigma}^0_M | i_0 \rangle \ , \end{aligned} \tag{5.15, 5.16}$$

where $\boldsymbol{\sigma}^{\,0}_M := \boldsymbol{\sigma}^0 \otimes \mathbb{1}^1 \otimes \cdots \otimes \mathbb{1}^{M-1}$. Thus, by equations (5.14) and (5.16), we have shown equation (5.11) for $i = 0$. ■

The expectation value of the $\mu$th spin measured along a direction $\mathbf{v} \in \mathbb{R}^3$ in a given $M$-qubits system $\psi \in \mathcal{PH}$ can thus be written in a vector form as follows

$$\mathrm{Tr}\left[ \left( \rho \left( \mathbb{1}^0 \otimes \cdots (\boldsymbol{\sigma} \cdot \mathbf{v})^\mu \cdots \otimes \mathbb{1}^{M-1} \right) \right] = \mathbf{n}^\mu \cdot \mathbf{v}^\mu = ||\mathbf{n}^\mu|| \cos\alpha \ , \tag{5.17}$$

where $\rho = |\psi\rangle\langle\psi|$ and

$$\mathbf{n}^{\mu} = \begin{pmatrix} \langle\psi|\mathbb{1}^0 \otimes \ldots \sigma_x{}^{\mu} \cdots \otimes \mathbb{1}^{M-1}|\psi\rangle \\ \langle\psi|\mathbb{1}^0 \otimes \ldots \sigma_y{}^{\mu} \cdots \otimes \mathbb{1}^{M-1}|\psi\rangle \\ \langle\psi|\mathbb{1}^0 \otimes \ldots \sigma_z{}^{\mu} \cdots \otimes \mathbb{1}^{M-1}|\psi\rangle \end{pmatrix} . \tag{5.18}$$

is the Bloch vector of the $\mu$th qubit. $\mathbf{v}^{\mu}$ is the vector chosen by the local observable to measure the $\mu$th spin and it is always chosen to be of norm 1. The angle $\alpha$ in Eq.(5.17) is the angle that the local observer can modify in order to maximize the expectation value, and it is defined in $[0, \pi]$.

The spin expectation value of the $\mu$th qubit depends thus on two parameters, the norm of the $\mu$th Bloch vector and the angle $\alpha$ between it and the direction of observation. Since $\alpha$ depends on the observer, we will denote it by the *extrinsic* parameter. It represents the lack of knowledge the observer introduces by measuring the spin in a given direction. For $\alpha = 0, \pi$, the observer introduces the minimum lack of knowledge on the qubit considered. Whereas, for $\alpha = \pi/2$, he increases the lack of knowledge to its maximum. However, the Bloch vector adds another condition to the expectation value for it to characterize the lack of knowledge one has on a given qubit. Let us take some examples seen above. The calculation of $\mathbf{n}^{\mu}$ for both qubits in the following state $|\psi_2\rangle = |0\rangle \otimes (1/\sqrt{2})(|0\rangle + |1\rangle)$ reads

$$\mathbf{n}^1 = \begin{pmatrix} 0 \\ 0 \\ 1 \end{pmatrix} \quad \mathbf{n}^2 = \begin{pmatrix} 1 \\ 0 \\ 0 \end{pmatrix} , \tag{5.19}$$

where 1 and 2 refer to the first and second qubits respectively. Whereas for the W and GHZ states, we obtain

$$\begin{aligned} \mathbf{n}^{\mu}_{\mathrm{W}} &= \begin{pmatrix} 0 \\ 0 \\ \frac{1}{3} \end{pmatrix} \\ \mathbf{n}^{\mu}_{\mathrm{GHZ}} &= \begin{pmatrix} 0 \\ 0 \\ 0 \end{pmatrix} , \end{aligned} \tag{5.20}$$

where $\mu = 1, 2, 3$ refers to each of the three qubits.

The degree by which a qubit is entangled to the system is seen by the norm of its Bloch vector. The more the qubit is entangled to the rest of the system, the smaller the norm of its spin representation in the Bloch sphere is, until reaching zero for maximally entangled qubits (see Figure 5.2). Thus, putting the expectation value in a vector form allows us to visualize geometrically the lack of knowledge a local observer has on a given qubit. That is, for spins on the surface of the sphere, if a lack of knowledge is present, then it would only be due to the *extrinsic* parameter. Whereas for those belonging to the ball of the sphere, entanglement also contributes to the lack of knowledge an observer has when measuring the spin of the qubit.

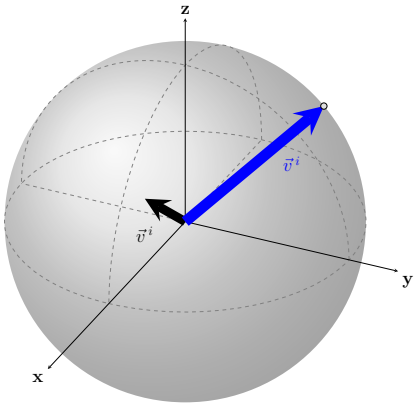


Figure 5.2: The Bloch sphere representation of the spin of a qubit that belongs to a generic state $\psi \in \mathcal{PH}$ of an $M$-qubits system. The black arrow, whose norm is less than 1, represents a qubit which is entangled to the system. Whereas the blue arrow, which norm is equal to 1, represents a separable qubit. The vector vanishes for a maximally entangled qubit.

The variance of the $\mu$th spin in a given $M$-qubits system $\rho = |\psi\rangle\langle\psi| \in \mathcal{PH}^{\otimes M}$ is

$$\mathrm{Var}\big[\,(\boldsymbol{\sigma}\cdot\mathbf{v})^{\mu}\,\big] = 1 - ||\,\langle(\boldsymbol{\sigma}\cdot\mathbf{v})\,{}^{\mu}_{M}\rangle_{\psi}\,||^2\,, \tag{5.21}$$

where

$$||\,\langle(\boldsymbol{\sigma}\cdot\mathbf{v})\,{}^{\mu}_{M}\rangle_{\psi}\,||^2 = ||\,\langle\psi|\mathbb{1}^0\otimes\ldots(\boldsymbol{\sigma}\cdot\mathbf{v})^{\,\mu}\cdots\otimes\mathbb{1}^{M-1}|\psi\rangle\,||^2\,.$$

In terms of the density matrix, the $\mu$th spin variance reads

$$\begin{aligned}\mathrm{Var}\big[\,(\boldsymbol{\sigma}\cdot\mathbf{v})^{\mu}\,\big] &= 1 - \left[\mathrm{Tr}\left(\rho\,(\boldsymbol{\sigma}\cdot\mathbf{v})^{\mu}_{M}\right)\right]^2 \\ &= 1 - \left[\mathrm{Tr}\left(\rho^{\mu}\,(\boldsymbol{\sigma}\cdot\mathbf{v})^{\mu}\right)\right]^2 \\ &= 1 - ||\mathbf{n}^{\mu}||^2\cos\alpha^2\,,\end{aligned} \tag{5.22}$$

where $\rho^{\,\mu}$ is defined in Eq.(5.12), and $\mathbf{n}^{\mu}$ is the Bloch vector of $\rho^{\,\mu}$. The angle $\alpha$ is defined in Eq.(5.17) and it is the angle between $\mathbf{v}$ and $\mathbf{n}^{\mu}$. The minimization of the variance coincides with the local observer choosing $\alpha = 0$. Thus, we have

$$\min_{\mathbf{v}^{\mu}}\mathrm{Var}\big[\,(\boldsymbol{\sigma}\cdot\mathbf{v})^{\mu}\,\big] = 1 - ||\mathbf{n}^{\mu}||^2\,, \tag{5.23}$$

which shows that the minimized spin variance is actually a distance squared in $\mathbb{R}^3$. Therefore, the minimized spin variance can be expressed as follows

$$\min_{\mathbf{v}^{\mu}}\mathrm{Var}\big[\,(\boldsymbol{\sigma}\cdot\mathbf{v})^{\mu}\,\big] = ||\tilde{\mathbf{n}}^{\mu}||^2 - ||\mathbf{n}^{\,\mu}||^2\,, \tag{5.24}$$

where $||\tilde{\mathbf{n}}^{\mu}|| = 1$. Physically, this would mean that the minimized spin variance of a given qubit indicates how mixed the qubit is since it is equal to the difference between the squared norm of a qubit's Bloch vector $\mathbf{n}^{\mu}$ and the squared norm of its Bloch vector $\tilde{\mathbf{n}}^{\mu}$ if it was completely separable. In Figure 5.3, we have plotted the variance of the $\mu$th spin as a function of the extrinsic parameter

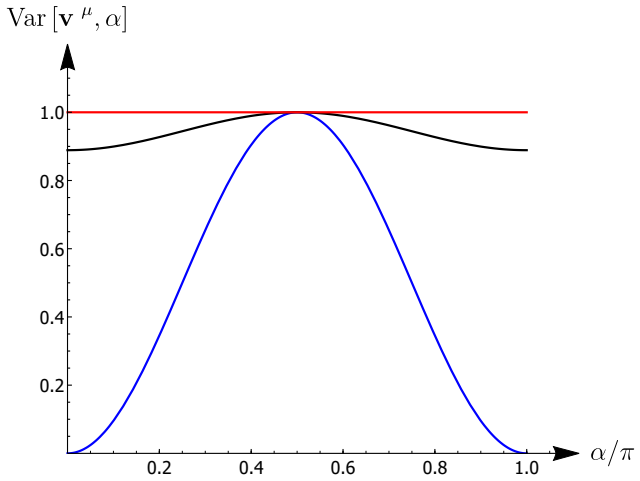


Figure 5.3: The figure depicts the spin variance in the case where *i*) the $\mu$th subsystem is maximally entangled to the rest of the system (curve in red). *ii*) The $\mu$th subsystem is entangled to the rest of the system (curve in black). *iii*) And the $\mu$th subsystem is fully separable from the rest of the system (curve in blue)

in the case of a fully separable subsystem, an entangled subsystem, and a maximally entangled subsystem. If the $\mu$th subsystem is fully separable, then the lack of knowledge can be canceled completely by the observer. That is, if $\alpha = 0, \pi$, the spin variance is equal to zero. If the $\mu$th subsystem is maximally entangled, then the lack of knowledge an observer has does not depend on him. It is completely intrinsic to the subsystem. This is shown in Figure 5.3, where the red curve does not depend on $\alpha$. However, if the subsystem is entangled, but not maximally entangled, the observer can still introduce and remove a small amount of a lack of knowledge.

## 5.4 The spin variance in terms of the spin probability distribution

A binary discrete distribution is characterized by a random variable $x$ which can only take two values, e.g. $x \in \{1, -1\}$ (Bernoulli process), the probability distribution function of $x$ can be parameterized as follows

$$\begin{aligned} p\left(x = 1|\Theta\right) &= \Theta \\ p\left(x = -1|\Theta\right) &= 1 - \Theta \,, \end{aligned} \tag{5.25}$$

where $0 \leq \Theta \leq 1$ and

$$\sum_{x \in \{1,-1\}} p\left(x|\Theta\right) = 1 \,. \tag{5.26}$$

This means that $x$ takes the value 1 with probability $\Theta$ and the value 0 with probability $1 - \Theta$. The expectation value of $x$ is

$$\mathbb{E}\left[x\right] = \sum_{x \in \{1,-1\}} p\left(x|\Theta\right)$$

$$\begin{aligned} &= 1 \cdot \Theta + (-1) \cdot (1 - \Theta) \\ &= 2\Theta - 1 \ , \end{aligned} \tag{5.27}$$

and its variance is

$$\begin{aligned} \mathrm{Var}\left[x\right] &= \mathbb{E}\left[\left(x - \mathbb{E}\left[x\right]\right)^2\right] \\ &= \mathbb{E}\left[\left(x + 1 - 2\Theta\right)^2\right] \\ &= \sum_{x \in \{1,-1\}} \left(x + 1 - 2\Theta\right)^2 p\left(x|\Theta\right) \\ &= \left(2 - 2\Theta\right)^2 \Theta + 4\Theta^2 \left(1 - \Theta\right) \\ &= 4\Theta\left(1 - \Theta\right) \ . \end{aligned} \tag{5.28}$$

We can now relate these calculations to the variance and expectation value of the spin of a given $\mu$th qubit in $\psi \in \mathcal{PH}^{\otimes M}$. In fact, since the spin of a qubit during a measurement behaves as a random variable that can take only two values; up or down (1 or $-1$), it can thus be represented by a binary distribution.

A projective-valued measure along a given direction $\mathbf{v}$ of the spin of the $\mu$th qubit in $\psi \in \mathcal{PH}^{\otimes M}$ is described by a set of projectors

$$\left\{\Pi^{\mu}_{+v},\, \Pi^{\mu}_{-v}\right\} ,$$

where

$$\Pi^{\mu}_{\pm v} = \mathbb{1}^0 \otimes \cdots \otimes \left(\frac{1}{2}\left(1 \pm \boldsymbol{\sigma} \cdot \mathbf{v}\right)\right)^{\mu} \otimes \cdots \otimes \mathbb{1}^{M-1} \ .$$

The probability of getting spin up (or down) along $\mathbf{v}$ (denoted $p\left(+v\right)^{\mu}$ and $p\left(-v\right)^{\mu}$ respectively) for a given qubit $\mu$ in $\psi \in \mathcal{PH}^{\otimes M}$ is[1]

$$\begin{aligned} p\left(\pm v\right)^{\mu} &= \langle\psi|\Pi^{\mu}_{\pm v}|\psi\rangle \\ &= \frac{1}{2}\left(1 \pm \langle\left(\boldsymbol{\sigma} \cdot \mathbf{v}\right)^{\mu}\rangle_M\right) \ , \end{aligned} \tag{5.29}$$

where

$$\langle\left(\boldsymbol{\sigma} \cdot \mathbf{v}\right)^{\ \mu}\rangle_M = \langle\psi|\mathbb{1}^0 \otimes \ldots \left(\boldsymbol{\sigma} \cdot \mathbf{v}\right)^{\ \mu} \cdots \otimes \mathbb{1}^{M-1}|\psi\rangle \ ,$$

Now, as we did above in Eq.(5.25), we can parameterize the probability distribution $\{p\left(+v\right)^{\mu}, p\left(-v\right)^{\mu}\}$ as follows

$$\begin{aligned} p\left(+v|\Theta\right)^{\mu} &= \Theta^{\mu} \\ p\left(-v|\Theta\right)^{\mu} &= 1 - \Theta^{\mu} \ , \end{aligned} \tag{5.30}$$

[1] In the case of one qubit for example, the expectation value of $\sigma_x$ in the state $|0\rangle$ is given by $\langle 0|\sigma_x|0\rangle = \langle 0|\Big(|+\rangle\langle +| - |-\rangle\langle -|\Big)|0\rangle = \langle 0|\Pi_{+x}|0\rangle - \langle 0|\Pi_{-x}|0\rangle = p\left(+x\right) - p\left(-x\right)$, where $\{|0\rangle, |1\rangle\}$ and $\{|+\rangle, |-\rangle\}$ are the set of eigenstates of $\sigma_z$ and $\sigma_x$ respectively. Thus, the probability of getting spin up (or down) along $x$ for a given state $|\psi\rangle$ is

$$p\left(\pm x\right) = \langle\psi|\Pi_{\pm x}|\psi\rangle \ ,$$

where $\Pi_{\pm} = \frac{1}{2}\left(\mathbb{1} + \sigma_x\right)$.

where $\mu$ denotes the $\mu$th qubit. Thus, from equations (5.29) and (5.30), we get the spin expectation value of the $\mu$th qubit in terms of $\Theta^\mu$

$$\langle (\boldsymbol{\sigma}\cdot\mathbf{v})^{\ \mu}\rangle_M = 2\Theta^\mu - 1\ , \tag{5.31}$$

which is similar to Eq.(5.27). And finally, the spin variance of the $i$th qubit in terms of $\Theta^\mu$ reads

$$\mathrm{Var}\big[\,(\boldsymbol{\sigma}\cdot\mathbf{v})^\mu\,\big] = 4\Theta^\mu\,(1-\Theta^\mu)\ . \tag{5.32}$$

Note that, the maximum lack of knowledge we can get on the spin of the $\mu$th subsystem is when $\Theta^\mu = 1/2$, which gives $\mathrm{Var}\big[\,(\boldsymbol{\sigma}\cdot\mathbf{v})^\mu\,\big] = 1$. If $\Theta^\mu$ is equal to 1 or 0, $\mathrm{Var}\big[\,(\boldsymbol{\sigma}\cdot\mathbf{v})^\mu\,\big] = 0$.

## 5.5 The spin variance and the linear entropy

The von Neumann entropy of the $\mu$th qubit is

$$\begin{aligned} S_v^\mu &= -\,\mathrm{Tr}\,\rho^\mu\log\rho^\mu \\ &= -\,\mathrm{Tr}\left[\sum_i p_i\,|\psi_i\rangle\,\langle\psi_i|\log\left(\sum_j p_i\,|\psi_j\rangle\,\langle\psi_j|\right)\right], \end{aligned} \tag{5.33}$$

where $\rho^\mu$ is expressed in a diagonal form with respect to an orthonormal basis $\{|\psi_i\rangle\}$. Linear entropy is an approximation of von Neumann entropy and it is defined as follows [113, 24]

$$\begin{aligned} S_L^\mu &\simeq -\,\mathrm{Tr}\,\rho^\mu\,(\rho^\mu - 1) \\ &= 1 - \mathrm{Tr}\,\big[\,(\rho^\mu)^2\,\big]\ . \end{aligned} \tag{5.34}$$

An important thing to note here is that Linear entropy informs on the intrinsic lack of knowledge since it is expressed solely in terms of the density matrix of the considered subsystem. It is not expressed in terms of the vector $\mathbf{v}$, which is the direction of the local observer that can introduce more lack of knowledge. For a qubit subsystem, we have $\{|\psi_i\rangle\} = \{|+n\rangle\,,|-n\rangle\}$, such that (see Eq.(5.30))

$$\sum_i p_i\,|\psi_i\rangle\,\langle\psi_i| = \tilde{\Theta}\,|+n\rangle\,\langle+n| + \big(1-\tilde{\Theta}\big)\,|-n\rangle\,\langle-n|\ , \tag{5.35}$$

where the tilde denotes the probability distribution that minimizes the local lack of knowledge (since there is no influence of a local observer here). Putting the above expression of the $\mu$th density matrix in the Linear entropy defined in Eq.(5.34), we get

$$S_L^\mu = 2\tilde{\Theta}\,\big(1-\tilde{\Theta}\big)\ . \tag{5.36}$$

We thus have

$$\min_{\{\mathbf{v}_\mu\}} \mathrm{Var}\big[\,(\boldsymbol{\sigma}\cdot\mathbf{v})^\mu\,\big] = 2\,S_L^\mu \tag{5.37}$$

The proposed entanglement measure for a multipartite qubit system $|s\rangle \in P\mathcal{H}$ is thus

$$E(|s\rangle) = 2\sum_{\mu=0}^{M-1} S_L^\mu\ . \tag{5.38}$$

## 5.6 Chapter conclusions

In this Chapter, we have shown that if the lack of knowledge an observer has about a given subsystem depends completely on him, then the subsystem is fully separable from the rest of the system. Whereas, for an entangled subsystem, there is an amount of lack of knowledge that the local observer has, which does not depend on him, and for a maximally entangled subsystem, the lack of knowledge a local observer has does not depend at all on him. This lack of knowledge can be measured through the spin variance of the subsystems. We have shown that the entanglement distance is actually the sum of the spin variances computed upon all the subsystems. We have also shown that the entanglement distance is equal to the sum of the local linear entropies. This means that, the physical interpretation of the proposed measure is the sum of the local mixedness.

# 6

# Applications of the entanglement distance

In this Chapter, we verify the efficacy of the proposed entanglement measure. We have published this work in Ref.[41]. We have first considered three different families of states: Briegel Raussendorf states $|r,\phi\rangle_M$, Greenberger-Horne-Zeilinger–like states (GHLS), $|\mathrm{GHZ},\theta\rangle_M$ and the W-like states (WLS), $|\mathrm{W},\theta,\varphi\rangle_M$. The three families of states depend on parameters that adjust their degree of entanglement. The first family of states we considered, has been introduced by Briegel and Raussendorf in Ref.[75]. For this reason, we named the elements in this family Briegel-Raussendorf states. The second family of states, in 6, is related to the Greenberger-Horne-Zeilinger states [74], since it contains one of these states. The third family of states is related to the $W$ state, which was named after Wolfgang Dür [30] who first reported the state together with Guifré Vidal, and Ignacio Cirac in 2002 [43].

In Ref.[26], Briegel and Raussendorf introduced two interesting notions: *Max. connectedness* and *persistency*. The first notion can be understood as follows: Suppose an $M$ qudits state $|\psi\rangle = \sum_{i=0}^{d} \chi_i \, |\phi_i^0\rangle \otimes |\phi_i^1\rangle \otimes \cdots \otimes |\phi_i^{M-1}\rangle$. $|\psi\rangle$ is said to be maximally connected if any two qubits can be projected, with certainty, into a pure Bell state, by measuring the rest of the qubits. For example: if we take the three-qubits $|\mathrm{GHZ}\rangle_3 = (1/\sqrt{2})\,(|000\rangle + |111\rangle)$ state, any two qubits can be projected with certainty to a pure Bell state. Whereas for example, this is not the case of the three-qubits $|\mathrm{W}\rangle_3 = (1/\sqrt{3})\,(|001\rangle + |010\rangle + |100\rangle)$ state. So *max. connectedness* is simply the degree of entanglement of a given state.
The second notion, i.e. *persistency*, is defined by the authors as the minimum number of local measurements such that, for all measurement outcomes, the state is completely disentangled. Roughly speaking, *persistency* defined by Briegel and Raussendorf in [26] is in a sense, the *robustness* defined by Vidal et al. in [157], which quantifies the endurance of entanglement against noise. Or in other words, it is the property that quantifies the operational effort that is needed to destroy all entanglement in a system.
Thus, Briegel and Raussendorf have shown that $|r,\phi\rangle_M$ and $|\mathrm{GHZ},\theta\rangle_M$ are both maximally connected and $|\mathrm{W},\theta,\varphi\rangle_M$ is not. However, $|r,\phi\rangle_M$ is more persistent than $|\mathrm{GHZ},\theta\rangle_M$ when $M \geq 4$. Below $M = 4$, they have the same persistency (robustness). They have also shown, that $|\mathrm{W},\theta,\varphi\rangle_M$ is more persistent than both of them $\forall\ M$.

Therefore, the first test about the efficiency of the proposed measure, we will be doing is to verify if and how the measure depicts the difference between $|r,\phi\rangle_M$ and $|\mathrm{GHZ},\theta\rangle_M$ when $M \geq 4$. Then, to see if the differences between $|\mathrm{W},\theta,\varphi\rangle_M$ and the two former families of states are detected in the entanglement distance.

We also took three other examples, to further test the entanglement distance. We have also considered a family of three-qubit states depending on two real parameters. With a suitable choice of these parameters, the state can be fully separable or bi-separable, whereas in the generic case, it is a genuine tripartite entangled state. The second example is a hybrid two-qudit system. In this example, we will compare the proposed entanglement measure to von Neumann's entropy. And the last example we will be seeing is a state of two qutrits in Section 6.

We will show that the entanglement distance provides an accurate description of all these cases. In the examples taken below, we will compute the entanglement distance given in Eq.(4.11) in the case of hybrid qudit systems. For the qubit states, we will compute the entanglement distance defined in Eq(4.9) and the entanglement metric (EM) defined in Eq.(4.16). We will see that the association of the entanglement measure with the information contained in the entanglement metric allows the classification of entangled qubit-states. We have published the work presented in this Chapter in Ref.[41].

## Greenberger-Horne-Zeilinger–like states

Let us consider the first family of $M$-qubit states, the GHZLS, defined according to

$$|\mathrm{GHZ},\theta\rangle_M = \cos(\theta)|0\rangle + \sin(\theta)e^{i\varphi}|2^M - 1\rangle\,. \tag{6.1}$$

For $\theta = k\pi/2$ and $\forall\varphi$, where $k \in \mathbb{Z}$, these states are fully separable, whereas $\theta = k\pi/2 + \pi/4$ $(\forall\varphi)$ selects the maximally entangled states. In this case, the trace for the Fubini-Study metric,

$$\mathrm{Tr}(g) = M - \cos^2(2\theta)\sum_{\nu=0}^{M-1}(v_3^\nu)^2\,, \tag{6.2}$$

is minimised by the values $v_3^\nu = 1$. The entanglement metric (EM) reads thus,

$$\tilde{g} = \sin^2(2\theta)J_M \tag{6.3}$$

where $J_M$ is the $M \times M$ matrix of ones. And, the entanglement measure for the GHZLS is

$$E(|\mathrm{GHZ},\theta\rangle_M) = \mathrm{Tr}\,\tilde{g} = M\sin^2(2\theta)\,. \tag{6.4}$$

**Remarks:**

1. If the state in Eq(6.1) is maximally entangled, the EM reads

$$\tilde{g} = J_M\,, \tag{6.5}$$

and the entanglement measure

$$E(|\mathrm{GHZ},\theta\rangle_M^{\max}) = M\,. \tag{6.6}$$

2. The family of maximally two-qubit entangled states obtained from Eq.(6.1) is the one containing all Bell-states.

We will now show that in the case of $M = 2, 3$, the maximally-entangled BRS and the maximally entangled GHZLS are equivalent. In fact, we will show that they only differ by local unitary transformations. We will show that in the case of $M = 2, 3$, the EMs of the maximally entangled states belonging to these two families are identical. We will also see that in the case of $M \geq 4$, the EMs of the maximally entangled states of the two families are different. This will be the first successful test of the validity of the entanglement distance since as said in the introduction of this Chapter, it has been shown [26], that above $M = 3$ the GHZ and BR states are not equivalent.

## Briegel Raussendorf states

The second family of states we consider is the one that was described by Briegel and Raussendorf in [26]. They considered three different arrangements of qubits: the first in a one-dimensional lattice (spin chain), the second, in a two-dimensional lattice, and the third, in a three-dimensional lattice. In what follows, we will only consider their first example, i.e. the spin chain case. They considered $M$ qubits prepared all in the state

$$|r, 0\rangle = \bigotimes_{\mu=0}^{M-1} \frac{1}{\sqrt{2}}(|0\rangle_\mu + |1\rangle_\mu) \, . \tag{6.7}$$

Each $M$-qubit state of the BRS class is derived by applying to the fully separable state in Eq.(6.7), the non-local unitary operator

$$U_0(\phi) = \exp(-i\phi H_0) = \prod_{\mu=1}^{M-1} \left( \mathbb{I} + \alpha \Pi_0^\mu \Pi_1^{\mu+1} \right) \, , \tag{6.8}$$

where $H_0 = \sum_{\mu=1}^{M-1} \Pi_0^\mu \Pi_1^{\mu+1}$ and $\alpha = (e^{-i\phi} - 1)$. We denote with $\Pi_0^\mu = (\mathbb{1} + \sigma_3^\mu)/2$ and $\Pi_1^\mu = (\mathbb{1} - \sigma_3^\mu)/2$ the projector operators onto the eigenstates of $\sigma_{\mu 3}$, $|0\rangle_\mu$ (with eigenvalue $+1$) and $|1\rangle_\mu$ (with eigenvalue $-1$), respectively, where $\mu$ denotes the $\mu$th qubit and $\sigma_{\mu 3}$ is the third Pauli matrix applied on the $\mu$th qubit.

The full operator (6.8) is diagonal on the states of the standard basis $\{|0 \cdots 0\rangle \, , \, |0 \cdots 01\rangle, \ldots, |1 \cdots 1\rangle\}$. In fact, each vector of the latter basis is identified by $M$ integers $n_0, \ldots, n_{M-1} = 0, 1$ as $|\{n\}\rangle = |n_{M-1} \; n_{M-2} \quad n_0\rangle$ and we can enumerate such vectors according to the binary integers representation $|k\rangle = |\{n^k\}\rangle$, with $k = \sum_{\mu=0}^{M-1} n_\mu^k 2^\mu$, where $n_\nu^k$ is the $\nu$-th digit of the number $k$ in binary representation and $k = 0, \ldots, 2^M - 1$. Then, the eigenvalue $\lambda_k$ of the operator (6.8), corresponding to a given eigenstate $|k\rangle$ of this basis, results

$$\lambda_k = \sum_{j=0}^{n(k)} \binom{n(k)}{j} \alpha^j \, , \tag{6.9}$$

where $n(k)$ is the number of ordered couples 01 inside the sequence of the base vector $|k\rangle$. For the initial state (6.7) we consistently get

$$|r,0\rangle_M = 2^{-M/2} \sum_{k=0}^{2^M-1} |k\rangle \,, \tag{6.10}$$

and, under the action of $U_0(\phi)$, one obtains

$$|r,\phi\rangle_M = 2^{-M/2} \sum_{k=0}^{2^M-1} \sum_{j=0}^{n(k)} \binom{n(k)}{j} \alpha^j |k\rangle \tag{6.11}$$

The non-local operator in Eq.(6.8) is periodic in time and generates entanglement oscillations of the chain. The qubits are fully separable in the case where $\phi = 2k\pi$, and they are maximally entanglement for the values $\phi = (2k+1)\,\pi$, $k \in \mathbb{Z}$. While for all other values of $\phi$, the chain is entangled.

Briegel Raussendorf states with $M = 2$

In the case of $M = 2$, i.e. two qubits, the BRS read

$$|r,\phi\rangle_2 = \frac{1}{2}\left(|0\rangle + e^{-i\phi}\,|1\rangle + |2\rangle + |3\rangle\right) \,, \tag{6.12}$$

The trace of the Fubini study metric for the BRS read

$$\begin{aligned} \mathrm{Tr}\, g = 2 - \left(\cos^2(\varphi/2)\left(v_1^1\right) + \sin(\varphi/2)\cos(\varphi/2)\left(v_2^1\right)\right)^2 + \\ - \left(\cos^2(\varphi/2)\left(v_1^2\right) - \sin(\varphi/2)\cos(\varphi/2)\left(v_2^2\right)\right)^2 \,. \end{aligned} \tag{6.13}$$

This equation has trivially the minimum for the normalized vectors $\tilde{\mathbf{v}}^1 = (\cos(\varphi/2),\, \sin(\varphi/2),\, 0)$ and $\tilde{\mathbf{v}}^2 = (\cos(\varphi/2),\, -\sin(\varphi/2),\, 0)$. The entanglement metric is thus

$$\tilde{g} = \begin{pmatrix} \sin^2(\varphi/2) & \sin^2(\varphi/2) \\ \sin^2(\varphi/2) & \sin^2(\varphi/2) \end{pmatrix} \,.$$

And the entanglement measure is

$$E(|r,\phi\rangle_2) = \mathrm{Tr}\,\tilde{g} = 2\sin^2(\varphi/2) \,. \tag{6.14}$$

**Remark:** The state in Eq.(6.12) is a maximally entangled state for $\phi = (2k+1)\,\pi$, $k \in \mathbb{Z}$. For this state, the EM reads

$$\tilde{g}_{\max} = \begin{pmatrix} 1 & 1 \\ 1 & 1 \end{pmatrix}$$

and the entanglement measure is

$$E(|r,\phi\rangle_2^{\max}) = \mathrm{Tr}\;\tilde{g} = 2 \,. \tag{6.15}$$

Both, the EM and the entanglement measure of the two-qubit maximally entangled BR state are similar to those of the two-qubit maximally entangled GHZ state (which represents the family of Bell states). From Proposition 4.2,

we have that the maximally entangled BRS is in the same class of entanglement as the maximally entangled GHZLS at $M = 2$.

Briegel Raussendorf states with $M = 3$

In the case of $M = 3$, we have

$$|r,\phi\rangle_3 = \frac{1}{2^{3/2}}\big(\,|0\rangle + e^{-i\phi}\,|1\rangle + e^{-i\phi}\,|2\rangle + e^{-i\phi}\,|3\rangle + |4\rangle + e^{-i\phi}\,|5\rangle + \\ + |6\rangle + |7\rangle\,\big) \tag{6.16}$$

The trace of the metric reads

$$\mathrm{Tr}\; g = 3 - \left(\cos^2(\varphi/2)\left(v_1^1\right) + \sin(\varphi/2)\cos(\varphi/2)\left(v_2^1\right)\right)^2 + \\ - \cos^4(\varphi/2)\left(v_1^2\right)^2 - \left(\cos^2(\varphi/2)\left(v_1^3\right) - \sin(\varphi/2)\cos(\varphi/2)\left(v_2^3\right)\right)^2 \;,$$

and it has the minimum for the normalized vectors $\tilde{\mathbf{v}}^1 = (\cos(\varphi/2),\, \sin(\varphi/2),\, 0)$, $\tilde{\mathbf{v}}^2 = (1,\, 0,\, 0)$ and $\tilde{\mathbf{v}}^3 = (\cos(\varphi/2),\, -\sin(\varphi/2),\, 0)$. It follows that the EM is

$$\tilde{g} = \sin^2(\varphi/2)\begin{pmatrix} 1 & \cos(\varphi/2) & 0 \\ \cos(\varphi/2) & 1+\cos^2(\varphi/2) & \cos(\varphi/2) \\ 0 & \cos(\varphi/2) & 1 \end{pmatrix}\;, \tag{6.17}$$

and the entanglement measure is

$$E(|r,\phi\rangle_3) = \mathrm{Tr}\;\tilde{g} = \sin^2(\varphi/2)\left(3 + \cos^2(\varphi/2)\right)\;. \tag{6.18}$$

**Remark:** If the state in Eq.(6.16) is maximally entangled, the EM reads

$$g_{\max} = \begin{pmatrix} 1 & \left(v_1^1\right)\left(v_3^2\right) & -\left(v_1^1\right)\left(v_1^3\right) \\ \left(v_1^1\right)\left(v_3^2\right) & 1 & -\left(v_3^2\right)\left(v_1^3\right) \\ -\left(v_1^1\right)\left(v_1^3\right) & -\left(v_3^2\right)\left(v_1^3\right) & 1 \end{pmatrix}\;, \tag{6.19}$$

and the entanglement measure is

$$E(|r,\phi\rangle_3^{\max}) = \mathrm{Tr}\;\tilde{g} = 3\;. \tag{6.20}$$

The trace of $g_{\max}$ does not depend on the vectors $\mathbf{v}^i$, where $i = 1, 2, 3$. Thus, to obtain the same entanglement metric of $|\mathrm{GHZ}\rangle_3$, one can choose the following normalized vectors: $\mathbf{v}^1 = (1,\, 0,\, 0)$, $\mathbf{v}^2 = (0,\, 0,\, 1)$ and $\mathbf{v}^3 = (-1,\, 0,\, 0)$. This suggests that each different metric, resulting from a different combination of the elements of $\mathbf{v}^i$, represents the entanglement metric of a different state that belongs to a family of states having the same entanglement. It is clear that the three-qubit maximally entangled BR state represents a family of states containing the GHZ state. According to Proposition 4.2, the maximally entangled BRS and GHZLS at $M = 3$ belong to the same class.

Briegel Raussendorf states with $M = 4$

For $M = 4$, we have

$$|r,\phi\rangle_4 = \frac{1}{4}\big(\big(\,|0\rangle + e^{-i\phi}\,|1\rangle + e^{-i\phi}\,|2\rangle + e^{-i\phi}\,|3\rangle + e^{-i\phi}\,|4\rangle + e^{-2i\phi}\,|5\rangle + \\ + e^{-i\phi}\,|6\rangle + e^{-i\phi}\,|7\rangle + |8\rangle + e^{-i\phi}\,|9\rangle + e^{-i\phi}\,|10\rangle + e^{-i\phi}\,|11\rangle + \\ + |12\rangle + e^{-i\phi}\,|13\rangle + |14\rangle + |15\rangle\,\big)\;. \tag{6.21}$$

The trace of the metric reads

$$\begin{aligned}\mathrm{Tr}\; g = 4 &- \left(\cos^2(\varphi/2)\left(v_1^1\right) + \sin(\varphi/2)\cos(\varphi/2)\left(v_2^1\right)\right)^2 - \cos^4(\varphi/2)\left(v_1^2\right)^2 \\ &- \cos^4(\varphi/2)\left(v_1^3\right)^2 - \left(\cos^2(\varphi/2)\left(v_1^3\right) - \sin(\varphi/2)\cos(\varphi/2)\left(v_2^3\right)\right)^2 \\ &- \left(\cos^2(\varphi/2)\left(v_1^4\right) - \sin(\varphi/2)\cos(\varphi/2)\left(v_2^4\right)\right)^2 \;,\end{aligned} \tag{6.22}$$

and it is minimized with the normalized vectors $\tilde{\mathbf{v}}^1 = (\cos(\varphi/2), \sin(\varphi/2), 0)$, $\tilde{\mathbf{v}}^2 = (1, 0, 0)$, $\tilde{\mathbf{v}}^3 = (1, 0, 0)$ and $\tilde{\mathbf{v}}^4 = (\cos(\varphi/2), -\sin(\varphi/2), 0)$. It follows that the EM is

$$\tilde{g} = \sin^2(\varphi/2)\begin{pmatrix} 1 & \cos(\varphi/2) & 0 & 0 \\ \cos(\varphi/2) & 1+\cos^2(\varphi/2) & 1 & 0 \\ 0 & 1 & 1+\cos^2(\varphi/2) & \cos(\varphi/2) \\ 0 & 0 & \cos(\varphi/2) & 1 \end{pmatrix}, \tag{6.23}$$

and the entanglement measure is

$$\mathrm{Tr}\,\tilde{g} = \sin^2(\varphi/2)\left(4 + \cos^2(\varphi/2)\right) \;, \tag{6.24}$$

**Remark:** If the state in Eq.(6.21) is maximally entangled, the EM reads

$$g_{\max} = \begin{pmatrix} 1 & \left(v_1^1\right)\left(v_3^2\right) & 0 & 0 \\ \left(v_1^1\right)\left(v_3^2\right) & 1 & 0 & 0 \\ 0 & 0 & 1 & -\left(v_3^3\right)\left(v_1^4\right) \\ 0 & 0 & -\left(v_3^3\right)\left(v_1^4\right) & 1 \end{pmatrix} . \tag{6.25}$$

and the entanglement measure is

$$E(|r,\phi\rangle_4^{\max}) = \mathrm{Tr}\;\tilde{g} = 4\;. \tag{6.26}$$

In the case of $M = 4$, some of the off-diagonal terms are equal to zero. Thus, whatever the choice of the vectors $\mathbf{v}^i$ is, the four-qubit maximally entanglement BRS will not be equivalent to the maximally entangled four-qubit GHZ state. Thus, according to Proposition 4.2, the maximally entangled BRS and GHLZS at $M = 4$ do not belong to the same class.

Briegel Raussendorf states with $M > 4$

For a general $M$-qubit state $|r,\phi\rangle_M$, the trace of $g$ results

$$\mathrm{Tr}(g) = \left\{ M - \sum_{\nu=0}^{M-1} \left[ v_3^\nu w_3^\nu + v_+^\nu w_-^\nu + v_-^\nu w_+^\nu \right]^2 \right\}, \tag{6.27}$$

where $v_\pm^\nu = v_1^\nu \pm i\, v_2^\nu$ and

$$\begin{aligned} w_-^\nu &= \sum_{k=0}^{2^M-1} \delta_{n_\nu^k,0}\, c_{k+2^\nu}^* c_k \;, \\ w_+^\nu &= \sum_{k=0}^{2^M-1} \delta_{n_\nu^k,1}\, c_{k-2^\nu}^* c_k \;, \\ w_3^\nu &= \sum_{k=0}^{2^M-1} (-1)^{n_\nu^k} |c_k|^2 \;, \end{aligned} \tag{6.28}$$

with $c_k = 2^{-M/2}\lambda_k$. The trace is minimized by setting $\tilde{v}_+^\nu = w_-^{\nu_\star}/\|\mathbf{w}^\nu\|$, $\tilde{v}_-^\nu = w_+^{\nu_\star}/\|\mathbf{w}^\nu\|$ and $\tilde{v}_3^\nu = w_3^\nu/\|\mathbf{w}^\nu\|$. From the latter, we get the entanglement measure for a general M-qubit BRS

$$E(|r,\phi\rangle_M) = \left(M - \sum_{\nu=0}^{M-1} \|\mathbf{w}^\nu\|^2\right) . \tag{6.29}$$

**Remark:** We do not depict the EM in the case of $M > 4$ because we are not interested in classifying the BRS beyond $M = 4$.

### W-like states

The third family of $M$-qubit states we consider is the one of the W-like states. We can define a generalized WLS according to the following induction

$$\begin{cases} |W,\alpha_1,\alpha_2\rangle_3 = \sin\alpha_1\cos\alpha_2\,|1\rangle + \sin\alpha_1\sin\alpha_2\,|2\rangle + \cos\alpha_1\,|4\rangle \\ \\ |W,\alpha_1,\ldots,\alpha_{M-1}\rangle_M = \sin\alpha_1\,|W,\alpha_2,\ldots,\alpha_{M-1}\rangle_{M-1} + \cos\alpha_1\,|2^{M-1}\rangle \end{cases} . \tag{6.30}$$

The maximally entangled state reads

$$|W\rangle_M^{\max} = \frac{1}{\sqrt{M}} \sum_{i=1}^{M} |2^{i-1}\rangle . \tag{6.31}$$

Note that the sum over $i$ is taken from 1 to $M$ in this example (and not from 0 to $M-1$) only for the purpose of simplifying the following calculations. We will return to the old notation in the next example. The above maximally entangled state is selected by the following angles

$$\begin{cases} \alpha_{M-1} = \dfrac{\pi}{4} \\ \alpha_{M-2} = \arctan\sqrt{2} \\ \alpha_{M-3} = \arctan\dfrac{1}{\cos\alpha_{M-2}} \\ \alpha_{M-4} = \arctan\dfrac{1}{\cos\alpha_{M-3}} \\ \vdots \\ \alpha_2 = \arctan\dfrac{1}{\cos\alpha_3} \\ \alpha_1 = \arccos\dfrac{1}{\sqrt{M}} . \end{cases} \tag{6.32}$$

Whereas to obtain a fully separable state, the angles have to respect the following mathematical induction

$$\begin{cases} \alpha_1 = k\pi , \quad \forall \sum_{i=2}^{M-1} \alpha_i \\ \alpha_1 = \dfrac{k\pi}{2} , \quad P(\alpha_2,\alpha_{M-1}) , \end{cases} \tag{6.33}$$

where the function $P$ is described as follows

$$P(\alpha_1,\alpha_2,\alpha_3)=\begin{cases}\alpha_1=k\pi\ , & \forall\ \alpha_2,\ \alpha_3\\ \alpha_1=\frac{k\pi}{2} & ,\ \begin{cases}\alpha_2=k\pi\ ,\forall\ \alpha_3\\ \alpha_2=\alpha_3=\frac{k\pi}{2}\end{cases}\end{cases}\ .$$

$$=\begin{cases}\alpha_1=k\pi\ ,\forall\ \alpha_2,\ \alpha_3\\ \alpha_1=\frac{k\pi}{2}\ , & P(\alpha_2,\alpha_3)\ ,\end{cases}\ .$$

for $k\in\mathbb{Z}$. The trace of the Fubini-Study metric in this case reads

$$\begin{aligned}\mathrm{Tr}\left(g\left(\mathbf{v}\right)\right)=\ M-&\left(\sum_{\mu=1}^{M-2}U_\mu\left(\alpha_\mu\right)^2\ \left(v_{\mu 3}\right)^2\right)+\\ &-U_{M-1}\left(\alpha_1,\ldots,\alpha_{M-1}\right)^2\left(v_{(M-1)3}\right)^2+\\ &-\ U_M\left(\alpha_1,\ldots,\alpha_{M-1}\right)^2\left(v_{M3}\right)^2\ ,\end{aligned}\tag{6.34}$$

where the functions $U$ are constructed with the following induction rule

$$\begin{cases}U_0=-1\\ U_1\left(\alpha\right)=-\cos 2\alpha\\ U_2\left(\alpha_1,\alpha_2\right)=\cos^2\alpha_1+\sin^2\alpha_1\,U_1\left(\alpha_2\right)\\ U_3\left(\alpha_1,\alpha_2,\alpha_3\right)=\cos^2\alpha_1+\sin^2\alpha_1\,U_2\left(\alpha_2,U_1\left(\alpha_3\right)\right)\\ \vdots\\ U_{M-2}\left(\alpha_1,\ldots,\alpha_{M-2}\right)=\cos^2\alpha_1+\sin^2\alpha_1\,U_{M-3}\left(\alpha_2,\ldots,U_1\left(\alpha_{M-2}\right)\right)\\ U_{M-1}\left(\alpha_1,\ldots,\alpha_{M-1}\right)=\cos^2\alpha_1+\sin^2\alpha_1\,U_{M-2}\left(\alpha_2,\ldots,-U_1\left(\alpha_{M-2}\right)\right)\\ U_M\left(\alpha_1,\ldots,\alpha_{M-1}\right)=\cos^2\alpha_1+\sin^2\alpha_1\,U_{M-2}\left(\alpha_2,\ldots,U_1\left(\alpha_{M-2}\right)\right)\ .\end{cases}$$

The $\mathrm{tr}\left(g\left(\mathbf{v}\right)\right)$ of the WLS is minimized by the values $\tilde{v}_3^{\mu}=1$, where $\mu$ denotes the qubit and 3 indicates the direction $z$. It follows that the entanglement measure in this case is

$$\begin{aligned}\mathrm{E}\left(\left|W,\alpha_1,\ldots,\alpha_{M-1}\right\rangle_M\right)=\ M-&\sum_{\mu=1}^{M-2}U_\mu\left(\alpha_\mu\right)^2-\ U_{M-1}\left(\alpha_1,\ldots,\alpha_{M-1}\right)^2+\\ &-U_M\left(\alpha_1,\ldots,\alpha_{M-1}\right)^2\ .\end{aligned}\tag{6.35}$$

If the WLS are maximally entangled (i.e. (6.31)), the Fubini Study metric reads

$$\tilde{g}_{\,\mathrm{Max}}\left(\left|W\right\rangle_M\right)=\frac{4}{M\times M}\begin{pmatrix}(M-1) & -1 & -1 & \cdots & -1\\ -1 & (M-1) & -1 & \cdots & -1\\ \vdots & \vdots & \vdots & \ddots & \vdots\\ -1 & -1 & -1 & \cdots & (M-1)\end{pmatrix}$$

The W-like states at $M=3$

At $M = 3$, the WLS read

$$|W, \theta, \varphi\rangle_3 = \sin\theta\cos\varphi\,|001\rangle + \sin\theta\sin\varphi\,|010\rangle + \cos\theta\,|100\rangle\ . \tag{6.36}$$

These states are fully separable at $\theta = 0 + k\pi$, $\forall\varphi$ and at $\theta = \pi/2 + k\pi$, $\varphi = k\pi/2$, where $k \in \mathbb{Z}$. And they are bi-separable at $\theta = \pi/2 + k\pi$ and $\varphi = pi/4 + k\pi$, and also at $\theta = kpi/4$ and $\varphi = k\pi/2$. And finally, they are maximally entangled (see Eq.6.32) at

$$\begin{cases} \varphi = \dfrac{\pi}{4} \\ \\ \theta = \arctan\sqrt{2} \end{cases} \tag{6.37}$$

The trace of the Fubini Study metric is

$$\begin{aligned} \text{Tr } g = 3 - \cos^2(2\theta)\left(v_3^1\right)^2 - \left[\cos^2(\theta) + \sin^2(\theta)\cos(2\varphi)\right]^2\left(v_3^2\right)^2 \\ - \left[\cos^2(\theta) - \sin^2(\theta)\cos(2\varphi)\right]^2\left(v_3^3\right)^2\ , \end{aligned} \tag{6.38}$$

and it is trivially minimized by $\tilde{\mathbf{v}}_1 = \tilde{\mathbf{v}}_2 = \tilde{\mathbf{v}}_3 = (0,\,0,\,1)$. Thus, the entanglement distance for the three qubits WLS is

$$E(|W\theta, \varphi\rangle_3) = \text{Tr }\tilde{g} = 3 - \cos^2(2\theta) - 2\cos^4(\theta) - 2\sin^4(\theta)\cos^2(2\varphi)\,. \tag{6.39}$$

**Remark:** From Eq.(6.31), we get the EM for the maximally entangled WLS at $M = 3$

$$g_{\text{Max}} = \begin{pmatrix} 1 - \dfrac{\left(v_3^1\right)^2}{9} & g_{12} & g_{13} \\ \\ g_{21} & 1 - \dfrac{\left(v_3^2\right)^2}{9} & g_{23} \\ \\ g_{31} & g_{32} & 1 - \dfrac{\left(v_3^3\right)^2}{9} \end{pmatrix}\ . \tag{6.40}$$

We notice that the trace still depends on the directions $\mathbf{v}^i$, where $i = 1, 2, 3$ and to minimize it, we should choose $\tilde{\mathbf{v}}^1 = \tilde{\mathbf{v}}^2 = \tilde{\mathbf{v}}^3 = (0, 0, 1)$. With this choice, the reduced EM becomes

$$\tilde{g}_{\text{Max}} = \frac{4}{9}\begin{pmatrix} 2 & -1 & -1 \\ -1 & 2 & -1 \\ -1 & -1 & 2 \end{pmatrix} \tag{6.41}$$

This shows that the EM of the maximally entangled WLS cannot be equivalent to the EM of the maximally BRS in Eq.(6.19) and of the maximally GHLS in Eq.(6.5) for two reasons: *i*) on the contrary of $g_{\text{Max}}$(BR) and $g_{\text{Max}}$(GHZ), the trace of $g_{\text{Max}}(\text{W}) < 3$ , $\quad \forall\left(v_3^1, v_3^2, v_3^3\right) \setminus (0, 0, 0)$, and *ii*) the off-diagonal terms in Eq.(6.40) depend on the choice of $\left(v_3^1, v_3^2, v_3^3\right)$ that should minimize the trace. In fact, the off-diagonal terms cannot take any values, they take only the value $-4/9$, coming from replacing the values of $\left(v_3^1, v_3^2, v_3^3\right)$, which minimize the trace, in $g_{12}$, $g_{13}$, $g_{23}$. The off-diagonal terms will thus never be equal to those in $g_{\text{Max}}$(BR) and $g_{\text{Max}}$(GHZ). Therefore, according to Proposition 4.2, the maximally entangled WLS does not belong to the class of the maximally entangled BRS and GHLS at $M = 3$.

### Three-qubit states depending on two parameters

The last family of M-qubit states we consider is

$$\begin{aligned}|\varphi,\gamma,\tau\rangle_3 =& \cos(\gamma)|0\rangle[\cos(\tau)|00\rangle + \sin(\tau)|11\rangle] \\ &+ \sin(\gamma)|1\rangle[\sin(\tau)|00\rangle + \cos(\tau)|11\rangle]\,.\end{aligned} \tag{6.42}$$

These states are fully separable for $\gamma = 0, \pi/2$ and $\tau = 0, \pi/2$ whereas they are bi-separable for $\tau = \pi/4$. In this case, the trace of the Fubini-Study metric is

$$\begin{aligned}\mathrm{Tr}(g) = \big\{&3 - \cos^2(2\gamma)\cos^2(2\tau)[(v_3^0)^2 + (v_3^1)^2] \\ &-[\sin(2\gamma)\sin(2\tau)v_1^2 + \cos(2\gamma)v_3^2]^2\big\}\end{aligned} \tag{6.43}$$

and it is minimised by the values $\tilde{\mathbf{v}}_3^\mu = (0,0,1)$, $\nu = 0,1$ and

$$\begin{aligned}\tilde{v}_3^0 &= \frac{\sin(2\gamma)\sin(2\tau)}{\sqrt{\sin^2(2\gamma)\sin^2(2\tau) + \cos^2(2\gamma)}}\,, \\ \tilde{v}_3^1 &= 0\,, \\ \tilde{v}_3^2 &= \frac{\cos(2\gamma)}{\sqrt{\sin^2(2\gamma)\sin^2(2\tau) + \cos^2(2\gamma)}}\,.\end{aligned} \tag{6.44}$$

Consistently, the entanglement measure for these states results to be

$$E(|\varphi,\gamma,\tau\rangle_3) = 2\sin^2(2\tau) + 3\sin^2(2\gamma)\cos^2(2\tau)\,. \tag{6.45}$$

### Hybrid two-qudit states depending on one parameter

As an example of application to hybrid qudit systems, we consider the projective Hilbert space $P\mathcal{H} = P(\mathcal{H}_2 \otimes \mathcal{H}_3)$, *i.e.* the product of qubit and qutrit states. Let us denote the elements of a basis in such Hilbert space with $|\alpha, j\rangle$, where $\alpha = \pm$ and $j = 0,1,2$ and consider the following family of single-parameter states

$$|s,\theta\rangle = \cos(\theta)|+,0\rangle + \sin(\theta)|-,2\rangle\,. \tag{6.46}$$

We expect the state with a higher degree of entanglement will correspond to $\theta = \pi/4$. Note that this is not a maximally entangled state since the component $|1\rangle$ of the second Hilbert space is absent. From Eq.(4.12), we have

$$A_0 = \begin{pmatrix} 1 & i\cos(2\theta) & 0 \\ -i\cos(2\theta) & 1 & 0 \\ 0 & 0 & 1-\cos^2(2\theta) \end{pmatrix}. \tag{6.47}$$

In the case of qutrits, the generators $\mathbf{T}_\mu$ can be represented by the Gell-Mann matrices. By direct calculation, one can verify that the only non-null matrix

elements for $A_1$ are the following

$$\begin{aligned}
(A_1)_{11} &= \cos^2(\theta)\,,\\
(A_1)_{22} &= \cos^2(\theta)\,,\\
(A_1)_{33} &= \cos^2(\theta)\sin^2(\theta)\,,\\
(A_1)_{44} &= \sin^2(\theta)\,,\\
(A_1)_{55} &= \sin^2(\theta)\,,\\
(A_1)_{66} &= 3\cos^2(\theta)\sin^2(\theta)\,,\\
(A_1)_{77} &= 1\,,\\
(A_1)_{88} &= 1\,.
\end{aligned}$$

Thus, from Eq. (4.14) we have

$$E(|s,\theta\rangle) = 2\sin^2(2\theta)\,. \tag{6.48}$$

In (6.48), $\theta = \pi/4$ provides the maximally entangled state.

In Section 6.1, we will compare entanglement measure $E(|s,\theta\rangle)/2$ with von Neumann entropy

$$\mathcal{E}[\rho(\theta)] = -\cos^2(\theta)\log_2[\cos^2(\theta)] - \sin^2(\theta)\log_2[\sin^2(\theta)] \tag{6.49}$$

of the density matrix $\rho(\theta) = |s,\theta\rangle\langle s,\theta|$ associated to the same state.

### $M$-qudit states depending on two parameters

Let us consider an $M$-qutrit system, that has a projecive Hilbert space $P\mathcal{H} = P\left(\mathcal{H}_3 \otimes \cdots \otimes \mathcal{H}_3\right)$, that is to say, the product of $M$ qutrit states. We have considered the following generalization of the GHZLS states to qutrits,

$$\begin{aligned}
|s,\theta,\phi\rangle_M = \sin(\theta)\cos(\phi)|0,\ldots,0\rangle + \\
\sin(\theta)\sin(\phi)|1,\ldots,1\rangle + \cos(\theta)|2,\ldots,2\rangle\,,
\end{aligned} \tag{6.50}$$

which is a family of 2-parameter states. We have,

$$\begin{aligned}
(A_\mu)_{11} &= \sin^2(\theta)\,,\\
(A_\mu)_{22} &= \sin^2(\theta)\,,\\
(A_\mu)_{33} &= \frac{1}{4}\sin^2(\theta)\left(3+\cos(2\theta)-2\sin^2(\theta)\cos(4\phi)\right)\,,\\
(A_\mu)_{44} &= \sin^2(\theta)\sin^2(\phi)+\cos^2(\theta)\,,\\
(A_\mu)_{55} &= \sin^2(\theta)\sin^2(\phi)+\cos^2(\theta)\,,\\
(A_\mu)_{66} &= 3\sin^2(\theta)\cos^2(\theta)\,,\\
(A_\mu)_{77} &= \sin^2(\theta)\cos^2(\phi)+\cos^2(\theta)\,,\\
(A_\mu)_{88} &= \sin^2(\theta)\cos^2(\phi)+\cos^2(\theta)\,,
\end{aligned}$$

for $\mu = 0,\ldots,M-1$. Thus, it results

$$E(|s,\theta,\phi\rangle_M) = \frac{M}{4}\sin^2(\theta)\left[9+7\cos(2\theta)-2\sin^2(\theta)\cos(4\phi)\right]\,. \tag{6.51}$$

In Section 6.1, we compare the entanglement measure $E(|s,\theta,\phi\rangle_M)/M$ of the states (6.50) with von Neumann entropy

$$\mathcal{E}(\rho(\theta,\phi)) = -a^2\log_2(a^2) - b^2\log_2(b^2) - c^2\log_2(c^2)\,, \tag{6.52}$$

where $\rho(\theta,\phi) = |s,\theta,\phi\rangle_{22}\langle s,\theta,\phi|$ is the density matrix associated with the same states in the case $M=2$. Here, $a=\sin(\theta)\cos(\phi)$, $b=\sin(\theta)\sin(\phi)$ and $c=\cos(\theta)$.

## 6.1 Results

### Entanglement measure

In Fig.6.1, we plot the measure $E(|r,\phi\rangle_M)/M$ vs $\phi/(2\pi)$ according to Eq.(6.29), for the multi-qubit states (6.11) in the case $M=3,4,7,9$. Figure 6.1 shows that the entanglement distance provides a correct estimation of the degree of entanglement for the BRS in all the cases considered. In particular, for the fully separable states ($\phi=0,2\pi$), it is zero, whereas, for the maximally entangled states ($\phi=\pi$), it provides the maximum possible value for the trace, that is $E(|r,\pi\rangle_M)/M=1$. This implies that the expectation values on the maximally entangled states of the operators $\tilde{\mathbf{v}}_\nu\cdot\boldsymbol{\sigma}_\nu$ ($\nu=0,\ldots,M-1$) are zero (see Lemma 4.2).

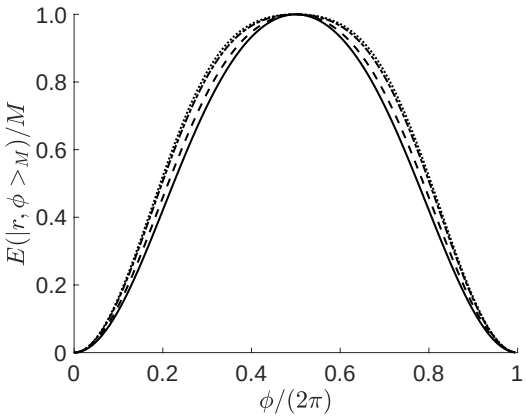


Figure 6.1: The figure reports the entanglement measure $E(|r,\phi\rangle_M)/M$ vs $\phi/(2\pi)$ for the states (6.11) in the cases $M=3$ (continuous line), $M=4$ (dashed line), $M=7$ (dot-dashed line) and $M=9$ (dotted line).

The entanglement distance successfully passes a second test. When applied on the GHZLS (Eq.(6.4)), it provides zero in the case of fully separable states ($\theta=0,\pi$), and provides 1 for the maximally entangled states ($\theta=\pi/2$). In figure 6.2, we compare the curves $E(|r,\phi\rangle_M)/M$ vs $\phi/(2\pi)$ in continuous line and $E(|GHZ,\theta\rangle_M)/M$ vs $2\theta/\pi$ in dashed line, for the case $M=3$. In the case of the maximally entanglement states, the expectation values of the operators $\tilde{\mathbf{v}}_\nu\cdot\boldsymbol{\sigma}_\nu$ ($\nu=0,\ldots,M-1$) is zero.

The entanglement distance is also tested on the WLS and it provides consistent results. The 3D plot in Figure 6.3 depicts $E\left(|W,\theta,\varphi\rangle_3\right)/3$ as a

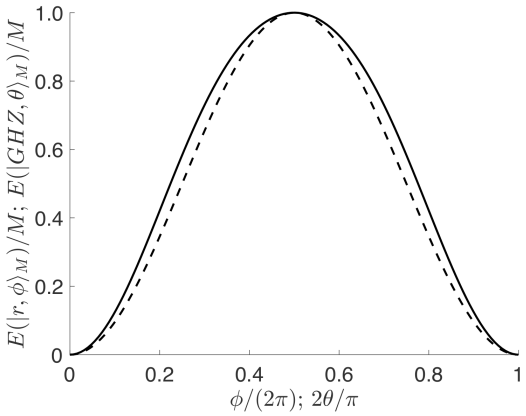


Figure 6.2: In this figure we compare the entanglement measures $E(|r,\phi\rangle_M)/M$ vs $\phi/(2\pi)$ for the states (6.11) in continuous line, and $E(|GHZ,\theta\rangle_M)/M$ vs $2\theta/\pi$ for the states (6.1) in dashed line, for the case $M = 3$.

function of $\theta/\pi$ and $\varphi/\pi$, where we clearly see that the measure is zero at $\theta = 0 + k\pi$, $\forall\varphi$ and also at $\theta = \pi/2 + k\pi$, $\varphi = k\pi/2$, which are the angles at which the WLS are fully separable. It displays local maxima at $\theta = \pi/2 + k\pi$ and $\varphi = \pi/4 + k\pi$, and at $\theta = k\pi/4$ and $\varphi = k\pi/2$. And finally, the maxium value of $E\left(|W,\theta,\varphi\rangle_3\right)/3$ are at $\theta = \pi/4 + k\pi$ and $\varphi/\pi \approx 0.3 \Rightarrow \varphi \approx \arctan\sqrt{2}$.

In Fig. 6.4, we report in a 3D plot the measure $E(|\varphi,\gamma,\tau\rangle_3)/3$ as a function of $\gamma/\pi$ and $\tau/\pi$ according to Eq. (6.45), for the states (6.42). The measure (4.11) catches in a surprisingly clear way the entanglement properties of this family of states. In particular, $E(|\varphi,\gamma,\tau\rangle_3)/3$ is null in the case of fully separable states ($\gamma = 0, \pi/2, \pi$ and $\tau = 0, \pi/2, \pi$) and it is maximum (with value 1) in the case of maximally entangled states ($\gamma = \pi/4, 3\pi/4$ and $\tau = 0, \pi/2, \pi$). In addition,

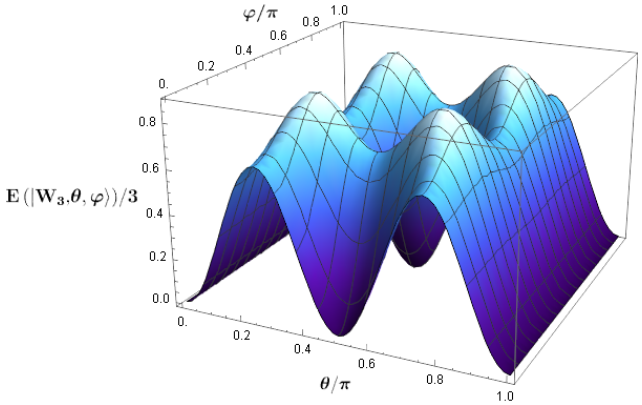


Figure 6.3: The figure reports the three-dimensional plot of the entanglement measure $E\left(|W,\theta,\varpi\rangle_3\right)/3$ in Eq.(6.39) as a function of $\theta/\pi$ and $\varphi/\pi$ of the state in Eq.(6.36)

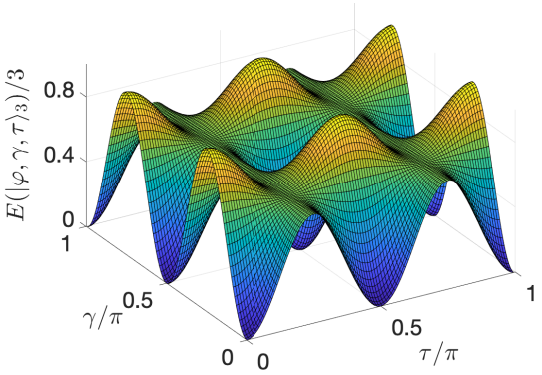


Figure 6.4: The figure reports the three dimensional plot of the entanglement measure $E(|\varphi,\gamma,\tau\rangle_3)/3$ as a function of $\gamma/\pi$ and $\tau/\pi$ for the states (6.42).

the case of bi-separable states ($\tau = \pi/4$) results in $0 < E(|\varphi,\gamma,\tau\rangle_3)/3 < 1$.

Figure 6.5 refers to the hybrid two-qudit states (6.46). Here, we compare the curves of entanglement measure $E(|s,\theta\rangle)/2$ vs $\theta/\pi$ of states (6.46) in a continuous line, and the von Neumann entropy $\mathcal{E}(|s,\theta\rangle)$ vs $\theta/\pi$ in dashed line, for the same states. This figure clearly shows that although these two curves are different, they strongly agree in the quantification of the entanglement of the different states. Note that the highly entangled state associated with $\theta = \pi/4$ has an entanglement measure of 1, lower than the maximally entangled state of this Hilbert space which, using (4.22), report a value of 7/6.

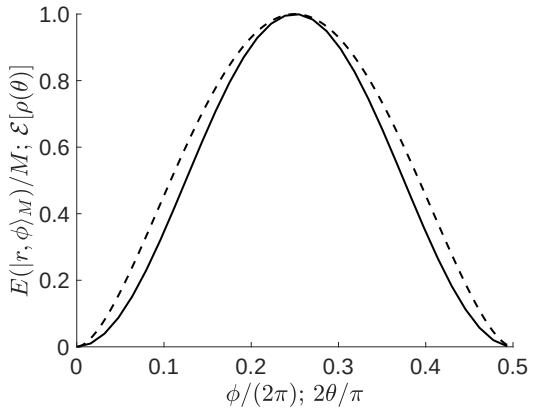


Figure 6.5: The figure compares the entanglement measure $E(|r,\phi\rangle_M)/M$ vs $\phi/(2\pi)$ in a continuous line for the hybrid two-qudit states (6.46), and the von Neumann entropy $\mathcal{E}[\rho(\theta)]$ vs $\theta/\pi$ in dashed lines for the same states.

In Fig. 6.6, we report the entanglement measure $E(|s,\theta,\phi\rangle_M)/M$ as a function of $\theta/\pi$ and $\phi/\pi$ given in Eq. (6.51), for the multi-qubit states (6.50). Even in this example, the measure (4.11) catches in a surprisingly clear way the entanglement properties of this family of multi-qudit states. In particular, $E(|s,\theta,\phi\rangle_M)/M$ is null in the case of fully separable states, *i.e.* for $\theta = 0$, $\forall\phi$

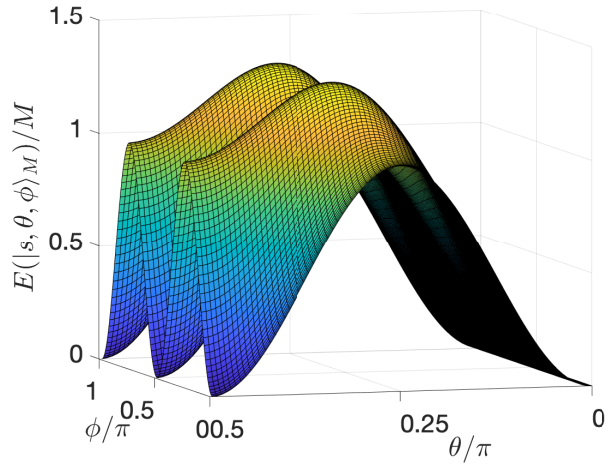


Figure 6.6: The plot shows the entanglement measure $E(|s,\theta,\phi\rangle_M)/M$ in (6.51) as a function of $\theta/\pi$ and $\phi/\pi$ for the states (6.50).

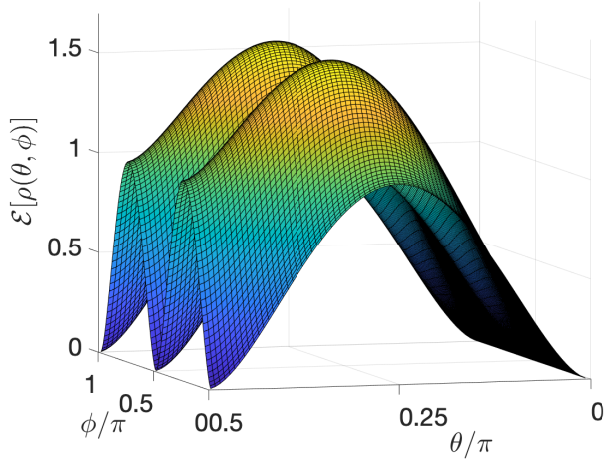


Figure 6.7: The figure shows $\mathcal{E}[\rho(\theta,\phi)]$ as a function of $\theta/\pi$ and $\phi/\pi$ given in Eq. (6.52). The density matrix is associated with the states (6.50), $\rho(\theta,\phi) = |s,\theta,\phi\rangle_{22}\langle s,\theta,\phi|$ in the case $M = 2$.

and $\theta = \pi/2$, $\phi = 0, \pi/2, \pi$. In case of $\phi = 0, \pi$, the entanglement measure changes over $\theta$ and shows local maximum for $\theta = \pi/4$. For $\theta = \pi/2$, the measure changes over $\phi$ displaying local maxima for $\phi = \pi/4, 3\pi/4$. Furthermore, the state corresponding to $\sin(\theta)\cos(\phi) = \sin(\theta)\sin(\phi) = \cos(\theta) = 1/\sqrt{3}$ is a maximally entangled state to which corresponds an entanglement measure (4.22) of value $4/3$.

In Fig. 6.7, we report the 3D plot for the von Neumann entropy $\mathcal{E}[\rho(\theta,\phi)]$ (see Eq. (6.52)) as a function of $\theta/\pi$ and $\phi/\pi$. The entropy is calculated for the density matrix $\rho(\theta,\phi) = |s,\theta,\phi\rangle_{22}\langle s,\theta,\phi|$ associated to the family of two-qudit states (6.50). The comparison between the figures 6.6 and 6.7 clearly shows

that, although the functions $E(|s,\theta,\phi\rangle_M)/M$ and $\mathcal{E}[\rho(\theta,\phi)]$ are different, they fully agree, in the entanglement estimation, for the states $|s,\theta,\phi\rangle$.

### Eigenvalues analysis for $M$-qubit states

In the case of multi-qubit states, further interesting characteristics of the entanglement come from the analysis of the entanglement metric's eigenvalues. In fig. 6.8, we compare the plots of the eigenvalues of $\tilde{g}$ for $|r,\phi\rangle_M$ vs $\phi/(2\pi)$ (dotted lines), with the plot of the unique not vanishing eigenvalue of $\tilde{g}$ for GHZLS vs $2\theta/\pi$ (continuous line), in the case $M=7$. When $\phi \neq 0, 2\pi$ the EM of the BRS, $\tilde{g}$, has exactly $M$ non-zero eigenvalues. On the other hand, the GHZLS have only one non-vanishing eigenvalue. Although the value of the latter is greater than the eigenvalues of the BRS (see Fig. 6.8), the GHZLS appear weak, in the sense of entanglement, since there exist $M-1$ directions with null minimum distance between states. This fact makes the class of the BRS robust in the sense of entanglement. In fact, the minimum distance between states in a random direction is greater than the minimum eigenvalue of the metric and, therefore, greater than zero. Within the scenario that we have proposed, the entanglement has the physical interpretation of an obstacle to the minimum distance squared between infinitesimally close states. In fact, by defining the distance squared between a given state represented by the vector $|U,s\rangle$ and an infinitesimally close state associated with the vector $|dU,s\rangle$ as $ds^2 = \mathrm{Tr}[g(\mathbf{v})]dr^2$ where $\sum_\mu (d\xi^\mu)^2 = dr^2$, it results

$$ds^2 \geq E(|s\rangle)dr^2\,. \tag{6.53}$$

This shows that the minimum distance squared density $ds^2/dr^2$, obtained by varying the vectors $\mathbf{v}$, is bounded from below by the entanglement measure $E(|s\rangle)$. For fully separable states, the minimum distance density is zero whereas, for maximally entangled states, it results $M$ at the very best. Finally, from the analysis of the eigenvalues we can investigate the sensitivity of different states

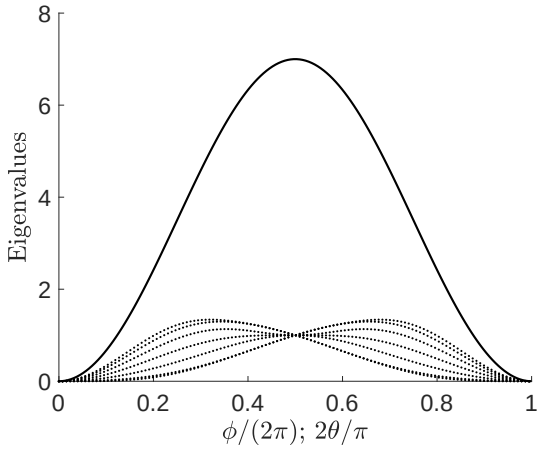


Figure 6.8: Plot of the $\tilde{g}$ eigenvalues for the state $|r,\phi\rangle_M$ vs $\phi/(2\pi)$ in dotted lines and the unique not vanishing eigenvalue of $\tilde{g}$ for the state GHZLS vs $2\theta/\pi$ in continuous line, for the case $M=7$.

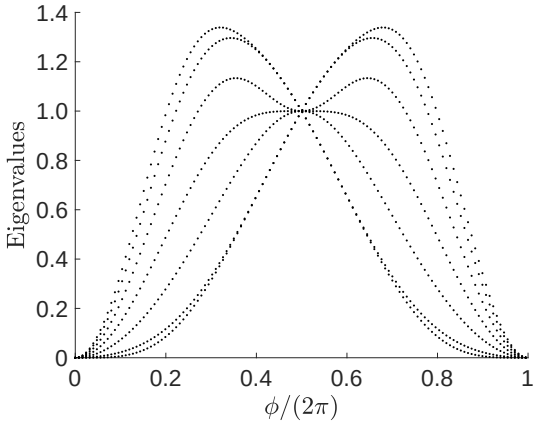


Figure 6.9: The figure plots the $\tilde{g}$ eigenvalues for the state $|r,\phi\rangle_M$ vs $\phi/(2\pi)$ for the case $M = 7$.

to small variations. Fig. 6.9 shows that at different points in parameter space corresponds different state sensitivity of $|r,\phi\rangle_7$. For instance, if we move out of $\phi = \pi/2$, following the eigenvector's direction corresponding to the maximum eigenvalue of $\tilde{g}$, we find a greater distance than moving along the eigenvector's of the maximally entangled state at $\phi = \pi$. Such analysis can be profitably used within quantum metrology applications.

## 6.2 Chapter conclusions

The goal of this Chapter was to verify the validity of the entanglement distance that we proposed in Ref.[41] and illustrated in Chapter 4. We undertook the following tests

- We have seen that the entanglement distance catches in a precise way the entanglement properties of the following examples: the GHZ-like states (GHZLS), the Briegel-Raussendorf states (BRS), defined in [75], the W-like states (WLS), a three-qubit state depending on two parameters and a hybrid two-qudit state depending on one parameter.

- In the case of $M = 3$, we have observed that the entanglement distance gives the same result for the GHZLS and BRS, and it is smaller for the WLS. This means that, at $M = 3$ , GHZLS and BRS have the same amount of entanglement and that the WLS is less entangled.

- It has been shown [19, 156] that two pure states $|\psi\rangle$ and $|\phi\rangle$ can be obtained with certainty from each other by means of LOCC if and only if they are related by local unitary operations (LUs). In Chapter 4 (Proposition 4.2), we have seen that if two states have different EMs, they cannot be transformed into each other by means of local unitary operations. We observed that, at $M = 3$, the entanglement metrics of the GHLZS and the BRS differ only by LUs. Whereas the entanglement metric of the WLS cannot be transformed into the one of the GHLZS or the BRS. This means that the BRS and the GHZLS can be transformed

into each other with certainty via LOCC, while the state W cannot be transformed into any of them with certainty via LOCC.

- In the case of $M = 4$, we have shown that the BRS and the GHZLS still have the same entanglement distance, but that they cannot be transformed into each other by LUs, since their entanglement metrics are different. This simply means that at $M = 4$, the GHLZS and the BRS cannot be transformed into each other with certainty by LOCC. However, the question of whether they can be transformed into each other by SLOCC remains open.

- With the information gathered from both, the entanglement distance and the entanglement metric, we are able to classify multipartite qubit states via LOCC. At $M = 2$, there is only one class of entangled states (Bell states), because all the entanglement metrics of entangled two-qubit states can be transformed into each other via LUs. At $M = 3$, there are two classes of genuine tripartite entangled states: the BRS (containing the GHZLS) and the WLS. And, for $M > 3$, the classification becomes complicated.

- It remains an open and interesting question as to how to relate the entanglement metric to SLOCC.

- Briegel-Raussendorf, showed in [26], that at $M = 3$, the GHZLS and the BRS have the same persistency and they are both max. connected. And for $M > 3$, the BRS are more persistent than the GHZLS, but they are both max. connected. With the analysis of the eigenvalues of the entanglement metrics, we have extracted an interesting property from the entanglement metric, namely its rank informs on the robustness of a state. we have seen that, although they have the same entanglement distance, at $M > 3$, the entanglement metric of the BRS has a bigger rank than the one of the GHZLS. This suggests that the rank of the entanglement metric informs on the robustness of the studied state.

- In the case of hybrid qudit states, we have seen that the entanglement distance and the von Neumann entropy agree on the quantification of entanglement of different states.

# 7

# Entanglement distance for mixed states

In this Chapter, we present our original work done in Ref.[154]. In this work, we have been interested in quantifying entanglement in mixed states. Extensive literature is devoted to the study of entanglement in multipartite systems. whereas, the study of entanglement in mixed multipartite states has been addressed, e.g., with a Schmidt measure [56] or with a generalization of concurrence [42, 34]. In recent years, approaches focusing on entanglement estimation have been proposed and derived from a statistical distance. [22] concept, as, for instance, the quantum Fisher information [124, 94, 149, 140]. Although many entanglement measures for mixed systems have been proposed so far. The topic remains open, as it is by no means an easy problem to tackle. In the case of pure states, entanglement and correlation are completely equivalent, therefore an appropriate measure of quantum correlation can provide also an entanglement measure. On the contrary, in the case of mixed states, one can observe states that manifest correlations detached from entanglement. In this Chapter, we construct a quantum correlation measure for multipartite states and show that the entanglement distance seen in Chapter 4 is a special case of the one constructed in this Chapter for mixed states. Then, from the quantum correlation measure, we will construct an entanglement measure for mixed states. This will be done in Section 7.2. Thus, a review of quantum correlations is given before in Section 7.1.

## 7.1 Quantum correlations in multipartite mixed states

A mixed quantum system $\rho$ composed of $M$ subsystems each associated with a Hilbert space $\mathcal{H}$, is said to be separable or unentangled if it can be prepared by means of LOCC [2], i.e. if

$$\rho = \sum_i p_i \sigma_1^{(i)} \otimes \sigma_2^{(i)} \otimes \cdots \otimes \sigma_M^{(i)} \ , \tag{7.1}$$

where $\sigma^i$ represents the density matrix of subsystem $i$ and it is not necessarily a projector. Any state that does not have the above form is entangled.

However, the theory of mixed-state entanglement is more complex than it seems to be. In fact, pure states can be either unentangled or entangled. On the

other hand, mixed entangled states can display other types of non-classical correlations such us *steering* [36] and *nonlocality* [27]. Moreover, the mystery of quantum mechanics does not stop here: even unentangled states when mixed can display a non-classical behavior that can be exemplified by the so-called quantum discord [119, 84]. In fact, it has been shown [60] that almost all mixed

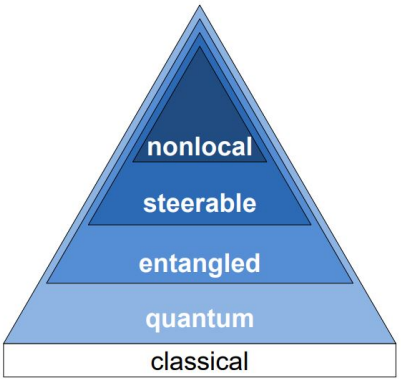


Figure 7.1: There are several types of non-classical correlations in the case of mixed quantum states. The figure is taken from [2].

quantum states of two or more subsystems display *quantum correlations*, even in the absence of entanglement. The only states which may be regarded as classically correlated form a negligible corner of the subset of separable states. Within the set of entangled states, one can distinguish some layers of other forms of non-classicity. In particular, some, but not all, entangled states are steerable, and some, but not all, steerable states are non-local (see Figure 7.1). Steering is the possibility of manipulating the state of one subsystem by making measurements on the other [36]. And, nonlocality, best known for violating the EPR local realism [54], represents the most radical description of quantumness. Thus, the mixing of quantum states gives rise to quantum correlation, which encompasses all types of quantumness of which entanglement represents only one layer.

It is thus very hard to construct an entanglement measure for a multipartite mixed state, as it must have the ability to extract the degree of entanglement from quantum correlation. One way to overcome the difficulty is to first build a good measure for quantum correlation, i.e. one that extracts quantum correlations from the classical ones, and then see how to build a measure for entanglement, i.e. extracting entanglement from quantum correlation. First, we need to define the set of all quantum correlated states $\mathcal{QC}$, to be able to construct a measure of quantum correlation acting on $\mathcal{QC}$. One way to do this is to define the set of all classical mixed states $\mathcal{C}$ since the set of all quantum correlated states is the complementary of $\mathcal{C}$, i.e. $\mathcal{QC} \equiv \bar{\mathcal{C}}$ (see Figure 7.1 ).

However, this is still not easy to do. We will see why shortly. Adesso et al. in [2] elegantly showed a simple way to define the set of all classical mixed states

$\mathcal{C}_{AB}$ in the case of a system composed of two subsystems $A$ and $B$

$$\mathcal{C}_{AB} := \left\{\rho_{AB} \quad | \quad \rho_{AB} = \sum_{ij} p_{ij} \left|i\right\rangle \left\langle i\right|_A \otimes \left|j\right\rangle \left\langle j\right|_B \right\} , \tag{7.2}$$

where $\left|i\right\rangle \left\langle i\right|_A$ and $\left|j\right\rangle \left\langle j\right|_B$ are orthonormal bases for both subsystems $A$ and $B$ and $\{p_{ij}\}$ is a joint probability distribution. They also defined the sets of one-sided $\mathcal{C}$

$$\mathcal{C}_A := \left\{\rho_{AB} \quad | \quad \rho_{AB} = \sum_{i} p_i \left|i\right\rangle \left\langle i\right|_A \otimes \rho_B^{(i)} \right\} , \tag{7.3}$$

and

$$\mathcal{C}_B := \left\{\rho_{AB} \quad | \quad \rho_{AB} = \sum_{j} p_j \, \rho_A^{(j)} \otimes \left|j\right\rangle \left\langle j\right|_A \right\} , \tag{7.4}$$

where $\rho_B^{(i)}$ and $\rho_A^{(j)}$ are quantum states and the classical states are represented by the orthonormal bases. They then defined a quantum correlated state $\rho_{AB}$ as follows[1]

**Definition 7.1.** *A state $\rho_{AB}$ has quantum correlations if it is not a classical state, i.e., if $\rho_{AB} \notin \mathcal{C}_A$ then $\rho_{AB}$ has one-sided quantum correlations, and if $\rho_{AB} \notin \mathcal{C}_{AB}$ then $\rho_{AB}$ has two-sided quantum correlations.*

Having defined the set of all quantum correlated states, they then gave the requirements for a bona fide one-sided quantum correlations measure $C_A(\rho_{AB})$ on bipartite quantum states.

(1) $C_A(\rho_{AB}) = 0$ if $\rho_{AB} \in \mathcal{C}_A$, i.e. if the classicality is on the subsystem A.

(2) $C_A(\rho_{AB})$ is invariant under local unitary operations.

(3) $C_A(\rho_{AB})$ reduces to a measure of entanglement $E(\rho_{AB})$, if $\rho_{AB}$ is pure.

(4) $C_A(\rho_{AB})$ is monotonically non-increasing under any LOCC on the party whose quantumness is not being measured. In this case, we have

$$C_A\left(\left(\mathbb{1}_A \otimes \mathcal{E}_B^{\mathrm{LOCC}}\right) \rho_{AB}\right) \leq C_A(\rho_{AB}) \, .$$

We see from Adesso's work [2], that for a given system composed of only two subsystems, there are three ways of creating quantum correlations. That is, the state $\rho_{AB}$ is quantum correlated if i) $\rho_{AB} \notin \mathcal{C}_{AB}$ or ii) $\rho_{AB} \notin \mathcal{C}_A$ or iii) $\rho_{AB} \notin \mathcal{C}_B$. We can thus extend the definition to an $M$-partite mixed state $\rho$

**Definition 7.2.** *An $M$-partite state $\rho$ has quantum correlations if it is not a classical state, i.e., if $\rho \notin \mathcal{C}_\mu$, where $\mu$ is a given subsystem, then $\rho$ has $(M-1)$-sided quantum correlations, and if $\rho \notin \mathcal{C}_M$ then $\rho$ has $M$-sided quantum correlations, where $\mathcal{C}_M$ is the set of all classical correlated $M$-partite states.*

[1] Actually, this is one of many equivalent definitions they gave of quantum correlated states in their article. However, it is not necessary to discuss them all in the present work

In the above definition, $\mathcal{C}_\mu$ is defined as follows

$$\mathcal{C}_\mu := \left\{\rho \quad | \quad \rho = \sum_i p_i \left|i\right\rangle \left\langle i\right|_\mu \otimes \rho_{\mu_c}^{(i)}\right\} , \tag{7.5}$$

where $\mu_c$ denotes the complementary of $\mu$ (i.e. the part that is not classical). We also define $C_M$ as follows

$$\mathcal{C}_M := \left\{\rho \quad | \quad \rho = \sum_{i_1,\cdots i_M} p_{i_1,\cdots,i_M} \left|i_1\right\rangle \left\langle i_1\right| \otimes \left|i_2\right\rangle \left\langle i_2\right| \otimes \cdots \otimes \left|i_M\right\rangle \left\langle i_M\right| \right\} , \tag{7.6}$$

which is a fully classical set. For an M-partite density matrix $\rho \in \mathcal{H}P^{\otimes M} = \bigotimes_{\mu=0}^{M-1} \mathcal{H}P_\mu$, we define the set of requirements for a bona fide quantum correlation measure $C_\mu(\rho)$ on the $\mu$th subsystem

(1) $C_\mu(\rho) = 0$ if $\rho \in \mathcal{C}_\mu$, i.e. if the classicality is on the subsystem $\mu$.

(2) $C_\mu(\rho)$ is invariant under local unitary operations.

(3) $C_\mu(\rho)$ reduces to a measure of entanglement $E(\rho)$, if $\rho$ is pure.

(4) $C_\mu(\rho)$ is monotonically non-increasing under any LOCC on the party whose quantumness is not being measured:

$$C_\mu\left(\left(\mathbb{1} \otimes \cdots \mathcal{E}_{\mu^c}^{\mathrm{LOCC}} \cdots \otimes \mathbb{1}\right) \rho\right) \leq C_\mu(\rho) ,$$

where $\mathcal{E}_{\mu^c}^{\mathrm{LOCC}}$ is computed on the complementary of $\mu$.

## 7.2 Entanglement Distance for Mixed States

### Quantum Correlation Distance

We consider the Hilbert space $\mathcal{H} = \bigotimes_{\mu=0}^{M-1} \mathcal{H}_\mu$. The Hilbert-Schmidt distance $D$ between two general square matrices, $A$ and $B$, is given by

$$D(A,B) = \sqrt{\frac{1}{2}\,\mathrm{Tr}[(A-B)^\dagger (A-B)]} . \tag{7.7}$$

We derive from the latter, the distance between two close density matrices of a quantum state in $\mathcal{H}P^{\otimes M}$, by

$$d_{dm}^2(\rho, \rho + d\rho) = \frac{1}{2}\,\mathrm{Tr}[(d\rho)^\dagger (d\rho)] . \tag{7.8}$$

The Hilbert-Schmidt distance is not the only possible choice, e.g. the Bures' distance represents an appropriate alternative option. The infinitesimal variation $d\rho$ of state $\rho$ is

$$\begin{aligned} d\rho &= \sum_{j=0}^{M-1} d\tilde{U}^\mu \rho + \rho \sum_{\mu=0}^{M-1} d\tilde{U}^{\mu\dagger} \\ &= -i \sum_{\mu=0}^{M-1} \sum_{j=1}^{3} [\sigma_j^\mu , \rho] n_j^\mu d\xi^\mu , \end{aligned} \tag{7.9}$$

where

$$d\tilde{U}^{\mu} = -i(\boldsymbol{\sigma}_{\mathbf{n}})^{\mu} d\xi^{\mu} \tag{7.10}$$

and with $[\,,\,]$, we mean the commutator. Here and in the following we use the notation $(\boldsymbol{\sigma}_{\mathbf{n}})^{\mu} = (\mathbf{n}^{\mu} \cdot \boldsymbol{\sigma}^{\mu})$, and for $\mu = 0, \ldots, M-1$, we denote by $\sigma_1^{\mu}$, $\sigma_2^{\mu}$ and $\sigma_3^{\mu}$ the three Pauli matrices operating on the $\mu$-th qubit, where the index $\mu$ labels the spins. We have

$$d^2_{dm}(\rho, \rho + d\rho) = \sum_{\mu,\nu=0}^{M-1} g_{\mu\nu}(\rho, \mathbf{n}) d\xi^{\mu} d\xi^{\nu}\,, \tag{7.11}$$

where

$$g_{\mu\nu}(\rho, \mathbf{n}) = \frac{1}{2} \sum_{i,j=1}^{3} \mathrm{Tr}[\rho\{\sigma_i^{\mu}\,,\, \sigma_j^{\nu}\}\rho - 2\rho\sigma_i^{\mu}\rho\sigma_j^{\nu}] n_i^{\mu} n_j^{\nu}\,, \tag{7.12}$$

with $\{\,,\,\}$ we mean the anticommutator.

**Definition 7.3.** *We define the quantum correlation for the state $\rho$ as*

$$C(\rho) = \inf_{\{\mathbf{n}^{\nu}\}_{\nu}} \mathrm{Tr}(g(\rho, \mathbf{n}))\,. \tag{7.13}$$

Since $C(\rho)$ derives from a distance, we name it quantum correlation distance (QCD).

**Proposition 7.1.** *The quantum correlation is the minimum value of the trace of $g$ when the unit vectors are varied, therefore its numerical value is invariant under local unitary transformations. We have*

$$\sum_{\mu=0}^{M-1} g_{\mu\mu}(\rho, \mathbf{n}) = M\,\mathrm{Tr}(\rho^2) - \sum_{\mu=0}^{M-1} \sum_{i,j=1}^{3} \mathrm{Tr}[\rho\sigma_i^{\mu}\rho\sigma_j^{\mu}] n_i^{\mu} n_j^{\mu}\,. \tag{7.14}$$

*Thus, by defining the matrices $A^{\mu}(\rho)$, for $\mu = 0, \ldots, M-1$, whose entries are*

$$A^{\mu}_{ij}(\rho) = \mathrm{Tr}[\rho\sigma_i^{\mu}\rho\sigma_j^{\mu}]\,, \tag{7.15}$$

*we obtain the closed-form expression for the QCD of $\rho$,*

$$C(\rho) = \sum_{\mu=0}^{M-1} \Big( \mathrm{Tr}(\rho^2) - \lambda^{\mu}_{max}(\rho) \Big) = \sum_{\mu=0}^{M-1} C_{\mu}(\rho)\,, \tag{7.16}$$

*where, for $\mu = 0, \ldots, M-1$, $\lambda^{\mu}_{max}(\rho)$ is the maximum of the eigenvalues of $A^{\mu}(\rho)$, and $C_{\mu}(\rho) = \mathrm{Tr}(\rho^2) - \lambda^{\mu}_{max}(\rho)$ is the QCD of the subsystem $\mu$.*

The QCD is a directly computable measure of the degree of correlation of $\rho$. Remarkably, Eq. (7.16) contains two competing terms. The first term is named Purity, which takes account of the degree of statistical mixing of $\rho$, its upper bound 1 corresponds to a pure state. The second term ranges between 0 and 1 and derives from the degree of correlation of $\rho$, with the lower value, 0, corresponding to the higher correlation.

The time complexity of the obtained formula for the QCD is that of $D \times D$ matrix multiplications, that is $o(D^3)$, where $D$ is the dimension of the full Hilbert space. In particular, the QCD possesses a closed formula and do not require any optimization (other than finding the largest eigenvalue of $3 \times 3$ matrices). This is in contrast with other measures of quantum correlation which, to our best knowledge, all require time-costly optimization procedures, except for some specific classes of states [2].

**Theorem 7.1.** *The QCD* (7.16) *fulfills the following requirements for a bona fide measure of quantum correlation (see Section 7.1)*

*1*) $C_\mu(\rho) = 0$ if $\rho \in \mathcal{C}_\mu$, where $C_\mu(\rho) = 0$ is defined in (7.5), i.e. if $\rho$ is classical in the subsystem $\mu$.

*2*) $C(U\rho U^\dagger) = C(\rho)$, i.e. it is invariant under local unitary transformations.

*3*) In the case of a pure state $\rho = |\psi\rangle\langle\psi|$, $C(|\psi\rangle\langle\psi|)$ reduces to the measure of entanglement for pure states.

*Proof.*

*1*) Suppose the following states

$$\rho = \rho^{\mu_c} \otimes |0\rangle\langle 0|^{\mu} \ , \tag{7.17}$$

where $\mu$ denotes the $\mu$th subsystem and $\mu_c$ denotes the complementary subsystem. In the above example, the classicality is on the $\mu$th subsystem. We have

$$C_\mu(\rho) = \mathrm{Tr}\left(\rho^2\right) - \max_{\mathbf{n}_\mu} \mathrm{Tr}\left[\rho\left(\mathbb{1}_{\mu_c} \otimes (\boldsymbol{\sigma}\cdot\mathbf{n})_\mu\right)\rho\left(\mathbb{1}_{\mu_c} \otimes (\boldsymbol{\sigma}\cdot\mathbf{n})_\mu\right)\right] . \tag{7.18}$$

In this example, $\mathbf{n}_\mu = \mathbf{z}_\mu = (0,0,1)$ minimizes $C(\rho)$. Thus, we have

$$\begin{aligned} C_\mu(\rho) &= \mathrm{Tr}\left((\rho^{\mu_c})^2\right) \underbrace{\left(|0\rangle\langle 0|^{\mu}\right)^2\Big)}_{=1} - \mathrm{Tr}\left[(\rho^{\mu_c})^2\right] \underbrace{\mathrm{Tr}\left[|0\rangle\langle 0|^{\mu}\,\sigma_z\,|0\rangle\langle 0|^{\mu}\,\sigma_z\right]}_{=1} \\ &= \mathrm{Tr}\left((\rho^{\mu_c})^2\right) - \mathrm{Tr}\left((\rho^{\mu_c})^2\right) = 0 \ . \end{aligned} \tag{7.19}$$

Thus, for the above-taken example, where the classicality is taken to be on the subsystem $\mu$, the measure of correlation on subsystem $\mu$ is equal to zero. The example can be trivially extended to a general case $\rho = \sum_i \rho_i^{\mu_c} \otimes |i\rangle\langle i|^{\mu}$.

*2*) It is invariant under local unitary operations by construction.

*3*) In the case of a pure state $\rho = |\psi\rangle\langle\psi|$, $C(|\psi\rangle\langle\psi|)$ reduces to the measure of entanglement valid for pure states that we derived in Chapter 4.

■

### Entanglement Distance

As stated above, for a mixed state, the existence of quantum correlation is not a sufficient condition to guarantee the presence of entanglement. To extract from a given state $\rho$ its entanglement essence, we now propose a procedure of regularization of $\rho$, repurposing our measure of quantum correlations to catch the true degree of entanglement owned by $\rho$. In what follows, the regularization procedure is done for qubit systems. Given a state $\rho$, we consider all of its possible decomposition $\{p_j, \rho_j\}$, such that

$$\rho = \sum_j p_j \rho_j \,, \tag{7.20}$$

where $\sum_j p_j = 1$ and $\mathrm{Tr}[\rho_j] = 1$. Also, we consider all the possible local partial transformations on qubit $\mu$:

$$\rho_U^\mu(\{p_j, \rho_j, U_j^\mu\}) = \sum_j p_j U_j^\mu \rho_j U_j^{\mu\dagger} \,, \tag{7.21}$$

where, for each $j$, $U_j^\mu$ is an $SU(2)$ local unitary operator acting on qubit $\mu$.

**Definition 7.4.** *We define the entanglement measure for a mixed state $\rho$ as follows*

$$E(\rho) = \inf_{\{p_j,\rho_j\}} \Big\{ \sum_{\mu=1}^{M-1} \inf_{\{U_j^\mu\}} C_\mu \left(\rho_U^\mu(\{p_j, \rho_j, U_j^\mu\})\right) \Big\} \,. \tag{7.22}$$

Since the definition $E(\rho)$ derives from a distance, we named it entanglement distance (ED). Note that, similarly to the QCD, one can define $E_\mu(\rho)$ as the ED of subsystem $\mu$, simply discarding the complement in the sum on $\mu$ in (7.14).

**Lemma 7.1.** *The ED* (7.22) *fulfill the following property: $E_\mu(\rho) = 0$ if $\rho$ is separable in $\mu$.*

*Proof.*

*1*) $E_\mu(\rho) = 0$ if $\rho$ is separable in $\mu$. Indeed, it then admits a decomposition $\{p_j, \rho_j\}$, where, for each $j$, $\rho_j = (\mathbb{I}^\mu + \boldsymbol{\sigma}_{\mathbf{n}_j}^\mu)/2 \otimes \rho_j^{\mu C}$, where. Thus, it is always possible to determine local partial operators $U_j^\mu$, such that, after transformation (7.21), it results $\rho_U^\mu = \sum_j p_j |j\rangle\langle j|^\mu \otimes \rho_j^{\mu C}$ and, from property *1*), it follows our statement. It results $E(\rho) = 0$ if $\rho \in \mathcal{S}$, that is if $\rho$ is fully separable.

*2*) Reciprocally, if $E(\rho) = 0$, then $\rho$ is separable. First of all, we note that, for each $\mu = 0, \ldots, M-1$, $\lambda_{max}^\mu(\rho) \leq \mathrm{Tr}(\rho^2)$. In fact, for each $\mu$ and for each unit vector $\mathbf{n}^\mu$ it is possible to determine a unitary local operator $U$, so that $\mathrm{Tr}[(\rho(\boldsymbol{\sigma}_\mathbf{n})^\mu \rho(\boldsymbol{\sigma}_\mathbf{n})^\mu)] = \mathrm{Tr}[\tilde{\rho}\sigma_3^\mu \tilde{\rho}\sigma_3^\mu]$, where $\tilde{\rho} = U\rho U^\dagger$. Furthermore $\mathrm{Tr}[\tilde{\rho}\sigma_3^\mu \tilde{\rho}\sigma_3^\mu] = \sum_j \tilde{\rho}_{jj}^2 + 2\sum_{i\neq j} \pm|\tilde{\rho}_{ij}|^2 \leq \sum_j \tilde{\rho}_{jj}^2 + 2\sum_{i\neq j} |\tilde{\rho}_{ij}|^2 = \mathrm{Tr}[\tilde{\rho}^2] = \mathrm{Tr}[\rho^2]$. Moreover, for each pair $i \neq j$, $\exists\mu$ such that the term $|\tilde{\rho}_{ij}|^2$ appears in $\mathrm{Tr}[(\tilde{\rho}\sigma_3^\mu)^2]$ with a negative sign. Yet, $E(\rho) = 0$ implies that there exist a decomposition of $\rho$, let's say $\overline{\rho}$, for which

$$\sup_{\mathbf{n}^\mu} \mathrm{Tr}[\overline{\rho}(\boldsymbol{\sigma}_\mathbf{n})^\mu)\overline{\rho}(\boldsymbol{\sigma}_\mathbf{n})^\mu)] = \mathrm{Tr}[\overline{\rho}^2] \tag{7.23}$$

for each $\mu$. We hence have $|\overline{\rho}_{ij}|^2 = 0$ for each $i \neq j$. But this implies that $\overline{\rho}$ is diagonal and then $\rho$ separable.

■

For a given density matrix decomposition $\{p_j, \rho_j\}$, the minimization on the local unitary partial transformations, entailed by Eq. (7.22), can be addressed by studying the local minima of $C(\rho(\{p_j, \rho_j, U_j\}))$ under variation of $\{U_j\}$. Nevertheless, it can be proven that such fixed points do correspond only to cases where $E(\rho) = 0$, hence to separable states. Therefore, the minima of (7.22) in the case of non-separable states, do not correspond to fixed points, but rather to nonlocal (boundary) minima. Remarkably, these fixed points of the minimization procedure (7.22) can, at least in some cases, be realized by a decomposition $\{p_j, \rho_j\}$ including entangled pure states $\rho_j$. In particular, for two-qubits states diagonal in the Bell basis (the Bell-diagonal (BD) states, see [91, 1]) the fixed points can always be realized on the eigen-decomposition (hence, where the $\rho_j$ are Bell states). This of course greatly simplify the problem, as the full exploration of the $\{p_j, \rho_j\}$-space is avoided. It is worth emphasizing that BD states are representative of the larger class of two-qubits states of maximally mixed marginals (that is, for which $\forall\mu$ and $\forall j$, $\mathrm{Tr}[\rho\sigma_j^\mu] = 0$, see [91]), hence (7.22) is tractable in the same manner for this class of states. Leaning on numerical evidences, we further conjecture that, for a given state $\rho(\boldsymbol{\gamma})$ depending on parameters $\boldsymbol{\gamma} = (\gamma_1, \gamma_2, ...)$, the decomposition realizing the minimum (7.22) is the same in the whole parametric domain of $\boldsymbol{\gamma}$, and can hence be inferred from the fixed points found in the domains where this state is separable if such a domain exists. This suggests that the minimization over all possible decompositions $\{p_j, \rho_j\}$ might in fact possess *non-trivial* general solutions, depending on the considered class of states. Here, by "non-trivial solutions" of the minimization procedure, we mean solutions that do not require finding the decomposition of $\rho$ in terms of pure product-states $\rho_j = \bigotimes_\mu (\mathbb{I}^\mu + (\boldsymbol{\sigma}_{\mathbf{n}_j})^\mu)/2$. A subsequent more thorough work on such a classification of the solutions of this procedure could thus lead to an entanglement measure of relatively low computational cost, in particular for systems symmetric under qudit permutations, and with low rank$(\rho)$.

## 7.3 Chapter conclusions

In this Chapter, we saw that in the case of mixed states, one can observe states that manifest correlations detached from entanglement [118, 2]. we have constructed a quantum correlation measure for a multipartite state, that is boiled down to the entanglement distance in the case of a pure multipartite state. Then, via a regularization procedure applied to the quantum correlation measure, we constructed an entanglement measure for mixed multipartite states. This work is still in progress since we still need to prove that the entanglement distance fulfills all the requirements for a good entanglement measure, for mixed states. Also, note that the monotonicity requirement for the correlation measure is still not done. The work is still in progress, but we will see in the next chapter that, numerically, the two proposed measures accurately describe the correlation and entanglement properties of the examples we will take.

# 8

# Application of the entanglement measure for mixed states

We have published the work depicted here in Ref.[154]. In this Chapter, we apply measures defined in the previous Chapter to concrete examples. We report four examples of the application of quantum correlation and entanglement measures seen in the previous Chapter. We have considered two well-known classes of states: a general Bell diagonal (BD) state and Werner states (WS). In addition, we have applied the quantum correlation and entanglement measures to Werner state generalization to three qubits, and to a one-parameter three qubits mixed states interpolating between a bi-separable state and a genuine multipartite state, passing through a fully separable state.

## 8.1 Bell diagonal states

As a first and seminal example of applications of this procedure, we consider general BD states. They can be expressed as:

$$\begin{aligned}\rho_{BD}(\{p_\alpha\}) &= \sum_{\alpha=1}^{4} p_\alpha |\psi_\alpha\rangle\langle\psi_\alpha| \\ &= \frac{1}{4}\Big(\mathbb{I} + \sum_i c_i \sigma_i^0 \sigma_i^1\Big), \end{aligned} \tag{8.1}$$

where the $|\psi_\alpha\rangle$ are the four Bell states: $|\psi_\pm\rangle = \frac{1}{\sqrt{2}}(|00\rangle \pm |11\rangle)$ and $|\phi_\pm\rangle = \frac{1}{\sqrt{2}}(|01\rangle \pm |10\rangle)$. Furthermore, we have $\forall i$, $|c_i| \leq 1$, and the $c_i$ are such that the vector $(c_1, c_2, c_3)$, fully characterizing the state, belongs to the tetrahedron $\mathcal{T}$ of vertices $(-1, 1, 1)$, $(1, -1, 1)$, $(1, 1, -1)$, $(-1, -1, -1)$. The separable BD states belong to the octahedron $\mathcal{O}$ of vertices $(\pm 1, 0, 0)$, $(0, \pm 1, 0)$, $(0, 0, \pm 1)$, corresponding to the condition $\forall \alpha$, $p_\alpha \leq 2$, and the classical BD states are located on the Cartesian axis $(c_1, 0, 0)$, $(0, c_2, 0)$, $(0, 0, c_3)$ [91, 1].

Direct calculation yields the following result for the QCD of general BD states

$$C(\rho_{BD}(\{p_\alpha\}) = 2\sum_{\alpha=1}^{4} p_\alpha^2 - 4 \max_{P\{i,j,k,l\}} \Big\{p_i p_j + p_k p_l\Big\}, \tag{8.2}$$

where the maximum is taken on all permutations $P\{i, j, k, l\}$ of the indices $\{1, 2, 3, 4\}$. Figure 8.1 shows the QCD of BD states on a face of $\mathcal{T}$. We were

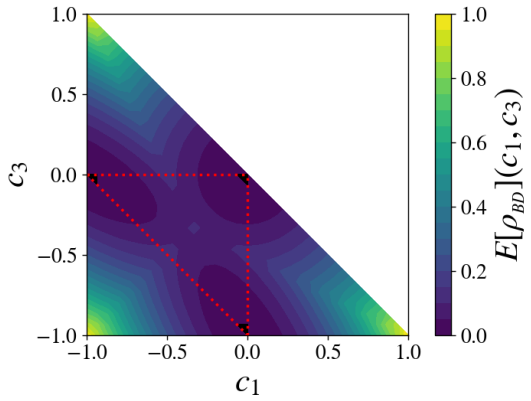


Figure 8.1: Quantum correlations $C[\rho_{BD}](c_1, c_2 = c_1, c_3)/2$ for a face of the BD state tetrahedron $\mathcal{T}$, corresponding to a mixture of three Bell states. The red dotted line defines the smaller triangle where the state is separable, according to the PPT criterion [121, 89]. The vertices of the large triangle correspond to pure Bell states. Those of the red dotted triangle, of vanishing QCD, correspond to equal-weight mixtures of two Bell states, which are evidently the three only *classical* states in the represented domain.

not able to find a simple analytic solution for the minimization procedure for the most general case of BD states. However, numerical minimization (for these calculations, we have applied a gradient steepest-descent method) provided us with empirical evidence that the procedure (22) also leads for these states to the squared concurrence, as shown in figure 8.2, which represent a face of the tetrahedral domain of BD states. It is interesting to note that the ED, as the concurrence and unlike the QCD, is constant on planes parallel to the boundary faces of the separability region: the ED of any given state indeed equates the QCD of the closest point located on a hinge of $\mathcal{T}$, hence the closest mixture of only two Bell states.

## 8.2 Werner states

Let us now consider the two-qubit Werner states (WS) [163], which stems as a special case of BD state, for which a simple analytical solution for the proposed procedure is available. WS are used as a testbed since they illustrate many features of mixed-states entanglement [16]. Using Eq. (8.1), they can simply be expressed as

$$\rho_W(p) = \rho_{BD}\big(\frac{p}{3}, \frac{p}{3}, \frac{p}{3}, (1-p)\big)\,. \tag{8.3}$$

Via direct calculations, one gets for the QCD of the WS

$$C(\rho_W(p)) = 2(1 - \frac{4}{3}p)^2\,. \tag{8.4}$$

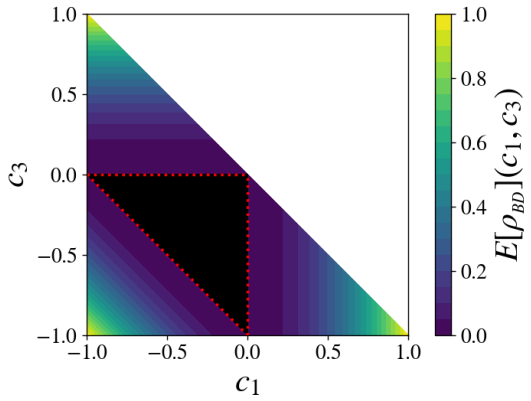


Figure 8.2: Entanglement distance $E[\rho_{BD}](c_1, c_2 = c_1, c_3)/2$ for a face of the BD state tetrahedron $\mathcal{T}$, corresponding to a mixture of three Bell states. The red dotted line defines the smaller triangle where the state is separable, according to the PPT criterion [121, 89] and a number of alternative derivations available in the literature (see e.g. [91]). Values below the threshold of $10^{-3}$ have been represented in black to emphasize that they correspond to a numerical zero, given the level of precision allowed by such time-costly minimization. The vertices of the large triangle correspond to pure Bell states, and those of the smaller black triangle to equal-weight mixtures of two Bell states.

WS yields a relatively simple solution to the minimization procedure. Indeed, as it can be easily verified, if we set

$$\begin{aligned} &U_{|\psi_+\rangle}(\theta) = U_z^\mu(\theta) U_x^\mu(\pi), \\ &U_{|\psi_-\rangle}(\theta) = U_z^\mu(\pi - \theta) U_x^\mu(\pi), \text{ and} \\ &U_{|\phi_+\rangle} = U_{|\phi_-\rangle} = \mathbb{I}, \end{aligned} \tag{8.5}$$

with $\mu = 0, 1$ arbitrarily chosen, the fixed points are found for $\theta = \arccos\left(\frac{3}{2p} - 2\right)$. This last expression has a solution if and only if $p \geq 1/2$, which is the parametric region of separability for $\rho_W(p)$ (as can be verified by application of the positive partial trace criterion, see [89]). Hence, $E(\rho_W) = 0$ for $p \geq 1/2$. For $p < 1/2$ numerical minimization yields $E(\rho_W) = 4p^2 - 4p + 1$. This corresponds to $\theta = 0$ uniformly on this whole domain, which is also the value previously determined at $p = 1/2$: hence, the minimum after this point cease to be a fixed point, but keeps the last position in terms of the parameters governing the rotations. One can understand this as the fixed point reaching the boundary of the parametric domain as the geometry of the state is changing continuously, becoming a simple point on a slope, located at this boundary. All together, for Werner states, the result of our entanglement measure exactly equates twice the square of the concurrence [165], that is

$$E(\rho_W(p)) = 2\Theta(1/2 - p)(1 - 2p)^2\,, \tag{8.6}$$

Fig. 8.3 shows $C(\rho_W(p))/2$ versus $p$, there it is clear that the only state with no quantum correlation, i.e. *classical state* according to the conventional terminology [2], is the one corresponding to the value $p = 3/4$, whereas the

maximally quantum-correlated state is that of $p = 0$. On the other hand, the state is entangled only in the region $p < 1/2$, and separable otherwise, a well-known fact that can be easily checked by application of the positive partial transpose (PPT) criterion [121, 89]. Alternatively, one can find, in the separable region, the expression of $\rho_W$ convex combination of (non-orthogonal) product states, using a more involved calculation resorting to the so-called Bloch representation.

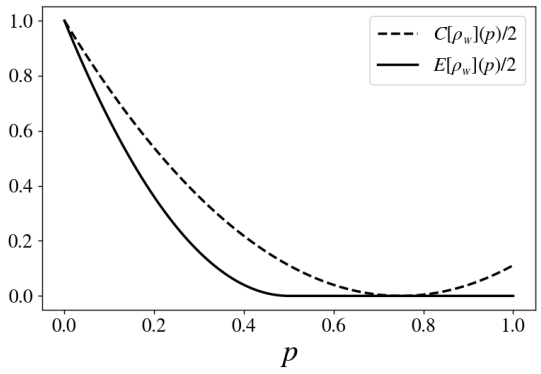


Figure 8.3: $C[\rho_W](p)/2$ and $E[\rho_W](p)/2$ versus $p$ for state (8.3). It is clear that the state $\rho_W(p = 0)$ is, as expected, the maximally-entangled, and that the states $\rho_W(p > 1/2)$ are fully-separable, as can be verified using the PPT criterion [121, 89]. This plot emphasizes that separable states can contain quantum correlation (i.e. not be classical). Note that, here $E[\rho_W](p)/2 = C_2^2[\rho_W](p)$, that is, the ED equates twice the squared concurrence for 2-qubits Werner states.

## 8.3 Generalized Werner states

Let us now consider as a multipartite example the following one-parameter density matrix

$$\rho_{W_3}(p) = p|GHZ_+\rangle\langle GHZ_+| + \frac{(1-p)}{8}\mathbb{I}_8\,, \tag{8.7}$$

where $|GHZ_+\rangle = (|000\rangle + |111\rangle)/\sqrt{2}$, $\mathbb{I}_8$ is the identity operator of the three-qubits Hilbert space and $0 \leq p \leq 1$. This is a generalization of the Werner states to three qubits, termed generalized Werner states [127, 49, 59]. The states $\rho_{W_3}(p)$ are known to be fully separable for $0 \leq p \leq 1/5$ [127, 142, 49] and genuinely multipartite entangled states in the region $3/7 < p \leq 1$ [80]. In the region $1/5 < p \leq 3/7$ the states $\rho_{W_3}(p)$ are bi-separable yet inseparable under any fixed bipartition [80]. Via direct calculations, one gets

$$C(\rho_{W_3}(p)) = 3p^2\,. \tag{8.8}$$

Numerical minimization provided the values for the ED shown in Fig. 8.4. There, we report in dotted line the QCD per qubit and continuous line the ED per qubit for the states $\rho_{W_3}(p)$. Fig. 8.4 clearly shows that $ED(\rho_{W_3}(p)) > 0$

only for $p > 3/7$, that is when the states are generally entangled. As for the region $1/5 < p \leq 3/7$ where ED should not be zero according to $ii$), we got numerical zero which we assume corresponds to very weak, but finite values. We interpreted this as a consequence of the fact that, in this region, the states $\rho_{W_3}(p)$ are not separable under any fixed bipartition, thus assuming the decomposition of the form $\sum_j \rho_j^1 \otimes \rho_j^{23} + \rho_j^2 \otimes \rho_j^{13} + \rho_j^3 \otimes \rho_j^{12}$. Hence the regularization procedure reaches easily small values for the ED.

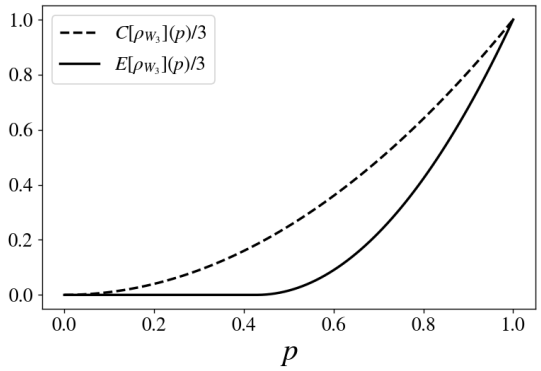


Figure 8.4: $C[\rho_{W_3}](p)/3$ (dotted line) and $E[\rho_{W_3}](p)/3$ (continuous line) versus $p$ for state (8.7). It is clear that the state $\rho_{W_3}(p = 1)$ is, as expected, the maximally entangled, and that the states $\rho_{W_3}(p > 3/7)$ are not separable. The latter are genuinely three-partite entangled states.

## 8.4 Three qubit states interpolating between bi-separable and genuine entangled states

Let us consider a further multipartite example, that is the one-parameter density matrix

$$\rho_3(p) = w_+ |GHZ_+\rangle\langle GHZ_+| + w_2 |\psi_2\rangle\langle\psi_2| + w\frac{(1-p)}{8}\mathbb{I}_8\,, \tag{8.9}$$

where

$$\begin{aligned} w_+ &= p[1 - 4p(1-p)]\,, \\ w_2 &= (1-p)[1 - 4p(1-p)]\,, \\ w &= 4p(1-p)\,, \end{aligned} \tag{8.10}$$

$|\psi_2\rangle = |0\rangle(|00\rangle + |11\rangle)/\sqrt{2}$ and $0 \leq p \leq 1$. For $p = 0$, $\rho_3(p = 0)$ is a pure bi-separable state, for $p = 1/2$, $\rho_3(p = 1/2)$ is a maximally mixed state of three qubits and for $p = 1$, $\rho_3(p = 1)$ is a pure maximally entangled state. Via direct calculations, one gets

$$C(\rho_3(p)) = \frac{(1-2p)^4}{2}\left[5 - 10p + 11p^2 - (1-p)\sqrt{1 - 2p(1-p)}\right]\,. \tag{8.11}$$

Using numerical minimization, we have obtained the results for the ED shown in Fig. 8.5. In this figure, we report in dotted line the QCD per qubit and

in continuous line the ED per qubit, for the states $\rho_3(p)$. Fig. 8.5 shows that $E(\rho_3(p)) > 0$ for $0 \leq p \lessapprox 0.18$ and for $0.81 \lessapprox p \leq 1$. Furthermore, the maximum value for ED per qubit in the region $0 \leq p \lessapprox 0.18$ is located at $p = 0$ and has the value $2/3$. $2/3$ is the maximum value for ED per qubit, in the case of bi-separable three qubits states. This confirms that the states of this region are stably bi-separable and that the state $|\psi_2\rangle\langle\psi_2|$ has the maximum local degree of entanglement. The maximum value for ED per qubit in the region $0.81 \lessapprox p \leq 1$ is located at $p = 1$ and has value 1. Therefore, the states of this region are not separable and, at least close to $p = 1$, are certainly genuinely entangled. For $0.18 < p < 0.81$ the entanglement is numerically null, thus suggesting the states of this region are separable or bi-separable yet inseparable under any fixed bipartition, hence not genuinely three-partite entangled states. Remarkably, the QCD is null only for the state corresponding to $p = 1/2$, which is the maximally mixed one.

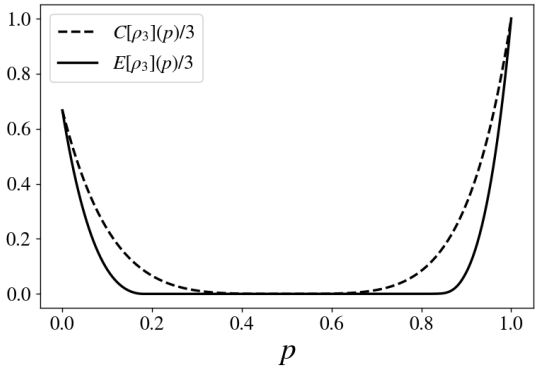


Figure 8.5: $C[\rho_3](p)/3$ (dotted line) and $E[\rho_3](p)/3$ (continuous line) versus $p$ for state (8.9). It is clear that the state $\rho_3(p = 1)$ is, as expected, the maximally entangled one, and that the states $\rho_3(p > 0.81)$ or $\rho_3(p < 0.18)$ are not separable.

## 8.5 Chapter conclusions

To test our quantum correlation and entanglement measures defined in the previous Chapter, we have applied them to two classes of mixed two-qubit states which are well-known entanglement properties, the Bell diagonal states and the Werner states, and we have verified the accordance between our measures and the expected results. Furthermore, we have applied the quantum correlation and entanglement measures to Werner state generalization to three qubits, and to a one-parameter family of three qubits mixed states. These latter interpolate between a bi-separable state and a genuine multipartite state, passing through a fully separable state. Also in these cases of multipartite states, then we have verified a satisfactory agreement between the behaviors deduced by our measures and the ones expected or already known in the literature.

# 9

# Conclusion of part II

The increasing interest in quantum information experimental applications, and the consequent demand for the development of skills in quantum state manipulation, has made pressing the development of effective measures of correlation and entanglement, valid for the general case of mixed multipartite states. Also, such measures are expected to be easily computable. For multipartite systems, a broad range of measures has covered pure states and mixed states, among which a Schmidt measure and a generalization of concurrence have been proposed. Nevertheless, the application of these measures to general multipartite mixed states still shows some issues. The work illustrated in this part can be summarized as follows

- We have constructed an entanglement measure, that we have named *entanglement distance*, for a general multipartite hybrid state from an adapted application of the Fubini Study metric, which is a metric defined in projective Hilbert spaces
- We have applied the entanglement distance to several examples, to verify its validity. And, we have seen that it actually gives precise predictions about the entanglement properties of different general hybrid multipartite states.
- Using the Hilbert Schmidt distance defined on the projective Hilbert space, we have also extended the entanglement distance to a measure of quantum correlation in mixed multipartite states, which we have proved its validity by applying it to some examples.
- Finally, from the quantum correlation measure, we have applied a regularization procedure to construct an entanglement measure for mixed multipartite states. And, it has been successfully applied to some entangled mixed states.

# 10

# Concluding remarks and further investigations

In this thesis, we have resorted to geometric methods to tackle two fairly distinct concepts which are: equilibrium phase transitions and quantum entanglement.

We have illustrated in **Part I** our proposed geometrical and topological analysis to characterize classical phase transitions. The proposed geometric and topological analysis is constructed from the microcanonical ensemble, which is the more fundamental statistical ensemble, as from it, we can generate the other statistical ensembles, i.e. canonical and grand-canonical. We have shown that peculiar behaviors of thermodynamic observables describing a given classical system at the phase transition point are rooted in more fundamental changes in the geometry of the energy level sets in phase space. In fact, geometric indicators, such as the Ricci curvature, undergo an abrupt change at the transition point. These geometric indicators are independent of the order parameter. Thus, the proposed geometric analysis can be applied also in the case of systems that undergo phase transitions in absence of a global symmetry breaking and consequently in the absence of an order parameter. A famous example of such a system is one that undergoes the Kosterlitz–Thouless (KT) phase transition, which manifests in several kinds of two-dimensional systems in condensed matter, such as the two-dimensional superconductors, the 2D liquid crystal or the XY ferromagnet. Our first original work [10, 8], was aimed at characterizing -from a geometric and topological point of view- the KT phase transition in the microcanonical ensemble. The KT phase transition is known to be an infinite-order phase transition in the canonical ensemble. However, using the proposed geometrical and topological analysis, we observed an abrupt change in the geometric indicator at a transition point, which led us to classify it as a second-order phase transition in the microcanonical ensemble. Our second work [9] consisted in describing the $\phi^4$ model, which is known to undergo a second-order phase transition. We have shown that in this model too, the geometric indicators undergo an abrupt change at the transition point. This suggests that phase transitions are the consequences of more fundamental changes in the geometry and topology of the phase space.

In **Part II**, we have characterized quantum entanglement through the study of projective Hilbert spaces $P(\mathcal{H})$. Our third original work [41], consisted in the construction of a measure of entanglement derived from an adapted

application of the Fubini-Study metric, which is a metric defined on $P(\mathcal{H})$. The proposed measure, which we named *entanglement distance*, can be applied to a multipartite hybrid quantum state. In fact, we have tested it on several different examples to confirm its validity. We have shown that the entanglement distance can be computed analytically. Moreover, through its study and the analysis of the Fubini Study metric, we could classify entangled pure states and find the same classification found in the literature. The success of the proposed entanglement measure for multipartite hybrid states led us to our fourth and last original work. In Ref.[154], we constructed a measure of quantum correlations in mixed multipartite states from the Hilbert Schmidt distance, defined in $P(\mathcal{H})$. We have shown that it boils down to the entanglement distance in the case of pure multipartite states. And, from a regularization procedure applied to the proposed measure of quantum correlation, we constructed an entanglement measure for mixed states, that we named *entanglement distance for mixed states*. Finally, both measures, i.e. the quantum correlation measure and the entanglement distance for mixed states have been tested in some examples, where we have shown that they clearly depict the quantum correlations and entanglement properties of the taken examples.

Further investigations can be conducted by bringing together the two topics studied in this work. One idea that might be pursued is the following: with the measurements of entanglement and quantum correlations of multipartite states proposed in this work, we can characterize entanglement and its evolution in quantum phase transitions. Another research line that can be conducted from this thesis is exporting to quantum phase transitions the geometric and topological methods used in the study of classical phase transitions. A well-known way to establish a formal link between classical and quantum systems stems from the mapping between the two fundamental operators in quantum physics and statistical physics, respectively, i.e. the unitary evolution operator $e^{-i\widehat{H}t}$ and the density matrix $e^{-\beta\widehat{H}}$, where $\hbar = 1$, that are formally related by the Wick rotation $t \to -it_E$, that is by means of an analytic continuation. Hence the Euclidean path integral of a field theory on a lattice is mapped onto a classical canonical partition function. Another promising mapping between quantum and classical systems prospectively allowing the use of geometrical-topological methods to study quantum phase transitions is provided by the Time Dependent Variational Principle (TDVP) in quantum mechanics. TDVP is a formulation of the time-dependent Schrödinger equation through the variation of an action functional which is required to be stationary under free variation of the time-dependent state. The TDVP, being a variational method, applies generically to any quantum system and its effectiveness depends on a reasonable choice of the initial ansatz for the state vector. Moreover, the important fact is that the dynamical equations worked out by means of the TDVP are formally classical but give the time evolution of actual quantum expectation values. Natural candidates to be initially tackled are the quantum optics Dicke model of the super-radiant phase transition and the Jaynes-Cummings model. These models can be mapped onto formally classical dynamical equations by means of the TDVP in order to apply the above-mentioned geometrical-topological methods, at the same time the Hilbert space geometrical methods developed to quantify the degree of entanglement could be also applied in parallel to figure

out if and to what extent the different phases correspond to entangled states of these systems.

# Appendices

# APPENDIX A

# Useful formulas for XY-2D model

## A.1 Derivatives and contractions of the potential energy with respect to generalized coordinates

Indexes in configuration space $\hat{\mu} = (i, j)$

$$V = J \sum_{(i,j)\in\Lambda} \left[2 - \cos(\theta_{(i+1,j)} - \theta_{(i,j)}) - \cos(\theta_{(i,j+1)} - \theta_{(i,j)})\right] \tag{A.1}$$

Gradient of the potential energy $V$

$$(\widehat{\nabla} V)^{(i,j)} = J \sum_{\mathbf{m}\in\mathbb{Z}, \|\mathbf{m}\|=1} \sin(\theta_{(i,j)} - \theta_{(i,j)+\mathbf{m}}) \tag{A.2}$$

Hessian of the potential

$$\begin{aligned}(\widehat{\mathrm{Hess}V})_{(i,j)(k,l)} = J\Bigg[\delta_{(i,j),(k,l)} \sum_{\|\mathbf{m}\|=1,\mathbf{m}\in\mathbb{Z}^2} \cos(\theta_{(k,l)} - \theta_{(k,l)+\mathbf{m}}) + \\ - \sum_{\|\mathbf{m}\|=1,\mathbf{m}\in\mathbb{Z}^2} \delta_{(i,j),(k,l)+\mathbf{m}} \ \cos(\theta_{(k,l)} - \theta_{(i,j)})\Bigg]\end{aligned} \tag{A.3}$$

## A.2 Derivatives of $f_{HP}$ and its contractions

Definition of $f_{HP}$

$$f_{HP} = \tilde{f}_{HP}(p^{\tilde{\mu}}) + \hat{f}_{HP}(q^{\hat{\mu}}) = \left(K(p^{\tilde{\mu}}) - \frac{P^2(p^{\tilde{\mu}})}{2N}\right) + V(q^{\hat{\mu}}) \tag{A.4}$$

Components of the gradient of $f_{HP}$

$$\nabla f_{HP} = \left(p^{\tilde{\mu}} - \frac{P\partial^{\tilde{\mu}} P}{N}\right)\partial_{\tilde{\mu}} + \partial^{\hat{\mu}} V \partial_{\hat{\mu}} \tag{A.5}$$

Module of the gradient of $f_{HP}$

$$\|\nabla f_{HP}\|^2 = 2\left(K - \frac{P^2}{2N}\right) + \|\widehat{\nabla} V\|^2 = 2\tilde{f}_{HP} + \|\widehat{\nabla} V\|^2 \tag{A.6}$$

when evaluated over the space corresponding to $P = 0$ it reduces to

$$\|\nabla f_{HP}\|^2\Big|_{\Sigma_0^P} = 2K + \|\widehat{\nabla} V\|^2 \tag{A.7}$$

Components of the hessian of $f_{HP}$

$$\begin{aligned}\mathrm{Hess} f_{HP} &= (\widetilde{\mathrm{Hess}}\tilde{f}_{HP})_{\tilde{\mu}\tilde{\nu}} \quad \mathrm{d}p^{\tilde{\mu}} \otimes \mathrm{d}p^{\tilde{\nu}} + (\widehat{\mathrm{Hess}}\hat{f}_{HP})_{\hat{\mu}\hat{\nu}} \quad \mathrm{d}q^{\hat{\mu}} \otimes \mathrm{d}q^{\hat{\nu}} \\ &= \left(\delta_{\tilde{\mu}\tilde{\nu}} - \frac{\partial_{\tilde{\mu}} P \partial_{\tilde{\nu}} P}{N}\right) \quad \mathrm{d}p^{\tilde{\mu}} \otimes \mathrm{d}p^{\tilde{\nu}} + (\widehat{\mathrm{Hess}} V)_{\hat{\mu}\hat{\nu}} \quad \mathrm{d}q^{\hat{\mu}} \otimes \mathrm{d}q^{\hat{\nu}}\end{aligned} \tag{A.8}$$

The Laplacian case is given by $g$-trace of the Hessian, i.e.

$$\begin{aligned}\Delta f_{HP} &= g^{\mu\nu}\mathrm{Hess}_{\mu\nu} = g^{\tilde{\mu}\tilde{\nu}}\widetilde{\mathrm{Hess}}_{\tilde{\mu}\tilde{\nu}} f_{HP} + g^{\hat{\mu}\hat{\nu}}\widehat{\mathrm{Hess}}_{\hat{\mu}\hat{\nu}} f_{HP} \\ &= \delta^{\tilde{\mu}\tilde{\nu}}\left(\delta_{\tilde{\mu}\tilde{\nu}} - \frac{\partial_{\tilde{\mu}} P \partial_{\tilde{\nu}} P}{N}\right) + \hat{\Delta} V \\ &= (N-1) + \hat{\Delta} V\end{aligned} \tag{A.9}$$

Components the double contraction of the Hessian of $f_{HP}$ with the gradient of $f_{HP}$

$$\begin{aligned}&\mathrm{Hess} f_{HP}(\nabla f_{HP}, \nabla f_{HP}) = (\nabla f_{HP})^{\mu}(\mathrm{Hess} f_{HP})_{\mu\nu}(\nabla f_{HP})^{\nu} \\ &= (\nabla f_{HP})^{\tilde{\mu}}(\mathrm{Hess} f_{HP})_{\tilde{\mu}\tilde{\nu}}(\nabla f_{HP})^{\tilde{\nu}} + (\nabla V)^{\hat{\mu}}(\mathrm{Hess} V)_{\hat{\mu}\hat{\nu}}(\nabla V)^{\hat{\nu}} \\ &= 2\left(K - \frac{P^2}{2N}\right) + \widehat{\mathrm{Hess}} V(\widehat{\nabla} V, \widehat{\nabla} V) \\ &= 2\tilde{f}_{HP} + \widehat{\mathrm{Hess}} V(\widehat{\nabla} V, \widehat{\nabla} V)\end{aligned} \tag{A.10}$$

Contraction of the Hessian of the function $f_{HP}$ with the gradient of total momentum $P$ is null

$$\begin{aligned}(\nabla P)^{\flat_{\mathrm{Hess} f_{HP}}} &= \imath_{\nabla P}\mathrm{Hess} f_{HP} = (\mathrm{Hess} f_{HP})_{\mu\nu}\partial^{\mu} P \, \mathrm{d}x^{\nu} \\ &= \left(\delta_{\tilde{\mu}\tilde{\nu}} - \frac{\partial_{\tilde{\mu}} P \partial_{\tilde{\nu}} P}{N}\right) \partial^{\tilde{\mu}} P \, \mathrm{d}x^{\tilde{\nu}} \\ &= \left(\delta_{\tilde{\mu}\tilde{\nu}} - \frac{\partial_{\tilde{\mu}} P \partial_{\tilde{\nu}} P}{N}\right) \partial^{\tilde{\mu}} P \, \mathrm{d}x^{\tilde{\nu}} = (\partial_{\tilde{\nu}} P - \partial_{\tilde{\nu}} P) \, \mathrm{d}x^{\tilde{\nu}} = 0\end{aligned} \tag{A.11}$$

# APPENDIX B

# Eisenhart Metric on Enlarged Configuration Space-Time

The natural motions of a standard Hamiltonian system, that is, having a quadratic kinetic energy term, can be identified with a geodesic flow on a Riemannian manifold. Among the other possibilities, Eisenhart proposed a geometric formulation of Hamiltonian/Newtonian dynamics by resorting to an enlarged configuration space-time $M \times \mathbb{R}^2$ having the local coordinates $(q^0, q^1, \ldots, q^i, \ldots, q^N, q^{N+1})$. This space can be endowed with a nondegenerate pseudo-Riemannian metric [55] whose arc length is

$$\begin{aligned} ds^2 &= (g_e)_{\mu\nu}\, dq^\mu dq^\nu \\ &= a_{ij}\, dq^i dq^j - 2V(q)(dq^0)^2 + 2\, dq^0 dq^{N+1} \end{aligned} \tag{B.1}$$

where $\mu$ and $\nu$ run from 0 to $N+1$ and $i$ and $j$ run from 1 to $N$. The following theorem holds.

**Theorem B.1** (Theorem (Eisenhart))**.** *The natural motions of a Hamiltonian dynamical system are obtained as the canonical projection of the geodesics of $(M \times \mathbb{R}^2, g_e)$ on the configuration space-time, $\pi : M \times \mathbb{R}^2 \mapsto M \times \mathbb{R}$. Among the totality of geodesics, only those whose arc lengths are positive definite and are given by*

$$ds^2 = c_1^2 dt^2 \tag{B.2}$$

*correspond to natural motions; the condition (B.2) can be equivalently cast in the following integral form as a condition on the extra coordinate $q^{N+1}$:*

$$q^{N+1} = \frac{c_1^2}{2} t + c_2^2 - \int_0^t L\, d\tau \ , \tag{B.3}$$

*where $c_1$ and $c_2$ are given real constants. Conversely, given a point $P \in M \times \mathbb{R}$ belonging to a trajectory of the system, and given two constants $c_1$ and $c_2$, the point $P' = \pi^{-1}(P) \in M \times \mathbb{R}^2$, with $q^{N+1}$ given by (B.3), describes a geodesic curve in $(M \times \mathbb{R}^2, g_e)$ such that $ds^2 = c_1^2 dt^2$.*

The explicit table of the entries of the Eisenhart metric is

$$g_e = \begin{pmatrix} -2V(q) & 0 & \cdots & 0 & 1 \\ 0 & a_{11} & \cdots & a_{1N} & 0 \\ \vdots & \vdots & \ddots & \vdots & \vdots \\ 0 & a_{N1} & \cdots & a_{NN} & 0 \\ 1 & 0 & \cdots & 0 & 0 \end{pmatrix} , \tag{B.4}$$

where $a_{ij}$ is the kinetic energy metric. The only non vanishing Christoffel symbols, for $a_{ij} = \delta_{ij}$, are

$$\Gamma^i_{00} = -\Gamma^{N+1}_{0i} = \partial_i V \ , \tag{B.5}$$

whence the geodesic equations

$$\frac{d^2 q^i}{ds^2} + \Gamma^i_{jk} \frac{dq^j}{ds} \frac{dq^k}{ds} = 0 \ ,$$

reduce to

$$\frac{d^2 q^0}{ds^2} = 0 \tag{B.6}$$

$$\frac{d^2 q^i}{ds^2} + \Gamma^i_{00} \frac{dq^0}{ds} \frac{dq^0}{ds} = 0 \ , \tag{B.7}$$

$$\frac{d^2 q^{N+1}}{ds^2} + \Gamma^{N+1}_{0i} \frac{dq^0}{ds} \frac{dq^i}{ds} = 0 \ ; \tag{B.8}$$

using $ds = dt$ one obtains

$$\frac{d^2 q^0}{dt^2} = 0 \ , \tag{B.9}$$

$$\frac{d^2 q^i}{dt^2} = -\frac{\partial V}{\partial q_i} \tag{B.10}$$

$$\frac{d^2 q^{N+1}}{dt^2} = -\frac{dL}{dt}. \tag{B.11}$$

Equation (B.9) states only that $q^0 = t$. The $N$ equations (B.10) are Newton's equations, and (B.11) is the differential version of (B.3).

The Riemann curvature tensor, associated with Eisenhart metric, has the following nonvanishing components

$$R_{0i0j} = \partial_i \partial_j V \ ; \tag{B.12}$$

thus the only nonzero component of the Ricci tensor is

$$R_{00} = \triangle V \ , \tag{B.13}$$

finally, the Ricci curvature is

$$K_R(q, \dot{q}) = R_{00} \dot{q}^0 \dot{q}^0 \equiv \triangle V \ , \tag{B.14}$$

so that $\triangle H/N$ is just

$$\frac{\triangle H}{N} = \frac{K_R(q, \dot{q})}{N} + 1 \ . \tag{B.15}$$

# APPENDIX C

# Some examples of projective spaces

The following Chapter is a summary of a personal work and of some lectures that can be found on youtube given by Prof.Wildberge.

We have defined a projective space $\mathbb{F}P^n$ over a field $\mathbb{F}$ in Chapter 2 as follows

$$\mathbb{F}P^n = \mathbb{F}^{n+1} \setminus (\{0\}/(v \sim \lambda v), \quad \lambda \in \mathbb{F}^*) \ ,$$

where $n$ can take any value in $\mathbb{N}$. let us first take $n = 2$ as an example. So, $n = 2$ means that we are looking at $\mathbb{F}P^2 = P\left(\mathbb{F}^3\right)$. Suppose $\mathbb{F} = \mathbb{R}$, we have thus $\mathbb{R}P^2 = P\left(\mathbb{R}^3\right)$, which is a real projective plane. A point $p \in \mathbb{R}P^2$ has coordinates $(x_0 : x_1 : x_2)$. we distinguish two situations

(1) $x_2 \neq 0$. Then
$p = [x_0 : x_1 : x_2] = \left[\frac{x_0}{x_2} : \frac{x_1}{x_2} : 1\right] = [\alpha : \beta : 1]$ for $\alpha, \beta \in \mathbb{R}$.

(2) $x_2 = 0$. Then
$p = [x_0 : x_1 : 0]$. This is a point at infinity in the direction $[x_0 : x_1]$

According to the first axiom posed at the beginning, we deduce that the set of $p = [x_0 : x_1 : 0]$ forms a line at infinity. Thus, we can think of $\mathbb{R}P^2$ as

$$\mathbb{R}P^2 \simeq \mathbb{R}^2 \cup \{\text{line at } \infty\} \tag{C.1}$$

The projective plane may be identified with the real plane extended by a line at infinity, which is homeomorphic to the quotient of the sphere $\mathbf{S}^2$ by the antipodal relation.

If $n = 1$, we are looking at $\mathbb{F}P^1 = P\left(\mathbb{F}^2\right)$. A point $p \in \mathbb{F}P^1$ has thus coordinates $[x_0 : x_1]$. Following the same reasoning as before, we distinguish two situations

(1) $x_1 \neq 0$. Then
$p = [x_0 : x_1] = \left[\frac{x_0}{x_1} : 1\right] = [\alpha : 1]$ for $\alpha \in \mathbb{F}$.

(2) $x_1 = 0$. Then
$p = [x_0 : 0] = [1 : 0]$. This is a fixed point.

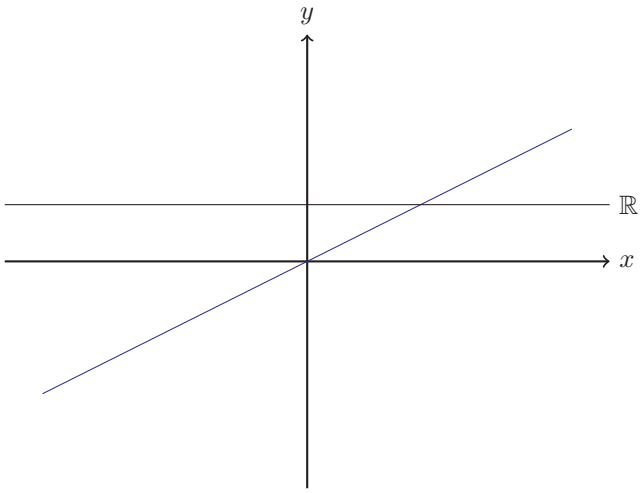


Figure C.1: $\mathbb{R}P^1$ can be seen as an extended line with a point at infinity.

If $\mathbb{F} = \mathbb{R}$, we get the real projective line $\mathbb{R}P^1 = P\left(\mathbb{R}^2\right)$, which is the projection of $\mathbb{R}$, called also the extended real line. We can think of the projective line as a line extended by a point at infinity. To see this, we can use the embedding of $\mathbb{R}$ in $\mathbb{R}^2$ (see Figure C.1) and consider that a point in $\mathbb{R}$ is given by the intersection of $\mathbb{R}$ with a line with equation $y = \alpha x$, where $\alpha \in \mathbb{R}$. The only line that is not projected onto $\mathbb{R}$ is the one parallel to it, i.e $y = 0$, which intersects $\mathbb{R}$ at infinity. Thus

$$\mathbb{R}P^1 = \mathbb{R} \cup \{\text{point at } \infty\} \ . \tag{C.2}$$

Note that in this example, we chose $\mathbb{R}$ to be parallel to the $x$ axis, but we could rotate the basis and choose another axis that will be parallel to $\mathbb{R}$. And, this will not change the result, i.e. the fact that $\mathbb{R}P^1$ is an extended line with a point at infinity. There is a second way to visualize the projective plane, which is by considering that $\mathbb{R}P^1 = P\left(\mathbb{R}^2\right)$ is the set of one-dimensional vector subspace in $\mathbb{R}^2$ (see Figure C.2). As for the projective plane, one ray is a point in this representation of the projective line. Thus, if we represent a ray with a vector $\vec{v} = (x, y) \in \mathbb{R}^2 \setminus \{0\}$, then any vector $\lambda\vec{v}$, where $\lambda \in \mathbb{R}^*$, will give the same ray, given by an equivalence class.

If $\mathbb{F} = \mathbb{C}$, we get the complex projective line

$$\mathbb{C}P^1 = \mathbb{C} \cup \{\text{point at } \infty\} \ , \tag{C.3}$$

which, as for the real projective line, it is the complex plane extended by a point at infinity.

The addition of the point at infinity $\{\infty\}$ to the complex plane $\mathbb{C}$, is also called the extended complex plane and denoted by $\mathbb{C} \cup \{\infty\} \equiv \mathbb{C}_\infty$ [44].

In what follows, we will show that topologically, $\mathbb{C}P^1$ is homeomorphic to a sphere in $\mathbb{R}^3$. More specifically, we will show that there is a one-to-one correspondence between the points of $\mathbb{C} \cup \{\infty\} \equiv \mathbb{C}_\infty$ and the unit sphere in $\mathbb{R}^3$

$$R = \{(x_1, x_2, x_3) \in \mathbb{R}^3 : x_1^2 + x_2^2 + x_3^3 = 1\} \ , \tag{C.4}$$

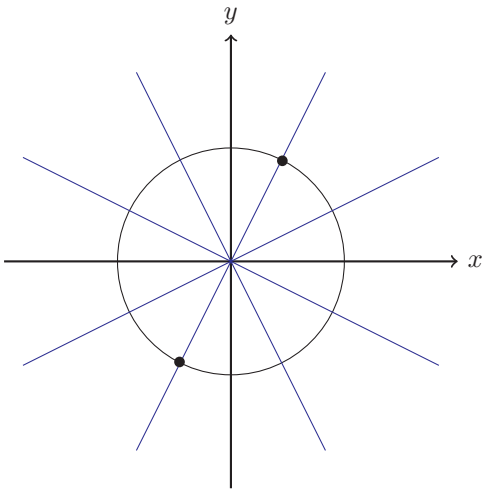


Figure C.2: $\mathbb{R}P^1$ is the set of all rays through the origin in $\mathbb{R}^2$. Topologically $\mathbb{R}^2 \simeq \mathbf{S}^1/_{(x\sim -x)}$

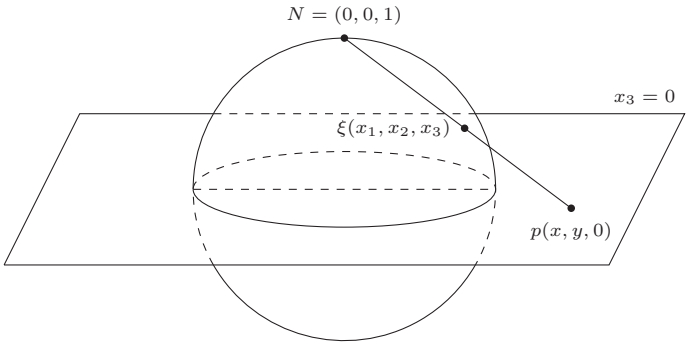


Figure C.3: Stenographic projection

called the Riemann sphere. This correspondence is what we call the stereographic projection. The idea is the following: imagine the complex plane that cuts a sphere in its equator (see Figure C.3). For any point $p$ on that plane, draw a straight line that connects it to the North Pole of the sphere. That straight line is going to intersect the sphere at some point $\xi$. If $p$ is on the exterior of the sphere it will intersect the northern hemisphere of the sphere. If $p$ is in the sphere's interior, the line will intersect the southern hemisphere of the sphere. And if $p$ lies on the sphere, it will itself be the intersection point. It is easy to see that the further away the point $p$ is on the plane, the closer its image projected on the sphere is to the North Pole. However, no point on the plane projects to the North Pole itself. The North Pole is only available to points at infinity on the plane because their projection moves toward the North Pole on the sphere. Thus, infinity is just a point and its projection is the North Pole of the sphere.

So, more formally suppose $N = (0, 0, 1)$ and $S = (0, 0, -1)$, the north and the South Poles of $R$ respectively. And suppose also that we identify $\mathbb{C}$ with

$\{(x_1, x_2, 0) : x_1, x_2 \in \mathbb{R}\}$ so that $\mathbb{C}$ cuts $R$ on along the equator. For $p \in \mathbb{C}$, let us consider the straight line in $\mathbb{R}^3$ through $p$ and $N$. This line intersects the sphere at exactly one point $\xi \neq N$. If $|p| < 1$, then $\xi$ is in the southern hemisphere and if $|p| > 1$, then $\xi$ is the northern hemisphere, and finally if $|p| = 1$, then $p = \xi$. The question now is, what happens to $\xi$ if $|p| \to \infty$?

The line in $\mathbb{R}^3$ passing trough $p$ and $N$ is given by

$$\{tN + (1-t)\, p : t \in \mathbb{R}\} \,. \tag{C.5}$$

Let $p = x + iy$. Knowing that $N = (0, 0, 1)$, we have that $tN + (1-t)\, p = ((1-t)\, x, (1-t)\, y, t)$, so that (C.5) can be written as

$$\{((1-t)\, x, (1-t)\, y, t) : t \in \mathbb{R}\} \,. \tag{C.6}$$

Now, we can find the coordinates of $\xi$ if we can find $t$ at which the line intersects $R$. Using equations C.4 and C.6, we get

$$\begin{aligned} &(1-t)^2\, x^2 + (1-t)^2\, y^2 + t^2 = 1 \\ &(1-t)^2\, |p|^2 + t^2 = 1 \,, \end{aligned}$$

which gives a quadratic equation on $t$

$$\left(1 + |p|^2\right) t^2 - 2|p|^2 t + \left(|p|^2 - 1\right) = 0 \,. \tag{C.7}$$

This equation has two solutions

$$\frac{|p|^2 - 1}{|p|^2 + 1} \,, \qquad \frac{|p|^2 + 1}{|p|^2 + 1} \,. \tag{C.8}$$

We will drop the second solution because it gives 1 and thus, using equation (C.6), gives the coordinates of the North Pole, which is not really interesting. So, using the first solution with Eq.(C.6), we get

$$x_1 = \frac{2x}{|p|^2 + 1} \,, \qquad x_2 = \frac{2y}{|p|^2 + 1} \,, \qquad x_3 = \frac{|p|^2 - 1}{|p|^2 + 1} \,. \tag{C.9}$$

We clearly see, using these coordinates, that if $|p| \to \infty$, we get $(0, 0, 1)$ which is the North Pole coordinate. Thus, the Riemann sphere is a complex projective space, which is formed by stereographically projecting the complex plane onto the sphere and including the point at infinity.

The Bloch sphere is a complex projective line. In fact, any quantum state of a spin 1/2 can be written in the following form

$$|\psi\rangle = \cos\frac{\theta}{2}\, |0\rangle + \sin\frac{\theta}{2} e^{i\phi}\, |1\rangle \;, \tag{C.10}$$

where $\theta \in [0, \pi]$ and $\phi \in [0, 2\pi]$ (see Figure C.4). As we did for the Riemann sphere, suppose we identify $\mathbb{C}$ with $\{(x_1, x_2, 0) : x_1, x_2 \in \mathbb{R}\}$ so that $\mathbb{C}$ cuts the Bloch sphere on along the equator. The stereographic projection of a quantum state $|\psi\rangle$ in the plane passing through the equator is given by the vector

$$\chi = \frac{\sin\dfrac{\theta}{2} e^{i\phi}}{\cos\dfrac{\theta}{2}} = \tan\frac{\theta}{2} e^{i\phi} \,, \tag{C.11}$$

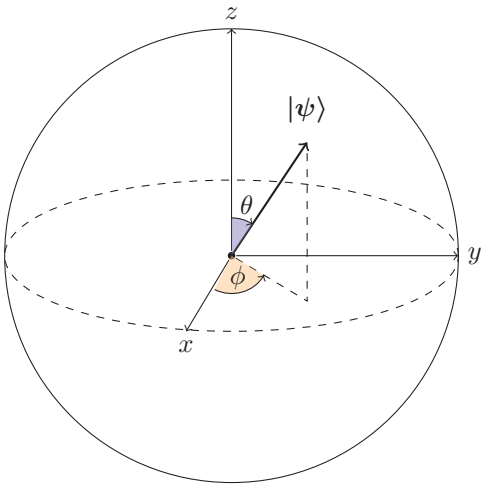


Figure C.4: Bloch sphere

which is the ratio of the coefficients in the state defined Eq.(C.10). The vector $\chi$ is shown in blue in Figure C.5. This ratio takes value in the $(x_1, x_2)$ plane plus a point at infinity, i.e. $\mathbb{C} \cup \{\infty\}$, corresponding to the stereographic projection of $|1\rangle$. The other basis state $|0\rangle$ is sent to the origin of the $(x_1, x_2)$ plane. By doing the projection of the Bloch sphere onto $\mathbb{C} \cup \{\infty\}$, we identify it with the Riemann sphere [102].

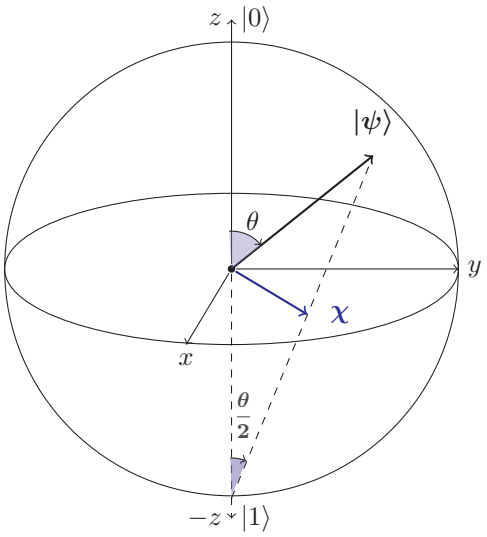


Figure C.5: Stereographic projection of the Bloch sphere

# APPENDIX D

# Differential geometry of Projective Hilbert spaces

The following Chapter is a summary of a personal work and of some lectures that can be found on youtube given by Prof.Frederic Schuller, and also other different small courses found on the internet. A more complete explanation can be found in [168, 45].

A projective Hilbert space is a complex projective space, and a complex projective space is a Khäler manifold, which is defined as a manifold with three mutually compatible structures: a complex structure, a symplectic structure, and a Riemannian structure. Thus, in this section, we will review the three structures.

## D.1 Complex manifolds

Let $M$ be a topological manifold of dimension $2n$, that is, X is a Hausdorff topological space such that each point of $M$ admits an open neighborhood $U$ which is homeomorphic to an open subset $V$ of $\mathbb{R}^{2n}$. Such a homeomorphism $x : U \to V$ is called *coordinate neighborhood.*

**Definition D.1.** *A local complex chart $(U, z)$ is an open subset $U \subseteq M$ and an homeomorphism $z : U \to V := z(U) \subset \mathbb{C}^n (\equiv \mathbb{R}^{2n})$. Two local complex charts $(U_\alpha, z_\alpha)$ and $(U_\beta, z_\beta)$ are compatible if the map $f_{\beta\alpha} := z_\beta \circ z_\alpha^{-1} : z_\alpha(U_\alpha \cup U_\beta) \to z_\beta(U_\alpha \cup U_\beta)$ is holomorphic[1]. The map $f_{\beta\alpha}$ is called transition function pr coordinate change.*

**Definition D.2.** *A holomorphic atlas (or complex analytical atlas) of $X$ is a collection $A = \{(U_\alpha, z_\alpha)\}$ of local complex charts, such that $X = \cup_\alpha U_\alpha$, and such that all transition functions $f_{\alpha\beta}$ are biholomorphic, for each $\alpha$ and $\beta$*

**Definition D.3.** *Complex manifolds are differentiable manifolds with a holomorphic atlas.*

The crucial difference between a real manifold of even dimension and a complex manifold is that for the latter, the transition functions are holomorphic. We will discuss complex manifolds in more detail in a moment. However, there

[1] A holomorphic function is infinitely differentiable and locally equal to its own Taylor series

is an intermediate notion that we shall first review as it will be useful for the study of complex manifolds, which is the notion of *almost complex manifolds*

**Definition D.4.** *An almost complex manifold is a smooth manifold equipped with a smooth linear complex structure on each tangent space. More formally, if a manifold $M$ admits a globally defined tensor $J$ of rank $(1,1)$ with the property*

$$J^2 = -\mathbb{1} \ , \tag{D.1}$$

*then $M$ is called an almost complex manifold. $\mathbb{1}$ is the identity operator. A globally defined $(1,1)$ tensor satisfying Eq.*(D.1) *is called an almost complex structure.*

Locally, this implies that at each given point $p \in M$, there is an endomorphism $J_p : T_pM \to T_pM$, that satisfies $(J_p)^2 = -\mathbb{1}_p$, where $T_pM$ denotes the tangent bundle on $p$. A tensor with rank $(1,1)$ can be defined by introducing a basis of real vector fields $\partial/\partial x^\mu$ in the tangent space, and a basis of dual one-forms $\mathrm{d}x^\mu$. The coordinates are denotes by $x^\mu$, $\mu = 1, \cdots, m$, where $m$ is the dimension of the almost complex manifold $M$. The tensor $J_p$ in local coordinates read

$$J_p = J^\nu_\mu(p) \frac{\partial}{\partial x^\nu} \otimes \mathrm{d}x^\mu \ , \tag{D.2}$$

where $J^\nu_\mu(p)$ are reals in this real basis. They can be complex if we complexify the basis, as we will see in a moment. In local coordinates, the condition for an almost complex structure in any point $p$ reads then

$$J^\rho_\mu(p) J^\nu_\rho(p) = -\delta^\nu_\mu \ . \tag{D.3}$$

Globally, having an almost complex structure means that one can define the $J_p$ in any patch and glue them together without encountering singularities. $J_p$ acts It acts on vector fields $X = X^\mu \partial/\partial x^\mu \in T_pM$, according to $J(X) = \left(X^\mu J^\nu_\mu\right) \partial/\partial x^\nu$.

If $M$ admits an almost complex structure, it must be even-dimensional. This can be seen as follows: suppose $M$ is $m$-dimensional, and let $J : TM \to TM$ be an almost complex structure. If $J^2 = \mathbb{1}$ then $[\mathrm{Det}(J)]^2 = \mathrm{Det}(J^2) = (-1)^m$. However, if $M$ is a real manifold, then $\mathrm{Det}\, J$ is a real number. Thus $m$ must be even $2n$ if $M$ has an almost complex structure.

We can complexify $T_pM$ by introducing linear combinations of vector fields with complex coefficients

$$Z = \frac{1}{2}\left(X + iY\right) \quad \text{and} \quad \bar{Z} = \frac{1}{2}\left(X - iY\right) \ , \tag{D.4}$$

where $X$, $Y \in T_pM$. $Z$ and $\bar{Z}$ belong thus to a complexified tangent space $T_pM^{\mathbb{C}}$. $J_p$ acts thus on $T_pM^{\mathbb{C}}$ as a complex linear map. In this case, the eigenvalues of $J_p$ are $\pm i$. More concretely, if one chooses a basis of $2n$ real vector fields in the tangent space $T_pM$, the almost complex structure takes the form

$$J_p = \begin{pmatrix} 0 & \mathbb{1}_{n\times n} \\ -\mathbb{1}_{n\times n} & 0 \end{pmatrix} \ , \tag{D.5}$$

and if one chooses a complexified basis, the almost complex structure is

$$J_p = \begin{pmatrix} i\mathbb{1}_{n\times n} & 0 \\ 0 & -i\mathbb{1}_{n\times n} \end{pmatrix} \ . \tag{D.6}$$

Thus, almost complex manifolds have even dimensional but are not complex, yet they inherit some of the properties of complex manifolds, as we will see below.

**Theorem D.1.** *Complex manifolds are almost complex.*

*Proof.* As we saw at the beginning of this section, complex manifolds allow for a holomorphic atlas, this means there exist local complex coordinates $z^\mu$ in a neighborhood $U$ of any given point $p \in M$. $J$ can thus be defined as follows

$$J = i\frac{\partial}{\partial z^\mu} \otimes \mathrm{d}z^\mu - i\frac{\partial}{\partial \bar{z}^\mu} \otimes \mathrm{d}\bar{z}^\mu \tag{D.7}$$

In contrast to the almost complex manifold, $J$ is defined on the patch $U$ and not only on a point $p$. For $J$ to be globally defined on $M$, we need to show that it keeps its form on the overlap of two patches $(U, z) \cap (V, w)$, Since, as we saw above, for complex manifolds, the transition functions are holomorphic, it follows that

$$J = i\frac{\partial}{\partial w^\mu} \otimes \mathrm{d}w^\mu - i\frac{\partial}{\partial \bar{w}^\mu} \otimes \mathrm{d}\bar{w}^\mu \ . \tag{D.8}$$

■

**Example D.1.** *The unit real sphere* $\mathbf{S}^2$ *defined in Eq.*(C.4) *in the previous chapter is a complex manifold. We used stereographic projection from the North Pole to the real plane* $\mathbb{R}^2$*, to show that* $\mathbb{C} \cup \{\infty\} \equiv \mathbb{C}P^1$.

**Example D.2.** *The complex projective space* $\mathbb{C}P^n$ *(see Eq.*(2.2) *in chapter 2 for a formal definition of* $\mathbb{C}P^n$*) is a complex manifold of dimension* $n$*. Suppose a atlas* $\{(U_i, \xi_i^a) \mid i = 1, \cdots n+1\}$*, where*

$$U_i = \{z^a | z^i \neq 0\} \quad \textit{and} \quad \xi_{\hat{i}}^a = \frac{z^a}{z^i} \ , \tag{D.9}$$

*where* $z^a$ *are the homogeneous coordinates, with* $a = 1, \cdots, n+1$*. On the overlap of two patches* $(U_l, \xi_{\hat{l}}^a) \cap (U_k, \xi_{\hat{k}}^a)$*, we have*

$$\frac{z^a z^k}{z^l z^k} = \frac{z^a}{z^l} = \xi_{\hat{l}}^a \ . \tag{D.10}$$

*There are* $n+1$ *charts that cover the entire space. The coordinates* $\xi_{\hat{i}}^a$ *are well defined on* $U_i$ *since* $z_i \neq 0$*. There are only* $n$ *independent coordinates since* $\xi_{\hat{i}}^{\hat{j}} = 1$*. Thus,* $\mathbb{C}P^n$ *is a complex manifold of dimension* $n$

## D.2 Symplectic manifolds

As we saw in the first part of the thesis, a symplectic manifold arises naturally as the phase space in classical Hamiltonian mechanics. It is actually a subset in the space of almost complex manifolds.

**Definition D.5.** *A symplectic manifold* $(M, \omega)$ *is a manifold* $M$ *equipped with a nondegenerate closed two-form* $\omega$*, called symplectic form. In local coordinates, we have*

$$\omega = \omega_{\mu\nu}(x)\, \mathrm{d}x^\mu \wedge \mathrm{d}x^\nu \ , \quad \mathrm{d}\omega = 0 \ . \tag{D.11}$$

The condition of being non-degenerate means that $\omega_{\mu\nu}$ is invertible, i.e.

$$\omega^{\mu\nu}\omega_{\nu\rho} = \delta^{\mu}_{\rho} \ . \tag{D.12}$$

An invertible antisymmetric matrix has an even number of rows and columns, so symplectic manifolds with even dimension.

**Example D.3.** *$\mathbb{R}^{2n}$ is a symplectic manifold. In fact, using a coordinate system, the symplectic form reads*

$$\omega = \mathrm{d}x^i \wedge \mathrm{d}x^y \ , \tag{D.13}$$

*and as a matrix*

$$\omega = \begin{pmatrix} 0 & \mathbb{1}_n \\ -\mathbb{1}_n & 0 \end{pmatrix} \ . \tag{D.14}$$

*The two-form is globally defined on $\mathbb{R}^{2n}$, it is closed and non-degenerate.*

**Example D.4.** *The complex projective space $\mathbb{C}P^n$ is symplectic. We will show this when we show that $\mathbb{C}P^n$ is a Kähler manifold since we will prove that Kähler manifolds are symplectic.*

**Theorem D.2.** *For $(M, \omega)$ a symplectic manifold with Riemannian metric $g$, $\exists$ a canonical almost complex structure $J$ compatible with $\omega$.*

The proof can be found in [111, 46].

*Proof.* Assume a globally defined metric

$$g = g_{\mu\nu}\, \mathrm{d}x^{\mu} \otimes \mathrm{d}x^{\nu} \ . \tag{D.15}$$

Let $A$ be a matrix defined on $M$, such that

$$\omega(X, Y) = g(AX, Y) \ , \tag{D.16}$$

which in local coordinates gives

$$A^{\nu}_{\mu}(x) = \omega_{\mu\rho}(x) g^{\rho\nu}(x) \ . \tag{D.17}$$

$\omega$ is anti-symmetric, so it is easy to show that $A$ is anti-hermitian with respect to the metric. From Eq.(D.17), we can deduce that $AA^{\dagger} = -A^2$ is hermitian and positive definite with respect to $g$. Thus, we can take the square-root of this matrix, and its inverse. In this way, we can define a matrix $J$ such that

$$J = \left(\sqrt{AA^{\dagger}}\right)^{-1} A \ , \tag{D.18}$$

where

$$J^2 = \left(AA^{\dagger}\right)^{-1} A^2 = -\mathbb{1} \ . \tag{D.19}$$

The tensor $J$ is globally defined since $g$ and $\omega$ are. Hence, $J$ defines an almost complex structure. ■

**Definition D.6.** *An almost complex structure $J$ is said to be compatible with the symplectic form $\omega$ if for all vector fields $X$, $Y$ we have*

$$\omega(JX, JY) = \omega(X, Y) \ , \quad \omega(X, JX) > 0 \ . \tag{D.20}$$

**Corollary D.1.** *The almost complex structure in* (D.18) *is compatible with $\omega$.*

There is a lot to say about symplectic geometry, but we only need a few notions for the following. That is why we stop here and now move on to the next concept: Khäler manifolds.

## D.3 Khäler manifolds

The concept of Khäler manifolds was first studied by Jan Arnoldus Schouten and David van Dantzig in 1930 and then introduced by Erich Kähler in 1933. Kähler manifolds are equipped with several compatible structures: complex, symplectic, and Riemannian, they can thus be described from different points of view. Let us first start defining the concept of a Hermitian metric

**Definition D.7.** *Let $M$ be a complex manifold, with Riemannian metric $g$ and complex structure $J$. If $g$ satisfies*

$$g(JX, JY) = g(X, Y) \ , \tag{D.21}$$

*for any two $X$ and $Y$ belonging to a complex vector bundle, then $g$ is said to be a Hermitian metric and $(M, g)$ is called a Hermitian manifold. If $(M, J)$ is an almost complex manifold, with a metric satisfying* (D.21)*, then $g$ is called an almost Hermitian metric, and $(M, g, J)$ is an almost Hermitian manifold.*

**Lemma D.1.** *Complex vector fields $Z$, $W$ are orthogonal with respect to a Hermitian metric.*

*Proof.* A complex vector field $Z$ satisfy $JZ = iZ$[2]. Thus, with respect to a Hermitian metric, we have

$$g(Z, W) = g(JZ, JW) = -g(Z, W) \ . \tag{D.24}$$

Therefore, $g(Z, W) = 0$. Similarly $g(\bar{Z}, \bar{W})$. It follows that the only nonzero elements are of the form $g(Z, \bar{W})$. ■

**Theorem D.3.** *A complex manifold $(M, J)$ always admits a Hermitian metric.*

*Proof.* Suppose $g$ is a Riemannian metric on $M$, we do not know if $g(JX, JY) = g(X, Y)$. However, we can define a metric $h$ such that

$$h(X, Y) = \frac{1}{2}\left(g(X, Y) + g(JX, JY)\right) \ . \tag{D.25}$$

It is clear that $h$ satisfies Eq.(D.21). ■

**Definition D.8.** *Let $(M, J, g)$ be a Hermitian manifold. We can define a two-form $\omega$ as*

$$\omega(X, Y) = g(JX, Y) \ . \tag{D.26}$$

[2]On a complex tangent bundle $TM^{\mathbb{C}}$ of a manifold $M$, we can define projector operators

$$P^{\pm} = \frac{1}{2}\left(\mathbb{1} \mp iJ\right) \ . \tag{D.22}$$

Since the eigenvalues of $J$ are $\pm i$ (see Eq.(D.6)), the above defined projectors satisfy $\left(P^{\pm}\right)^2 = P^{\pm}$, $P^+ + P^- = \mathbb{1}$ and $P^+ + P^- = 0$. Now, consider an arbitrary element $W \in TM^{\mathbb{C}}$ and define

$$Z \equiv P^+(W) = \frac{1}{2}(W - iJ(W)) \quad \text{and} \quad \bar{Z} \equiv P^-(W) = \frac{1}{2}(W + iJ(W)) \ . \tag{D.23}$$

It is clear that $J(Z) = iZ$ and $J(\bar{Z}) = -i\bar{Z}$.

*This is a two-form because it is antisymmetric with respect to $X$ and $Y$. Indeed*

$$\omega(X,Y) = \underbrace{g(JX,Y) = g(J^2X,JY)}_{g \text{ is a Hermitian metric}} = -g(X,JY) = -g(JY,X) = \omega(X,Y) \ . \tag{D.27}$$

*This is called a fundamental form.*

In local real coordinates, the components of the fundamental form are

$$\omega_{\mu\nu}(x) = J^\rho_\mu(x) g_{\rho\nu}(x) \ , \tag{D.28}$$

where $\omega_{\mu\nu} = -\omega_{\nu\mu}$.

**Corollary D.2.** *The fundamental form is non-degenerate.*

*Proof.* From Eq.(D.28), we can deduce $\omega^{\mu\rho}\omega_{\rho\nu} = \delta^\mu_\nu$. ■

**Corollary D.3.** *The fundamental form $\omega$ is compatible with $J$, in the sense of* (D.20).

*Proof.* We have

$$\omega(JX,JY) = \omega(J^2X,JY) = \omega(J^3X,J^2Y) = \omega(JX,Y) = \omega(X,Y) \ , \tag{D.29}$$

and

$$\omega(X,JX) = g(JX,JX) = g(X,X) > 0 \ , \tag{D.30}$$

since $g$ is a Riemannian metric. ■

**Definition D.9.** *Let $M$ be a complex manifold with Hermitian metric $g$ and fundamental two-form $\omega$. If $\omega$ is closed i.e. $\mathrm{d}\omega = 0$, then $M$ is called a Khäler manifold, $g$ a Khäler metric, and $\omega$ a Khäler form.*

When $(M,g,J)$ is an almost Hermitian manifold, with closed fundamental two-form $\omega$, then $M$ is called almost Khäler. All Khäler manifolds are also symplectic since the Khäler form is closed and non-degenerate. However, the opposite is not always true.

We will now express the Khäler metric and the Khäler form with local complex coordinates. In a local holomorphic chart $\varphi = (z^1, \cdots, z^n) : U \to \mathbb{C}^n$ of $M$, we can distinguish real coordinates $(x^1, \cdots, x^n, y^1, \cdots, y^n)$, defined by $z^i = x^i + iy^i$. These give distinguished complex-valued one-forms $\mathrm{d}z^i = \mathrm{d}x^i + i\,\mathrm{d}y^i$ and $\mathrm{d}\bar{z}^i = \mathrm{d}x^i - i\,\mathrm{d}y^i$ on $U$. These complex-valued one-forms have their dual, which are the complex-valued vector fields

$$\frac{\partial}{\partial z^i} = \frac{1}{2}\left(\frac{\partial}{\partial x^i} - i\frac{\partial}{\partial y^i}\right) \ , \quad \text{and} \quad \frac{\partial}{\partial \bar{z}^i} = \frac{1}{2}\left(\frac{\partial}{\partial x^i} + i\frac{\partial}{\partial y^i}\right) \ . \tag{D.31}$$

They are defined on a complex tangent space $T_pM^{\mathbb{C}}$, where $p \in M$. The hermitian metric in Eq.(D.21) can be extended by complex linearity to be defined on $T_pM^{\mathbb{C}}$. Thus, we can write $g$ first as follows

$$g = g_{ij}\,\mathrm{d}z^i \otimes \mathrm{d}z^j + g_{\bar{i}\,\bar{j}}\mathrm{d}\bar{z}^i \otimes \mathrm{d}\bar{z}^j + g_{\bar{i}\,j}\mathrm{d}\bar{z}^i \otimes \mathrm{d}z^j + g_{i\,\bar{j}}\,\mathrm{d}z^i \otimes \mathrm{d}\bar{z}^j \ , \tag{D.32}$$

where $g_{ij} = g\left(\frac{\partial}{\partial z^i}, \frac{\partial}{\partial z^j}\right)$. The fact that the metric is Hermitian will simply Eq.(D.32). On one hand, we have

$$g\left(J\frac{\partial}{\partial z^i}, J\frac{\partial}{\partial z^j}\right) = g\left(i\frac{\partial}{\partial z^i}, i\frac{\partial}{\partial z^j}\right) = -g\left(\frac{\partial}{\partial z^i}, \frac{\partial}{\partial z^j}\right) = -g_{ij} \ , \tag{D.33}$$

and on the other hand

$$g\left(J\frac{\partial}{\partial z^i}, J\frac{\partial}{\partial z^j}\right) = g\left(\frac{\partial}{\partial z^i}, \frac{\partial}{\partial z^j}\right) = g_{ij} \ . \tag{D.34}$$

Thus, $g_{ij} = 0$. Similarly $g_{\bar{i}\,\bar{j}} = 0$. Let us now compute $g_{\bar{i}\,j}$ and $g_{i\,\bar{j}}$.

$$g_{\bar{i}\,j} = g\left(\frac{\partial}{\partial \bar{z}^i}, \frac{\partial}{\partial z^j}\right) = \frac{1}{2}\Big[g\left(\frac{\partial}{\partial x^i}, \frac{\partial}{\partial x^j}\right) + g\left(\frac{\partial}{\partial y^i}, \frac{\partial}{\partial y^j}\right) + i\left(g\left(\frac{\partial}{\partial y^i}, \frac{\partial}{\partial x^j}\right) - g\left(\frac{\partial}{\partial x^i}, \frac{\partial}{\partial y^j}\right)\right)\Big] \ .$$

Using again the fact the $g$ is Hermitian, and using the fact that $J\left(\frac{\partial}{\partial x}\right) = \frac{\partial}{\partial y}$ and $J\left(\frac{\partial}{\partial y}\right) = -\frac{\partial}{\partial x}$ (Eq.(D.5)), we get

$$g\left(\frac{\partial}{\partial y^i}, \frac{\partial}{\partial x^j}\right) = g\left(J\frac{\partial}{\partial x^i}, -J\frac{\partial}{\partial y^j}\right) = -g\left(\frac{\partial}{\partial x^i}, \frac{\partial}{\partial y^j}\right) \ . \tag{D.35}$$

We also have

$$g\left(\frac{\partial}{\partial x^i}, \frac{\partial}{\partial x^j}\right) = g\left(\frac{\partial}{\partial y^i}, \frac{\partial}{\partial y^j}\right) \ . \tag{D.36}$$

Therefore, we obtain

$$g_{\bar{i}\,j} = g\left(\frac{\partial}{\partial x^i}, \frac{\partial}{\partial x^j}\right) - ig\left(\frac{\partial}{\partial x^i}, \frac{\partial}{\partial y^j}\right) \ . \tag{D.37}$$

Using the same arguments as those applied so far, we also get

$$g_{i\,\bar{j}} = g\left(\frac{\partial}{\partial x^i}, \frac{\partial}{\partial x^j}\right) - ig\left(\frac{\partial}{\partial x^i}, \frac{\partial}{\partial y^j}\right) = g_{\bar{i}\,j} \ . \tag{D.38}$$

Finally, the Khäler metric in terms of local complex coordinates reads

$$g = g_{\bar{i}\,j}\left(\mathrm{d}\bar{z}^i \otimes \mathrm{d}z^j + \mathrm{d}z^i \otimes \mathrm{d}\bar{z}^j\right) \ . \tag{D.39}$$

From the above equation and the ones in (D.8) and (D.28), we get the expression of the fundamental form in local complex coordinates

$$\omega = 2ig_{\bar{i}\,j}\,\mathrm{d}z^i \otimes \mathrm{d}\bar{z}^j \ . \tag{D.40}$$

With the above equation, we show that the fundamental form is a type of complex structure. The fact that the fundamental form is closed has important consequences. If we compute $\mathrm{d}\omega$ from Eq.(D.40), we have

$$\mathrm{d}\omega = i\left(\partial_a g_{b\bar{c}}\right)\mathrm{d}z^a \wedge z^b \wedge \mathrm{d}\bar{z}^c + i\left(\partial_{\bar{a}} g_{b\bar{c}}\right)\mathrm{d}\bar{z}^a \wedge z^b \wedge \mathrm{d}\bar{z}^c = 0 \ . \tag{D.41}$$

From both terms of the equation, we get two parts that must both be equal to zero

$$\partial_a g_{b\bar{c}} - \partial_b g_{a\bar{c}} = 0 \ , \quad \text{and} \quad \partial_{\bar{a}} g_{b\bar{c}} - \partial_{\bar{c}} g_{b\bar{a}} = 0 \ . \tag{D.42}$$

This implies that, locally in the patch $U_i$, there must exist a function $K_i(z, \bar{z})$, called the *Khäler potential*, such that

$$g_{a\bar{b}} = \partial_a \partial_{\bar{b}} K_i \ . \tag{D.43}$$

The Khäler form thus reads

$$\omega = i\partial\bar{\partial} K_i \ . \tag{D.44}$$

Note that, the Khäler potential $K_i$ is only defined in the patch $U_i$. On the overlap on two patches $U_i \cup U_j$, the functions $K_i$ and $K_j$ do not necessarily have to be equal to each other but can be related by a *Khäler transformation*

$$K_i(z, \bar{z}) = K_j(z, \bar{z}) + f_{ij}(z) + \bar{f}_{ij}(\bar{z}) \ . \tag{D.45}$$

**Example D.5.** *The complex projective space $\mathbb{C}P^n$ is a Kähler manifold. If we define*

$$K_i = \log\left(\sum_{a=1}^{n+1} |\xi_i^a|^2\right) \tag{D.46}$$

*defined in Eq.*(D.9)*. On the overlap $U_i \cup U_k$ (see Eq.*(D.10)*), we get*

$$K_i = K_k - \log \xi_{\hat{k}}^i - \log \bar{\xi}_{\hat{k}}^{\bar{i}} \ . \tag{D.47}$$

*Thus, the Khäler transformation in Eq.*(D.45) *is satisfied. This means we can define a globally defined metric*

$$g_{a\bar{b}} = \partial_a \partial_{\bar{b}} K_i = \partial_a \partial_{\bar{b}} K_k \ , \tag{D.48}$$

*and similarly for the Khäler form. This Khäler metric and the Khäler potential in* (D.46) *is called the Fubini study metric.*

Finally, we conclude that a finite projective Hilbert space $P\mathcal{H}^n \cong \mathbb{C}P^n$ is a Khäler manifold, in which a Khäler metric, called *Fubini Study metric* is defined.

## D.4 Fubini Study metric

We saw that the Khäler metric is well-defined globally on $\mathcal{H}P^n$ (see Examples (D.5) and (D.2) in the previous section)

$$g = \underbrace{\left(\partial_\mu \partial_{\bar{\nu}} K\right)}_{g_{\mu\bar{\nu}}} \left(\mathrm{d}\bar{\xi}^\mu \otimes \mathrm{d}\xi^\nu + \mathrm{d}\xi^\mu \otimes \mathrm{d}\bar{\xi}^\nu\right) \ , \tag{D.49}$$

where

$$K = \log\left(\sum_{a=1}^{n+1} |\xi^a|^2\right) = \log\left(|\xi|^2\right) = \log\left(\xi_\alpha \, \bar{\xi}^\alpha\right) \ , \tag{D.50}$$

and

$$\xi^\alpha = \frac{z^\alpha}{z} \ . \tag{D.51}$$

$z$ in the denominator can be any homogeneous coordinates, provided that it is not equal to zero. To obtain the metric, we need to derive twice the Khäler potential in Eq.(D.50). However, written in this way, the Khäler potential yields $\partial\bar{\partial}K = \partial\bar{\partial}(\xi\bar{\xi}) = 0$. We can get rid of this issue by expressing the Khäler potential in the following way

$$\log\left(\sum_{i}^{n+1}\frac{z^i}{z}\right) = \log\left(1+\sum_{i=1}^{n}\frac{z^i}{z}\right). \tag{D.52}$$

Let us take an example. Suppose a projective plane $\mathbb{R}P^2$, described with homogeneous coordinates $(x, y, z)$ defined in $\mathbb{R}^3 \setminus \{0\}$. We can express, the homogeneous coordinates in terms of affine coordinates defined on a given plane $X = x/z$ and $Y = y/z$, i.e. $(x/z, y/z, 1)$. The Khäler potential reads then

$$K = \log\left(\sum_{i=1}^{3}(\xi^i)^2\right) = \log\left(1+\left(\frac{x}{z}\right)^2+\left(\frac{y}{z}\right)^2\right), \tag{D.53}$$

where $\xi^i = u^i/z$, $u^i = x, y, z$. We can thus write Eq.(D.53) as follows

$$K = \log\left(1+\sum_{i=1}^{2}(\xi^i)^2\right) = \log\left(1+|w|^2\right), \tag{D.54}$$

where $|w|^2$ is the vector norm in $\mathbb{R}^2$. The change in the coordinates (from homogeneous to affine) will not change the derivatives $\partial$, $\bar{\partial}$ in the metric, since $\xi^i = w^i, 1$. Thus, coming back to the case of complex coordinates, we have

$$\begin{aligned}\partial_\mu\partial_{\bar{\nu}}K &= \partial_\mu\partial_{\bar{\nu}}\log\left(1+w_\alpha\bar{w}^\alpha\right) = \partial_\mu\partial_{\bar{\nu}}\log\left(1+\delta_{\alpha\bar{\beta}}w^\alpha\bar{w}^\beta\right)\\ &= \frac{\left(1+|w|^2\right)\delta_{\mu\bar{\nu}}-w_\mu\bar{w}_\nu}{\left(1+|w|^2\right)^2}\,.\end{aligned} \tag{D.55}$$

Thus, the Fubini-Study metric in terms of the affine complex coordinates reads

$$\begin{aligned}\mathrm{d}s^2 &= g_{\mu\bar{\nu}}\,\mathrm{d}w^\mu\,\mathrm{d}\bar{w}^\nu\\ &= \frac{\left(1+|w|^2\right)|\,\mathrm{d}w|^2-(\bar{w}\,\mathrm{d}w)\,(w\,\mathrm{d}\bar{w})}{\left(1+|w|^2\right)^2}\,.\end{aligned} \tag{D.56}$$

We can come back now to the homogeneous coordinates, where $\left(1+|w|^2\right) = |\xi|^2$, and $w\,\mathrm{d}\bar{w} = \xi\,\mathrm{d}\bar{\xi}$. Thus, the Fubini Study in terms of the homogeneous complex coordinates reads

$$\mathrm{d}s^2 = \frac{|\xi|^2|\,\mathrm{d}\xi|^2-\left(\bar{\xi}\,\mathrm{d}\xi\right)\left(\xi\,\mathrm{d}\bar{\xi}\right)}{|\xi|^4}\,. \tag{D.57}$$

We have seen in Example D.5, that the complex projective space $\mathbb{C}P^n$ is a Khäler manifold. We have also seen in Definition 2.2, that a finite projective Hilbert space $P\mathcal{H}$ is complex projective space $\mathbb{C}P^n$. The finite projective Hilbert space is thus a Käler manifold. Therefore, we expect to have the Fubini Study

defined also in $P\mathcal{H}$. In fact, a quantum state defined in $P\left(\mathcal{H}^{n+1}\right) = P\mathcal{H}^n$ can be expressed as follows

$$|\psi\rangle = \sum_{i=0}^{n} a_i \, |e_i\rangle = [a_0 : a_1 : \cdots : a_n] \ . \tag{D.58}$$

Then, given two rays $|\psi\rangle$ and $|\phi\rangle$ on $P\mathcal{H}^n$, we can define a transition probability as follows

$$\cos(\theta)^2 = \frac{|\langle\phi|\psi\rangle|^2}{\langle\phi|\phi\rangle \langle\psi|\psi\rangle} \ , \tag{D.59}$$

where $\theta$ is the angle between the two rays. We saw in the previous chapter that a ray in a projective space is considered as a point in the projective space. Thus, the angle $\theta$ between two rays in $P\mathcal{H}^n$ can be thought of as a distance between two points $|\psi\rangle$ and $|\phi\rangle$. If we Taylor expand Eq.(D.59) up to the second order and if we set $\mathrm{d}\theta$ equal to $\mathrm{d}s$, where $\mathrm{d}s$ denotes an infinitesimal distance, and take $\phi = \psi + \mathrm{d}\psi$, we get

$$\mathrm{d}s^2 = \frac{\langle\psi|\psi\rangle \langle\mathrm{d}\psi|\,\mathrm{d}\psi\rangle - \langle\mathrm{d}\psi|\psi\rangle \langle\psi|\,\mathrm{d}\psi\rangle}{\langle\psi|\psi\rangle^2} \ . \tag{D.60}$$

This is the Fubini Study metric defined on projective Hilbert spaces, which is similar to the one seen in Eq.(D.57).

# APPENDIX E

# Generalized Gell-Mann matrices

As fundamental representation for the generators of the algebra of SU($d_\mu$), we use the generalized Gell-Mann matrices. These are the following $d_\mu^2 - 1$, $d_\mu \times d_\mu$ matrices. Let $E_{j,k}$ (for $j, k = 1, \ldots, d_\mu$ ) be the matrix with 1 as $(j, k)$-th entry and 0 elsewhere. We define

$$T_{\mu\ell} = (E_{j,k} + E_{k,j}) \,, \tag{E.1}$$

where $\ell = 2(k-j) + (j-1)(2d_\mu - j) - 1$ for $j = 1, \ldots, d_\mu - 1$, $k = j+1, \ldots, d_\mu$,

$$T_{\mu\ell} = -i(E_{j,k} - E_{k,j}) \,, \tag{E.2}$$

where $\ell = 2(k-j) + (j-1)(2d_\mu - j)$ for $j = 1, \ldots, d_\mu - 1$, $k = j+1, \ldots, d_\mu$ and

$$T_{\mu\ell} = \left[ \sum_{j=1}^{k} E_{j,j} - kE_{k+1,k+1} \right] \sqrt{\frac{2}{k(k+1)}} \,, \tag{E.3}$$

where $\ell = d_\mu(d_\mu - 1) + k$ for $k = 1, \ldots, d_\mu - 1$. In the case of $d_\mu = 2$, these generators are given in terms of the Pauli matrices according to $T_{\mu 1} = \sigma_{\mu 1}$, $T_{\mu 2} = \sigma_{\mu 2}$ and $T_{\mu 3} = \sigma_{\mu 3}$. In the case $d_\mu = 3$, the generators are given by the standard Gell-Mann matrices. In the general case, the following identity holds true,

$$\sum_{k=1}^{d_\mu^2 - 1} T_{\mu k} T_{\mu k} = \frac{2(d_\mu^2 - 1)}{d_\mu} \mathbb{1} \tag{E.4}$$

and, for each normalized state $|s_\mu\rangle \in \mathcal{H}_{d_\mu}$, it results

$$\sum_{k=1}^{d_\mu^2 - 1} \langle s_\mu | T_{\mu k} | s_\mu \rangle^2 = \frac{2(d_\mu - 1)}{d_\mu} \,. \tag{E.5}$$

For each normalized state $|s\rangle \in \mathcal{H}$ and unitary local operator $U_\mu : \mathcal{H}_{d_\mu} \to \mathcal{H}_{d_\mu}$, it results

$$\begin{aligned}
&\sum_{k=1}^{d_\mu^2-1} \langle s|U_\mu^\dagger T_{\mu_k} U_\mu|s\rangle^2 = \\
&\sum_{k=1}^{d_\mu^2-1} \sum_{\alpha=1}^{d_\mu^2-1} (n_\alpha^k)^2 \langle s|T_{\mu\alpha}|s\rangle^2 = \\
&\sum_{\alpha=1}^{d_\mu^2-1} \langle s|T_{\mu\alpha}|s\rangle^2 \sum_{k=1}^{d_\mu^2-1} (n_\alpha^k)^2 = \\
&\sum_{\alpha=1}^{d_\mu^2-1} \langle s|T_{\mu\alpha}|s\rangle^2 .
\end{aligned} \tag{E.6}$$

# Bibliography


[1] B. Aaronson, R. Lo Franco, and G. Adesso. Comparative investigation of the freezing phenomena for quantum correlations under nondissipative decoherence. *Phys. Rev. A*, 88:012120, Jul 2013. doi: 10.1103/PhysRevA.88.012120. URL https://link.aps.org/doi/10.1103/PhysRevA.88.012120.

[2] G. Adesso, T. R. Bromley, and M. Cianciaruso. Measures and applications of quantum correlations. *Journal of Physics A: Mathematical and Theoretical*, 49(47):473001, nov 2016. doi: 10.1088/1751-8113/49/47/473001. URL https://doi.org/10.1088/1751-8113/49/47/473001.

[3] V. I. Arnold, V. V. Kozlov, A. I. Neishtadt, and I. Iacob. *Mathematical aspects of classical and celestial mechanics*, volume 3. Springer, 2006.

[4] A. Barasiński and M. Nowotarski. Quantifying entanglement properties of qudit mixed states with incomplete permutation symmetry. *Physical Review A*, 95(4):042333, 2017.

[5] H. Barnum and N. Linden. Monotones and invariants for multi-particle quantum states. *Journal of Physics A: Mathematical and General*, 34(35): 6787, 2001.

[6] T. Bastin, S. Krins, P. Mathonet, M. Godefroid, L. Lamata, and E. Solano. Operational families of entanglement classes for symmetric n-qubit states. *Physical review letters*, 103(7):070503, 2009.

[7] J. L. Beckey, N. Gigena, P. J. Coles, and M. Cerezo. Computable and operationally meaningful multipartite entanglement measures. *Physical Review Letters*, 127(14):140501, 2021.

[8] G. Bel-Hadj-Aissa. High order derivatives of boltzmann microcanonical entropy with an additional conserved quantity. *Physics Letters A*, 384 (24):126449, 2020.

[9] G. Bel-Hadj-Aissa, M. Gori, V. Penna, G. Pettini, and R. Franzosi. Geometrical aspects in the analysis of microcanonical phase-transitions. *Entropy*, 22(4):380, 2020.

[10] G. Bel-Hadj-Aissa, M. Gori, R. Franzosi, and M. Pettini. Geometrical and topological study of the kosterlitz–thouless phase transition in the xy model in two dimensions. *Journal of Statistical Mechanics: Theory and Experiment*, 2021(2):023206, 2021.

[11] I. Bengtsson and K. Życzkowski. *Geometry of quantum states: an introduction to quantum entanglement*. Cambridge university press, 2017.

[12] C. H. Bennett and S. J. Wiesner. Communication via one-and two-particle operators on einstein-podolsky-rosen states. *Physical review letters*, 69 (20):2881, 1992.

[13] C. H. Bennett, G. Brassard, C. Crépeau, R. Jozsa, A. Peres, and W. K. Wootters. Teleporting an unknown quantum state via dual classical and einstein-podolsky-rosen channels. *Physical review letters*, 70(13):1895, 1993.

[14] C. H. Bennett, H. J. Bernstein, S. Popescu, and B. Schumacher. Concentrating partial entanglement by local operations. *Physical Review A*, 53(4):2046, 1996.

[15] C. H. Bennett, G. Brassard, S. Popescu, B. Schumacher, J. A. Smolin, and W. K. Wootters. Purification of noisy entanglement and faithful teleportation via noisy channels. *Physical review letters*, 76(5):722, 1996.

[16] C. H. Bennett, D. P. DiVincenzo, J. A. Smolin, and W. K. Wootters. Mixed-state entanglement and quantum error correction. *Phys. Rev. A*, 54:3824–3851, Nov 1996. doi: 10.1103/PhysRevA.54.3824. URL https://link.aps.org/doi/10.1103/PhysRevA.54.3824.

[17] C. H. Bennett, D. P. DiVincenzo, J. A. Smolin, and W. K. Wootters. Mixed-state entanglement and quantum error correction. *Physical Review A*, 54(5):3824, 1996.

[18] C. H. Bennett, D. P. DiVincenzo, C. A. Fuchs, T. Mor, E. Rains, P. W. Shor, J. A. Smolin, and W. K. Wootters. Quantum nonlocality without entanglement. *Physical Review A*, 59(2):1070, 1999.

[19] C. H. Bennett, S. Popescu, D. Rohrlich, J. A. Smolin, and A. V. Thapliyal. Exact and asymptotic measures of multipartite pure-state entanglement. *Physical Review A*, 63(1):012307, 2000.

[20] V. Berezinskii. Destruction of long-range order in one-dimensional and two-dimensional systems having a continuous symmetry group i. classical systems. *Sov. Phys. JETP*, 32(3):493–500, 1971.

[21] V. S. Bhaskara and P. K. Panigrahi. Generalized concurrence measure for faithful quantification of multiparticle pure state entanglement using lagrange's identity and wedge product. *Quantum Information Processing*, 16(5):118, 2017.

[22] S. L. Braunstein and C. M. Caves. Statistical distance and the geometry of quantum states. *Phys. Rev. Lett.*, 72:3439–3443, May 1994. doi: 10.1103/PhysRevLett.72.3439. URL https://link.aps.org/doi/10.1103/PhysRevLett.72.3439.

[23] S. L. Braunstein and C. M. Caves. Statistical distance and the geometry of quantum states. *Physical Review Letters*, 72(22):3439, 1994.

[24] G. K. Brennen. An observable measure of entanglement for pure states of multi-qubit systems. *arXiv preprint quant-ph/0305094*, 2003.

[25] H. J. Briegel and R. Raussendorf. Persistent entanglement in arrays of interacting particles. *Physical Review Letters*, 86(5):910, 2001.

[26] H. J. Briegel and R. Raussendorf. Persistent entanglement in arrays of interacting particles. *Phys. Rev. Lett.*, 86:910–913, Jan 2001. doi: 10.1103/PhysRevLett.86.910. URL https://link.aps.org/doi/10.1103/PhysRevLett.86.910.

[27] N. Brunner, D. Cavalcanti, S. Pironio, V. Scarani, and S. Wehner. Bell nonlocality. *Reviews of modern physics*, 86(2):419, 2014.

[28] D. Bruß, G. M. D'Ariano, M. Lewenstein, C. Macchiavello, A. Sen, U. Sen, et al. Distributed quantum dense coding. *Physical review letters*, 93(21): 210501, 2004.

[29] D. Bruß, M. Lewenstein, A. SEN, U. Sen, G. M. D'ARIANO, and C. Macchiavello. Dense coding with multipartite quantum states. *International Journal of Quantum Information*, 4(03):415–428, 2006.

[30] A. Cabello. Bell's theorem with and without inequalities for the three-qubit greenberger-horne-zeilinger and w states. *Physical Review A*, 65(3): 032108, 2002.

[31] L. Caiani, L. Casetti, C. Clementi, and M. Pettini. Geometry of dynamics, lyapunov exponents, and phase transitions. *Physical review letters*, 79 (22):4361, 1997.

[32] E. T. Campbell, H. Anwar, and D. E. Browne. Magic-state distillation in all prime dimensions using quantum reed-muller codes. *Physical Review X*, 2(4):041021, 2012.

[33] A. R. Carvalho, F. Mintert, and A. Buchleitner. Decoherence and multipartite entanglement. *Physical review letters*, 93(23):230501, 2004.

[34] A. R. R. Carvalho, F. Mintert, and A. Buchleitner. Decoherence and multipartite entanglement. *Phys. Rev. Lett.*, 93:230501, Dec 2004. doi: 10.1103/PhysRevLett.93.230501. URL https://link.aps.org/doi/10.1103/PhysRevLett.93.230501.

[35] L. Casetti. Efficient symplectic algorithms for numerical simulations of hamiltonian flows. *Physica scripta*, 51(1):29, 1995.

[36] D. Cavalcanti and P. Skrzypczyk. Quantum steering: a review with focus on semidefinite programming. *Reports on Progress in Physics*, 80(2): 024001, 2016.

[37] M. Cerruti-Sola, C. Clementi, and M. Pettini. Hamiltonian dynamics and geometry of phase transitions in classical xy models. *Physical Review E*, 61(5):5171, 2000.

[38] S.-J. Chang. Existence of a second-order phase transition in a two-dimensional $\varphi$ 4 field theory. *Physical Review D*, 13(10):2778, 1976.

[39] E. Chitambar. Local quantum transformations requiring infinite rounds of classical communication. *Physical review letters*, 107(19):190502, 2011.

[40] E. Chitambar and G. Gour. Quantum resource theories. *Reviews of modern physics*, 91(2):025001, 2019.

[41] D. Cocchiarella, S. Scali, S. Ribisi, B. Nardi, G. Bel-Hadj-Aissa, and R. Franzosi. Entanglement distance for arbitrary m-qudit hybrid systems. *Physical Review A*, 101(4):042129, 2020.

[42] V. Coffman, J. Kundu, and W. K. Wootters. Distributed entanglement. *Phys. Rev. A*, 61:052306, Apr 2000. doi: 10.1103/PhysRevA.61.052306. URL https://link.aps.org/doi/10.1103/PhysRevA.61.052306.

[43] V. Coffman, J. Kundu, and W. K. Wootters. Distributed entanglement. *Physical Review A*, 61(5):052306, 2000.

[44] J. B. Conway and J. B. Conway. The complex number system. *Functions of One Complex Variable I*, pages 1–10, 1978.

[45] H. S. M. Coxeter. *Projective geometry*. Springer Science & Business Media, 2003.

[46] A. C. Da Silva. Symplectic geometry. In *Handbook of differential geometry*, volume 2, pages 79–188. Elsevier, 2006.

[47] K. A. Dill, S. B. Ozkan, M. S. Shell, and T. R. Weikl. The protein folding problem. *Annu. Rev. Biophys.*, 37:289–316, 2008.

[48] M. J. Donald, M. Horodecki, and O. Rudolph. The uniqueness theorem for entanglement measures. *Journal of Mathematical Physics*, 43(9): 4252–4272, 2002.

[49] W. Dür and J. I. Cirac. Classification of multiqubit mixed states: Separability and distillability properties. *Phys. Rev. A*, 61:042314, Mar 2000. doi: 10.1103/PhysRevA.61.042314. URL https://link.aps.org/doi/10.1103/PhysRevA.61.042314.

[50] W. Dür, G. Vidal, and J. I. Cirac. Three qubits can be entangled in two inequivalent ways. *Physical Review A*, 62(6):062314, 2000.

[51] S. Dutta, A. Banerjee, and P. K. Panigrahi. Absolutely secure distributed superdense coding: Entanglement requirement for optimality. *Physica Scripta*, 2021.

[52] C. Duval, G. Gibbons, and P. Horváthy. Celestial mechanics, conformal structures, and gravitational waves. *Physical Review D*, 43(12):3907, 1991.

[53] S. Ecker, F. Bouchard, L. Bulla, F. Brandt, O. Kohout, F. Steinlechner, R. Fickler, M. Malik, Y. Guryanova, R. Ursin, et al. Overcoming noise in entanglement distribution. *Physical Review X*, 9(4):041042, 2019.

[54] A. Einstein, B. Podolsky, and N. Rosen. Can quantum-mechanical description of physical reality be considered complete? *Physical review*, 47(10):777, 1935.

[55] L. P. Eisenhart. Dynamical trajectories and geodesics. *Annals of Mathematics*, pages 591–606, 1928.

[56] J. Eisert and H. J. Briegel. Schmidt measure as a tool for quantifying multiparticle entanglement. *Phys. Rev. A*, 64:022306, Jul 2001. doi: 10.1103/PhysRevA.64.022306. URL https://link.aps.org/doi/10.1103/PhysRevA.64.022306.

[57] J. Eisert and H. J. Briegel. Schmidt measure as a tool for quantifying multiparticle entanglement. *Physical Review A*, 64(2):022306, 2001.

[58] S. Elitzur. Impossibility of spontaneously breaking local symmetries. *Physical review d*, 12(12):3978, 1975.

[59] C. Eltschka and J. Siewert. Entanglement of three-qubit greenberger-horne-zeilinger–symmetric states. *Phys. Rev. Lett.*, 108:020502, Jan 2012. doi: 10.1103/PhysRevLett.108.020502. URL https://link.aps.org/doi/10.1103/PhysRevLett.108.020502.

[60] A. Ferraro, L. Aolita, D. Cavalcanti, F. M. Cucchietti, and A. Acín. Almost all quantum states have nonclassical correlations. *Physical Review A*, 81(5):052318, 2010.

[61] R. Franzosi. Microcanonical entropy for classical systems. *Physica A: Statistical Mechanics and its Applications*, 494:302–307, 2018.

[62] R. Franzosi, M. Pettini, and L. Spinelli. Topology and phase transitions i. preliminary results. *Nuclear Physics B*, 782(3):189–218, 2007.

[63] G. Fubini. *Sulle metriche definite da una forma hermitiana: nota*. Office graf. C. Ferrari, 1904.

[64] C. A. Fuchs and J. Van De Graaf. Cryptographic distinguishability measures for quantum-mechanical states. *IEEE Transactions on Information Theory*, 45(4):1216–1227, 1999.

[65] H.-O. Georgii. Gibbs measures and phase transitions. In *Gibbs Measures and Phase Transitions*. de Gruyter, 2011.

[66] M. G. Ghahi and S. Mancini. Comment on "inductive entanglement classification of four qubits under stochastic local operations and classical communication". *Physical Review A*, 98(6):066301, 2018.

[67] M. Gharahi, S. Mancini, and G. Ottaviani. Fine-structure classification of multiqubit entanglement by algebraic geometry. *Physical Review Research*, 2(4):043003, 2020.

[68] G. Gibbons. Typical states and density matrices. *Journal of Geometry and Physics*, 8(1):147 – 162, 1992. ISSN 0393-0440. doi: 10.1016/0393-0440(92)90046-4. URL http://www.sciencedirect.com/science/article/pii/0393044092900464.

[69] V. Giovannetti, S. Mancini, D. Vitali, and P. Tombesi. Characterizing the entanglement of bipartite quantum systems. *Phys. Rev. A*, 67:022320, Feb 2003. doi: 10.1103/PhysRevA.67.022320. URL https://link.aps.org/doi/10.1103/PhysRevA.67.022320.

[70] V. Giovannetti, S. Mancini, D. Vitali, and P. Tombesi. Characterizing the entanglement of bipartite quantum systems. *Physical Review A*, 67 (2):022320, 2003.

[71] H. Goldstein, C. Poole, and J. Safko. Classical mechanics, 2002.

[72] D. Gottesman. Theory of quantum secret sharing. *Physical Review A*, 61 (4):042311, 2000.

[73] G. Gour and N. R. Wallach. Classification of multipartite entanglement of all finite dimensionality. *Physical review letters*, 111(6):060502, 2013.

[74] D. M. Greenberger, M. A. Horne, and A. Zeilinger. *Going Beyond Bell's Theorem*, pages 69–72. Springer Netherlands, Dordrecht, 1989. ISBN 978-94-017-0849-4. doi: 10.1007/978-94-017-0849-4_10. URL https://doi.org/10.1007/978-94-017-0849-4_10.

[75] D. M. Greenberger, M. A. Horne, and A. Zeilinger. Going beyond bell's theorem. *Bell's theorem, quantum theory and conceptions of the universe*, pages 69–72, 1989.

[76] D. H. Gross. *Microcanonical thermodynamics: phase transitions in" small" systems*. World Scientific, 2001.

[77] O. Gühne and G. Tóth. Entanglement detection. *Physics Reports*, 474 (1-6):1–75, 2009.

[78] O. Gühne, F. Bodoky, and M. Blaauboer. Multiparticle entanglement under the influence of decoherence. *Physical Review A*, 78(6):060301, 2008.

[79] Y. Guo. Strict entanglement monotonicity under local operations and classical communication. *Physical Review A*, 99(2):022338, 2019.

[80] O. Gühne and M. Seevinck. Separability criteria for genuine multiparticle entanglement. *New Journal of Physics*, 12(5):053002, may 2010. doi: 10.1088/1367-2630/12/5/053002. URL https://dx.doi.org/10.1088/1367-2630/12/5/053002.

[81] Z. Hadzibabic, P. Krüger, M. Cheneau, B. Battelier, and J. Dalibard. Berezinskii–kosterlitz–thouless crossover in a trapped atomic gas. *Nature*, 441(7097):1118–1121, 2006.

[82] B. Halperin and D. R. Nelson. Theory of two-dimensional melting. *Physical Review Letters*, 41(2):121, 1978.

[83] A. S. M. Hassan and P. S. Joag. Geometric measure for entanglement in n-qudit pure states. *Physical Review A*, 80(4):042302, 2009.

[84] L. Henderson and V. Vedral. Classical, quantum and total correlations. *Journal of physics A: mathematical and general*, 34(35):6899, 2001.

[85] M. Hillery, V. Bužek, and A. Berthiaume. Quantum secret sharing. *Physical Review A*, 59(3):1829, 1999.

[86] M. W. Hirsch. *Differential topology*, volume 33. Springer Science & Business Media, 2012.

[87] M. Horodecki. Entanglement measures. *Quantum Inf. Comput.*, 1(1): 3–26, 2001.

[88] M. Horodecki and J. Oppenheim. (quantumness in the context of) resource theories. *International Journal of Modern Physics B*, 27(01n03):1345019, 2013.

[89] M. Horodecki, P. Horodecki, and R. Horodecki. Separability of mixed states: necessary and sufficient conditions. *Physics Letters A*, 223 (1):1–8, 1996. ISSN 0375-9601. doi: https://doi.org/10.1016/S0375-9601(96)00706-2. URL https://www.sciencedirect.com/science/article/pii/S0375960196007062.

[90] M. Horodecki, P. Horodecki, and R. Horodecki. Mixed-state entanglement and distillation: Is there a "bound" entanglement in nature? *Physical Review Letters*, 80(24):5239, 1998.

[91] R. Horodecki and M. Horodecki. Information-theoretic aspects of inseparability of mixed states. *Phys. Rev. A*, 54:1838–1843, Sep 1996. doi: 10.1103/PhysRevA.54.1838. URL https://link.aps.org/doi/10.1103/PhysRevA.54.1838.

[92] R. Horodecki, P. Horodecki, M. Horodecki, and K. Horodecki. Quantum entanglement. *Reviews of modern physics*, 81(2):865, 2009.

[93] X.-M. Hu, C. Zhang, B.-H. Liu, Y. Cai, X.-J. Ye, Y. Guo, W.-B. Xing, C.-X. Huang, Y.-F. Huang, C.-F. Li, et al. Experimental high-dimensional quantum teleportation. *Physical Review Letters*, 125(23):230501, 2020.

[94] P. Hyllus, W. Laskowski, R. Krischek, C. Schwemmer, W. Wieczorek, H. Weinfurter, L. Pezzé, and A. Smerzi. Fisher information and multiparticle entanglement. *Phys. Rev. A*, 85:022321, Feb 2012. doi: 10.1103/PhysRevA.85.022321. URL https://link.aps.org/doi/10.1103/PhysRevA.85.022321.

[95] P. Hyllus, W. Laskowski, R. Krischek, C. Schwemmer, W. Wieczorek, H. Weinfurter, L. Pezzé, and A. Smerzi. Fisher information and multiparticle entanglement. *Physical Review A*, 85(2):022321, 2012.

[96] C. J. Isham. *Modern differential geometry for physicists*, volume 61. World Scientific Publishing Company, 1999.

[97] C. G. J. Jacobi and C. W. Borchardt. *Vorlesungen über dynamik*. G. Reimer, 1866.

[98] J. Joo, Y.-J. Park, S. Oh, and J. Kim. Quantum teleportation via a w state. *New Journal of Physics*, 5(1):136, 2003.

[99] F. S. Khan and M. Perkowski. Synthesis of multi-qudit hybrid and d-valued quantum logic circuits by decomposition. *Theoretical Computer Science*, 367(3):336–346, 2006.

[100] J. M. Kosterlitz. Nobel lecture: Topological defects and phase transitions. *Reviews of Modern Physics*, 89(4):040501, 2017.

[101] J. M. Kosterlitz and D. J. Thouless. Ordering, metastability and phase transitions in two-dimensional systems. *Journal of Physics C: Solid State Physics*, 6(7):1181, 1973.

[102] J.-w. Lee, C. H. Kim, E. K. Lee, J. Kim, and S. Lee. Qubit geometry and conformal mapping. *arXiv preprint quant-ph/0201014*, 2002.

[103] A. J. Leggett. Bose-einstein condensation in the alkali gases: Some fundamental concepts. *Reviews of modern physics*, 73(2):307, 2001.

[104] P. Levay. The geometry of entanglement: metrics, connections and the geometric phase. *Journal of Physics A: Mathematical and General*, 37(5):1821, 2004. URL https://iopscience.iop.org/article/10.1088/0305-4470/37/5/024.

[105] X. Li and D. Li. Classification of general n-qubit states under stochastic local operations and classical communication in terms of the rank of coefficient matrix. *Physical review letters*, 108(18):180502, 2012.

[106] I. Lifshitz, A. Y. Grosberg, and A. Khokhlov. Some problems of the statistical physics of polymer chains with volume interaction. *Reviews of Modern Physics*, 50(3):683, 1978.

[107] H.-K. Lo and S. Popescu. Concentrating entanglement by local actions: Beyond mean values. *Physical Review A*, 63(2):022301, 2001.

[108] J. Luc. Quantumness of states and unitary operations. *Foundations of Physics*, 50(11):1645–1685, 2020.

[109] P. Maraner. On the jacobi metric for a general lagrangian system. *Journal of Mathematical Physics*, 60(11):112901, 2019.

[110] O. A. McBryan and T. Spencer. On the decay of correlations in so (n)-symmetric ferromagnets. *Communications in Mathematical Physics*, 53: 299–302, 1977.

[111] D. McDuff and D. Salamon. *Introduction to symplectic topology*, volume 27. Oxford University Press, 2017.

[112] N. D. Mermin and H. Wagner. Absence of ferromagnetism or antiferromagnetism in one-or two-dimensional isotropic heisenberg models. *Physical Review Letters*, 17(22):1133, 1966.

[113] D. A. Meyer and N. R. Wallach. Global entanglement in multiparticle systems. *Journal of Mathematical Physics*, 43(9):4273–4278, 2002.

[114] A. Michael. Nielsen and isaac l. chuang. quantum computation and quantum information, 2000.

[115] A. F. MObius. *Der barycentrische Calcul ein neues Hülfsmittel zur analytischen Behandlung der Geometrie dargestellt und insbesondere auf die Bildung neuer Classen von Aufgaben und die Entwickelung mehrerer Eigenschaften der Kegelschnitte angewendet von August Ferdinand Mobius Professor der Astronomie zu Leipzig*. Verlag von Johann Ambrosius Barth, 1827.

[116] M. A. Nielsen and I. Chuang. Quantum computation and quantum information, 2002.

[117] M. A. Nielsen and G. Vidal. Majorization and the interconversion of bipartite states. *Quantum Inf. Comput.*, 1(1):76–93, 2001.

[118] H. Ollivier and W. H. Zurek. Quantum discord: A measure of the quantumness of correlations. *Phys. Rev. Lett.*, 88:017901, Dec 2001. doi: 10.1103/PhysRevLett.88.017901. URL https://link.aps.org/doi/10.1103/PhysRevLett.88.017901.

[119] H. Ollivier and W. H. Zurek. Quantum discord: a measure of the quantumness of correlations. *Physical review letters*, 88(1):017901, 2001.

[120] E. M. Pearson, T. Halicioglu, and W. A. Tiller. Laplace-transform technique for deriving thermodynamic equations from the classical microcanonical ensemble. *Phys. Rev. A*, 32:3030–3039, Nov 1985. doi: 10.1103/PhysRevA.32.3030. URL https://link.aps.org/doi/10.1103/PhysRevA.32.3030.

[121] A. Peres. Separability criterion for density matrices. *Phys. Rev. Lett.*, 77:1413–1415, Aug 1996. doi: 10.1103/PhysRevLett.77.1413. URL https://link.aps.org/doi/10.1103/PhysRevLett.77.1413.

[122] G. Pettini, M. Gori, R. Franzosi, C. Clementi, and M. Pettini. On the origin of phase transitions in the absence of symmetry-breaking. *Physica A: Statistical Mechanics and its Applications*, 516:376–392, 2019.

[123] M. Pettini. *Geometry and topology in Hamiltonian dynamics and statistical mechanics*, volume 33. Springer Science & Business Media, 2007.

[124] L. Pezzé and A. Smerzi. Entanglement, nonlinear dynamics, and the heisenberg limit. *Phys. Rev. Lett.*, 102:100401, Mar 2009. doi: 10.1103/PhysRevLett.102.100401. URL https://link.aps.org/doi/10.1103/PhysRevLett.102.100401.

[125] L. Pezzé and A. Smerzi. Entanglement, nonlinear dynamics, and the heisenberg limit. *Physical review letters*, 102(10):100401, 2009.

[126] U. Pinkall. Inequalities of willmore type for submanifolds. 1985.

[127] A. O. Pittenger and M. H. Rubin. Note on separability of the werner states in arbitrary dimensions1this work was supported in part by the national security agency.1. *Optics Communications*, 179(1):447–449, 2000. ISSN 0030-4018. doi: https://doi.org/10.1016/S0030-4018(00)00612-X. URL https://www.sciencedirect.com/science/article/pii/S003040180000612X.

[128] M. B. Plenio. Logarithmic negativity: a full entanglement monotone that is not convex. *Physical review letters*, 95(9):090503, 2005.

[129] M. B. Plenio and S. Virmani. An introduction to entanglement measures. *Quantum Inf. Comput.*, 7(1):1–51, 2007.

[130] S. Popescu and D. Rohrlich. Thermodynamics and the measure of entanglement. *Physical Review A*, 56(5):R3319, 1997.

[131] C. C. Pradzynski, R. M. Forck, T. Zeuch, P. Slavíček, and U. Buck. A fully size-resolved perspective on the crystallization of water clusters. *Science*, 337(6101):1529–1532, 2012.

[132] J. Provost and G. Vallee. Riemannian structure on manifolds of quantum states. *Communications in Mathematical Physics*, 76:289–301, 1980.

[133] K. Qi and M. Bachmann. Classification of phase transitions by microcanonical inflection-point analysis. *Physical review letters*, 120 (18):180601, 2018.

[134] E. M. Rains. Entanglement purification via separable superoperators. *arXiv preprint quant-ph/9707002*, 1997.

[135] M. Reed and B. Simon. *Methods of modern mathematical physics. vol. 1. Functional analysis*. Academic San Diego, 1980.

[136] D. Resnick, J. Garland, J. Boyd, S. Shoemaker, and R. Newrock. Kosterlitz-thouless transition in proximity-coupled superconducting arrays. *Physical Review Letters*, 47(21):1542, 1981.

[137] P. Ribeiro and R. Mosseri. Entanglement in the symmetric sector of n qubits. *Physical review letters*, 106(18):180502, 2011.

[138] P. Rungta, V. Bužek, C. M. Caves, M. Hillery, and G. J. Milburn. Universal state inversion and concurrence in arbitrary dimensions. *Physical Review A*, 64(4):042315, 2001.

[139] D. Saha and P. K. Panigrahi. N-qubit quantum teleportation, information splitting and superdense coding through the composite ghz–bell channel. *Quantum Information Processing*, 11(2):615–628, 2012.

[140] S. Scali and R. Franzosi. Entanglement estimation in non-optimal qubit states. *Annals of Physics*, 411:167995, 2019. ISSN 0003-4916. doi: https://doi.org/10.1016/j.aop.2019.167995. URL http://www.sciencedirect.com/science/article/pii/S0003491619302507.

[141] S. Scali and R. Franzosi. Entanglement estimation in non-optimal qubit states. *Annals of Physics*, 411:167995, 2019.

[142] R. Schack and C. M. Caves. Explicit product ensembles for separable quantum states. *Journal of Modern Optics*, 47(2-3):387–399, 2000. doi: 10.1080/09500340008244050. URL https://www.tandfonline.com/doi/abs/10.1080/09500340008244050.

[143] M. O. Scully and M. S. Zubairy. Quantum optics, 1999.

[144] L. Sheridan and V. Scarani. Security proof for quantum key distribution using qudit systems. *Physical Review A*, 82(3):030301, 2010.

[145] D. E. Smith. *History of modern mathematics*. Number 1. J. Wiley & Sons, 1896.

[146] J. Sperling and I. Walmsley. Entanglement in macroscopic systems. *Physical Review A*, 95(6):062116, 2017.

[147] J. Sperling and I. A. Walmsley. Entanglement in macroscopic systems. *Phys. Rev. A*, 95:062116, Jun 2017. doi: 10.1103/PhysRevA.95.062116. URL https://link.aps.org/doi/10.1103/PhysRevA.95.062116.

[148] E. Study. Kürzeste wege im komplexen gebiet. *Mathematische Annalen*, 60(3):321–378, 1905.

[149] G. Tóth. Multipartite entanglement and high-precision metrology. *Phys. Rev. A*, 85:022322, Feb 2012. doi: 10.1103/PhysRevA.85.022322. URL https://link.aps.org/doi/10.1103/PhysRevA.85.022322.

[150] H. Touchette. Legendre-fenchel transforms in a nutshell. *URL http://www. maths. qmul. ac. uk/˜ ht/archive/lfth2. pdf*, 2005.

[151] V. Vedral and M. B. Plenio. Entanglement measures and purification procedures. *Physical Review A*, 57(3):1619, 1998.

[152] V. Vedral, M. Plenio, K. Jacobs, and P. Knight. Statistical inference, distinguishability of quantum states, and quantum entanglement. *Physical Review A*, 56(6):4452, 1997.

[153] V. Vedral, M. B. Plenio, M. A. Rippin, and P. L. Knight. Quantifying entanglement. *Physical Review Letters*, 78(12):2275, 1997.

[154] A. Vesperini, G. Bel-Hadj-Aissa, and R. Franzosi. Entanglement and quantum correlation measures for quantum multipartite mixed states. *Scientific Reports*, 13(1):2852, 2023.

[155] G. Vidal. Entanglement of pure states for a single copy. *Physical Review Letters*, 83(5):1046, 1999.

[156] G. Vidal. Entanglement monotones. *Journal of Modern Optics*, 47(2-3): 355–376, 2000.

[157] G. Vidal and R. Tarrach. Robustness of entanglement. *Physical Review A*, 59(1):141, 1999.

[158] G. Vidal and R. F. Werner. Computable measure of entanglement. *Physical Review A*, 65(3):032314, 2002.

[159] M. Walter, B. Doran, D. Gross, and M. Christandl. Entanglement polytopes: multiparticle entanglement from single-particle information. *Science*, 340(6137):1205–1208, 2013.

[160] M. Walter, D. Gross, and J. Eisert. Multipartite entanglement. *Quantum Information: From Foundations to Quantum Technology Applications*, pages 293–330, 2016.

[161] T.-C. Wei and P. M. Goldbart. Geometric measure of entanglement for multipartite quantum states. *arXiv preprint quant-ph/0212030*, 2002.

[162] T.-C. Wei and P. M. Goldbart. Geometric measure of entanglement and applications to bipartite and multipartite quantum states. *Physical Review A*, 68(4):042307, 2003.

[163] R. F. Werner. Quantum states with einstein-podolsky-rosen correlations admitting a hidden-variable model. *Phys. Rev. A*, 40:4277–4281, Oct 1989. doi: 10.1103/PhysRevA.40.4277. URL https://link.aps.org/doi/10.1103/PhysRevA.40.4277.

[164] A. Wong and N. Christensen. Potential multiparticle entanglement measure. *Physical Review A*, 63(4):044301, 2001.

[165] W. K. Wootters. Entanglement of formation of an arbitrary state of two qubits. *Phys. Rev. Lett.*, 80:2245–2248, Mar 1998. doi: 10.1103/PhysRevLett.80.2245. URL https://link.aps.org/doi/10.1103/PhysRevLett.80.2245.

[166] W. K. Wootters. Entanglement of formation of an arbitrary state of two qubits. *Physical Review Letters*, 80(10):2245, 1998.

[167] Z. Wu, J. K. Block, and G. M. Bruun. Liquid crystal phases of two-dimensional dipolar gases and berezinskii-kosterlitz-thouless melting. *Scientific Reports*, 6(1):1–10, 2016.

[168] C. R. Wylie. *Introduction to projective geometry*. Courier Corporation, 2011.

[169] G. Xu. Geometric quaternionic quantum mechanics. 2020.

[170] C.-N. Yang and T.-D. Lee. Statistical theory of equations of state and phase transitions. i. theory of condensation. *Physical Review*, 87(3):404, 1952.